Universidade do Minho
Escola de Medicina

Rogério Cristiano Rocha de Castro

Deciphering the mechanisms underlying the role of interleukin-10 in cognitive function

julho de 2021

Deciphering the mechanisms underlying the role of interleukin-10 in cognitive function
Rogério Cristiano Rocha de Castro
UMinho | 2021

Universidade do Minho
Escola de Medicina

Rogério Cristiano Rocha de Castro

Deciphering the mechanisms underlying the role of interleukin-10 in cognitive function

Dissertação de Mestrado
Mestrado em Ciências da Saúde

Trabalho efetuado sob a orientação de
Doutora Susana Cristina Roque Oliveira
e de
Doutora Palmira da Conceição de Araújo Barreira da Silva

julho de 2021

DIREITOS DE AUTOR E CONDIÇÕES DE UTILIZAÇÃO DO TRABALHO POR TERCEIROS

Este é um trabalho académico que pode ser utilizado por terceiros desde que respeitadas as regras e boas práticas internacionalmente aceites, no que concerne aos direitos de autor e direitos conexos.

Assim, o presente trabalho pode ser utilizado nos termos previstos na licença abaixo indicada.

Caso o utilizador necessite de permissão para poder fazer um uso do trabalho em condições não previstas no licenciamento indicado, deverá contactar o autor, através do RepositóriUM da Universidade do Minho.

Licença concedida aos utilizadores deste trabalho

Atribuição-NãoComercial-SemDerivações

CC BY-NC-ND

https://creativecommons.org/licenses/by-nc-nd/4.0/

AGRADECIMENTOS

Embora a presente dissertação de Mestrado seja, pelo seu desígnio académico, um projeto individual, há contributos de natureza diversa que não podem deixar de ser realçados. Por essa razão, desejo expressar o meu tributo a todos os animais de laboratório empregues para o triunfo deste trabalho, recordando que a experimentação animal é um privilégio de paladar azedo. Pretendo, além disso, manifestar a minha gratidão: À Doutora Susana Roque e à Doutora Palmira Barreira-Silva por terem aceitado este desafio árduo de me orientarem, por terem enriquecido o meu pensamento crítico e por me terem proporcionado inumeráveis momentos de discussão. À Professora Doutora Margarida Correia-Neves por me inspirar na expansão dos meus horizontes. À equipa *MCN* – em particular à Ângela Géros-Mesquita, à Cláudia Serre-Miranda e à Sónia Gomes – pela sua hospitalidade e colaboração nos procedimentos experimentais concretizados. À Doutora Patrícia Monteiro e ao Doutor Luís Jacinto pela gentileza nas correções das análises de dados. À Doutora Joana Alves e ao Doutor Nuno Cerca do Centro de Engenharia Biológica por terem amavelmente disponibilizado a câmara de anaerobiose e o equipamento para a realização dos qRT-PCR. Aos técnicos, investigadores e docentes responsáveis pelo funcionamento do Mestrado em Ciências da Saúde, por auxiliarem a levar a bom porto esta dissertação. Ao Engenheiro António Machado pelas fantásticas sessões de mentoria. À minha mãe, ao meu pai e ao meu irmão por primarem, permanentemente, pela minha educação. À Safira pelo carinho e ao Dimitri pela determinação. Ao Vítor Hugo Ribeiro por estimular, incondicionalmente, o meu desenvolvimento pessoal e profissional e pelo inestimável suporte emocional. Ao grupo *Las Plagas* – à Carolina Pereira, à Raquel Correia, à Sara Ferreira e à Susana Lima – pela amizade, pelas doses diárias de bom humor e pelo amparo nos períodos mais sombrios. À Joana Costa por ter acreditado sempre no meu potencial e por ter ajudado a tornar a Academia Minhota uma segunda casa. À Universidade do Minho, à Escola de Medicina (EMUM) e ao Instituto de Investigação em Ciências da Vida e Saúde (ICVS) por terem disponibilizado as infraestruturas que possibilitaram a realização deste trabalho. E, por fim, ao Programa Operacional Regional do Norte de Portugal – NORTE 2020 no âmbito dos projetos NORTE-01-0145-FEDER-000013 e NORTE-01-0145-FEDER-000023; à Plataforma de Microscopia Científica do ICVS, membro da infraestrutura nacional da Plataforma Portuguesa de Bioimagem – PPBI no contexto do projeto PPBI-POCI-01-0145-FEDER-022122, ambos ao abrigo do Acordo de Parceria – Portugal 2020, através do Fundo Europeu de Desenvolvimento Regional; e à Fundação para a Ciência e Tecnologia mediante fundos nacionais vinculados aos projetos UIDB/50026/2020 e UIDP/50026/2020 pelo suporte financeiro.

STATEMENT OF INTEGRITY

I hereby declare having conducted this academic work with integrity. I confirm that I have not used plagiarism or any form of undue use of information or falsification of results along the process leading to its elaboration.

I further declare that I have fully acknowledged the Code of Ethical Conduct of the University of Minho.

RESUMO

A função cognitiva refere-se aos processos mentais internos críticos para as atividades quotidianas, como a memória. A imunovigilância do cérebro é crucial para a cognição. A ausência de células T e níveis aumentados de citocinas pró-inflamatórias têm sido associados a comprometimentos cognitivos. No entanto, o papel das citocinas anti-inflamatórias, como a interleucina-10 (IL-10), tem sido pouco estudado. Aqui, o efeito da ausência de IL-10 na função cognitiva foi investigado em murganhos fêmeas BALB/c jovens-adultas IL-10 *knockout* (KO) e irmãs de tipo selvagem (WT). A ausência de IL-10 prejudicou a memória de referência espacial dependente do hipocampo no *Barnes-maze test*. Curiosamemente, neste teste, os murganhos IL-10 KO mostraram uma redução nas estratégias dependentes do hipocampo principalmente durante as fases de metestro e diestro do ciclo estríco. Não foram observados problemas locomotores nos murganhos IL-10 KO, no entanto, a deficiência de IL-10 comprometeu a exploração no *open-field test*. Embora a ausência de IL-10 tivesse aumentado os níveis basais de corticosterona e de expressão genética de marcadores pró-inflamatórios no cólon, estes parâmetros não se correlacionaram com o desempenho comportamental. Usando as variáveis comportamentais analisadas, o genótipo (WT *vs* IL-10 KO) foi classificado por *support vector machine models* com uma precisão de até 89,3%. Adicionalmente, a ausência de IL-10 diminui o número de neurónios e volume do hipocampo dorsal, mas não do ventral. Além disso, no hipocampo, a deficiência de IL-10 modulou negativamente a dinâmica das espinhas dendríticas e diminuiu a arborização dendrítica dos neurónios granulares do giro dentado dorsal e ventral e piramidais do *cornu ammonis*-1 e -3, que são conhecidos por suportar a aprendizagem e memória. Ademais, análises por citometria de fluxo mostraram que a ausência de IL-10 influenciou o perfil leucocitário no sangue pelo aumento do número total de neutrófilos e da sua percentagem dentro dos leucócitos e diminuição da percentagem dentro dos leucócitos de eosinófilos, células *natural-killer*, células B e células T. Além disso, no sangue, a deficiência de IL-10 aumentou a percentagem de células T $CD4^+$ efetoras de memória, que foram previamente associadas a uma pior função cognitiva em idosos saudáveis. A ausência de IL-10 também aumentou o número total de leucócitos nos nódulos linfáticos cervicais profundos, sugerindo um aumento do recrutamento de células para o sistema linfático do cérebro. Por fim, através de um tratamento antibiótico, um protocolo para a depleção do microbioma intestinal de murganhos IL-10 KO foi otimizado. Após 3 dias de tratamento, os antibióticos reduziram os níveis de expressão genética de *16s* nas fezes sem proliferação fúngica, proporcionando uma etapa inicial para explorar o papel do microbioma intestinal na função cognitiva de murganhos IL-10 KO. No geral, estes resultados não só suportaram que a ausência de IL-10 impactou as habilidades cognitivas, mas também destacaram potenciais mecanismos subjacentes à ação dessa citocina anti-inflamatória, que podem ser contribuintes importantes para o desenvolvimento de novas terapias para comprometimentos cognitivas baseadas em IL-10.

Palavras-chave: Citocina; Função cognitiva; Hipocampo; Interleucina-10; Sistema imunitário.

ABSTRACT

Cognitive function refers to internal mental processes critical for daily life activities, such as memory. Brain immune surveillance has proven to be crucial for cognitive function. T cell absence and increased levels of pro-inflammatory cytokines have been associated with impaired cognition. However, the role of anti-inflammatory cytokines, such as interleukin-10 (IL-10), has been poorly studied. Here, the effect of IL-10 absence in cognitive function was investigated in young-adult female BALB/c IL-10 knockout (KO) and wild-type (WT) littermate mice. IL-10 absence impaired the hippocampal-dependent spatial reference memory in the Barnes-maze test. Interestingly, in this test, IL-10 KO mice showed a reduction in hippocampal-dependent strategies mainly during the metestrus and diestrus phases of the estrous cycle. No locomotor disabilities were observed in IL-10 KO mice however IL-10 deficiency impaired exploration in the open-field test. Although IL-10 absence has led to higher basal levels of corticosterone and increased gene expression levels of pro-inflammatory markers in the colon, these parameters did not correlate with the behavioral performance. Using the behavioral variables analyzed, the genotype (WT *vs* IL-10 KO) was classified by support vector machine models with an accuracy of up to 89.3%. Moreover, IL-10 absence led to a decreased number of neurons and volumetric atrophy of the dorsal, but not of the ventral hippocampus. Additionally, in the hippocampus, IL-10 deficiency negatively modulated the dendritic spine dynamics and decreased the dendritic arborization of dorsal and ventral dentate gyrus granule neurons and *cornu ammonis*-1 and -3 pyramidal neurons, which are known to support learning and memory. Furthermore, flow cytometry analysis showed that IL-10 absence impacted the leukocyte profile in the blood by increasing the total number of neutrophils and its percentage within leukocytes and decreasing the percentage of eosinophils, natural-killer cells, B cells, and T cells within leukocytes. Also, in the blood, IL-10 deficiency increased the percentage of effector memory $CD4^+$ T cells, which were previously associated with a worst cognitive function of healthy aged individuals. IL-10 absence also increased the total number of leukocytes in the deep cervical lymph nodes, suggesting an increased cell recruitment to the lymphatic system of the brain. Lastly, through an antibiotic treatment, a protocol for gut microbiome depletion of IL-10 KO mice was optimized. After 3 days of treatment, antibiotics reduced the gene expression levels of *16s* in the feces without fungal overgrowth, providing an initial step to explore the role of the gut microbiome in the cognitive function of IL-10 KO mice. Overall, these results not only supported that IL-10 absence impacted cognitive abilities but also highlighted the potential mechanisms underlying the action of this anti-inflammatory cytokine, which may be important contributors to the development of new IL-10-based therapies for cognitive impairments.

Key-words: Cytokine; Cognitive function; Hippocampus; Immune system; Interleukin-10.

TABLE OF CONTENTS

LIST OF ABBREVIATIONS AND ACRONYMS

A

ACTH Adrenocorticotropin hormone

AKT Protein kinase B

ANOVA Analysis of variance

APCs Antigen-presenting cells

AUC Area under the curve

B

B2m *β_2 microglobulin* gene expression

BBB Blood-brain barrier

Bcl B cell lymphoma

BCSFB Blood- cerebrospinal fluid barrier

BDNF Brain-derived neurotrophic factor

BMT Barnes-maze test

bp Base pairs

BT Burrowing test

C

CA *Cornu ammonis*

CCFCT Contextual and cued fear conditioning test

CD Cluster of differentiation

cDNA Complementary deoxyribonucleic acid

CFUs Colony-forming units

CM Central memory

CN Catalog number

CNS Central nervous system

CRH Corticotropin-releasing hormone

CS Conditional stimulus

CSF Cerebrospinal fluid

Ct Threshold cycle

D

d Cohen's D

dCA1 Dorsal *cornu ammonis* 1

dCA3 Dorsal *cornu ammonis* 3

dcLN Deep cervical lymph nodes

DCs Dendritic cells

dDG Dorsal dentate gyrus

DDS Distal dendritic segment

DG Dentate gyrus

DH Dorsal hippocampus

DNA Deoxyribonucleic acid

E

EC Entorhinal cortex

ELISA Enzyme-linked immunosorbent assay

EM Effector memory

EMUM School of Medicine, University of Minho

F

FST Forced swim test

G

G Relative centrifugal force

GA Genetic algorithm

gcl Granule cell layer

GFP Green fluorescent protein

GR Glucocorticoid receptor

H

HPA Hypothalamic-pituitary-adrenal

I

IBD Inflammatory bowel disease

IC^{high} High inflammation cluster

IC^{low} Low inflammation cluster

ICVS Life and Health Sciences Research Institute

Ido *Indoleamine 2,3-dioxygenase* gene expression

IFN Interferon

Ifnγ *Interferon γ* gene expression

IL Interleukin

IL-10R Interleukin-10 receptor

ingLN Inguinal lymph nodes

Inos *Inducible nitric oxide synthase* gene expression

IQR Interquartile range

ISF Interstitial fluid

Its2 *Fungal internal transcribed spacer 2* gene expression

J

JAK Janus kinase

K

KO Knockout

L

LPS Lipopolysaccharide

LTD Long-term depression

LTP Long-term potentiation

M

MBP Myelin basic protein

MDF Metestrus and diestrus females

MHC Major histocompatibility complex

ml Molecular layer

Mpigr *Mouse polymeric immunoglobulin receptor* gene expression

MWMT Morris water maze test

N

NK Natural killer

NORT Novel object recognition test

NS Non-statistical significance

NSCs Neural stem cells

O

OFT Open-field test

ORBEA Órgão Responsável pelo Bem-Estar Animal

OVA Ovalbumin

P

pcl Pyramidal cell layer

PCR Polymerase chain reaction

PDS Proximal dendritic segment

PEF Proestrus and estrus females

PFA Paraformaldehyde

PFC Prefrontal cortex

PI3K Phosphatidylinositol-4,5--bisphosphate-3-kinase

pl Polymorph layer

PP Perforant path

Q

qRT-PCR Quantitative real-time polymerase chain reaction

R

r Pearson's correlation coefficients

RNA Ribonucleic acid

ROC Receiver-operating characteristic

ROUT Robust regression and outlier removal

r_u Rosenthal's R

S

SCID Severe combined immune deficiency

SEM Standard error of the mean

SGZ Subgranular zone

so *Stratum oriens*

sr *Stratum radiatum*

STAT Signal transducer and activator of transcription

SVM Support vector machine

T

TAP Temporoammonic path

TGF transforming growth factor

TNF Tumor necrosis factor

Tnf *Tumor necrosis factor* gene expression

TST Tail suspension test

U

US Unconditional stimulus

V

vCA1 Ventral *cornu ammonis* 1

vCA3 Ventral *cornu ammonis* 3

vDG Ventral dentate gyrus

VH Ventral hippocampus

W

W Kendall's Coefficient of Concordance

WT Wild-type

Y

YMT Y-maze test

Ywhaz *14-3-3 ζ protein* gene expression

#

16s *16s* gene expression

α

η^2 Eta Squared

η_p^2 Partial Eta Squared

ρ Spearman's rank correlation coefficient

ϕ_c Cramér's V

LIST OF FIGURES

LIST OF TABLES

CHAPTER 1

INTRODUCTION

1.1 What is the cognitive function?

Attempts to understand the cognitive functioning of the human mind and its processes date back at least to Classical Antiquity, when Ancient Greek philosophers, such as Plato and his student Aristotle, tried to explain the nature of knowledge and the act of thinking. At that period, the roots of the current term cognition began to develop from the Latin verb *cognoscere* which means to know or to recognize. The term cognition then derived to cognitive function (Benjafield, Kingstone and Smilek, 2010) and was defined as the internal mental processes that underlie the way humans perceive, remember, speak, think, make decisions, and solve problems (Fisher, Chacon and Chaffee, 2019). Cognitive function is thus critical for daily life activities, as it is necessary to refine all the information that humans receive about the world around them and to interact safely with it (Michalos, 2014).

1.1.1 Learning and memory as a major domain of cognitive function

Contributions of several fields, including biology, informatics, linguistics, neurosciences, philosophy, and psychology, made it possible to describe cognitive function as a non-unitary concept. Cognition is rather considered to be a set of all mental abilities related to knowledge, which are organized into distinct cognitive domains that operate synergistically in the regulation of animal behaviors and actions (Benjafield, Kingstone and Smilek, 2010). Cognitive domains have been categorized by different authors (Mesulam, 2000; Lezak *et al.*, 2004), however, a complete consensus has not yet been reached. Despite this, six main cognitive domains are reported reasonably in humans (**Figure 1**): complex attention, language, executive function, social cognition, perceptual-motor function, and learning and memory (Sachdev *et al.*, 2014). Within each cognitive domain, there are a series of specific subdomains which provide a whole spectrum of elements necessary for mental abilities related to knowledge (Mesulam, 2000; Harvey, 2019). The separation of cognitive domains was initially supported by brain injury studies that connected brain structures to the impairment of specific cognitive processes (Babcock, 1930). Even so, the cognitive domains are not independent of each other as they can operate synergistically in nature. For instance, elements of executive function have been reported to influence and exert control over the most basic cognitive processes related to social and perceptual activities (Al-Aidroos, Said and Turk-Browne, 2012; Harvey, 2019).

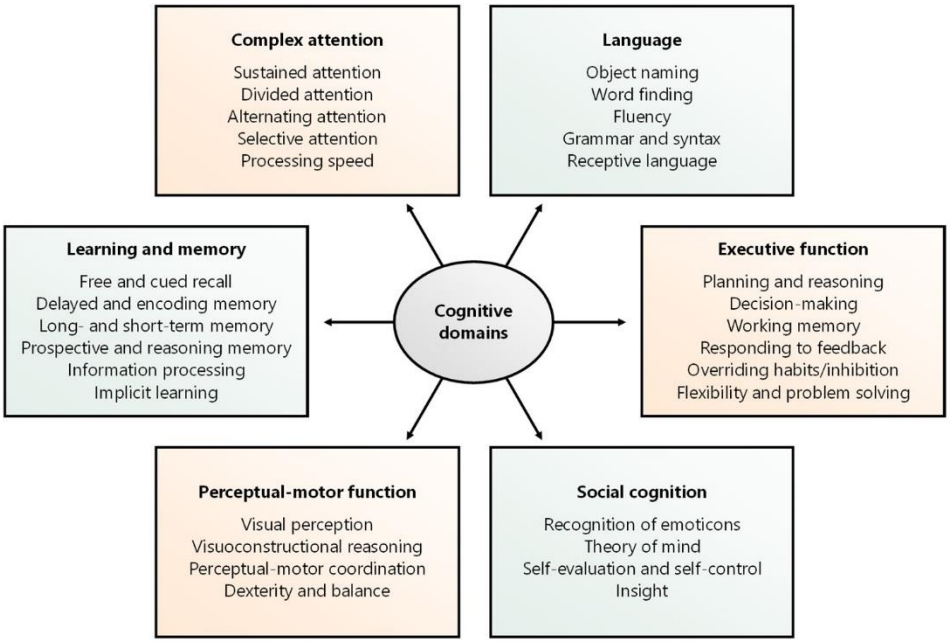

Figure 1. Domains of cognitive function. Mental abilities related to knowledge can be organized into six distinct cognitive domains: complex attention, language, executive function, social cognition, perceptual-motor function, and learning and memory. Within each cognitive domain, a list of the main specific subdomains is depicted. Adapted (Sachdev *et al.*, 2014).

Complex attention is a multifaceted cognitive domain that encompasses several subdomains accountable for attention skills: (1) selective attention – the process of focusing on relevant and important information and disregarding irrelevant ones; (2) divided attention – the ability to perform two tasks at once; (3) alternating attention – the process to successfully shift between tasks; and (4) sustained attention – the ability to maintain attention over time (Posner, 2011; Petersen and Posner, 2012). Processing speed is also a subdomain of complex attention and refers to the time needed to perform a mental task (Salthouse, 1996). Complex attention is frequently impaired in several conditions including major depressive disorder, schizophrenia, Alzheimer's disease, and other degenerative brain disorders (Diamond *et al.*, 2008; Knowles, David and Reichenberg, 2010; Haworth *et al.*, 2016).

Language is a cognitive domain that includes the mental abilities vital to effectively understand and formulate language. In humans, language skills are assessed by measures of fluency, object naming, and response to instructions (Lezak *et al.*, 2004; Harvey, 2019). Aphasia, which is characterized by the loss or impairment of language skills, is commonly associated with conditions involving stroke, brain damage, or degenerative brain disorders (Fonseca, Ferreira and Pavão-Martins, 2017). Growing evidence suggests that ultrasonic vocalizations, used by rodents to communicate and transmit their emotional state, are also connected to the cognitive domain of language (Fischer and Hammerschmidt, 2011; Portfors and Perkel, 2014; Simola, 2015).

Executive function refers to a family of mental skills that underpin goal-directed behavior and manifest

control over other cognitive processes in the orchestration of complex tasks. There is a general agreement that there are three core executive function subdomains: (1) working memory – the process of holding and manipulating information in the mind; (2) overriding habits/inhibition – the ability to cancel internal predispositions and to do what is most appropriate in each situation; and (3) flexibility – the capacity to constantly adapt behaviors in response to changes in the environment. From these, high-order executive functions, such as reasoning, problem solving, and planning, are assembled. Damage to the executive function system generally results in a manifestation of impulsivity, inefficient cognitive processing, and organizational deficits (Diamond, 2013; Sira and Mateer, 2014; Harvey, 2019).

Social cognition is defined as the ability to perceive, recognize, manipulate, and behave concerning socially relevant information (Adolphs, 2001). This domain includes abilities that allow the recognition of social cues, reading of facial expressions, manifestation of empathy, motivation, behavior change in response to social feedback, and development of insight (Sachdev *et al.*, 2014; Beaudoin and Beauchamp, 2020). The existence of socially inappropriate behaviors is being reported as a prominent feature of some brain pathologies, such as frontotemporal neurocognitive disorder (Sachdev *et al.*, 2014).

Perceptual-motor function is the capacity to interact with the environment by combining the use of the senses with motor skills. Through perception skills, meaningful auditory, gustatory, olfactory, tactile, and visual sensory information is gathered and used by motor skills to coordinate body movements and convey behavioral responses (Rosenbaum, Carlson and Gilmore, 2001; Harvey, 2019). Motor skills are generally divided into two classes: fine skills, which are involved in tasks that require a high degree of control and dexterity, and gross skills, which guarantee balance, coordination, reaction time, and physical strength (Gonzalez, Alvarez and Nelson, 2019). Several conditions, including agnosia, autism spectrum disorder, and Down syndrome, are characterized by impaired perceptual or motor skills (Virji-Babul *et al.*, 2006; Linkenauger *et al.*, 2012; Harvey, 2019).

Learning and memory are considered to be the source of knowledge (Huemer, 1999). This cognitive domain is responsible for collecting and maintaining information from past experiences with the purpose of using them later to influence future actions. Processes of learning and memory involve three stages: (1) encoding – the registration and acquisition of information; (2) storage – the preservation of information over time; and (3) retrieval – the process whereby stored information is brought back into conscious awareness or otherwise affects ongoing behavior unconsciously (Roediger and Karpicke, 2005). Memory can take different forms, thus distinct types of memory are consistently considered (**Figure 2**): sensory memory, short-term memory, and long-term memory (Camina and Güell, 2017).

Sensory memory is the ability to briefly retain large amounts of sensory information immediately

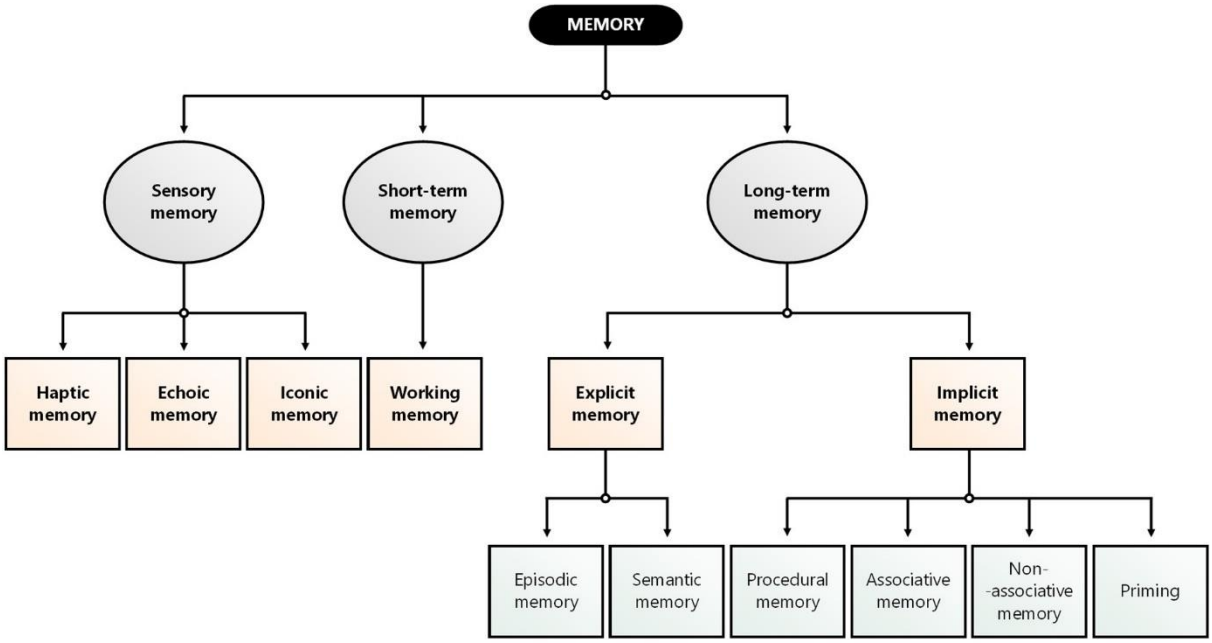

Figure 2. Classification of memory types. Memory processes can be divided into three distinct categories: sensory memory, short-term memory, and long-term memory. Within each memory type, a list of the main specific subdomains is depicted. The subdomain of working memory also falls under the cognitive domain of executive function. Adapted (Camina and Güell, 2017).

following its presentation. It provides a detailed, non-manipulated representation of the entire sensory experience, however, only lasts milliseconds and is mostly outside conscious awareness. Usually, in less than a second, relevant sensory information is quickly transferred to short-term memory (Brewin, 2014). It is assumed that there is a sensory memory subdomain for each of the five senses (hearing, taste, touch, sight, and smell), still, only three of these domains have been extensively studied: (1) haptic memory – retains data acquired through touch; (2) echoic memory – retains information that is gathered through sight; and (3) iconic memory – retains information gathered through auditory stimuli (Camina and Güell, 2017).

Short-term memory is the ability to keep a small amount of information in an active, readily available state for a short period (Camina and Güell, 2017). The modal model of Atkinson and Shiffrin contextualizes short-term memory as a step between sensory memory and long-term memory. According to them, a storage unit in short-term memory with limited capacity receives sensory information that decays rapidly. Through rehearsal, this information could be transferred to long-term memory for permanent storage (Atkinson and Shiffrin, 1968). Baddeley and Hitch later proposed that a multicomponent working memory should be considered, rather than a single storage unit in short-term memory (Baddeley and Hitch, 1974). By definition, whereas short-term memory can only hold information, working memory has components that allow the retention and processing of information necessary for complex cognitive tasks. For this reason, working memory is categorized as a subdomain that falls under both the cognitive domains of executive function and learning and memory (Diamond,

2013). The current model of Baddeley proposes the existence of four integral components of working memory: (1) central executive – responsible for attention control and cognitive processing; (2) phonological loop – ensures retention of verbal information; (3) visuospatial sketchpad – accountable for storing visual and spatial information; and (4) episodic buffer – capable of integrating information from different sources temporarily (Baddeley, 2000; Grigorenko, Mambrino and Preiss, 2012; Camina and Güell, 2017).

Long-term memory refers to theoretically unlimited storage of information to be maintained for long periods, even for a lifetime. Long-term memory can be broken down into explicit/declarative memory and implicit/non-declarative memory. Explicit memory refers to information that can be consciously evoked and is further divided into episodic memory – responsible for storing unique personal experiences, including information about the time and location of events (also known as reference memory) – and semantic memory – accountable for storing information about meanings, interpretations and concepts related to general facts (Kolb and Whishaw, 2003; Dickerson and Eichenbaum, 2010; Brem, Ran and Pascual-leone, 2013). In contrast, implicit memory comprises all unconscious memories. Within implicit memory, four subdomain emerge: (1) procedural memory – participates in the recalling of motor and executive skills that are necessary to perform a task; (2) associative memory – refers to the storage and retrieval of information resulting from an association with other sets of information, as is the case of Pavlovian conditioning; (3) non-associative memory – denotes newly learned behaviors due to repeated exposure to a single stimulus; and (4) priming – an effect whereby exposure to a certain stimulus influences the response to a subsequent one (Kolb and Whishaw, 2003; Camina and Güell, 2017).

Memory impairments are a widespread symptom in a variety of conditions. Virtually any neurological, neurodegenerative, toxic, or traumatic damage to brain structures involved in memory, may lead to memory impairments (Kolb and Whishaw, 2003). In addition to Alzheimer's disease, which is accounts for two-thirds of dementia syndromes in people over 65 years old (Arlt, 2013), memory impairments are described in a range of pathologies, from Parkinson's disease (Goldman *et al.*, 2012), Huntington's disease (Stout *et al.*, 2011), and epilepsy (Dupont *et al.*, 2001), to major depressive disorder (Pantzar *et al.*, 2014), post-traumatic stress disorder (Jonathan *et al.*, 2011), and schizophrenia (Schaefer *et al.*, 2013). Memory function may also be transiently influenced by hormonal alterations during pregnancy (Wilson *et al.*, 2011) and menopause (Kocoska-Maras *et al.*, 2013) and compromised by traumatic brain injury (Stulemeijer *et al.*, 2010), stroke (Al-Qazzaz *et al.*, 2014) or toxic events related to alcohol (Kapaki *et al.*, 2005) or drug use (Chavant *et al.*, 2011). Additionally, with age comes the increased likelihood of developing memory loss. It is estimated that about 40% of people over 65 years old have age-related memory impairments (Small, 2002).

1.1.2 Brain atlas of learning and memory: focus on the hippocampus

Memories are not stored in just one part of the brain. A great deal of neural specialization occurs, such that various brain regions are responsible for handling different aspects of information (**Figure 3**).

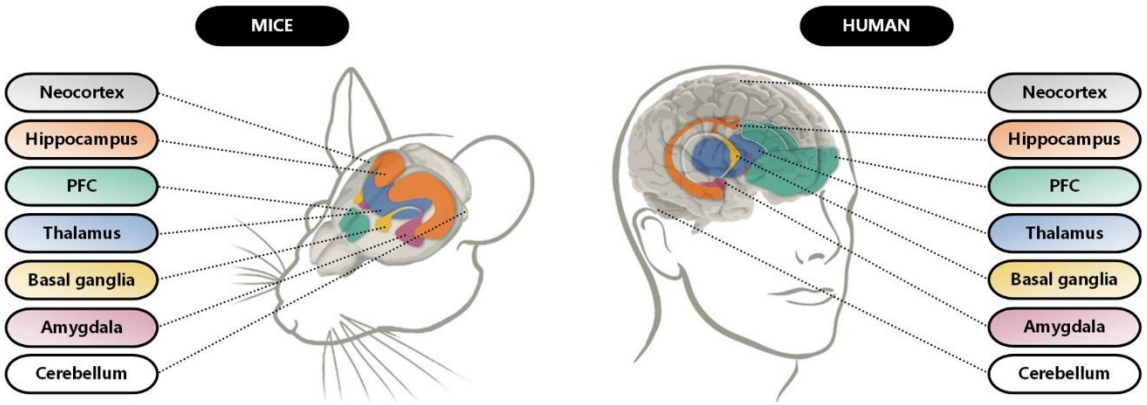

Figure 3. Brain regions associated with memory. The main brain regions involved in memory function are greatly conserved between rodents and humans. PFC – prefrontal cortex. Adapted (Flores *et al.*, 2018).

Working memory, for instance, depends heavily on the prefrontal cortex (PFC) and the thalamus. The function of PFC in working memory is to maintain information in a highly active, easily accessible state (Kane and Engle, 2002). Patients with damage PFC often display problem solving and planning deficits, and monkeys who receive PFC injuries have impaired working memory (Curtis and D'Esposito, 2003; Gazzaniga *et al.*, 2013). The PFC shares dense reciprocal connectivity with the thalamus, which in turn supports PFC activity during working memory maintenance (Nadeau, 2008; Bolkan *et al.*, 2017). Implicit memories rely on the basal ganglia and the cerebellum, which play a central role in how motor actions are learned, remembered, and coordinated (Packard and Knowlton, 2002; Gazzaniga *et al.*, 2013). There are at least three other important areas of the brain that are involved in explicit memories: the neocortex, the amygdala, and the hippocampus. The neocortex is the largest part of the brain cortex and is involved in memory consolidation. Over time, information initially processed in the hippocampus can be transferred to the neocortex as general knowledge (Wiltgen *et al.*, 2004). The amygdala, in contrast, is crucially involved in regulating memories of emotionally charged events. Findings indicate that acute stress exposure influences amygdala-dependent memory consolidation processes (Roozendaal, McEwen and Chattarji, 2009; Sah, Sun and Gooch, 2020). Lastly, the hippocampus is where episodic memories are formed and retrieved for later use. Damage to the hippocampus usually results in an inability to form new episodic memories (Craver, 2003; Camina and Güell, 2017).

Both in humans and rodents, the hippocampal formation comprises the dentate gyrus (DG), the *cornu ammonis* (CA), and the adjacent parahippocampal cortices (Lopez-Rojas and Kreutz, 2016). It is organized in a laminar fashion and its connectivity is mostly unidirectional, which configures the classical hippocampal trisynaptic circuit model of information processing (Andersen, Bliss and Skrede, 1971). In this loop circuitry, inflow signals from the entorhinal cortex (EC) are propagated by excitatory synapses to the CA and DG and then redirected back into the EC (**Figure 4**). The major excitatory input to the hippocampus arises from the EC layer 2 that terminate in the DG and CA3 (perforant path; PP) and from EC layer 3 that cease in the CA1 (temporoammonic path; TAP). Within the DG, granule cells project their axons, the mossy fibers, to the CA3, where pyramidal neurons are interconnected via recurrent connections. These pyramidal neurons will convey signal input towards the CA1, through Shaffer collaterals. To close the loop, CA1 pyramidal neurons send their axons to the subiculum or directly to deep layers of the EC (Neves, Cooke and Bliss, 2008; Deng, Aimone and Gage, 2010).

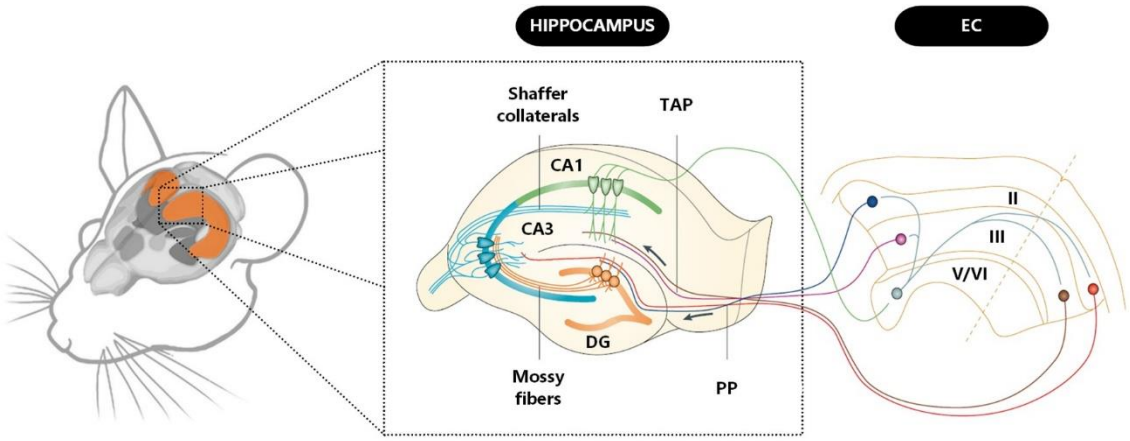

Figure 4. The classic hippocampal trisynaptic circuit. The basic functional unit of the hippocampus corresponds to the classical trisynaptic circuit. The signal follows an EC → DG → CA3 → CA1 sequence, to be then conveyed to the subiculum or directly to the EC. The hippocampus is also home to a rich diversity of interneurons, which send projections, namely to the granule cells of the DG (not shown in the figure). CA - *cornus ammonis*; DG – dentate gyrus; EC – entorhinal cortex; PP – perforant path; TAP – temporoammonic path. Adapted (Neves, Cooke and Bliss, 2008; Deng, Aimone and Gage, 2010).

The description given above of the classic hippocampal trisynaptic circuit is, however, narrow in light of recent knowledge. Currently, the classic circuit is considered far more complex, involving many recurrent collaterals and interneurons that modulate hippocampal activity (Witter, 1993; McBain and Fisahn, 2001). Additionally, the hippocampus is now considered one of the most connected areas of the brain, allowing it to receive and process information from and to multiple brain regions important in different cognitive abilities (Femenía *et al.*, 2012; Small *et al.*, 2012). Although the classic circuit is replicated along the entire dorsal-ventral axis of the hippocampus, the dorsal and ventral hippocampal

subregions establish additional different connections with other brain areas. The ventral hippocampus (VH) connects with the amygdala, the bed nucleus of the stria terminalis, and the dorsal and ventral striatum (Felix-Ortiz and Tye, 2014; Lebow and Chen, 2016). Additionally, it also establishes connections with the PFC and other brain structures associated with the hypothalamic-pituitary-adrenal (HPA) axis (**Figure 5**), namely the hypothalamus (Sweeney and Yang, 2015; Liu and Carter, 2018). In contrast, the dorsal hippocampus (DH) establishes important connections with the retrosplenial and anterior cingulate cortices, the septal and mammillary nuclei, the dorsal striatum, and the thalamus (Wyss and Groen, 1992; Atallah, Rudy and O'Reilly, 2008; Aggleton *et al.*, 2010; Wang, John and Barbas, 2021).

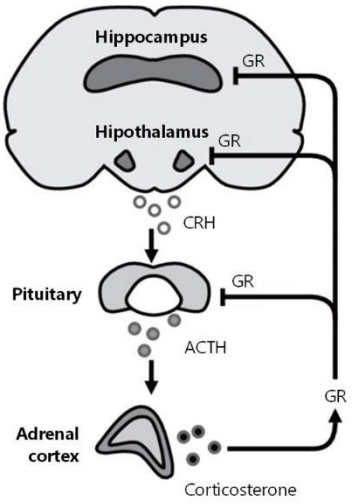

Figure 5. The hypothalamic-pituitary-adrenal axis. This axis is controlled by the hypothalamic and higher brain centers, such as the hippocampus. When activated by stress and other factors, CRH from the paraventricular hypothalamic area stimulates the release of ACTH from the anterior pituitary, which in turn triggers the release of glucocorticoids (corticosterone in rodents) from the adrenal cortex. The secreted glucocorticoids exert widespread effects on body functions, including cellular metabolism and immune functions, and via their GR, are responsible for the termination of the axis activation through a negative feedback loop applied on the central axis components. ACTH – adrenocorticotropin hormone; CRH – corticotropin-releasing hormone; GR – glucocorticoid receptor. Adapted (Kitraki *et al.*, 2016).

Considering the distinct connections that the dorsal and ventral hippocampal subregions establish with other brain areas, a functional specialization of the hippocampal dorsal-ventral axis emerges. While the VH integrates brain circuits responsible for anxiety and fear, reward-seeking behavior, stress response, affective states, neuroendocrine functions, and social behaviors with a strong emotional component, the DH has been shown to participate mainly in exploration, spatial orientation, and navigation tasks (Saper, Scammell and Lu, 2005; Dong and Swanson, 2006; Nollet *et al.*, 2011; Mahan and Ressler, 2012; Hartley *et al.*, 2014; Strange *et al.*, 2014). The importance of the DH in spatial orientation and navigation, specifically, was evidenced by studies of brain injury in animal models. Using

the Morris water maze test (MWMT) – a paradigm classically used to assess spatial memory of rodents (Morris, 1984) – Moser and colleagues showed that lesions in the DH of rats produced spatial memory deficits (Moser *et al.*, 1995). In the same line of experiments, it was also demonstrated that lesions in the VH did not interfere with spatial memory (Bannerman *et al.*, 2002).

The DH is known to harbor a great density of place cells which are vital for spatial memory encoding. Place cells allow the mental construction of allocentric space representations – "independent from the point of view" – by firing specifically when an animal is at a given location of a certain environment. Each environment is defined by a unique firing pattern of active place cells. The same place cells participate in allocentric space representations of different environments, however, the firing pattern between them is different from one environment to the next (O'Keefe, Dostrovsky and J. O'Keefe, 1971; Moser, Kropff and Moser, 2008). On the subject of allocentric spatial representations, it becomes also important to mention grid cells and head direction cells. Grid cells reside with a higher density on the EC dorsal subregion and exhibit spatially modulated firing patterns, much like the hippocampal place cells (Hafting *et al.*, 2005). Head direction cells encode the directional heading of an animal concerning its environment by firing specifically when the head of an animal point in a specific direction (Taube, 2007).

Postnatal hippocampal neurogenesis has also been proposed as a novel mechanism that may mediate hippocampal-dependent spatial memory (Suk-yu, Ang and Kwok-Fai, 2015). Interestingly, the subgranular zone (SGZ) of the hippocampal DG is considered one of the two consensual cytogenic niches where neural stem cells (NSCs) persist in the postnatal brain under normal physiological conditions – the second one is the subventricular zone lining the brain lateral ventricles (Kempermann, Song and Gage, 2015). Within the postnatal SGZ, NSCs can generate two distinct cell lineages: neuronal – giving rise to new glutamatergic neurons (neurogenesis) that establish synapses within the pre-existing circuits in the DG – and astroglial – giving rise to new astrocytes (astrogliogenesis) in the postnatal hippocampus (Bonzano *et al.*, 2018). Studies have shown that ablation of hippocampal neurogenesis by x-ray in rats led to impaired memory function (Alam *et al.*, 2018), and the genetically driven expansion of NSCs in the hippocampus rescued the age-related decline of spatial memory in old mice (Berdugo-Vega *et al.*, 2020).

It is suggested that the mechanisms of structural plasticity in the hippocampus also contribute to spatial memory. In fact, decreased hippocampal volume has been linked to cognitive impairments. Several studies found that the hippocampal volume of patients with Alzheimer's disease and other varieties of dementia was reduced when compared to healthy controls (Petten, 2004; Vijayakumar and Vijayakumar, 2012). In healthy young males, the hippocampal volume was also reported to be positively correlated with their cognitive abilities, namely with declarative memory (Pohlack *et al.*, 2014). In animal

studies, it was revealed that transgenic mice expressing human apolipoprotein E4, which has been implicated as a potential genetic risk factor for dementia (Chia-Chen *et al.*, 2013), in the brain presented spatial memory deficits in the MWMT when compared to the wild-type (WT) counterpart. Interestingly, these cognitive impairments were associated with hippocampal volume loss and increased levels of pro-inflammatory markers in the hippocampus (Yin *et al.*, 2011).

Alterations of the dendritic arborization of hippocampal neurons have also been reported as a structural plasticity mechanism involved in hippocampal-dependent memory. For instance, female and male rats trained in hippocampal-dependent tasks such as MWMT displayed an increased dendritic arborization of CA1 and CA3 neurons in the DH when compared to non-trained naïve rats (Espino, Gómez and Durán, 2020). In the DG of male rats, it was also described that spatial learning increased the complexity of the dendritic arborization of adult newborn neurons (Tronel *et al.*, 2010). Additionally, decreased dendritic arborization of CA1 hippocampal neurons occurs in patients with autism spectrum disorder and altered dendritic arborization of CA3 hippocampal neurons is present in patients with schizophrenia (Kolomeets, Orlovskaya and Uranova, 2007; Kulkarni and Firestein, 2012).

The complex mechanisms underlying the encoding, storage, and retention of spatial memories in the hippocampus are also assumed to involve synaptic plasticity (Frankfurt and Luine, 2015). Synaptic plasticity covers both structural changes, including dendritic spine dynamics, and the resulting physiological processes: long-term potentiation (LTP) and long-term depression (LTD) – considered the foundations of learning and memory (Bear and Malenka, 1994; Yang, Lu and Zuo, 2018). Dendritic spines are small protrusions in neuronal dendrites where more than 90% of excitatory synapses in the central nervous system (CNS) occur (Kirov, Sorra and Harris, 1999). A strong relationship between dendritic spine density in the hippocampus and learning and memory has been demonstrated using different behavioral assessments. It was shown that a better behavioral performance of rats in the MWMT is associated with a higher dendritic spine density in the pyramidal cells of CA1 (Moser, Trommald and Andersen, 1994; Conrad *et al.*, 2012; Eilam-Stock *et al.*, 2012). In the hippocampus, it has also been demonstrated that increased dendritic spine density is associated with LTP, and decreased dendritic spine density is related to LTD (Matsuzaki *et al.*, 2004; Bosch and Hayashi, 2012; Frankfurt and Luine, 2015).

1.2 Modulators of cognitive function

Cognitive function was originally thought to be exclusively regulated by endogenous CNS processes, with neurogenesis and hippocampal plasticity processes contributing to the encoding, storage,

and retention of memories (Frankfurt and Luine, 2015; Suk-yu, Ang and Kwok-Fai, 2015). Increasingly, it is becoming clear that other organ systems and processes including the cellular and molecular components of the immune system (Marin and Kipnis, 2013), the resident bacteria of the gastrointestinal tract – the gut microbiome – and the metabolites they produce (Gareau, 2016), the HPA axis (Jameison and Dinan, 2001), and the sex hormones, such as progesterone and estrogen (Ali, Begum and Reza, 2018), may affect the CNS and modulate cognitive function.

1.2.1 How is the central nervous system protected from threats?

The CNS is universally perceived as the command center of the body by monitoring internal organ function, coordinating behavioral performance, including cognition, and responding to environmental changes (Gazzaniga *et al.*, 2013). Anatomically, the CNS is protected from endogenous and exogenous threats by the cerebrospinal fluid (CSF) and the meninges (**Figure 6**).

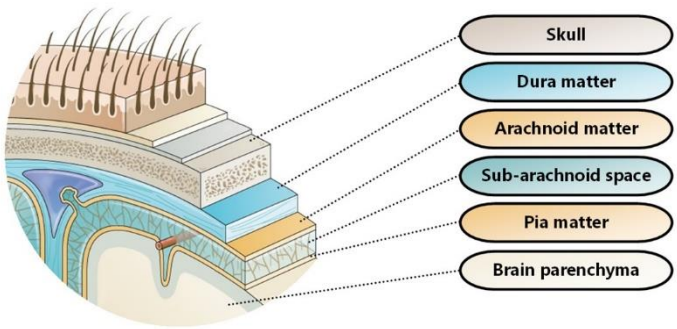

Figure 6. The architecture of the brain meninges. The meninges are composed of three membranes: the dura mater attached to the skull, the arachnoid mater, and the pia mater interacting in the brain parenchyma. Adapted (Parker *et al.*, 2019).

The meninges are composed of the pia matter that intimately covers the brain parenchyma, a non-vascularized arachnoid matter, and a heavily vascularized dura matter, that is attached to the skull. Between the arachnoid and the pia matter lies the sub-arachnoid space that contains the CSF (Strominger, Demarest and Laemle, 2012). The CNS is additionally protected from the entry of potentially damaging neurotoxins and other factors within the blood by an endothelial blood-brain barrier (BBB) and a blood-CSF barrier (BCSFB), jointly maintained by tight junctions that prevent unregulated leakage (Daneman and Prat, 2015; Johanson and Johanson, 2018).

For decades, the CNS has been seen as an immune-privileged system, because of its limited interactions with the immune system, especially under homeostatic, healthy conditions. Several

characteristics of the CNS, in addition to the presence of the BBB and the BCSFB, were thought to limit the capacity for an immune response in the brain, as reviewed elsewhere (Louveau, Harris and Kipnis, 2015).

The absence of classical lymphatic drainage in the CNS was an initial claim suggesting the immune-privilege of the brain (Louveau, Harris and Kipnis, 2015). This was, however, disputed by experiments showing that tracers injected into the CSF and the brain interstitial fluid (ISF) found their way to deep cervical lymph nodes (dcLN) in the vicinity of the brain (Kida, Pantazis and Weller, 1993). These results were also confirmed using cells: green fluorescent protein (GFP)-expressing cluster of differentiation (CD)4^+ T cells injected into the EC and the ventricles and GFP-expressing monocytes injected into the EC were able to migrate from the lesion site and drain primarily in the dcLN (Goldmann *et al.*, 2006; Kaminski *et al.*, 2012). Afferent to the dcLN, several mechanisms have been proposed to explain the clearance of waste products and leukocytes from the CNS. The BBB, the BCSFB, and the pia mater – which is the largest interface between brain ISF and CSF – are not absolute barriers, and permeability to small molecules is dependent on concentration gradients, size, and solubility. For larger molecules, simple diffusion is not efficient, therefore, the clearance of several compounds is dependent on specific active transporter mechanisms (Deane *et al.*, 2003; Zlokovic, 2012; Zhao *et al.*, 2015; Papadopoulos, Herz and Kipnis, 2020). Removal of cellular debris and toxic molecules in the brain is also mediated by phagocytosis and digestion by the microglia (Janda, Boi and Carta, 2018). Additionally, the brain has adapted to use a unique paravascular route in which fluids may freely exchange between the ISF and the CSF along with the glymphatic system (Iliff *et al.*, 2012; Bacyinski *et al.*, 2017). Downstream of the glymphatic system, water, and small molecules drain from the CSF into the bloodstream through arachnoid granulations, however, macromolecules and leukocytes are unlikely to be transferred through this route (Louveau, Harris and Kipnis, 2015). Surprisingly, recent findings reproduced the XVIII century postulates of the Italian anatomist Paolo Mascagni, in which the existence of meningeal lymphatic vessels was described (Bucchieri *et al.*, 2015). A novel route for the drainage of macromolecules and leukocytes within the CNS was, thus, established from the lymphatic vessels in the meninges, specifically in the dura mater, to the dcLN (Aspelund *et al.*, 2015; Louveau *et al.*, 2015). A recent study revealed that the rupture of the meningeal lymphatic vessels in mice was able to impair the glymphatic system and lead to cognitive deficits, which demonstrated the essential role of meningeal lymphatic vessels in maintaining brain homeostasis (Da Mesquita *et al.*, 2018).

Two other initial claims that were suggested to consider the CNS an immune-privileged site were the lack of antigen-presenting cells (APCs) and the low major histocompatibility complex (MHC) class II expression in the brain (Louveau, Harris and Kipnis, 2015). Actually, the brain parenchyma is only

recurrently surveyed by its resident leukocyte, the microglia. Microglia form a self-renewing highly specialized cell population of innate sentinels in the brain (Huang *et al.*, 2018). Microglia have been reported to express MHC class II in inflammatory conditions, and thus function as APCs (Schetters *et al.*, 2018). Because microglia do not appear capable of migrating from the brain parenchyma to the vascular system, their role in the induction of an adaptive immune response is constrained to the antigen presentation to brain infiltrating leukocytes (Herz, Johnson and McGavern, 2015). Besides microglia, the brain parenchyma seems to differ from other tissues as it is devoid of APCs during normal conditions. However, following closer examination, significant populations of dendritic cells (DCs) are present among the leukocytes found in the meninges and in the choroid plexus – the organ that secretes CSF from the selective filtration of blood plasma (Hart and Fabre, 1981). In these locations, DCs are in an ideal position to access CSF and inspect material crossing the brain barriers, thus ensuring the detection of a variety of insults to the brain (Fischer, Bonifas and Reichmann, 2000; Kostulas *et al.*, 2002; Walsh *et al.*, 2014). Once activated, DCs function as potent APCs, by traveling to the dcLN (Karman *et al.*, 2004).

Like DCs, a diverse repertoire of innate and adaptive leukocytes have been described within CNS borders, including in the meninges. Additionally, the continuous influx of leukocytes into the CNS has also been demonstrated (Hickey, 2001). For instance, it is estimated that in the CSF of healthy individuals alone, there are about 3,000 leukocytes per ml, 80% of which phenotypically characterized as central memory (CM) $CD4^+$ T cells (Engelhardt and Ransohoff, 2005). Several routes of leukocyte entry into the CNS have now been characterized (Ransohoff, Kivisäkk and Kidd, 2003). Under normal physiological conditions, the first route of leukocyte migration into the CNS follows the formation of the CSF. In this route, leukocytes may extravasate across the fenestrated endothelium of the choroid plexus (Carrithers *et al.*, 2002). In a second route, leukocytes may also extravasate across the capillaries at the pia matter surface into the subarachnoid space, where they can interact with APCs (Hickey, 1999). In another route, leukocytes can enter the CNS directly from the bloodstream, by crossing the BBB, although the efficiency of this event is considered quite low (Ransohoff, Kivisäkk and Kidd, 2003). These routes reveal that leukocytes can pass through the CNS, providing it with immunological surveillance (Hickey, 2001) and demonstrating that the interaction between the immune system and the CNS is far more complex than was assumed.

1.2.2 The interaction between leukocytes and cognitive function

Currently, the notion that the CNS enjoys immune privileges is still accepted, but it is clear that

the immune system and the CNS are interconnected by a wide variety of coordinated mechanisms that are not limited to pathology, but also extend to homeostatic functions (Louveau, Harris and Kipnis, 2015; Papadopoulos, Herz and Kipnis, 2020). Indeed, key roles for leukocytes are being reported in several healthy brain functions, including spatial learning and memory and adult hippocampal neurogenesis (Kipnis *et al.*, 2004; Ziv *et al.*, 2006; Brynskikh *et al.*, 2008).

Animal models lacking peripheral leukocytes have provided experimental evidence to support this theory. Both severe combined immune deficiency (SCID) mice – lacking functional B and T cells – and nude mice – deficient in mature T cells – present hippocampal-dependent spatial learning and memory impairment in several cognitive tests, when compared to the WT counterpart. Importantly, these cognitive deficits were reverted after immune system restoration, specifically with T cells (Kipnis *et al.*, 2004; Brynskikh *et al.*, 2008; Ron-Harel *et al.*, 2008). Interestingly, SCID mice with impaired hippocampal--dependent memory expressed lower levels of genes encoding proteins related to presynaptic activity in the hippocampus, which were restored to normal levels after immune system reestablishment (Ron-Harel *et al.*, 2008). In another experiment (**Figure 7**), WT mice were initially depleted of their adaptive immunity by irradiation and then injected with bone marrow cells from WT or SCID mice.

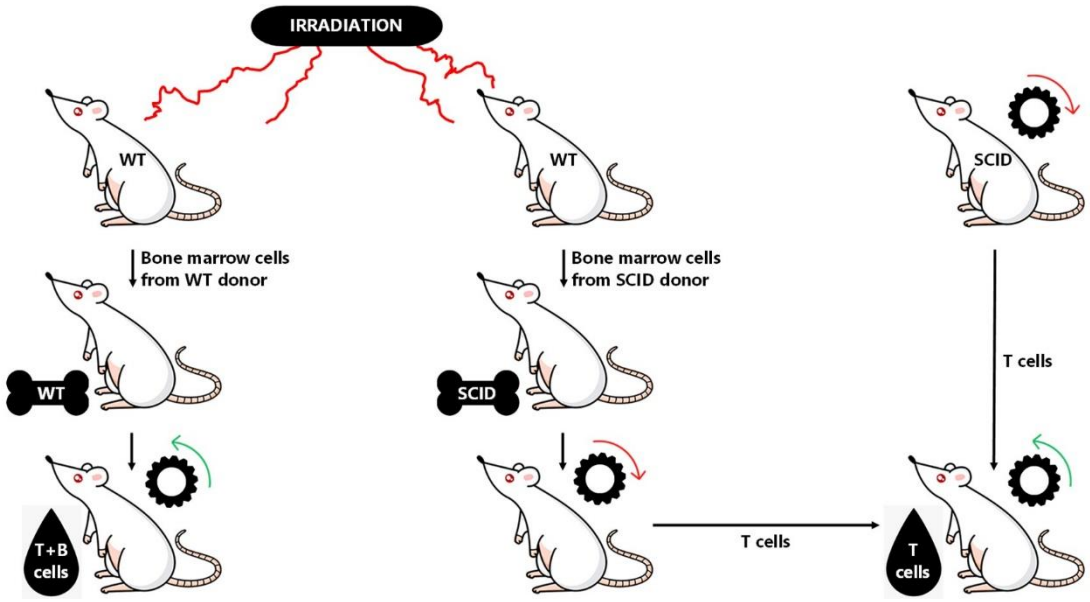

Figure 7. Immune system availability and cognitive function. Depletion of adaptive immunity from WT mice by irradiation, followed by injection of bone marrow cells from SCID mice impairs cognitive function, whereas replacement of bone marrow cells of WT mice does not. The cognitive decline observed in SCID mice and irradiated WT mice reloaded with SCID-derived bone marrow is reversible by the injection of T cells from WT donors. SCID – severe combined immune deficiency; WT – wild-type. Adapted (Kipnis *et al.*, 2008).

Irradiated WT mice replenished with autologous bone marrow exhibited a hippocampal-dependent

memory similar to naïve WT mice. In contrast, irradiated WT mice reloaded with SCID-derived bone marrow exhibited an impaired spatial learning, comparable to that of naïve SCID mice. Moreover, the cognitive function of WT mice reloaded with SCID-derived bone marrow was restored after transplantation of T cells obtained from naïve WT donors (Brynskikh *et al.*, 2008). Additionally, a study revealed that mice depleted from $CD4^+$ T cells presented impaired spatial learning and memory in the MWMT, along with a significant reduction in hippocampal neurogenesis (Wolf *et al.*, 2009). Acute suppression of T cells using the immunosuppressive drug fingolimod (FTY720), currently used in the treatment of multiple sclerosis, was also sufficient to cause cognitive deficits in adult WT mice (Derecki *et al.*, 2010). Following the animal models, also in humans, an association between leukocytes and cognitive function was already acknowledged. In a cohort of healthy aged individuals, lower numbers of effector memory (EM) $CD4^+$ T cells and higher numbers of naïve $CD8^+$ T cells and B cells in the blood were associated with a better cognitive function. Additionally, blood EM $CD4^+$ T cells were found to be predictors of executive function and memory, even when considering factors known to influence cognitive performance in aged individuals, such as age, gender, education, and mood (Serre-Miranda *et al.*, 2015).

Some authors argue that one of the mechanisms underlying the role of T cells in cognitive function may be hippocampal neurogenesis (Schwartz and Shechter, 2010). Schwartz and colleagues demonstrated that hippocampal neurogenesis induced by an enriched environment was associated with the recruitment of T cells to the hippocampus. The authors also showed that hippocampal neurogenesis was markedly impaired in SCID mice when compared to the WT counterpart. However, transferring WT splenocytes into SCID mice was able to partially revert those deficits in hippocampal neurogenesis. Interestingly, similar results were obtained using nude mice instead of SCID mice, thus ensuring that the impaired hippocampal neurogenesis observed was T cell-dependent. Additionally, to assess whether hippocampal neurogenesis was dependent on the presence of CNS-specific T cells, transgenic mice possessing mainly T cells receptors for myelin basic protein (MBP; a CNS-specific antigen) or ovalbumin (OVA; a non-CNS-specific antigen) were used. While mice with MBP-specific T cells presented higher hippocampal neurogenesis and improved spatial learning in the MWMT, when compared to the WT animals, mice with OVA-specific T cells showed impaired hippocampal neurogenesis and spatial learning (Ziv *et al.*, 2006). These findings imply that the CNS-specific T cells present pro-cognitive properties (Kipnis, Gadani and Derecki, 2012) and are required for hippocampal neurogenesis (Ziv *et al.*, 2006).

Despite this, other mechanisms that may explain the role of T cells in cognitive function have been described, including neurotransmission modulation. A study revealed that cognitive impairments in the MWMT induced by neurotransmitter dysfunctions can be overcome by T cell-based vaccination using

copolymer-1, a weak agonist of numerous self-reactive T cells (Kipnis *et al.*, 2004). In reality, neurotransmitters can be released from T cells, which may influence neurotransmission (Ogawa *et al.*, 2003; Pacheco *et al.*, 2006). Moreover, it is known that neurotransmitters, such as glutamate, dopamine, acetylcholine, and serotonin, interact directly with T cells, leading to the modulation of various functions, including cytokine secretion, as reviewed elsewhere (Franco *et al.*, 2007).

1.2.3 Cytokines as modulators of cognitive function

The effect of T cells on cognitive function might also be mediated via cytokines (Kipnis, Gadani and Derecki, 2012). Cytokines are a large and diverse family of extracellular polypeptides/glycoproteins of low molecular weight with cell-signaling properties that can be transiently induced and secreted by virtually all nucleated cells. Different types of cytokines had been discovered, including interleukins (IL), lymphokines, interferons (IFN), tumor necrosis factor (TNF), and chemokines. The downstream effect of a given cytokine occurs through a high-affinity bond to its receptor that is expressed on the surface of a target cell. This phenomenon can happen in an autocrine, paracrine, or endocrine way and lead to a series of effects including differentiation, proliferation, and activation of the target cell (Correa *et al.*, 2007; Ferreira *et al.*, 2019; Testar, 2019). Cytokines can respond to diverse types of insults including inflammation, infections, and traumas throughout the body. In the CNS, cytokines can interact directly with the brain, since they can cross BBB and BCSFB and are constitutively expressed by microglia, astrocytes and even neurons (Banks, Kastin and Broadwell, 1995; Galic, Riazi and Pittman, 2012).

Growing evidence has shown the determinant role of cytokines in cognitive function. A study revealed that after performing a cognitive evaluation, the meninges of MWMT-trained mice had an increased accumulation of IL-4-producing $CD4^+$ T cells than non-trained naïve mice. Moreover, the cognitive evaluation of IL-4 knockout (KO) mice revealed severe spatial memory deficits in the MWMT, combined with a pro-inflammatory meningeal phenotype (increased levels of TNF and IL-12) when compared to WT controls. In another experiment, WT mice were initially depleted of their immune system by irradiation and then injected with bone marrow cells from IL-4 KO mice. This also resulted in cognitive impairment and pro-inflammatory meningeal phenotype. Additionally, IL-4 KO mice injected with T cells from WT mice reversed cognitive impairment and attenuated the pro-inflammatory meningeal phenotype, when compared to non-injected IL-4 KO mice (Derecki *et al.*, 2010). These results support an indirect mode of T cell-mediated support of spatial learning and memory dependent on IL-4. However, the effects of IL-4 do not cease here, since this cytokine has been shown to induce astrocytic expression of

brain-derived neurotrophic factor (BDNF), which is known to play a critical role in the synaptic plasticity underlying the encoding, storage, and retention of certain forms of memory and hippocampal neurogenesis (Heldt *et al.*, 2007; Ron-Harel *et al.*, 2008; Derecki *et al.*, 2010). Curiously, it has been described that CNS-specific T cells and $CD4^+$ T cells were also able to increase BDNF expression in the brain parenchyma (Ziv *et al.*, 2006; Wolf *et al.*, 2009).

In another study that was carried out using IL-13 KO mice, the results of the behavioral characterization demonstrate that animals lacking IL-13 had impaired spatial learning and memory in the MWMT when compared to WT mice. Additionally, after the behavioral characterization, the meninges of MWMT-trained WT mice had an increased accumulation of $CD4^+$ T cells and higher levels of BDNF than non-trained WT mice. This was not the case for IL-13 KO mice, since the MWMT-training did not affect the number of $CD4^+$ T cells in the meninges nor the BDNF concentration (Brombacher *et al.*, 2017). Controversially, while IL-13 absence in mice showed a detrimental effect in cognitive function, in a cohort of healthy aged individuals, increased concentrations of IL-13, along with higher concentrations of IL-1β and IL-8, in the blood were associated with a worst cognitive function (Serre-Miranda *et al.*, 2020), which highlight the need to perform more in-depth studies to decipher the mechanisms by which immune modulators affect the functioning of the CNS. Additionally, in this study, IL-1β, IL-1-receptor antagonist, IL-6, IL-13, IFN-γ-induced protein-10, and TNF were found to be negatively associated with memory. Higher plasma concentrations of IL-1β also negatively predicted executive function, even when considering factors known to influence cognitive performance in aged individuals, such as age, gender, education, and mood (Serre-Miranda *et al.*, 2020). Specifically, the pro-inflammatory cytokine IL-1β has already been shown to have a detrimental effect on cognitive function. It has been widely described that IL-1β administration in rodents, both in the CNS and in the periphery, induces hippocampal-dependent memory deficits during the MWMT and impair hippocampal plasticity by suppressing LTP, as reviewed elsewhere (Huang and Sheng, 2010).

IL-6 is also being described as having a negative effect in cognitive function. In fact, increased plasma levels of IL-6 are inversely correlated with cognitive performance and hippocampal volume of patients with Alzheimer's disease and healthy controls (Lyra *et al.*, 2021). An animal study also revealed that young, but not old, IL-6 KO mice presented a better performance in the novel object recognition test (NORT) – a paradigm classically used to assess recognition memory of rodents (Bevins and Besheer, 2006) – than the aged-matched WT controls (Bialuk, Jakubów and Winnicka, 2019). Additionally, blockade of endogenous IL-6 in rats using anti-IL-6 antibodies resulted in an improvement of cognitive function in hippocampal-dependent tasks and prolongation of LTP in the hippocampus when compared

to control mice (Balschun *et al.*, 2004). In the same line of experiments, exogenous administration of IL-6 in the CNS also led to inhibited LTP in the hippocampus (Tancredi *et al.*, 2000) and increased plasma levels of adrenocorticotropin hormone (ACTH) and corticosterone, as reviewed elsewhere (Wichers and Maes, 2002). Since it is increasingly recognized that elevated glucocorticoids are associated with poor cognitive functioning (Ouanes and Popp, 2019), HPA axis hyperactivation after exogenous administration of IL-6 might be a mechanism underlying the role of IL-6, and thus cytokines, in cognitive function.

The role of the pro-inflammatory cytokine IFN-γ in cognitive function modulation was also already deciphered. Mice lacking IFN-γ presented a better hippocampal-dependent memory than WT littermates in the NORT and in the MWMT. Moreover, IFN-γ KO mice displayed an increased hippocampal volume and number of neurons in the CA1 subregion of the DH, when compared to WT mice. IFN-γ KO mice also displayed improved hippocampal neurogenesis and synaptic plasticity, and enlarged dendritic arborization of the DG granule and CA1 pyramidal neurons (Monteiro *et al.*, 2015). An *in vitro* study also demonstrated that in embryonic neuronal cultures, IFN-γ inhibits the dendritic arborization and the synapse formation rate of hippocampal neurons (Kim *et al.*, 2002).

All the reports described above support the importance of cytokines in the support of the CNS. The association of major cytokines, such as IL-1β, IL-4, IL-6, IL-13, and IFN-γ, with cognitive function has been previously highlighted and is supported by studies that show their differential actions in learning and memory, neurogenesis, and hippocampal plasticity processes (Baier *et al.*, 2009; Derecki *et al.*, 2010; Huang and Sheng, 2010; Monteiro *et al.*, 2015; Brombacher *et al.*, 2017). However, there are cytokines with high biological importance, such as the anti-inflammatory IL-10, which have not yet seen their role deciphered in this context.

1.3 The biological properties of interleukin-10

IL-10 was discovered in 1989 (Fiorentino, Bond and Mosmann, 1989) and is to date one of the most studied suppressive molecules of the immune system. This cytokine is produced by most leukocytes of the innate and adaptive immune systems, including macrophages, DCs, neutrophils, eosinophils, B cells, and $CD4^+$ and $CD8^+$ T cells (Saraiva and O'Garra, 2010). Within the CNS, IL-10 is also mainly produced by microglia and astrocytes, as reviewed elsewhere (Lobo-Silva *et al.*, 2016). IL-10 plays a critical role in preventing inflammatory and autoimmune conditions by limiting the inflammatory response. When binds to its receptor (IL-10R), IL-10 activates a series of signaling cascades mediated by the Janus kinase (JAK) signal transducer and activator of transcription (STAT) pathway which regulate the

inflammatory response by decreasing cytokine gene expression, namely of pro-inflammatory ones, and down-regulating the expression of MHC class II, and thus antigen presentation to T cells (Moore *et al.*, 2001; Murray, 2006). Additionally, through activation of the phosphatidylinositol-4,5-bisphosphate-3--kinase (PI3K)/protein kinase B (AKT) pathway, IL-10 binding to the IL-10R has been shown to prevent apoptosis by enhancing the expression of the anti-apoptotic factors B cell lymphoma (Bcl)-2 and Bcl-xl and attenuating the expression of caspase-3 (Moore *et al.*, 2001; Lobo-Silva *et al.*, 2016).

Since the IL-10R is constitutively expressed on most hematopoietic cells (Howes, Gabryšová and O'Garra, 2014) and a few nonhematopoietic cell types, including neurons (Zhou *et al.*, 2009), the processes mediated by IL-10 have important implications in the crosstalk between microglia, astrocytes, and neurons at the CNS level. Specifically, it was already reported that IL-10 can: (1) inhibit the production of pro-inflammatory cytokines, namely IL-1β and TNF, by microglia, protecting astrocytes from excessive inflammation (Balasingam and Yong, 1996; Ledeboer *et al.*, 2002); (2) constrain its own expression levels and the expression of the IL-10R in astrocytes and microglia by an autoregulatory mechanism, protecting the CNS from unbalanced inflammatory responses (Ledeboer *et al.*, 2002); (3) potentiate the astrocytic production of transforming growth factor (TGF)-β, a molecule known to have anti-inflammatory and neuroprotective effects in the CNS, which, in turn, attenuated microglial activation (Norden *et al.*, 2014); (4) increase neuronal survival and overcome the neurotoxic effects of excessive glutamate (Zhou *et al.*, 2009); and (5) regulate adult neurogenesis in the subventricular zone by reducing the differentiation of NSCs into new neurons (Perez-Asensio *et al.*, 2013; Pereira *et al.*, 2015). Consistently with the latter, in the absence of IL-10, neuronal differentiation of NSCs in the subventricular zone is enhanced and the formation of new neurons is increased (Perez-Asensio *et al.*, 2013). However, in this study the role of IL-10 in neurogenesis was only assessed in the subventricular zone, leaving the second consensual cytogenic niche of the adult brain, the SGZ of the hippocampal DG, which is crucial for cognitive abilities, to be addressed.

Notably, in addition to the evidence identifying IL-10 as a regulator of the CNS, several studies directly associated altered IL-10 production or signaling to patients and animal models of neurological diseases, ranging from neuropathic pain (George *et al.*, 2004) and Alzheimer's disease (Kiyota *et al.*, 2012), to Parkinson's disease (Arimoto *et al.*, 2007) and multiple sclerosis (Boxel-Dezaire *et al.*, 1999; Hesse *et al.*, 2011). Moreover, considering the case of multiple sclerosis, intracranial IL-10 administration during experimental autoimmune encephalitis, accelerated disease remission, and reduced disease severity and mortality (Cua *et al.*, 2001), which demonstrated a direct action of IL-10 in the CNS.

Several studies using lipopolysaccharide (LPS) injection into rodents have also revealed potential functions of IL-10 in the modulation of CNS physiology and behavior. LPS injection is used to mimic the

entrance of bacterial-derived compounds and induce sickness behavior into the host (Krueger *et al.*, 1994). IL-10 administration before LPS injection reverted the deleterious behavioral effects of LPS, namely in the reduction of mobility and social exploration in rats (Bluthé *et al.*, 1999). In another study, LPS injection led to altered hippocampal plasticity processes by reducing LTP in rats, which was abrogated by IL-10 administration (Lynch *et al.*, 2004). It was also described that after LPS injection, mice lacking IL-10 presented increased levels of pro-inflammatory cytokines and reduced levels of BDNF and nerve growth factor in the hippocampus when compared to LPS-injected WT mice. Moreover, LPS-injected IL-10 KO mice also revealed cognitive impairments in a hippocampal-dependent memory task when compared to the WT counterpart (Richwine *et al.*, 2009), giving a first evidence that during an inflammatory challenge by LPS injection, IL-10 is critical for cognitive function.

Without previous exposure to an inflammatory challenge by LPS injection, IL-10 administration by itself was capable to induce increased motor activity and abnormal exploratory patterns in mice (Harvey *et al.*, 2006). In another study, it was also described that female, but not male mice lacking IL-10 presented increased signs of depressive-like behavior when compared to the gender-matched non-littermate WT controls. Importantly, this phenotype in female IL-10 KO mice was partially reverted by IL-10 administration. Additionally, female, but not male mice overexpressing IL-10 also displayed fewer signs of depressive-like behavior than the gender-matched non-littermate WT controls (Mesquita *et al.*, 2008), which indicates that the effect of IL-10 in the modulation of animal behaviors could be gender-specific. Recently it was also reported that IL-10 KO mice from microglia ($Cx3cr1^{CreER}$) showed increased depressive- and anxious-like behaviors compared to their WT littermates (Yang *et al.*, 2021), indicating that, within the CNS, IL-10 production by microglia alone is crucial for emotional stability.

The role of IL-10 in the support of mental processes was extended to hippocampal-dependent cognitive abilities by a report showing that mice with lower IL-10 expression demonstrated increased signs of depressive-like behavior, alongside with impaired spatial learning and memory in the MWMT, when compared to WT littermates (Zhang *et al.*, 2020). Also noteworthy is the human study supporting that high IL-10 plasma levels are positively associated with high arithmetic intelligence scores in healthy young adults (Jung *et al.*, 2019). Also in humans, a IL-10 gene polymorphism was found to have reduced promoter activity (Steinke *et al.*, 2004). Surprisingly, in patients with schizophrenia, this IL-10 gene polymorphism was associated with reduced serum IL-10 levels and worse cognitive function (Xiu *et al.*, 2016). Lastly, preliminary data from our laboratory also showed that male mice lacking IL-10 presented cognitive impairments in hippocampal-dependent tasks, reduced dendritic arborization of DG hippocampal neurons, and alteration of the leukocyte profile in the blood and lymph nodes (unpublished

data). These results provide insight that IL-10 may be modulating the cognitive function of male mice and unravel clues to potential mechanisms that may mediate this process.

Despite this, other mechanisms may contribute to the crosstalk between IL-10 and cognitive function. Among them is the IL-10 induced alterations in HPA axis activation. It is known that under basal conditions, IL-10 KO mice may present higher corticosterone levels (Smith *et al.*, 1999). This condition is consistently reported to be associated with impaired cognitive function (Ouanes and Popp, 2019), shrinkage of the dendritic arborization of hippocampal neurons (Alfarez *et al.*, 2009), and alteration of the leukocyte profile in the blood (Deutsch *et al.*, 2007; Davis, Maney and Maerz, 2008). Therefore, HPA axis hyperactivation should be considered as a potential mechanism underlying the role of IL-10 in cognitive function.

Another mechanism that may contribute to this association between IL-10 and cognition is the gut-brain axis, in which the gut microbiome cooperates with its host in the regulation of mental processes (Morais, Schreiber and Mazmanian, 2021). Actually, since they were generated in 1993, IL-10 KO mice have been characterized as an animal model for studying inflammatory bowel disease (IBD) (Kühn *et al.*, 1993; Sturlan *et al.*, 2001), a chronic colon inflammatory condition whose symptoms include mainly misbalanced gut microbiome (dysbiosis), diarrhea, abdominal pain, and rectal bleeding (Keubler *et al.*, 2015). Dysbiosis in IL-10 KO mice leads to a gut microbiome with less diversity and richness than the WT counterpart (Maharshak *et al.*, 2013; Singh *et al.*, 2016). Since certain animal behaviors appear to correlate with the composition of the gut microbiome, and disruptions in microbial communities have been implicated in several neurological disorders (Morais, Schreiber and Mazmanian, 2021), it is imperative that the potential impact that the gut microbiome may have in the cognitive function of IL-10 KO mice be addressed.

In summary, there is mounting evidence strongly suggesting the crucial role of IL-10 in the modulation of cognitive function. However, the mechanisms by which this association may occur still need further clarification. Additionally, considering the reports indicating that the effect of IL-10 in the modulation of animal behaviors could be gender-specific and the preliminary data from our laboratory in male IL-10 KO mice supporting the protective role of IL-10 in cognitive abilities, becomes crucial to evaluate the cognitive behavior of female mice and the mechanisms underlying this association.

CHAPTER 2

RESEARCH OBJECTIVES

CHAPTER 2 – **RESEARCH OBJECTIVES**

Despite the growing number of studies showing that IL-10 may impact different cognitive abilities, including learning and memory, the role of this anti-inflammatory cytokine as a modulator of cognitive function in the healthy brain is far from being understood. Of utmost interest, the mechanisms by which IL-10 may influence cognitive abilities also need further enlightenment, as they could be important contributors to the development of novel IL-10-based therapies for cognitive impairments.

In this thesis, the central hypothesis is that IL-10 absence might modulate cognitive abilities of mice, which in turn may be mechanistically associated with alterations in the colon inflammatory profile, hippocampal plasticity processes, HPA axis activation, leukocyte profile in the blood and lymph nodes, and gut microbiome. To test this hypothesis, the work conducted in this thesis was divided into 2 parts:

Part 1: Characterization of the mechanisms underlying the role of IL-10 in cognitive function

With the aim to characterize the cognitive behavior of female mice lacking IL-10 and decipher mechanisms underlying the role of IL-10 in cognitive function, six research objectives were designed:

i. Study the behavioral performance of adult constitutive IL-10 KO female mice and WT littermates in hippocampal-dependent cognitive tasks;
ii. Assess the impact of hormonal fluctuation that occurs during the estrous cycle in the cognitive function of IL-10 KO female mice;
iii. Analyze the influence of the colon inflammatory profile in the cognitive data of IL-10 KO mice;
iv. Understand the impact of IL-10 deficiency in hippocampal plasticity processes associated with cognitive function;
v. Explore the HPA axis activity of IL-10 KO mice and its correlation with the cognitive behavior profile;
vi. Evaluate the leukocyte profile in the blood and lymph nodes (namely dcLN) of IL-10 KO mice and its correlation with the cognitive behavior profile.

Part 2: Optimization of a gut microbiome depletion protocol

With the aim to characterize the potential impact that the gut microbiome modulation may have in the cognitive function of IL-10 KO mice, a research objective was designed:

vii. Optimization of an effective protocol for gut microbiome depletion of IL-10 KO mice.

CHAPTER 3

MATERIALS AND METHODS

3.1 Ethics statement

The experimental procedures performed in this thesis were conducted in accordance with the Portuguese national authority for animal experimentation, Direção Geral de Alimentação e Veterinária (DGAV), and the local committee responsible for animal welfare, Órgão Responsável pelo Bem-Estar Animal (ORBEA) of the EMUM–ICVS: process number ORBEA EM/ICVS-I3Bs_007/2020. All experimental procedures were performed by researchers trained in laboratory animal sciences and licensed by DGAV. Animals were kept and handled under the guidelines in the Decree-Law no. 1/2019, which makes the first amendment to the Decree-Law no. 113/2013 of the Portuguese Parliament, transposing the Directive no. 2010/63/EU on the protection of animals used for scientific purposes of the European Parliament and of the Council.

3.2 Animal model and experimental groups

Constitutive IL-10 KO (IL-$10^{-/-}$) mice produced by gene targeting (Kühn *et al.*, 1993) and backcrossed to BALB/c background were kindly provided by Dr. Anne O'Garra (National Institute for Medical Research, London, United Kingdom) and were crossed with WT (IL-$10^{+/+}$) mice on a BALB/c background (Charles River Laboratories, Barcelona, Spain). The F1 progeny, heterozygous BALB/c IL-10 KO (IL-$10^{+/-}$) mice, were crossed in the animal facility of the EMUM–ICVS to preserve the mice colony and to generate both WT littermate and IL-10 KO mice. WT littermate mice were used as controls in all experimental procedures to minimize genetic variability (Holmdahl and Malissen, 2012). Sterile standard diet (catalog number [CN]: 4RF25 during gestation and postnatal periods, and CN: 4RF21 after weaning; Mucedola SRL, Settimo Milanese, Italy) and water were given *ad libitum* to all animals. Mice were maintained under standard laboratory conditions on a 12/12 h light/dark cycle (lights on at 8:00 a.m. and lights off at 8:00 p.m.) with a room temperature of 22-24 °C, and relative humidity of 55%. Cages were environmentally enriched with a wooden wool roll and soft paper for nesting. At postnatal day 7-14, mice were identified by toe tattoo ink puncture and genotyped by polymerase chain reaction (PCR). After weaning, at postnatal day 21-28, female IL-10 KO and WT mice were group-housed (4-6 mice per cage) in separate housing cages so that there was no modulation of the gut microbiome by animals of distinct genotypes (Robertson *et al.*,

2019). At 3-6 months, female IL-10 KO and WT mice were used in all experimental procedures. Animal welfare was monitored at least once a week throughout the animal's life. Mice were excluded from the experimental procedures and humanely euthanized, whenever a humane endpoint was reached (Burkholder *et al.*, 2012). The humane endpoints predefined were: weight loss ≥ 20% within a week; occurrence of signs of dehydration and reduction of skin turgor without recovery potential; inability to eat or drink; lack of responsiveness to manual stimulation; existence of open or infected wounds without healing potential; and presence of debilitating chronic diarrhea, rectal prolapses, or tumors.

Part 1: Characterization of the mechanisms underlying the role of IL-10 in cognitive function

For the behavior evaluation and mechanistic characterization, 4 independent sets were performed. In each one, female animals were divided according to their genotype: IL-10 KO and WT mice (**Table 1**).

Table 1. Animal sample size used per set for behavioral assessment.

Set number	Experimental group – Sample size	
	WT	IL-10 KO
Set 1	15	13
Set 2	20	22
Set 3	15	13
Set 4	8	12
Total	**58**	**60**

Part 2: Optimization of a gut microbiome depletion protocol

For the optimization of the gut microbiome depletion protocol, 2 independent sets were performed. In each one, female animals were divided into four experimental groups: IL-10 KO and WT control mice and, IL-10 KO and WT mice submitted to an antibiotic treatment (**Table 2**).

Table 2. Animal sample size used per set for gut microbiome depletion protocol optimization.

Set number	Experimental group – Sample size			
	WT control	IL-10 KO control	WT treated	IL-10 KO treated
Set 1	3	3	12	12
Set 2	3	3	3	3
Total	**6**	**6**	**15**	**15**

3.3 Identification by toe tattoo ink puncture method

At postnatal day 7-14, mice were identified by toe tattoo ink puncture, as previously described

(Castelhano-Carlos *et al.*, 2010; M. Chen *et al.*, 2016). Briefly, a 30-gauge needle, previously immersed in animal green tattoo paste (CN: 329AA; Ketchum Manufacturing Company, New York, USA), was used to puncture a different toe in each animal in one of the four feet. The needle was inserted into the superficial layer of the skin and left on the toe for 2 s. Excess ink on the toe was cleaned with soft paper.

3.4 Genotyping

For deoxyribonucleic acid (DNA) isolation, the tissue samples collected from the tail tip were incubated with 300 μL of 50 mM sodium hydroxide solution for 50 min at 98 °C. Then, 30 μL of 1 M Tris-HCl neutralizing buffer (pH = 8.0) was added, and debris was removed through centrifugation for 6 min at 15,000 relative centrifugal force (G). The supernatant containing the isolated DNA was transferred to a sterile nuclease-free tube.

For the genotyping PCR, 2 μL of template DNA and the oligonucleotide primers listed in **Table 3** were used. The primer sense 1 and the primer antisense 1 amplify the IL-10 WT allele (137 base pairs [bp]), while the primer sense 1 and the primer antisense 2 amplify the IL-10 KO allele (312 bp).

Table 3. List and sequence of the PCR oligonucleotide primers used for mice genotyping.

Name	Database code	Sequence
Primer sense 1	oIMR9573_IL10common	5'-CTT GCA CTA CCA AAG CCA CA-3'
Primer antisense 1	oIMR9574_IL10wt	5'-GTT ATT GTC TTC CCG GCT GT-3'
Primer antisense 2	oIMR7376_IL10mutant	5'-CCA CAC GCG TCA CCT TAA TA-3'

Table 4 summarizes the concentration of the reagents present in the genotyping mixture used to perform the PCR. A 96-well thermal cycler (CN: 4484075, Thermo Fisher Scientific, Massachusetts, USA) was used with a protocol designed to have an initial denaturation step (3 min at 94 °C), followed by 40 cycles of denaturation (30 s at 94 °C), primer annealing (60 s at 64 °C), and extension (60 s at 72 °C), and, lastly, a final extension step (2 min at 72 °C). PCR products were analyzed using a 1.5% (w/v) gel of agarose (CN: A9539; Sigma-Aldrich, Missouri, USA) in TAE buffer (40 mM tris-base, 20 mM acetic acid, and 1 mM ethylenediaminetetraacetic acid; pH = 7.4). GreenSafe Premium (6 μL.100 mL^{-1}; CN: MB1320; Nzytech, Lisbon, Portugal) was added to the gel to allow the visualization of DNA bands. Then, 2 μL of 6 × concentrate DNA loading dye (CN: CN0611; Thermo Fisher Scientific) were added to the samples, and all volume was loaded into the agarose gel. The GRS ladder 100 bp (NC: GL041.0050; Grisp, Porto, Portugal) was used to access the size of the bands. The electrophoresis ran at 100 V for

30 min. Lastly, the resulting gel was visualized under ultraviolet radiation using the Gel Doc EZ System (Bio-Rad, California, USA).

Table 4. Genotyping mixture composition used for PCR.

Reagent	Concentration	Manufacturer
Taq buffer (CN: AB0301B)	1× concentrate	Thermo Fisher Scientific, Massachusetts, USA
Taq DNA polymerase (CN: AB0301B)	0.03 $U.\mu L^{-1}$	
Magnesium chloride (CN: AB0301B)	2.0 mM	
dNTPs (CN: R0192)	0.2 mM	
Primer sense 1	1.0 μM	STAB Vida, Lisbon, Portugal
Primer antisense 1	1.0 μM	
Primer antisense 2	1.0 μM	
Dimethyl sulfoxide (CN: D8418)	2%	Sigma-Aldrich, Missouri, USA
Nuclease-free water (CN: LSKNF0500)	Up to 10 μL	Millipore, Massachusetts, USA

3.5 Behavioral assessment

In *Part 1* of this thesis, IL-10 KO and WT mice were submitted to distinct behavioral tests to assess cognitive function. Four independent sets of behavioral assessments were performed (**Table 5**).

Table 5. Battery of tests of each set of behavioral assessment.

Set number	Behavioral test							
	OFT	YMT	NORT	BMT	CCFCT	FST	TST	BT
Set 1	×			×		×*	×*	×*
Set 2	×			×				
Set 3	×	×	×		×			
Set 4	×	×#	×#		×			

BMT - Barnes-maze test; BT - burrowing test; CCFCT - contextual and cued fear conditioning test; FST - forced swim test; NORT – novel object recognition test; OFT – open-field test; TST - tail suspension test; YMT – Y-maze test. *Information related to this behavioral test will not be presented as they are out of the scope of this thesis. #Information related to this behavioral test will not be presented due to problems in data acquisition during the performance of the behavioral test.

The batteries of tests of the behavioral sets 1 and 2 were carried out by other researchers in a period before the start date of this thesis. Analysis and interpretations of the results were carried out by me. In at least one of the sets, the Y-maze test (YMT), the NORT, the Barnes-maze test (BMT), and the contextual and cued fear conditioning test (CCFCT) were performed. The open-field test (OFT) was performed in all sets to control for locomotion, general and vertical exploration, and anxious-like behavior. Before starting the behavioral tests, mice were gently handled by the same researcher every day for at least a week. Behavioral assessments took place between 9:00 a.m. and 7:00 p.m. and, during their performance, the researcher

was blinded to genotype. On all behavioral testing days, mice were transported to the testing room and left for habituation to the room conditions for 30 min before the test initiation.

3.5.1 Open-field test

The OFT is commonly used to assess novel environment exploration, locomotor activity, and provide an initial screen for anxious-like behavior (Prut and Belzung, 2003). The OFT apparatus consists of a highly illuminated square arena measuring 43.2 cm (length) × 43.2 cm (width) × 30.5 cm (height) made from white plastic. Mice were placed individually in the center of the arena and allowed to freely explore it for 5 min. Their movement was traced using a 16-beam infrared system (CN: ENV-258; Med Associates, Vermont, USA). The resulting data was analyzed using the Activity Monitor Software (CN: SOF-812; Med Associates), considering two previously defined areas: a central and an outer area. The central area was defined as a square measuring 14.4 cm (length) × 14.4 cm (width) in the center of the OFT arena. The average velocity of the mice was used to assess locomotor activity. The total distance traveled was used to evaluate general exploration and the number and duration of rearings (the rodent's behavior of standing on its hind legs) were collected to assess vertical exploration (Sturman, Germain and Bohacek, 2018). Anxious-like behavior was assessed by the percentage of distance in the center of the OFT arena. Typically, a thigmotactic phenotype is an indication of anxious-like behavior (Prut and Belzung, 2003; Seibenhener and Wooten, 2015).

3.5.2 Y-maze test

Spatial short-term memory, which is a hippocampal-dependent cognitive function (Kraeuter, Guest and Sarnyai, 2019), was evaluated through the 2-trial YMT. The YMT apparatus consists of a 3-arm maze shaped like a capital Y with each arm spaced at an angle of 120 degrees, elevated 20 cm from the floor, and under dim light. Each arm measures 50.0 cm (length) × 10.0 cm (width) × 15.0 cm (height) and contains, at its end, a distinct spatial geometric cue. In the first trial (training trial; **Figure 8A**), mice were allowed to explore only 2 arms of the arena, since the third arm was closed for exploration, for 10 min. After this period, mice were returned to their home cage. In the second trial (testing trial; **Figure 8B**), which was performed 1 h later, mice were allowed to explore the arena with the 3 arms available for exploration, for 5 min. Testing trials were video-recorded, and the time in the novel arm and number of arm alternations were manually measured using the behavioral scoring software Observador v.0.2.7

(Department of Pharmacology - University of Athens, Athens, Greece). The natural tendency of mice to explore new environments serves as the basis of the YMT, thus mice should visit the novel arm more often in the testing trial (Kraeuter, Guest and Sarnyai, 2019; Sultana, Ogundele and Lee, 2019).

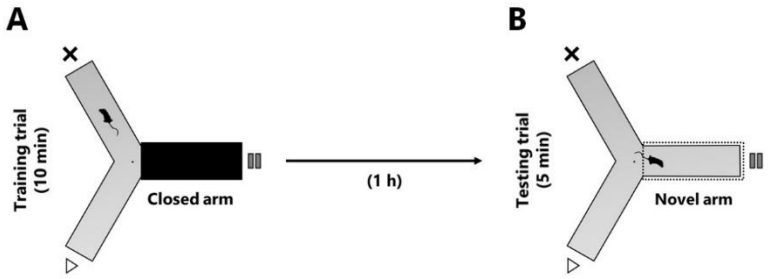

Figure 8. Representation of the 2-trial Y-maze test protocol. A. In the first trial (training trial), the exploration of the arena for 10 min was conditioned to only 2 arms, since the third arm (closed arm) was blocked. **B.** After 1 h, in the second trial (testing trial), the third arm (novel arm) was opened, and the exploration of the entire arena was allowed for 5 min. A distinct spatial geometric cue was placed at the end of each arm to allow mice orientation. In both trials, mice started the exploration from the same location in the center of the arena.

3.5.3 Novel object recognition test

Recognition short-term memory was assessed through the NORT (Bird, 2017). The NORT apparatus consists of a dimly illuminated square arena measuring 40.0 cm (length) × 40.0 cm (width) × 40.0 cm (height) and made of black acrylic. Mice were accustomed to the arena for 20 min in 3 consecutive days (habituation trials; **Figure 9A**). On the fourth day, two distinct trials were performed. In the first trial, two identical 3-dimensional objects were symmetrically placed on one side of the arena (training trial: **Figure 9B**), and mice were allowed to freely explore both of them for 10 min. The second trial (testing trial) was carried out 1 h later. One of the identical objects was replaced by a novel one with a similar size but different

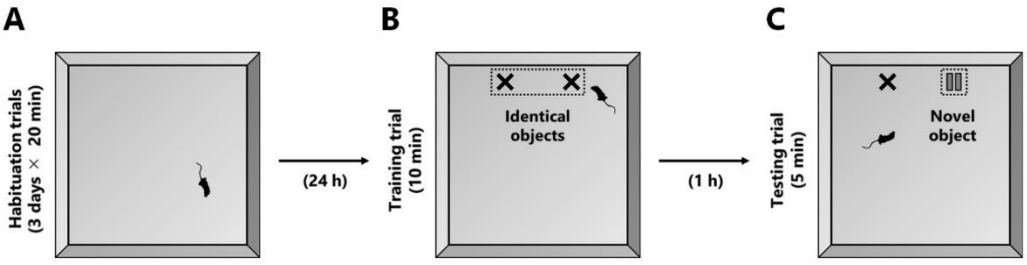

Figure 9. Representation of the novel object recognition test protocol. A. For 3 consecutive days, mice were familiarized with the arena for 20 min a day (habituation trials). **B.** In the first trial of the fourth day (training trial), two identical objects placed inside the arena were allowed to be explored for 10 min. **C.** After 1 h, in the second trial of the fourth day (testing trial), one of the identical objects was replaced by a distinct one (novel object), and the exploration of the arena was allowed for 5 min.

shape, color, and texture, and mice were then returned to the arena and allowed to freely explore both objects for 5 min (testing trial; **Figure 9C**). Testing trials were video-recorded, and the time spent exploring each one of the objects was manually measured using the behavioral scoring software Observador v.0.2.7 (Department of Pharmacology - University of Athens). Mice were considered to be exploring whenever the nose was facing one of the objects. Since NORT is based on the innate preference of mice to explore novel objects rather than familiar ones, short-term recognition memory was assessed by the exploration time that mice spent exploring the novel object (Bevins and Besheer, 2006; Leger *et al.*, 2013).

3.5.4 Barnes-maze test

The BMT was used to assess spatial reference memory, which is a hippocampal-dependent cognitive function (Matthew, 2018). This test was first described by Carol Barnes in 1979, as a useful alternative to the MWMT and the radial arm maze test, which are more stressful and physically demanding, and require water immersion or food deprivation (Gawel *et al.*, 2019). The BMT apparatus consists of a custom-made gray circular arena measuring 80.0 cm (diameter) × 100.0 cm (height) with 12 equidistant open holes measuring 5.0 cm (diameter) located 2.0 cm from the border (**Figure 10**). Directly above the arena, a light bulb was placed to create a mildly anxiogenic environment. In this open and illuminated arena, the natural behavior of mice is the attempt to find shelter where they can take refuge. (Gawel *et al.*, 2019). Mice were able to find shelter in an escape chamber placed under one of the open holes, the target hole. The escape chamber measuring 20.0 cm (length) × 9.0 cm (width) × 9.0 cm (height) contained bedding material on the bottom to mimic a shelter. Mice were able to locate the target hole through visual cues surrounding the arena. The arena can be virtually divided into 4 quadrants, including the target quadrant containing the target hole and the two neighboring open holes.

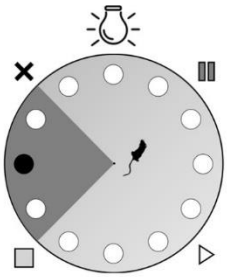

Figure 10. Representation of the Barnes-maze test arena. A gray circular arena with 12 equidistant open holes. The target hole (in black) contained an escape chamber that allowed mice to take shelter. Directly above the arena, a light bulb was placed, and surrounding the maze visual cues were positioned. The target quadrant containing the target hole is shown in dark gray.

The BMT was carried out over 6 consecutive days, with the learning phase taking place in the first 5 days and the probe trial on the sixth day. In the learning phase, each animal was submitted to 3 daily training trials with a duration of 120 s each and an inter-trial interval of approximately 15 min. The spatial location of the target hole during all training trials remained unchanged to allow the assessment of spatial reference memory (Matthew, 2018). Before the beginning of the test, mice were habituated to the escape chamber. Each learning phase trial started by placing the mice inside a black starting cylinder measuring 15.0 cm (diameter) × 10.0 cm (height) at the center of the BMT arena which was removed after a few seconds, allowing mice to freely explore the apparatus. Mice that failed to find the target hole within 120 s were gently guided to its location and the light bulb turned off. For those mice, 120 s were recorded as the latency to enter the target hole. For mice that successfully found the target hole and entered the escape chamber before the 120 s, the light bulb was immediately turned off as a memory reinforcement and the trial ended. All animals remained in the escape chamber for 20 s with the light bulb turned off. On the sixth day, reference memory was assessed by a probe trial during which the escape chamber was removed from the target hole, leaving the target hole in conditions similar to the remaining open holes. Mice were allowed to explore the arena in these conditions for 60 s.

All trials were video-recorded and analyzed using the video tracking software Ethovision XT v.12 (Noldus, Wageningen, Netherlands). In the learning phase trials, the latency to enter the target hole, the total distance traveled, and the time spent in the target quadrant was assessed, and in the probe trial, the latency to reach the target hole for the first time, the total distance, the time spent in the target quadrant, and the number of nose pokes in each open hole was measured. Also, in all trials, the heatmap output of the video tracking software with the path taken by the mice in the attempt to find the target hole was manually classified into seven predefined search strategies (**Figure 11**). The classification of mice paths in search strategies was inspired by similar classification schemes previously developed for the MWMT (Brody and Holtzman, 2006; Rogers *et al.*, 2017). Briefly, 3 blocks of search strategies were considered: the hippocampal-dependent, the exploratory, and the freezing strategies. The hippocampal-dependent strategies comprise the direct encounter (immediate displacement to the target hole), and the direct approach (immediate approach to the target hole and at least one of the neighboring open holes). The exploratory strategies include the serial exploration (exploration of at least 3 consecutive open holes), the mixed exploration (exploration of at least 3 consecutive open holes passing more than once through the center of the arena), and the random exploration (no exploration of 3 consecutive open holes). The freezing strategies contain the freeze in the periphery (displacement to the periphery), and the freeze in the center (without displacement).

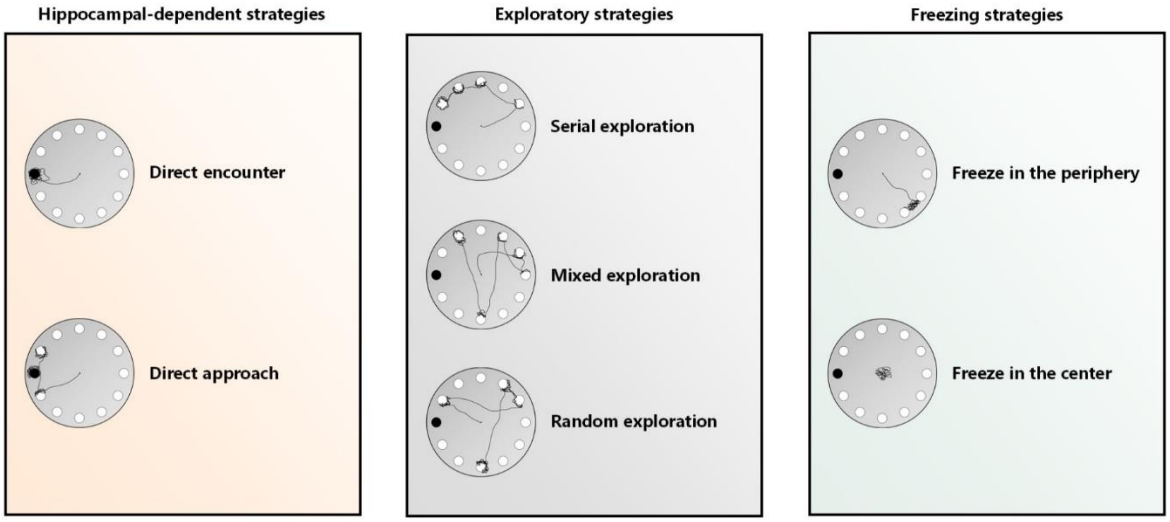

Figure 11. Representation of the search strategies used to classify the paths taken by the mice in the Barnes-maze test. From left to right, the blocks of hippocampal-dependent, exploratory, and freezing strategies are presented. The black lines represent prototypes of a path taken by the mice. The location of the target hole is represented in black.

3.5.5 Contextual and cued fear conditioning test

Associative memory was assessed in the contextual and cued fear conditioning test (CCFCT), which is commonly used to assess hippocampal-dependent cognitive function and the integrity of extrahippocampal memory circuits (Curzon, Rustay and Browman, 2009). The CCFCT consists of two unrelated arenas (contexts) with distinct characteristics. In the first context, an innocuous conditional stimulus (CS; an auditory cue) is contingently paired with an aversive unconditional stimulus (US; a foot shock) that triggers a Pavlovian response. The CS-US pairings are the basis to evaluate spatial (context) and non-spatial (cued) associative memory (Kim and Jung, 2006). The CCFCT was conducted under dim light in acrylic arenas measuring 20.0 cm (length) × 16.0 cm (width) × 20.5 cm (height). Each arena contained a stainless-steel shock grid floor (CN: VFC-008-LP; Med Associates), where animals were placed. Each trial was video-recorded, and the conditioned response of mice was manually measured in two independent evaluations using the behavioral scoring software Observador v.0.2.7 (Department of Pharmacology - University of Athens). In the first evaluation, only freezing behavior was considered as a conditioned response, which is a species-specific response to fear and has been defined as the absence of movement for a minimum of 1 s (Curzon, Rustay and Browman, 2009). In contrast, in the second evaluation, in addition to freezing behavior, other phenotypes such as tail rattle, vigorous grooming, vivid tremor, and intense jumping, were also considered as a conditioned response since they had not been observed before the CS-US pairings. The CCFCT was conducted over 3 days:

Day 1: Conditioning

Mice were placed in a white arena (Context A; **Figure 12A**) and received 3 CS-US pairings: an auditory cue (90 dB; 20 s) and a foot shock (0.5 mA; 2s). The interval between pairings was 40 s, and the first auditory cue presentation started at 160 s after the animals were placed into the arena. After the 3 CS-US pairings, conditioned response was measured for 30 s.

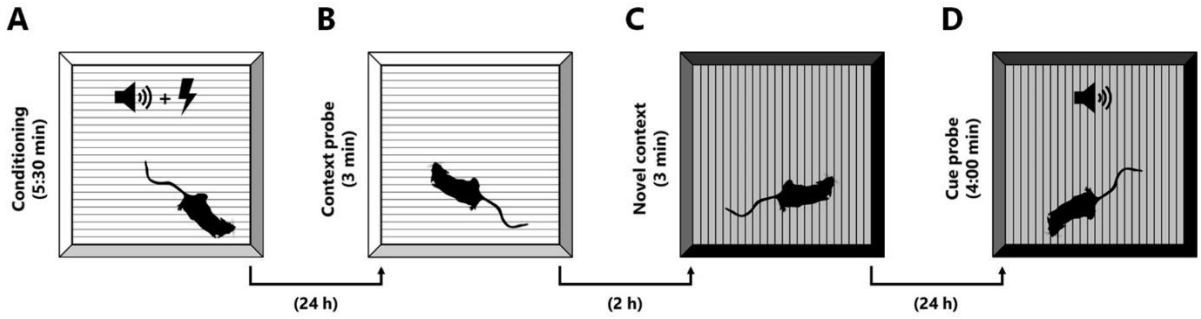

Figure 12. Representation of the contextual and cued fear conditioning test protocol. **A.** On the first day, after a 160 s habituation period, the mice were submitted to 3 CS-US pairings between an auditory cue and a foot shock in context A to trigger a Pavlovian conditioned response. **B**. On the second day, the mice returned to context A for 3 min to perform the context probe. **C.** After 2 h, mice were placed in a novel context (Context B) for 3 min to assess the context discrimination index. **D.** On the last day of the CCFCT, the cue probe was performed by returning the mice to context B, where the auditory cue was presented.

Day 2: Context probe and context discrimination index

To evaluate spatial associative memory in a context probe, mice were placed again in the white arena (Context A; **Figure 12B**), where they had been 24 h earlier for the CS-US pairings. The conditioned response was measured for 3 min. Two hours later, the animals were placed in a novel arena (Context B; **Figure 12C**) lined with a black plasticized coating previously sprayed with vanilla oil to alter both spatial and non-spatial references. The researcher wore a different style of gloves and lab coat. The conditioned response was measured again for 3 min, and the context discrimination index was calculated as:

$$\textit{Context discrimination index} = \frac{\textit{Conditioned response in context A - Conditioned response in context B}}{\textit{Conditioned response in context A + Conditioned response in context B}}$$

Day 3: Cue probe:

To assess non-spatial associative memory in a cue probe, mice were placed 24 h later in Context B with the same test setting (**Figure 12D**). After 160 s, an auditory cue (90 dB; 20 s) was presented and the conditioned response was subsequently measured for 60 s.

3.6 Estrous cycle phase determination

Vaginal smears were performed at the end of each behavioral testing day. For that, a drop of sterile 0.9% saline solution was inserted into the vagina and a cell suspension was collected with a small plastic inoculation loop, which was then used to perform a vaginal smear on a non-coated glass slide. Vaginal smears were air-dried, fixed in 96% ethanol solution for 12 h, and stained using a conventional Papanicolaou protocol (Berkan *et al.*, 1986). Vaginal smears were analyzed under a light microscope (CN: BX53; Olympus, Hamburg, Germany) and the stage of the estrous cycle was determined based on the presence or absence of leukocytes, cornified epithelial, and nucleated epithelial cells. Female mice were considered to be in the proestrus phase when nucleated epithelial cells were dominant; estrus phase when there was a large abundance of cornified epithelial cells; metestrus phase when there was a mixture of all three cell types; and diestrus phase when there was a large proportion of leukocytes in the vaginal smears (Byers *et al.*, 2012). To analyze the impact of the estrous cycle on behavioral data, for each behavioral testing day, female mice were divided into two subgroups, as previously proposed by other authors (Chari *et al.*, 2020). Proestrus and estrus mice have been combined in one subgroup (PEF), while metestrus and diestrus mice have been combined in another (MDF), as shown in **Figure 13**.

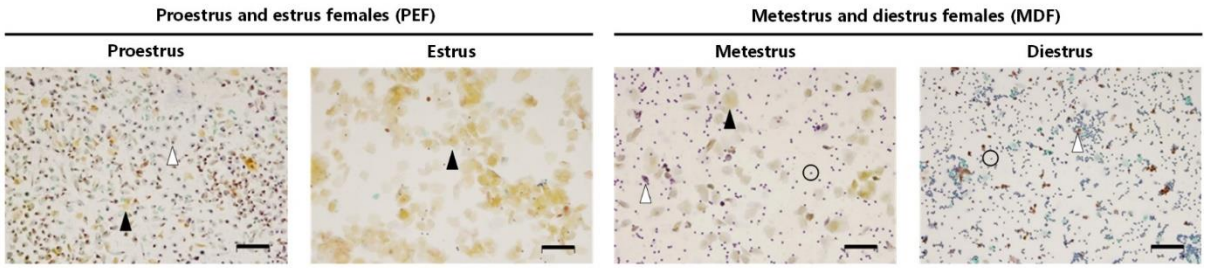

Figure 13. Vaginal smears representing each estrous cycle phase. From left to right, proestrus, estrus, metestrus, and diestrus phases are depicted. Three cell types were identified: leukocytes (circles), cornified epithelial (black arrows), and nucleated epithelial cells (white arrows). For each behavioral testing day, mice in proestrus and estrus were grouped in one subgroup (PEF) and mice in metestrus and diestrus in another (MDF). Scale bar = 100 μm.

3.7 Serum corticosterone measurements

At the end of the behavioral testing, blood samples were collected to assess serum corticosterone levels. Blood sampling to sterile nuclease-free tubes was performed by tail-clipping during the diurnal nadir (between 08.00 a.m. and 09:00 a.m.) and the nocturnal zenith (between 07.00 p.m. and 08:00 p.m.) of the following day for a maximum period of 2 min. The serum was isolated through centrifugation for

5 min at 15,000 G and stored at -80 °C until further use. Subsequent serum corticosterone levels were measured by a corticosterone enzyme-linked immunosorbent assay (ELISA) kit, following the instructions provided by the manufacturer (CN: ADI-901-097; Enzo Life Sciences, New York, USA).

3.8 Tissue collection

Mice that finished the allocated experimental procedures, at the experimental endpoint, were anesthetized with an intraperitoneal injection of ketamine (75 mg/kg; Imalgene 1000; Merial, Lyon, France) and medetomidine (1 mg/kg; Domitor; Orion Pharma, Espoo, Finland) and posteriorly dissected.

Part 1: Characterization of the mechanisms underlying the role of IL-10 in cognitive function

Mice submitted to the behavior evaluation were transcardially perfused with cold sterile 0.9% saline solution after anesthesia. The distal colon, the inguinal lymph nodes (ingLN) and dcLN, and the brain were collected. The colons were immediately frozen in dry ice and stored at -80 °C until further processing for ribonucleic acid (RNA) expression analysis (**Section 3.9**) and the lymph nodes were immediately processed for immunophenotyping (**Section 3.12**). The brains were separated into two groups depending on the intended purpose: hippocampal stereological analysis, or hippocampal 3-dimensional neuronal reconstruction and dendritic spine characterization. For hippocampal stereological analysis, brains were fixed and kept in a 4% paraformaldehyde (PFA) solution, with constant agitation for at least 24 h until further processing (**Section 3.10**). For hippocampal 3-dimensional neuronal reconstruction and dendritic spine characterization, brains were immersed in Golgi-Cox staining (1% mercury chloride, 1% potassium dichromate, and 1% potassium chromate) for 14 days with gentle agitation, and then moved to a 30% sucrose solution until further processing (**Section 3.11**).

Part 2: Optimization of a gut microbiome depletion protocol

After anesthesia, cervical dislocation was performed. Mice were immediately dissected, and the cecum was removed and examined (**Section 3.13**).

3.9 Colon inflammatory profile evaluation

The distal colon of each animal was collected at the experimental endpoint, and the expression levels of pro-inflammatory marker genes were evaluated by quantitative real-time PCR (qRT-PCR).

3.9.1 Colon RNA extraction

For RNA extraction, the frozen distal colon samples were transferred into 1 mL of TripleXtractor (CN: GB23.0100; Grisp), mechanically dissociated using a 20-gauge needle, and incubated for 5 min at room temperature. Then, 200 μL of chloroform were added, and the samples were shacked vigorously for 10 s and incubated for 3 min at room temperature. Phase separation was performed through centrifugation for 15 min at 6,000 G and 4 °C. The aqueous phase was subsequently transferred into a sterile nuclease-free tube and 500 μL of isopropanol was added. The samples were incubated for 10 min at room temperature and then centrifuged for 10 min at 7500 G and 4 °C. The RNA pellet was washed in 1 mL of a 75% ethanol solution and centrifuged again for 5 min at 2500 G and 4 °C. Lastly, the RNA pellet was resuspended in 20 μL of nuclease-free water (CN: LSKNF0500; Millipore, Massachusetts, USA). RNA concentration was assessed using the NanoDrop 1000 Spectrophotometer (ThermoFisher Scientific, Massachusetts, EUA) and the samples were diluted to a final concentration of 0.5 μg of RNA per μL.

3.9.2 Complementary DNA synthesis

The complementary DNA (cDNA) synthesis was performed using the iScript Advanced cDNA Synthesis Kit (CN: 1725038; Bio-Rad). To 15 μL of RNA template sample (corresponding to 7.5 μg of RNA) were added 4 μL of 5 × concentrate iScript Advanced Reaction Mix and 1 μL of iScript Advanced Reverse Transcriptase. cDNA synthesis was carried out in a 96-well thermal cycler (CN: 4484075, Thermo Fisher Scientific) by incubating the samples for 20 min at 46 °C followed by 1 min at 95 °C. cDNA samples were kept at -20 °C until further use.

3.9.3 Quantitative real-time PCR of colon inflammatory marker genes

The gene expression levels were evaluated by qRT-PCR on a CFX96 Touch qRT-PCR System (Bio-Rad). A reaction mixture was prepared and 19 μL of it were added to 1 μL of the cDNA template sample. The reaction mixture reagents were diluted to a final concentration of 1 × concentrate SsoFast EvaGreen Supermix (CN: 172-5202; Bio-Rad), and 0.5 $\mu M.L^{-1}$ of each specific oligonucleotide primer (**Table 6**). The qRT-PCR protocol was designed to have an initial activation step (1 min at 95 °C), followed by 40 cycles of denaturation (15 s at 95 °C), primer annealing (20 s at the optimized annealing

temperature), and extension (20 s at 72 °C). Product fluorescence intensity was detected at the end of each extension step. A melting curve was performed at the end of the qRT-PCR protocol by monitoring product fluorescence intensity from 65 °C to 95 °C, with a temperature increase rate of 0.5 °C.5 s^{-1}. The expression levels of the target genes – *indoleamine 2,3-dioxygenase (Ido)*, *interferon γ (Ifnγ)*, *inducible nitric oxide synthase (Inos)*, and *tumor necrosis factor (Tnf)* – were normalized for the expression level of the reference genes – *β₂ microglobulin (B2m)*, and *14-3-3 ζ protein (Ywhaz)*. Data analysis was performed in the software CXF Maestro (Bio-Rad), considering the ΔΔ threshold cycle (Ct) quantification method and the efficiency of the qRT-PCR protocol (Livak and Schmittgen, 2001).

Table 6. List, sequence, and optimized annealing temperature of the oligonucleotide primers used in the qRT-PCR of colon inflammatory marker genes.

Gene	Sense sequence	Antisense sequence	AT (°C)
Ido	5'-GGC TTC TTC CTC GTC TCT CTA TTG-3'	5'-TGA CGC TCT ACT GCA CTG GAT AC-3'	58
Ifnγ	5'-CAA CAG CAA GGC GAA AAA GG-3'	5'-GGA CCA CTC GGA TGA GCT CA-3'	58
Inos	5'-CTC GGA GGT TCA CCT CAC TGT-3'	5'-GCT GGA AGC CAC TGA CAC TT-3'	59
Tnf	5'-TGC CTA TGT CTC AGC CTC TTC-3'	5'-GAG GCC ATT TGG GAA CTT CT-3'	58
*B2m**	5'-CCT TCA GCA AGG ACT GGT CT-3'	5'-TCT CGA TCC CAG TAG ACG GT-3'	58
*Ywhaz**	5'-TAG GTC ATC GTG GAG GGT CG-3'	5'-GAA GCA TTG GGG ATC AAG AAC TT-3'	58

AT – annealing temperature. *Used as a reference gene.

3.10 Hippocampal stereological analysis

Brains were processed for hippocampal stereological analysis as previously described (Keuker, Vollmann-Honsdorf and Fuchs, 2001). After fixation with 4% PFA, brains were embedded in glycolmethacrylate (Tecnovit, 7100; Heraeus Kulzer, Werheim, Germany) and 30 μm thick coronal brain sections were obtained using a microtome (CN: RM2125-RTS; Leica Biosystems, Wetzlar, Germany). Every other section was collected on a non-coated glass slide, stained with Giemsa for 2 min, and coverslipped using entellan (CN: 1.07961; Sigma-Aldrich). Each brain was coded to keep the researcher blind to the genotype. The hippocampus was analyzed according to its main anatomical subregions: DG, CA1, and CA3. The DG (molecular layer [ml], granule cell layer [gcl], and polymorph layer [pl]) and CA1 and CA3 (*stratum oriens* [so], pyramidal cell layer [pcl], and *stratum radiatum* [sr]) layers were delimited according to the mouse brain atlas (Mackenzie-Graham *et al.*, 2004). The hippocampal stereological analysis was further divided accordingly to the dorsal-ventral axis. For each genotype, 6 animals were analyzed and, for each one, the 2 brain hemispheres were evaluated independently (total of 12 brain hemispheres per genotype). Volumes of the different hippocampal subregions were determined using

Cavalieri's principle (Gundersen *et al.*, 1988). Briefly, every fourth section was used, and the reconstruction of the cross-sectional area of each hippocampal subregion was assessed by manual tracing. The volume of each hippocampal subregion was then calculated from the cross-sectional area of each hippocampal subregion and the distance between the systematically sampled sections. The number of neurons in the DG-gcl and the CA1-pcl and CA3-pcl was estimated using the optical fractionator method (West, Slomianka and Gundersen, 1991). For this, we randomly superimposed a grid layout onto every traced cross-sectional area of each hippocampal subregion, with each grid space measuring 150 μm (length) × 150 μm (width) for the DG and 200 μm (length) × 200 μm (width) for the CA1 and CA3. On the top left corner of each grid space, a virtual 3-dimensional counting box was placed. For the DG, the counting box measured 20 μm (length) × 20 μm (width) × 15 μm (height) and for the CA1 and CA3 measured 40 μm (length) × 40 μm (width) × 15 μm (height). Neurons were counted whenever their nucleus (identified by size, shape, and the prominent nucleoli) came into focus within each counting box. Estimations of volume and number of neurons were performed using the tracing software StereoInvestigator (MBF Bioscience, Vermont, USA) and a motorized light microscope (CN: BX53; Olympus).

3.11 Hippocampal 3-dimensional neuronal reconstruction and dendritic spine characterization

Brains were processed for 3-dimensional neuronal reconstruction and dendritic spine characterization as previously described (Gibb and Kolb, 1998). After staining with Golgi-Cox solution for 21 days and transferring to a 30% sucrose solution, 200 μm thick coronal brain sections were sliced in a 6% sucrose solution using a vibratome (CN: VT1000-S; Leica Biosystems). Every section was blotted dry onto a gelatin-coated glass slide, alkalinized in an 18.7% ammonia solution, revealed in Dektol (CN: 516-0270; Kodak, New York, USA), fixed in Kodak Rapid Fix (CN: 146-4106; Kodak), dehydrated in a series of decreasing concentration ethanol solutions, cleared with xylene and coverslipped using entellan (CN: 1.07961; Sigma-Aldrich). All incubation steps were done in a dark room. Each brain was coded to keep the researcher blind to the genotype. Neurons of the main anatomical subregions of the hippocampus (DG, CA1, and CA3) were reconstructed according to the mouse brain atlas (Mackenzie-Graham *et al.*, 2004). The reconstruction of the DG neurons was further divided accordingly to the dorsal-ventral axis. For each genotype, 6 animals were analyzed and, for each one, 6 neurons per subregion were reconstructed independently (total of 36 neurons per genotype in each subregion). Brain sections containing the

subregions of interest were randomly searched, and a maximum of 3 neurons per section was selected for reconstruction in every subregion. The neurons selected for reconstruction met the following predefined criteria: (1) full Golgi-Cox solution impregnation along the entire dendritic arborization; (2) complete dendrites without truncated branches; and (3) isolation from neighboring impregnated neurons, astrocytes, or blood vessels. For each selected neuron, all branches of the dendritic arborization (both apical and basal arborizations in the case of the CA1 and CA3 neurons) were reconstructed by manual tracing. A 3-dimensional analysis of the reconstructed neurons was performed using the software NeuroExplorer (MicroBright Field, Vermont, USA). The length and complexity of the dendritic arborization were examined by the total dendritic length, the number of dendritic ends, and the arrangement of the dendrites using a 3-dimensional version of the Sholl analysis of intersections (Sholl, 1956). The number of dendritic intersections with concentric spheres positioned at radial intervals of 10 μm from the center of the neuronal soma was registered. After the neuronal reconstruction, the dendritic spine density of the selected neurons was calculated as the number of dendritic spines in a 30 μm length dendritic segment. Both proximal and distal dendritic segments to the neuronal soma were evaluated in each neuron. The evaluation of the dendritic spine density of the CA1 and CA3 neurons was performed independently in the apical and basal arborizations. Each dendritic spine in the selected segments was manually counted and morphological classified as thin, thick, mushroom, or ramified (Figure 14), as previously reported by other authors (Harris, Jensen and Tsao, 1992; Risher *et al.*, 2014; Maiti *et al.*, 2015).

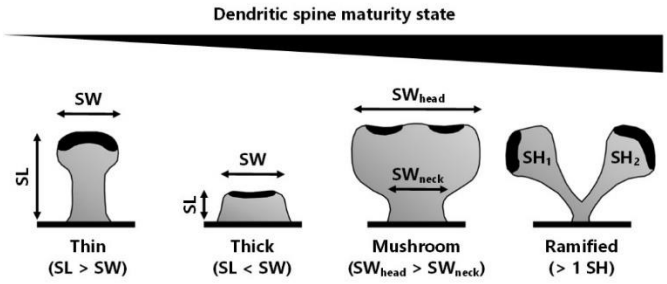

Figure 14. Dendritic spine morphological classification. From left to right, dendritic spines and are shown in ascending order of maturity state. The dendritic spine formation starts with thin filopodia-like structures (thin spines), which become mature wide-headed (mushroom spines), or, occasionally, cup-shaped structures (ramified spines) through a series of developmental stages. The morphological criteria for the classification assignment of each dendritic spine are shown. Abbreviations: SH - spine head; SL - spine length; SW - spine width. Adapted (Maiti *et al.*, 2015).

Briefly, in ascending order of maturity state, dendritic spines were considered: thin when the spine length was higher than spine width; thick when the spine length was lower than spine width; mushroom when the spine head was thicker than the spine neck; or ramified when the spine had more

than one spine head. The hippocampal 3-dimensional neuronal reconstruction and the dendritic spine characterization were performed using the tracing software Neurolucida (MicroBright Field) and a motorized light microscope (CN: BX53; Olympus).

3.12 Flow cytometry analysis

Flow cytometry was used to phenotypically evaluate the leukocyte profile in the blood and the ingLN and dcLN of IL-10 KO and WT mice.

3.12.1 Blood

At the end of the behavioral testing, blood samples were collected to heparin-coated capillaries by tail-clipping. To perform the leukocyte profile evaluation, 50 μL of blood were incubated for 20 min with a combination of monoclonal antibodies (**Table 7**), diluted in FACS buffer (0.50% bovine serum albumin and 0.01% sodium azide in PBS [137mM sodium chloride, 2.7mM potassium chloride, 10mM disodium hydrogen phosphate, and 1.8mM potassium dihydrogen phosphate; pH = 7.2]). An unstained control was performed to assess the level of autofluorescence in the samples and a single stained control for each antibody was used to determine the compensation matrix to overcome fluorochrome spectral overlap. Erythrocytes were lysed by incubation for 10 min in ACK lysis buffer (0.15 mM ammonium chloride, 10 mM potassium bicarbonate, and 0.10 mM ethylenediaminetetraacetic acid; pH = 7.2), and the samples were washed twice in FACS buffer. Samples were centrifuged for 5 min at 550 G between washes. All incubation steps were done at room temperature in the dark. After the last centrifugation, the cell pellet was resuspended in 100 μL of FACS buffer. All samples were acquired (minimum of 10^6 $CD45^+$ events per sample) on a LSR II Flow Cytometer (BD Biosciences, New Jersey, USA) equipped with the software FACSDiva v.9 (BD Biosciences). Data were analyzed using the software FlowJo v.10.7.1 (BD Biosciences). The gating strategies used to assess the percentage of the major leukocyte populations of the innate and adaptive immune systems in the blood are represented respectively in **Supplementary figures 1 and 2**. To evaluate the number of leukocytes per μL, 10 μL of blood were incubated with 10 μL of anti-mouse CD45 (clone: 30-F11) PE antibody (BioLegend, California, USA) at a dilution of 1:200 in FACS buffer, for 15 min. Then, samples were incubated for 15 min with 370 μL of ACK lysis buffer. All incubation steps were done at room temperature in the dark. Lastly, 10 μL of AccuCheck Counting Beads (CN: PCB100; Invitrogen, California, USA) were added and all samples were acquired (minimum of 2,000

counting bead events per sample) using the same equipment previously described in the blood phenotyping. The number of leukocytes per μL of peripheral blood was estimated using the software FlowJo v.10.7.1 (BD Biosciences) and following the instructions provided by the counting beads manufacturer.

Table 7. List of monoclonal antibodies used for the leukocyte profile evaluation by flow cytometry.

Antibody	Clone	Coupled fluorochrome	Working dilution	Manufacturer
Anti-mouse CD3	145-2C11	PE-Cy7	1:100	BioLegend, California, USA
Anti-mouse CD19	6D5	PerCP-Cy5.5		
Anti-mouse CD45	104	BV786		
Anti-mouse CD44	IM7	APC	1:200	
Anti-mouse CD4	GK1.5	BV450	1:400	
Anti-mouse CD8	53-6.7	BV500	1:800	
Anti-mouse Ly6C	HK1.4	BV711	1:1200	
*Anti-mouse Ly6G**	1A8	BV650		
*Anti-mouse CD49b**	DX5	FITC	1:50	eBioscience, California, USA
Anti-mouse CD62L	MEL-14	PE	1:100	

*Not used in the leukocyte profile evaluation of the lymph nodes.

3.12.2 Inguinal and deep cervical lymph nodes

Single-cell suspensions of the lymph nodes were obtained by mechanical dissociation in complete RPMI medium (RPMI 1640 Medium [CN: 11875101; Gibco, California, USA], 10% heat-inactivated fetal bovine serum [CN: TMS-013-B; Sigma-Aldrich], 100 $U.mL^{-1}$ of penicillin-streptomycin [CN: 15140148; Gibco], and 1mM sodium pyruvate). The Countess Automated Cell Counter (CN: C10227; Invitrogen) was used to evaluate the total number of leukocytes in the lymph nodes by the trypan blue dye exclusion method. To perform the leukocyte phenotyping, 10^6 lymph node cells were incubated for 20 min with the same combination of monoclonal antibodies used for the peripheral blood (but in this case without the anti-mouse Ly6G and CD49b antibodies; **Table 7**). An unstained control and a single stained control for each antibody were also performed. Afterward, the samples were washed twice in FACS buffer and centrifuged for 5 min at 550 G between washes. Then, samples were fixed with 200 μL of 2% PFA for 30 min and, again, washed and centrifuged twice. All incubation steps were done at room temperature and in the dark. After the last centrifugation, the cell pellet was resuspended in 100 μL of FACS buffer. Samples were acquired within 24 h using the same equipment previously described in the blood phenotyping. Data were analyzed using the software FlowJo v.10.7.1 (BD Biosciences). The gating strategy used to assess the percentage of the major leukocyte populations in the lymph nodes is represented in **Supplementary figure 3**.

3.13 Gut microbiota depletion protocol

In *Part 2* of this thesis, mice were submitted to a gut microbiome depletion protocol. Two independent gut microbiome depletion protocol optimization sets were performed.

3.13.1 Antibiotic treatment

The gut microbiome depletion was induced by a 10-day antibiotic treatment performed by oral gavage, as previously described (Hill *et al.*, 2010; Kennedy, King and Baldridge, 2018). Briefly, for 10 consecutive days, treated mice were subjected to daily oral gavage of freshly prepared antibiotic cocktail containing ampicillin (1 $mg.mL^{-1}$; CN: A9518), gentamicin (11 $mg.Kg^{-1}$; CN: G4918), metronidazole (11 $mg.Kg^{-1}$; CN: M1547), neomycin (11 $mg.Kg^{-1}$; CN: N6386), and vancomycin (4.5 $mg.Kg^{-1}$; CN: V2002), manufactured by Sigma-Aldrich, diluted in sterile water and delivered with a stainless-steel feeding tube without prior sedation of the mice. Age- and genotype-matched control mice received water *ad libitum* only. To assess the possible negative impact of antibiotic treatment on animal welfare, body weight and general signs of sickness and distress were monitored every day. After the antibiotic treatment, the cecum was collected, weighed and its longitudinal area was calculated using the software ImageJ (National Institutes of Health, Maryland, USA).

3.13.2 Fecal sample collections and quantification of colony-forming units

The day before and throughout the 10-day antibiotic treatment, fecal samples were collected to evaluate the effectiveness of the gut microbiome depletion by quantification of colony-forming units (CFUs) of aerobic and anaerobic bacteria, and by relative quantification of bacterial and fungal genes by qRT-PCR (**Table 8**). For the collection of fecal samples, mice were placed into individual boxes under a laminar flow hood in sterile conditions and left for 10 min to defecate. For the quantification of CFUs, 1-2 fecal pellets were placed into pre-weighed sterile nuclease-free tubes prefilled with 1 mL of cold sterile 0.9% saline solution. Then, the weight of the fecal pellet was calculated. All steps were done on ice. For qRT-PCR, 1-2 fecal pellets were placed into sterile nuclease-free tubes and stored at -80 °C until further use.

The fecal pellets placed in cold sterile 0.9% saline solution were disintegrated by bashing with a small sterile plastic inoculation loop and vigorous shaking. Five serial dilutions of 1.10^{-1} made in cold sterile 0.9% saline solution of the fecal suspension were made and 100 µL of each one were then plated

Table 8. Fecal samples collections.

Set number	Evaluation method	Antibiotic treatment time (days)										
		0	1	2	3	4	5	6	7	8	9	10
Set 1	Aerobic cultivation	×*			×				×			×
	Anaerobic cultivation	×*			×				×			×
	qRT-PCR	×			×				×			
Set 2	Aerobic cultivation	×	×		×		×					×
	Anaerobic cultivation	×	×		×			×				

*Fecal samples from day 0 of the antibiotic treatment of set 1 for aerobic and anaerobic cultivation of bacteria were unutilized due to an experimental problem.

on Columbia 5% sheep blood agar plates (CN: 43049; bioMérieux, Marcy-l'Étoile, France). Plates for the quantification of CFUs of aerobic bacteria were incubated aerobically at 37 °C with 5% carbon dioxide for 48 h, while for the quantification of CFUs of anaerobic bacteria, were incubated at room temperature in anaerobic conditions for 96 h. At the end of incubation time, the number of aerobic and anaerobic CFUs.mg^{-1} of feces was calculated.

3.13.3 Fecal DNA extraction and quantitative real-time PCR of bacterial and fungal genes

DNA was extracted from fecal pellets using the NucleoSpin DNA Stool kit (CN: 740472.50; Macherey-Nagel, Düren, Germany). DNA concentration was assessed using the NanoDrop 1000 Spectrophotometer (ThermoFisher Scientific) and the samples were diluted to a final concentration of 6.25 µg of RNA per µL and kept at -20 °C. The relative quantification of bacterial and fungal genes was evaluated by qRT-PCR on a CFX96 Touch qRT-PCR System (Bio-Rad). To perform the qRT-PCR, a reaction mixture was prepared and 12 µL of it were added to 8 µL of the DNA template sample (corresponding to 50 ng of DNA). The reaction mixture reagents were diluted to a final concentration of 1 × concentrate SsoFast EvaGreen Supermix (CN: 172-5202; Bio-Rad), and 0.5 µM.L^{-1} of each specific oligonucleotide primer (**Table 9**). The qRT-PCR protocol was designed to have an initial activation step (2 min at 98 °C), followed by 40 cycles of denaturation (5 s at 98 °C) and primer annealing/extension (5 s at the optimized annealing temperature). Product fluorescence intensity was detected at the end of each extension step. A melting curve was performed at the end of the qRT-PCR protocol by monitoring product fluorescence intensity from 65 °C to 95 °C, with a temperature increase rate of 0.5 °C.5 s^{-1}. The expression levels of the target genes – bacterial *16s ribosomal RNA (16s)*, and *fungal internal transcribed spacer 2 (Its2)* – were normalized for the expression level of the reference gene – *mouse polymeric immunoglobulin receptor (Mpigr)*. Gene expression throughout the 10-day antibiotic treatment was further relativized for

the gene expression on day 0 of the antibiotic treatment for each mouse. Data analysis was performed in the software CXF Maestro (Bio-Rad), considering the ΔΔ Ct quantification method and the efficiency of the qRT-PCR protocol (Livak and Schmittgen, 2001).

Table 9. List, sequence, and optimized annealing temperature of the oligonucleotide primers used in the qRT-PCR of gut microbiota genes.

Gene	Sense sequence	Antisense sequence	AT (°C)
16s	5'-GGT GAA TAC GTT CCC GG-3'	5'-TAC GGC TAC CTT GTT ACG ACT T-3'	60
Its2	5'-GCA TCG ATG AAG AAC GCA GC-3'	5'-TTG ATA TGC TTA AGT TCA GCG G-3'	60
*Mpigr**	5'-TTT GCT CCT GGG CCT CCA AGT T-3'	5'-AGC CCG TGA CTG CCA CAA ATC A-3'	59

AT – annealing temperature. *Used as a reference gene.

3.14 Data analysis

Statistical data analysis was performed using the software IBM SPSS Statistics v.26 (International Business Machines Corporation, New York, USA) and GraphPad Prism v.8 (GraphPad Software, California, USA). Additionally, computational data analysis was achieved using custom-written MATLAB codes (**Annex 1**) on the software MATLAB R2020b (MathWorks, Massachusetts, USA).

3.14.1 Statistical data analysis

The normal distribution was assessed by the Kolmogorov-Smirnov test and the Levene test was used to assess whether the variances were similar. Statistical significance was considered for p-values < 0.05. Data with normal distribution were presented as mean ± standard error of the mean (SEM), otherwise were presented as median ± interquartile range (IQR). Outlier data points in the behavioral performance results were removed using the robust regression and outlier removal (ROUT) method with Q = 1%. For behavioral tests that were performed on more than one animal set, the z-score value of each data point was calculated, and the distinct animal sets were then combined. Non-behavioral results of the distinct animal sets were also combined but without the z-score transformation. To compare two groups within a data set, the two-tailed independent samples Student's t-test was applied, when normal distribution was confirmed, otherwise the Mann-Whitney U test was used. To compare the distributions of two non-stratified categorical features, the Fisher's exact test was used. To compare the distributions of two categorical features, one of them being stratified, the Cochran-Armitage χ^2 test for trend was applied. To compare more than two groups, the two-way analysis of variance (ANOVA) was

used as a parametric approach and the Kruskal-Wallis *H* test as a non-parametric approach. If an evaluation of two or more groups along time was required, a two-way repeated-measures ANOVA was performed to data sets with normal distribution, and the Friedman test to data sets with non-normal distribution. As a *post hoc* analysis, the Sidak's multiple comparisons test was applied to data sets previously analyzed by the two-way ANOVA or the two-way repeated-measures ANOVA, and the Dunn's multiple comparisons test to data sets previously analyzed by the Kruskal-Wallis *H* test or the Friedman test. To correlate the data sets with each other, the Pearson's correlation coefficients (*r*) test was performed for data with normal distribution, and the Spearman's rank correlation coefficient (ρ) test for data with non-normal distribution. Lastly, effect size statistics (**Table 10**) were used to quantify the relationship strength between two variables, regardless of the sample size.

Table 10. Interpretation of effect size statistics.

Effect size	Interpretation			Reference
	Small	Medium	Large	
D	$d < 0.50$	$0.50 \leq d < 0.80$	$d \geq 0.80$	(Cohen, 1988)
r_u	$r_u < 0.30$	$0.30 \leq r_u < 0.50$	$r_u \geq 0.50$	
ϕ_c	$\phi_c < 0.30$	$0.30 \leq \phi_c < 0.50$	$\phi_c \geq 0.50$	
η^2	$\eta^2 < 0.06$	$0.06 \leq \eta^2 < 0.14$	$\eta^2 \geq 0.14$	
η_p^2	$\eta_p^2 < 0.09$	$0.09 \leq \eta_p^2 < 0.25$	$\eta_p^2 \geq 0.25$	(Cohen *et al.*, 2002)
W	$W < 0.10$	$0.10 \leq W < 0.30$	$W \geq 0.30$	(Kendall and Smith, 1939)

Distinct effect size statistics were applied in each of the statistical tests performed, as follow: the Cohen's D (*d*) effect size for the two-tailed independent samples Student's *t*-test and the Sidak's multiple comparisons test; the Rosenthal's R (r_u) effect size for the Mann-Whitney *U* test and the Dunn's multiple comparisons test; the Cramér's V (ϕ_c) effect size for the Fisher's exact test and the Cochran-Armitage χ^2 test for trend; the Eta Squared (η^2) effect size for the Kruskal-Wallis *H* test; the Partial Eta Squared (η_p^2) effect size for the two-way ANOVA and the two-way repeated-measures ANOVA; and the Kendall's Coefficient of Concordance (*W*) effect size for the Friedman test.

3.14.2 Computational data analysis

Unsupervised machine learning: an algorithm for data clustering

To split a data set into *k* clusters so that the data points in the same cluster are more similar to each other than those in other clusters, an unsupervised machine learning *k*-means clustering algorithm

was developed. Briefly, based on a partitioning strategy, the *k*-means clustering algorithm assigned membership to data points by measuring the distance from every data point to the centroid position of the designated *k* clusters. The centroid positions of the designated *k* clusters were recalculated, and the membership assignment of each data point was progressively refined until the best possible assignment was yielded – when the within-cluster variance was minimized, and the between-cluster variance was maximized in a data set. To determine the optimal number of *k* clusters into which the data set should be clustered, the elbow method was used. For that, the *k*-means clustering algorithm ran on the dataset for a range of *k* values (from $k = 1$ to $k = 5$), and for each *k* value, the silhouette coefficient value was assessed as a confidence measure (Rousseeuw, 1987). However, the final quality of the membership assignment of each data point is largely dependent on the initial centroid positions at the beginning of the partitioning process. These initial centroid positions are randomly generated each time the *k*-means clustering algorithm starts, which are different over time (Fong *et al.*, 2014). To minimize this problem, the *k*-means clustering algorithm repeated for 100 × the partitioning process for each *k* value (100 × from $k = 1$ to $k = 5$). In each portioning process, the silhouette coefficient value was also assessed, and at the end of the 100 × partitioning processes, for each *k* value, the average silhouette coefficient value was calculated. The *k* value with the highest average silhouette coefficient value was selected for the final membership assignment of each data point.

Supervised machine learning: a hybrid algorithm for feature selection and data classification

To perform a binary classification of a data set, a supervised machine learning support vector machine (SVM) model was used, as previously described (Mountrakis, Im and Ogole, 2011; Nayak, Naik and Behera, 2015). Briefly, the SVM model with a linear kernel was trained. To perform the training, a 10-fold cross-validation step was performed by splitting the original data set into 10 subsets of similar size. Nine of them were considered the training data subset and the remaining one was considered the testing data subset. The SVM model training procedure created a linear hyperplane in a high-dimensional space using the features present in the training data subset. The linear hyperplane maximized the margins of separation of the data points of one class from those of the other class. The SVM model then aimed to classify the data points of the testing data subset, by assessing on which side of the linear hyperplane the data points were placed on. Lastly, the classification accuracy (accuracy = 1 - error) of the testing data subset was calculated. The time required for computing the SVM model is increased and the accuracy of the classification is adversely affected by data sets with a large number of features, a phenomenon that is known as the curse of dimensionality (Bellman, 1957). Thus, the exclusion of

redundant or irrelevant features before the classification by the SVM model is a very effective manner to improve classification accuracy. Here, a hybrid algorithm for feature selection and data classification was designed through the use of a genetic algorithm (GA) that optimizes the feature combination (by the presence or absence of a given feature) that generates the best classification accuracy in the SVM model – creating the GA + SVM model. The GA, initially conceptualized by John Holland, is a global search-optimization method based on Darwin's principle of natural selection and population genetics (Holland, 1975; Zhao *et al.*, 2011). The algorithm takes a random population of individuals, each one with a candidate solution of feature combinations, and applies the Darwinian principle known as the survival of the fittest, to find the individual with the optimized feature combination. In this case, the fittest individual is the one that generates the best classification accuracy in the SVM model. The GA was developed to have 50 generations. In each generation, a population of 500 individuals was classified through the SVM model. The population was replaced in each generation by a novel one created by 3 genetic operators: crossover, mutation, and rescue, as follows. The individuals that generate a classification error > 0.5 were automatically discarded, in each generation. In contrast, the fittest survivors were selected as the parental population. To the individuals of the parental populations was performed a random single feature crossover to produce the crossover population of feature combinations (75% of the novel population = 375 individuals). Also, to the individuals of the parental population was executed a 10% feature mutation (presence of a given feature becomes absent and *vice versa*) to produce the mutated population of feature combinations (24% of the novel population = 120 individuals). Lastly, the GA used an evolutionary strategy of rescuing the fittest individuals across generations, creating the elite population of feature combinations (1% of the novel population = 5 individuals). The crossover, the mutated, and the elite populations of feature combinations were then merged to create the novel population that replace the previous one and entered the GA in the following generation. When the 50^{th} generation was reached, the GA algorithm ended and the optimized individual feature combination that generated the best classification accuracy in the SVM model was retrieved and interpreted. The flowchart depicting the architectural concept of the GA-SVM model is represented in **Supplementary figure 4**.

CHAPTER 4

RESULTS

4.1 Cognitive behavior characterization

In *Part 1* of this thesis, to characterize the cognitive function of female IL-10 KO mice compared to their WT littermates, distinct behavioral tests were performed to evaluate spatial reference memory, spatial and recognition short-term memory, and spatial and non-spatial associative memory.

4.1.1 IL-10 absence impaired hippocampal-dependent spatial reference memory

IL-10 KO mice and WT littermates and were tested in BMT (**Figure 15A**) to assess spatial reference memory, which relies on the integrity of the hippocampus (Matthew, 2018). Both IL-10 KO and WT mice were able to successfully learn the location of the target hole during the learning phase of the BMT. The learning curve was independent of the genotype (time factor: $F_{(14, 952)} = 10.60$, $p < 0.001$,

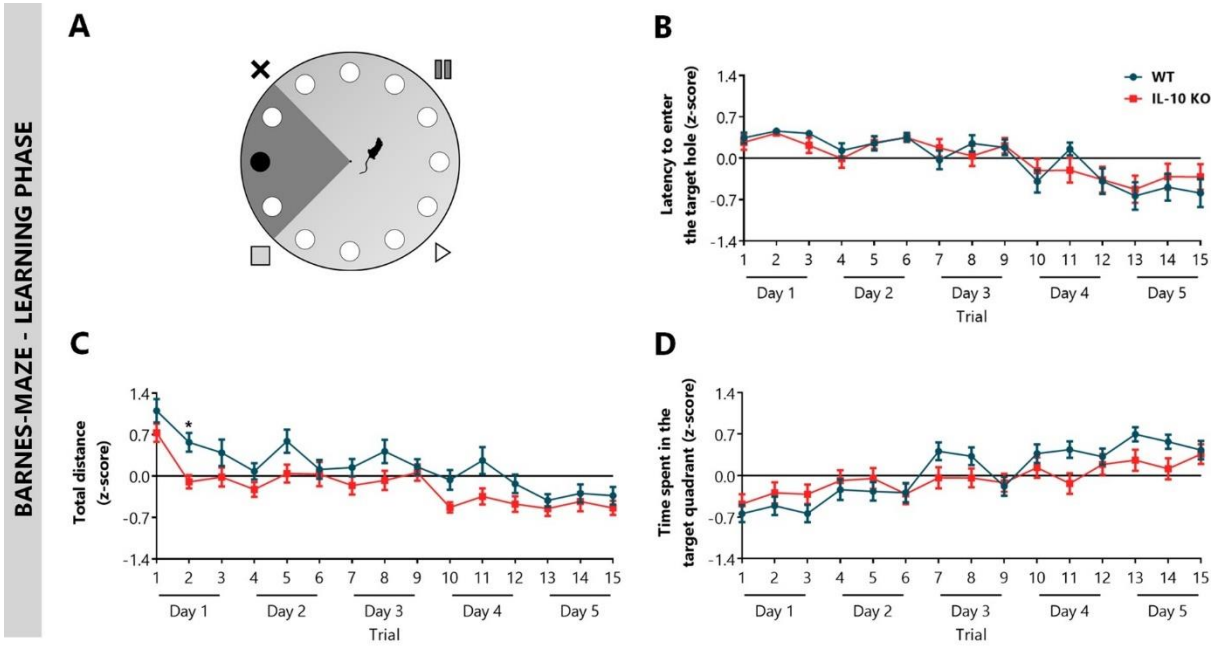

Figure 15. IL-10 absence did not impact spatial reference memory during the learning phase of the Barnes-maze test. **A.** Representation of the Barnes-maze test arena. A gray circular arena with 12 equidistant open holes contained in one of them (target hole - in black) an escape chamber that allowed the mice to take shelter. Directly above the arena, a light bulb was placed, and surrounding the maze visual cues were positioned. The target quadrant containing the target hole is shown in dark gray. **B.** Latency to enter the target hole. **C.** Total distance traveled in the arena. **D.** Time spent in the target quadrant. Data presented as mean ± SEM of z-scores of the values from two independent sets. $n_{WT} = 35$; $n_{IL\text{-}10\ KO} = 35$. Statistical analysis was performed by a two-way repeated-measures ANOVA. * $p < 0.05$.

$\eta_p^2 = 0.13$; genotype factor: $F_{(1, 68)} < 0.01$, $p = 0.996$, $\eta_p^2 < 0.01$; interaction: $F_{(14, 952)} = 0.73$, $p = 0.749$, $\eta_p^2 = 0.01$; **Figure 15B**). Moreover, IL-10 KO and WT mice significantly reduced the distance traveled in the arena during the learning phase of the BMT. Although IL-10 KO mice seem to move less than WT littermates, a *post hoc* analysis revealed significant differences only on trial 2 of the first testing day (trial 2: $p = 0.04$; $d = 0.82$; time factor: $F_{(14, 952)} = 11.74$, $p < 0.001$, $\eta_p^2 = 0.15$; genotype factor: $F_{(1, 68)} = 14.42$, $p < 0.001$, $\eta_p^2 = 0.17$; interaction: $F_{(14, 952)} = 0.80$, $p = 0.669$, $\eta_p^2 = 0.01$; **Figure 15C**). During the learning phase, both IL-10 KO and WT mice increased the time spent in the target quadrant, where the target hole is located. No differences were detected between genotypes (time factor: $F_{(14, 952)} = 10.37$, $p < 0.001$, $\eta_p^2 = 0.13$; genotype factor: $F_{(1, 68)} = 1.04$, $p = 0.311$, $\eta_p^2 = 0.02$; interaction: $F_{(14, 952)} = 2.02$, $p = 0.014$, $\eta_p^2 = 0.03$; **Figure 15D**).

To assess spatial memory retrieval, the probe trial was conducted by removing the escape chamber from the target hole (**Figure 16A**). According to the learning phase, both genotypes traveled same distances in the BMT arena during the probe trial ($U = 526.00$, $p = 0.313$, $r_u = 0.12$; **Figure 16B**).

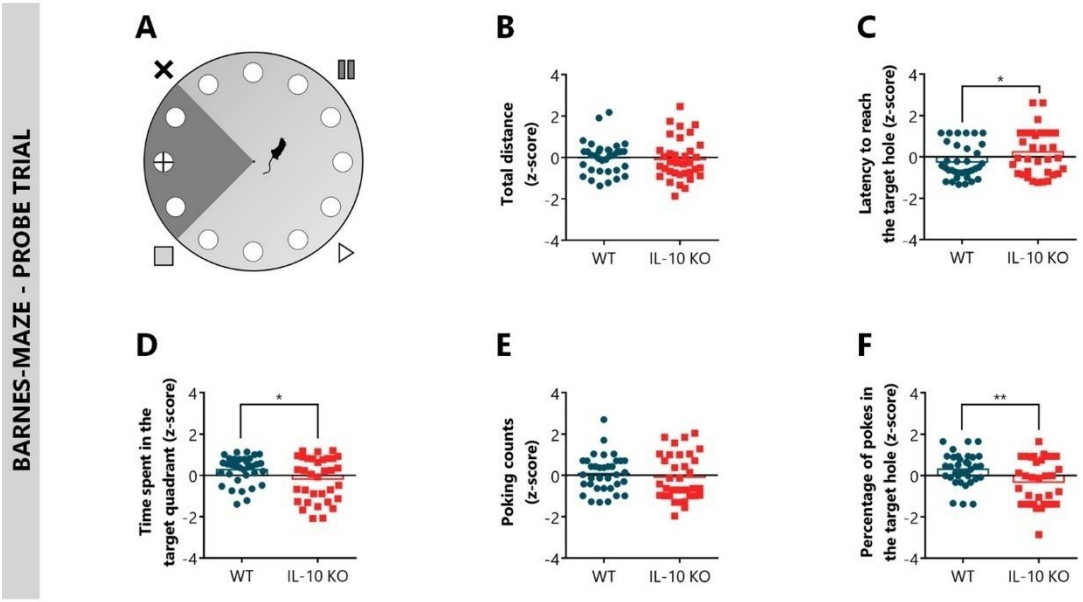

Figure 16. IL-10 absence impaired spatial reference memory during the probe trial of the Barnes-maze test. A. Representation of the Barnes-maze test arena. A gray circular arena contained 12 equidistant open holes. The former location of the target hole is shown with the + marker. Directly above the arena, a light bulb was placed, and surrounding the maze visual cues were positioned. The target quadrant containing the former location of the target hole is shown in dark gray. **B.** Total distance traveled in the arena. **C.** Latency to reach the former location of the target hole for the first time. **D.** Time spent in the target quadrant. **E.** Total number of nose pokes in the open holes. **F.** Percentage of nose pokes in the former location of the target hole. Data presented as median (**B**) or mean (**C-F**) of z-scores of the values from two independent sets. Each dot represents an animal. $n_{WT} = 35$; $n_{IL\text{-}10\ KO} = 35$. Statistical analysis was performed by Mann-Whitney *U* test (**B**) or a two-tailed independent samples *t*-test (**C-F**). * $p < 0.05$; ** $p < 0.01$.

However, in this trial, IL-10 KO mice took longer to reach the former location of the target hole for the first time ($t_{(68)} = 2.08$, $p = 0.041$, $d = 0.50$; **Figure 16C**) and spent less time in the target quadrant ($t_{(68)} = 2.44$, $p = 0.017$, $d = 0.58$; **Figure 16D**), when compared to WT littermates. Interestingly, although IL-10 KO mice performed a similar total number of nose pokes in the open holes ($t_{(68)} = 0.72$, $p = 0.472$, $d = 0.17$; **Figure 16E**), they were less correct than WT mice when poking the former location of the target hole ($t_{(68)} = 2.73$, $p = 0.008$, $d = 0.65$; **Figure 16F**).

Additionally, the classification of the paths taken by mice to find the location of the escape chamber revealed significant differences in the search strategies performed by mice of distinct genotypes during the learning phase of the BMT ($\chi^2_{(1)} = 42.79$, $p < 0.001$, $\phi_c = 0.20$; **Figure 17A**). Specifically, IL-10 KO mice performed less hippocampal-dependent strategies over time, namely the direct encounter ($\chi^2_{(1)} = 6.05$, $p = 0.014$, $\phi_c = 0.23$) and the direct approach ($\chi^2_{(1)} = 4.08$, $p = 0.043$, $\phi_c = 0.19$), than WT littermates. Regarding the exploratory strategies, no differences were found between genotypes in the serial exploration ($\chi^2_{(1)} = 2.80$, $p = 0.094$, $\phi_c = 0.11$), in the mixed exploration ($\chi^2_{(1)} = 0.56$, $p = 0.456$, $\phi_c = 0.07$), nor in the random exploration ($\chi^2_{(1)} = 0.55$, $p = 0.457$, $\phi_c = 0.07$). Lastly, concerning the freezing strategies, although IL-10 KO mice perform more freezing in the periphery ($\chi^2_{(1)} = 8.52$, $p = 0.004$, $\phi_c = 0.17$) when compared to WT controls, no differences were found between genotypes in the freezing

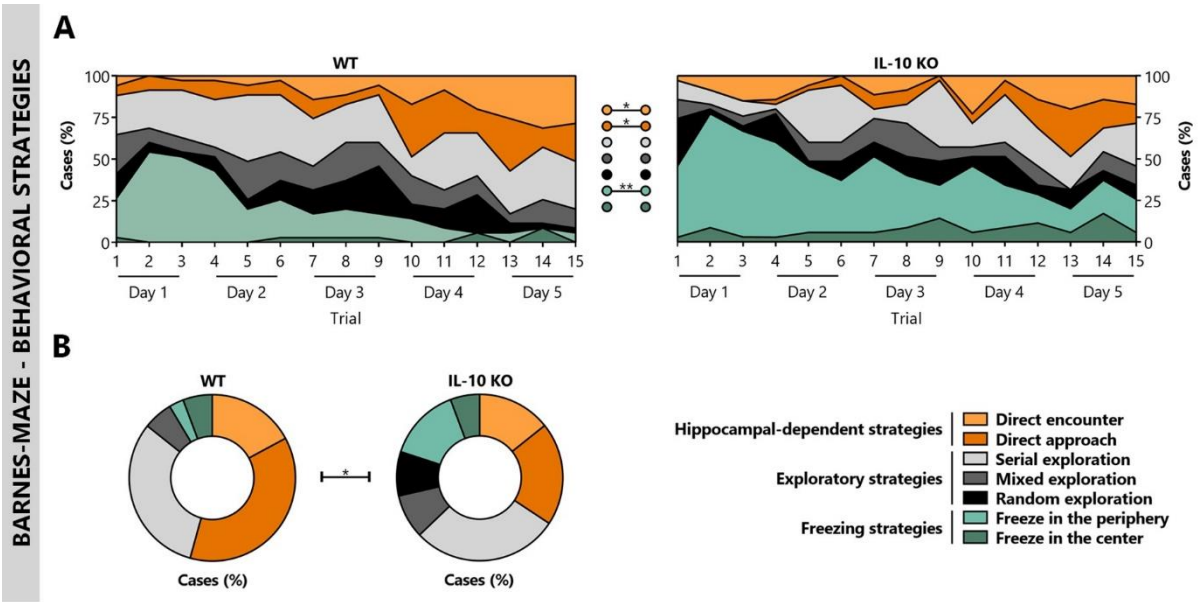

Figure 17. IL-10 absence led to a decreased percentage of hippocampal-dependent strategies used by mice to find the location of the escape chamber in the Barnes-maze test. A. Search strategies performed during the learning phase. **B.** Search strategies adopted during the probe trial. Data presented as the percentage of cases from two independent sets. $n_{WT} = 35$; $n_{IL\text{-}10\ KO} = 35$. Statistical analysis was performed by a Cochran-Armitage χ^2 test for trend. * $p < 0.05$; ** $p < 0.01$.

strategy in the center of the arena ($\chi^2_{(1)} = 0.11$, $p = 0.744$, $\phi_c = 0.05$). In the probe trial, the search strategies analysis showed significant differences in the search strategies performed by mice of distinct genotypes, with IL-10 KO mice performing a lower percentage of hippocampal-dependent strategies and a higher percentage of freezing strategies than WT mice ($\chi^2_{(1)} = 5.00$, $p = 0.025$, $\phi_c = 0.27$; **Figure 17B**). Overall, these results suggest that IL-10 absence impaired hippocampal-dependent spatial reference memory.

4.1.2 No alterations in spatial and recognition short-term memory were observed in IL-10 KO mice

IL-10 KO and WT mice were tested in the YMT (**Figure 18A**) and in the NORT (**Figure 18D**) to assess, respectively, spatial and recognition short-term memory. Both tests are based on the innate exploratory instinct of rodents and involve the hippocampus (Broadbent *et al.*, 2010; Kraeuter, Guest and Sarnyai, 2019). In the YMT, IL-10 KO and WT mice spent similar times exploring the novel arm ($t_{(26)} = 0.55$, $p = 0.589$, $d = 0.20$; **Figure 18B**). The value of this variable was in most mice of both genotypes greater than the cut-off value that indicates a random exploration of the novel arm (33.3% dotted line; **Figure 18B**). Additionally, IL-10 KO mice explored less the YMT arena than WT controls, as shown by

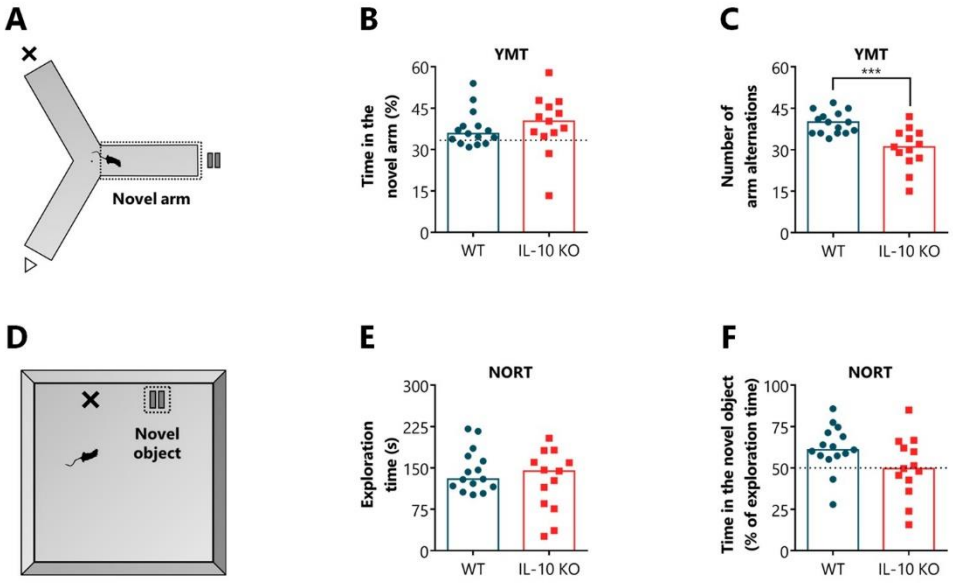

Figure 18. IL-10 absence did not impact spatial and recognition short-term memory. A. Representation of the testing trial of the Y-maze test. The novel arm location is highlighted. **B.** Percentage of time in the novel arm. The dotted line depicts the cut-off for a random time in the novel arm (33.3%). **C.** Total number of arm alternations. **D.** Representation of the testing trial of the novel object recognition test. The novel object location is highlighted. **E.** Total time that mice spent exploring both objects. **F.** Percentage of exploration time spent in the novel object. The dotted line depicts the cut-off for a random time in the novel object (50%). Data presented as mean of the values from one set. Each dot represents an animal. NORT – novel object recognition test; YMT – Y-maze test. $n_{WT} = 15$; $n_{IL\text{-}10\ KO} = 13$. Statistical analysis was performed by a two-tailed independent samples *t*test. *** $p < 0.001$.

the lower number of arm alternations ($t_{(26)} = 4.22$, $p < 0.001$, $d = 1.57$; **Figure 18C**). Concerning the NORT, both genotypes presented similar total exploration times ($t_{(26)} = 1.01$, $p = 0.321$, $d = 0.38$; **Figure 18E**). The percentage of exploration time spent in the novel object was also similar between genotypes ($t_{(26)} = 1.88$, $p = 0.072$, $d = 0.70$; **Figure 18F**). However, the mean exploration time of IL-10 KO mice was very close to the cut-off value that indicates a random exploration of the novel object (50% dotted line; **Figure 18F**). Globally, these results suggest that IL-10 absence did not impact spatial and recognition short-term memory.

4.1.3 IL-10 deficiency did not impact spatial and non-spatial associative memory

The CCFCT evaluated hippocampal-dependent memory and the integrity of extrahippocampal memory circuits (Curzon, Rustay and Browman, 2009). In this test, the Pavlovian conditioned response was measured in two independent evaluations: (1) considering the freezing behavior, which is the typical species-specific response to fear, as the only conditioned response (Curzon, Rustay and Browman, 2009), and (2) considering other phenotypes (tail rattle, vigorous grooming, vivid tremor, and intense jumping) besides freezing as the conditioned response since they had not been observed before the CS-US pairings in this mice strain.

Concerning the first evaluation (**Supplementary figure 5**), both IL-10 KO and WT mice had similar basal times of freezing behavior before conditioning ($p = 0.997$, $d = 0.44$). However, after conditioning, IL-10 KO mice exhibited longer time of freezing behavior than WT mice ($p = 0.002$, $d = 0.67$), as revealed by a *post hoc* analysis of a two-way repeated-measures ANOVA (time factor: $F_{(4, 184)} = 36.96$, $p < 0.001$, $\eta_p^2 = 0.44$; genotype factor: $F_{(1, 46)} = 2.25$, $p = 0.141$, $\eta_p^2 = 0.05$; interaction: $F_{(4, 184)} = 2.81$, $p = 0.027$, $\eta_p^2 = 0.06$). No differences between genotypes were detected in the following trials (context probe: $p = 0.997$, $d = 0.10$; novel context: $p > 0.999$, $d = 0.12$; cue probe: $p = 0.997$, $d = 0.12$), nor in the context discrimination index ($t_{(46)} = 0.54$, $p = 0.593$, $d = 0.16$).

In the second evaluation, considering other phenotypes besides freezing as the conditioned response, IL-10 KO and WT mice had similar times of conditioned behaviors before ($p = 0.999$, $d = 0.40$) and after conditioning ($p = 0.113$, $d = 0.52$; **Figure 19A**). During the second testing day, IL-10 KO mice performed a similar time of conditioned behaviors during the context probe as WT mice ($p > 0.999$, $d = 0.06$), indicating that all mice recognized the context where they had been 24 h earlier. Switching to the novel context, both genotypes decreased the time of conditioned behaviors to levels similar to those of before conditioning ($p = 0.897$, $d = 0.53$), and presented a similar context discrimination index

($t_{(46)} = 0.90$, $p = 0.374$, $d = 0.26$; **Figure 19B**). Lastly, in the cue probe, mice increased the time of conditioned behaviors after the auditory cue presentation to levels similar to those of context probe, independently of the genotype (cue probe: $p = 0.10$, $d = 0.50$; time factor: $F_{(4, 184)} = 123.50$, $p < 0.001$, $\eta^2_p = 0.73$; genotype factor: $F_{(1, 46)} = 3.76$, $p = 0.059$, $\eta^2_p = 0.08$; interaction: $F_{(4, 184)} = 1.64$, $p = 0.167$, $\eta^2_p = 0.03$). Overall, these results indicate that IL-10 deficiency did not impact the hippocampal-dependent spatial associative memory nor the integrity of the extrahippocampal memory circuits involved in the non-spatial associative memory.

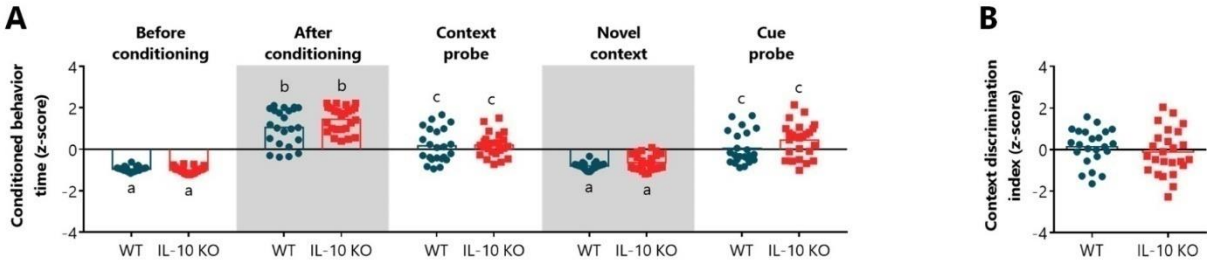

Figure 19. IL-10 absence did not impact spatial and non-spatial associative memory as assessed by the conditioned behavior time. A. Time that mice spent performing conditioned behaviors in each of the trials of the contextual and cued fear conditioning test. **B.** Context discrimination index considering the time that mice spent performing conditioned behaviors in the context probe and the novel context trials. Data presented as mean of z-scores of the values from two independent sets. Each dot represents an animal. $n_{WT} = 23$; $n_{IL\text{-}10\ KO} = 25$. Statistical analysis was performed by a two-way repeated-measures ANOVA (**A**) or a two-tailed independent samples *t*-test (**B**). Distinct and equal letters denote, respectively, statistically and non-statistically significant differences for $p < 0.05$ ("a" is significantly different from "b" and "c"; "b" is significantly different from "c").

4.1.4 IL-10 KO mice showed general and vertical exploration deficits but did not present locomotor nor anxious-like behavior alterations

The OFT (**Figure 20A**) was performed at the beginning of the behavioral assessment to assess locomotion, exploration, and anxious-like behavior. This test revealed that the general exploration of IL-10 KO mice was impaired, as they moved less than WT mice ($t_{(115)} = 3.52$, $p < 0.001$, $d = 0.65$; **Figure 20B**). Moreover, IL-10 KO mice did not present locomotor deficits nor anxious-like behavior alterations in the OFT, as the average velocity ($t_{(74)} = 1.00$, $p = 0.320$, $d = 0.23$; **Figure 20C**) and the percentage of distance traveled in the center of the arena ($t_{(115)} = 0.21$, $p = 0.835$, $d = 0.04$; **Figure 20D**) was similar to WT mice. The analysis of the vertical exploration showed a decrease in the duration ($t_{(74)} = 2.03$, $p = 0.046$, $d = 0.47$; **Figure 20E**) and number ($t_{(74)} = 2.26$, $p = 0.027$, $d = 0.52$; **Figure 20F**) of rearings of IL-10 KO mice compared to their WT counterpart, indicating that IL-10 absence led to vertical exploration deficits.

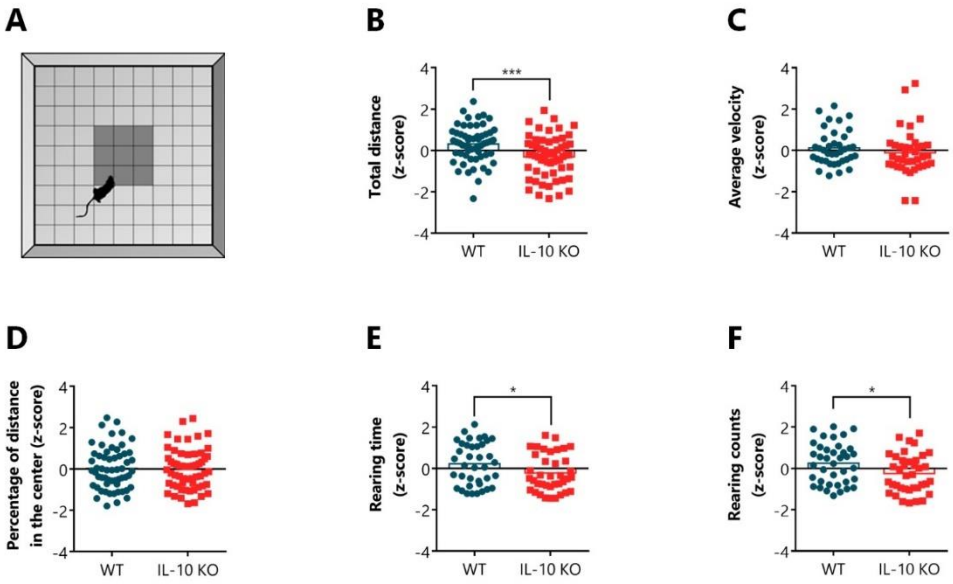

Figure 20. IL-10 absence impaired general and vertical exploration but did not affect locomotion nor anxious-like behavior. **A.** Representation of the open-field test arena. The center area of the arena is shown in dark gray. **B.** Total distance traveled in the arena. **C.** Average velocity in the trial. **D.** Percentage of distance traveled in the center of the arena. **E.** Time performing vertical exploration (rearings). **F.** Total number of rearings. Data presented as mean of z-scores of the values from four (**B**; **D**) or three (**C**; **E-F**) independent sets. Each dot represents an animal. n_{WT} = 58; $n_{IL\text{-}10\ KO}$ = 60 (**B**; **D**); n_{WT} = 38; $n_{IL\text{-}10\ KO}$ = 38 (**C**; **E-F**). Statistical analysis was performed by a two-tailed independent samples *t*test. * $p < 0.05$; *** $p < 0.001$.

4.1.5 Mice genotype (WT *vs* IL-10 KO) can be classified by SVM models using behavioral variables related to cognitive function

To examine if the variables obtained by the behavioral characterization were able to classify the mice genotype (WT *vs* IL-10 KO), the SVM model was used in the data sets from Set 1 + Set 2, Set 3, and Set 4. To assess if the classification accuracy could be raised by the exclusion of redundant or irrelevant variables, the hybrid GA + SVM model for feature selection and classification was also used in the same data set combination. The fitness of the classification models trained before and after feature selection by the GA for each data set was compared in terms of classification accuracy, sensitivity, and specificity. Since receiver-operating characteristic curves (ROC) and its area under the curve (AUC) analysis are significant discrimination tools of the performance of binary classification models (Flach, Hernández-Orallo and Ferri, 2011), they were also used to assess the fitness of the classification models. The results from the fitness of each classification model, the number of features used in the classification, and the elapsed time for algorithm processing are presented in **Table 11** and **Figure 21**.

On set 1 + set 2, the behavioral variables obtained in the OFT and BMT were used to classify the genotype of 70 animals (n_{WT} = 35; $n_{IL\text{-}10\ KO}$ = 35). In this data set, the use of all variables through the

Table 11. Fitness of the SVM and GA + SVM classification models performed for genotype classification.

Classification method		Initial number of features	Final number of features	Accuracy (%)	AUC	Sensitivity	Specificity	Elapsed time (s)
Set 1 + Set 2	*SVM*	7	7	70.6	0.75	0.77	0.64	0.23
	GA + SVM	7	3	75.0	0.81	0.83	0.67	1397.7
Set 3	*SVM*	15	15	75.0	0.84	0.80	0.69	0.32
	GA + SVM	15	5	89.3	0.88	1.00	0.77	1734.83
Set 4	*SVM*	11	11	50.0	0.44	0.13	0.75	0.26
	GA + SVM	11	3	60.0	0.54	0.50	0.67	1517.12

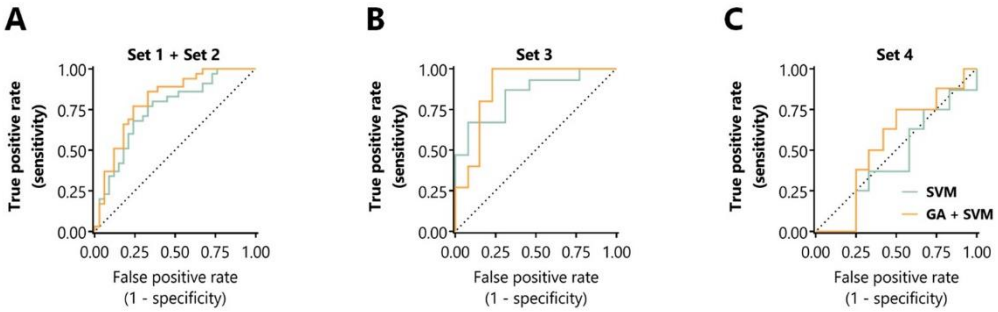

Figure 21. ROC curves of the SVM and the GA + SVM classification models performed for genotype classification. The variables of the behavioral tests performed in each set were used to train the classification models. **A.** ROC curves of the classification models trained before and after feature selection by the GA with variables of the open-field test and the Barnes-maze test of set 1 + set 2. **B.** ROC curves of the classification models trained before and after feature selection by the GA with variables of the open-field test, the Y-maze test, the novel object recognition test, and the contextual and cued fear conditioning test of set 3. **C.** ROC curves of the classification models trained before and after feature selection by the GA with variables of the open-field test and the contextual and cued fear conditioning test of set 4. The dotted line depicts the chance level. GA – genetic algorithm; ROC – receiver-operating characteristic; SVM – support vector machine.

SVM model led to a classification accuracy of 70.6%, far above the chance level (50.0%). After feature selection by the GA, 3 variables (total distance traveled in the OFT, latency to reach the target hole for the first time, and the number of pokes in the target hole on the probe trial of the BMT) were selected as the combination that generates the best classification accuracy. In the GA + SVM model, the classification accuracy increased to 75.0%, and the values of AUC, sensitivity, and specificity were higher than the SVM model alone. In contrast, on set 3, the behavioral variables obtained in the OFT, YMT, NORT, and CCFCT were used to classify the genotype of 28 animals (n_{WT} = 15; $n_{IL\text{-}10\ KO}$ = 13). The use of all variables through the SVM model led to a classification accuracy of 75.0%. However, the classification accuracy was further increased by the GA to 89.3%. In this data set, the sensitivity of the GA + SVM model was 1.00, indicating that all WT mice were successfully classified. The GA + SVM model selected the number of arm alternations in the YMT, the time exploring the novel object in the NORT, and the time of conditioned behaviors in the context probe, novel context, and cue probe of the CCFCT as the feature combination that generates the best classification accuracy. Lastly, on set 4, the behavioral variables

obtained in the OFT and CCFCT were used to predict the genotype of 20 animals (n_{WT} = 8; $n_{IL\text{-}10\ KO}$ = 12). In this data set, the use of all variables through the SVM model led to a classification accuracy equal to the chance level (50.0%). The GA + SVM model not only increased the classification accuracy to 60.0%, but also enlarged the values of AUC, sensitivity, and specificity. In this data set, the GA selected 3 features (total distance traveled in the OFT, the time of conditioned behaviors in the novel context of the CCFCT, and the discrimination index of the CCFCT) as the feature combination that generates the best classification accuracy. Overall, the GA + SVM classification models had classification accuracies higher than the chance level in all data set combinations, indicating that the mice genotype (WT *vs* IL-10 KO) can be classified through behavioral variables related to cognitive function.

4.2 Influence of the estrous cycle in the cognitive behavior characterization

The behavior of female mice could be influenced by hormonal fluctuation that occurs during the estrous cycle (Meziane *et al.*, 2007). Thus, to analyze the impact of the estrous cycle phase on behavioral data, vaginal smears were harvested immediately after each behavioral testing day and female mice of both genotypes were divided into two subgroups: PEF and DMF.

4.2.1 The estrous cycle influenced the behavior of IL-10 KO mice in the Barnes-maze test

The estrous cycle did not impact the spatial reference memory during the learning phase of the BMT of both genotypes (latency to enter the target hole: $F_{(42,\ 360)} = 0.53$, $p = 0.993$, $\eta_p^2 = 0.06$; total distance traveled in the arena: $F_{(42,\ 360)} = 1.16$, $p = 0.237$, $\eta_p^2 = 0.12$; time spent in the target quadrant: $F_{(42,\ 360)} = 1.11$, $p = 0.344$, $\eta_p^2 = 0.11$; **Supplementary figure 6A-C**). Additionally, the estrous cycle did not impact the behavior of both genotypes during the probe trial of the BMT (total distance traveled in the arena: $\chi^2_{H(3)} = 1.99$, $p = 0.575$, $\eta^2 = 0.04$; latency to reach the former location of the target hole: $\chi^2_{H(3)} = 5.60$, $p = 0.133$, $\eta^2 = 0.11$; time spent in the target quadrant: $\chi^2_{H(3)} = 0.48$, $p = 0.923$, $\eta^2 = 0.10$; total number of nose pokes in the open holes: $\chi^2_{H(3)} = 3.95$, $p = 0.267$, $\eta^2 = 0.04$; percentage of nose pokes in the former location of the target hole: $\chi^2_{H(3)} = 0.75$, $p = 0.861$, $\eta^2 = 0.09$; **Supplementary figure 6D-H**). The analysis of the search strategies used by mice to find the location of the escape chamber in the BMT revealed significant differences in the search strategies performed by IL-10 KO mice when

compared to WT littermates both on the PEF ($\chi^2_{(1)}$ = 16.76, p < 0.001, ϕ_c = 0.30) and MDF subgroups ($\chi^2_{(1)}$ = 12.79, p < 0.001, ϕ_c = 0.23) during the learning phase of the BMT (**Figure 22A**). Both IL-10 KO PEF ($\chi^2_{(1)}$ = 3.90, p = 0.048, ϕ_c = 0.30) and IL-10 KO MDF ($\chi^2_{(1)}$ = 6.52, p = 0.011, ϕ_c = 0.34) mice performed more freezing in the periphery of the BMT arena when compared to the WT counterparts. However, while IL-10 KO PEF mice perform less serial exploration than WT PEF mice ($\chi^2_{(1)}$ = 6.03, p = 0.014, ϕ_c = 0.42), IL-10 KO MDF mice perform less direct encounter than WT MDF mice ($\chi^2_{(1)}$ = 4.41, p = 0.036, ϕ_c = 0.34). Moreover, no general differences were found between WT mice of the PEF and MDF subgroups ($\chi^2_{(1)}$ = 0.01, p = 0.912, ϕ_c = 0.01) nor IL-10 KO mice of the PEF and MDF subgroups ($\chi^2_{(1)}$ = 1.02, p = 0.314, ϕ_c = 0.07). In the probe trial (**Figure 22B**), although the search strategies analysis exposed differences between IL-10 KO and WT mice on the MDF subgroup ($\chi^2_{(1)}$ = 4.07, p = 0.044, ϕ_c = 0.61), no differences were detected between genotypes on the PEF subgroup ($\chi^2_{(1)}$ = 0.56, p = 0.454, ϕ_c = 0.18). Also, no differences were found between WT mice of the PEF and MDF subgroups ($\chi^2_{(1)}$ = 1.02, p = 0.312, ϕ_c = 0.26). However, in this trial, IL-10 KO MDF mice performed less hippocampal-dependent strategies and more freezing strategies than IL-10 KO PEF mice ($\chi^2_{(1)}$ = 4.06, p = 0.044, ϕ_c = 0.56), which shows that the estrous cycle was impacting the search strategies used by IL-10 KO mice to find the location of the escape chamber in the probe trial of the BMT.

During YMT and NORT, no vaginal smears were collected, so the role of the estrus cycle in the spatial and recognition short-term memory of IL-10 KO and WT mice was not evaluated.

The estrous cycle did not influence the conditioning behavior during the CCFCT of both genotypes since no differences were found between mice in the PEF and MDF subgroups in this test (conditioning behavior through the 3 testing days: $F_{(12, 77)}$ = 0.33, p = 0.981, η^2_p = 0.05; context discrimination index: $\chi^2_{H(3)}$ = 2.52, p = 0.471, η^2 = 0.03; **Supplementary figure 6I-J**).

Lastly, the estrous cycle did not impact the behavior of both genotypes in the OFT (total distance traveled: $\chi^2_{H(3)}$ = 3.16, p = 0.368, η^2 = 0.01; average velocity: $\chi^2_{H(3)}$ = 3.19, p = 0.363, η^2 = 0.01; percentage of distance traveled in the center of the arena: $\chi^2_{H(3)}$ = 0.06, p = 0.996, η^2 = 0.18; time performing vertical exploration: $\chi^2_{H(3)}$ = 1.93, p = 0.587, η^2 = 0.07; total number of rearings: $\chi^2_{H(3)}$ = 1.20, p = 0.754, η^2 = 0.11; **Supplementary figure 6K-O**).

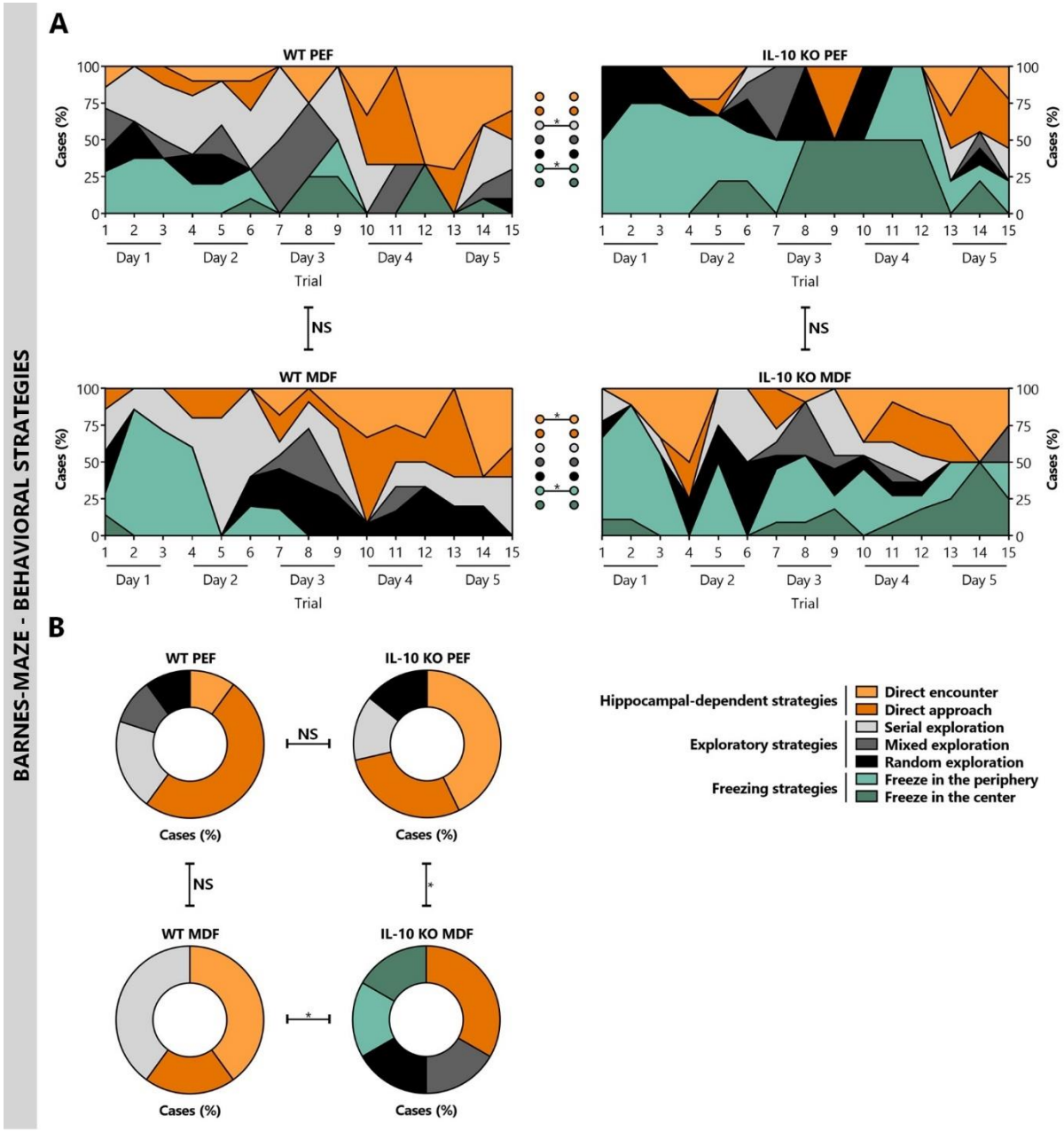

Figure 22. The estrous cycle influenced the strategies used by IL-10 KO mice to find the location of the escape chamber in the Barnes-maze test. A. Search strategies performed during the learning phase. **B.** Search strategies adopted during the probe trial. Data presented as the percentage of cases from one set. MDF – metestrus and diestrus females; NS – non-statistical significance; PEF – proestrus and estrous females. $n_{WT\ PEF}$ = 3-10; $n_{IL\text{-}10\ KO\ PEF}$ = 2-9; $n_{WT\ MDF}$ = 5-12; $n_{IL\text{-}10\ KO\ MDF}$ = 4-11 (**A**); $n_{WT\ PEF}$ = 10; $n_{IL\text{-}10\ KO\ PEF}$ = 7; $n_{WT\ MDF}$ = 5; $n_{IL\text{-}10\ KO\ MDF}$ = 6 (**B**). Statistical analysis was performed by a Cochran-Armitage χ^2 test for trend. * $p < 0.05$.

4.3 Influence of the colon inflammatory profile in the cognitive behavior characterization

It is established that IL-10 KO mice could spontaneously develop IBD (Sturlan *et al.*, 2001; Scheinin *et al.*, 2003), a condition characterized by increased colon inflammation (Rubin, Shaker and

Levin, 2012) that can impact the behavior of female mice (Nyuyki *et al.*, 2018). Thus, to analyze the impact of the colon inflammatory profile on behavioral data, the gene expression levels of pro-inflammatory markers were assessed by qRT-PCR.

4.3.1 IL-10 absence led to increased gene expression levels of pro-inflammatory markers in the colon

IL-10 KO mice presented higher gene expression levels of *Ido* ($U = 713.50$, $p < 0.001$, $r_U = 0.49$; **Figure 23A**), *Ifnγ* ($U = 1186.00$, $p = 0.009$, $r_U = 0.24$; **Figure 23B**), *Inos* ($U = 1076.50$, $p = 0.001$, $r_U = 0.30$; **Figure 23C**), and *Tnf* ($U = 815.50$, $p < 0.001$, $r_U = 0.44$; **Figure 23D**) than WT mice, in the colon.

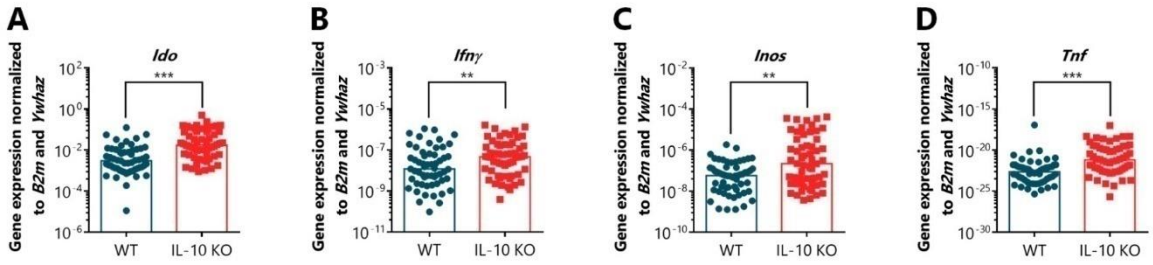

Figure 23. IL-10 absence led to increased gene expression levels of pro-inflammatory markers in the colon. Gene expression levels of *Ido* (**A**), *Ifnγ* (**B**), *Inos* (**C**), and *Tnf* (**D**) in the colon. The gene expression levels of pro-inflammatory markers were quantified through qRT-PCR and normalized to the gene expression levels of *B2m* and *Ywhaz* reference genes. Data presented as median of the values from four independent sets. Each dot represents an animal. $n_{WT} = 57$; $n_{IL\text{-}10\ KO} = 58$. Statistical analysis was performed by a Mann-Whitney *U* test. ** $p < 0.01$; *** $p < 0.001$.

4.3.2 IL-10 KO mice could be divided into 2 groups according to the colon inflammatory profile

To analyze the impact of the colon inflammatory profile on behavioral data, all mice were divided into *k* clusters according to the expression levels of pro-inflammatory markers in the colon. Executing a *k*-means clustering algorithm with *k* values ranging from 1 to 5, the optimal number of clusters was determined as being $k = 2$ (average silhouette coefficient value: 0.93; **Figure 24A**). With $k = 2$, all mice were successfully assigned, as the silhouette coefficient value of each one was higher than zero (**Figure 24B**). The gene expression levels of pro-inflammatory markers in the colon of mice assigned to the cluster 2 was higher than those assigned to the cluster 1 (*Ido*: $U < 0.01$, $p < 0.001$, $r_U = 0.63$; *Ifnγ*: $U = 233.50$, $p < 0.001$, $r_U = 0.46$; *Inos*: $U = 128.00$, $p < 0.001$, $r_U = 0.53$; *Tnf*: $U = 194.00$, $p < 0.001$, $r_U = 0.49$; **Figure 24C**). The proportion of WT and IL-10 KO mice in each cluster after the membership assignment was distinct (Fisher's exact test : $p < 0.001$; **Figure 24D**). While all WT mice

($n_{WT\ CLUSTER\ 1}$ = 57) were assigned to the cluster 1, 71% of IL-10 KO mice were assigned to the cluster 1 ($n_{IL\text{-}10\ KO\ CLUSTER\ 1}$ = 41) and the remaining 29% constituted the entire cluster 2 ($n_{IL\text{-}10\ KO\ CLUSTER\ 2}$ = 17).

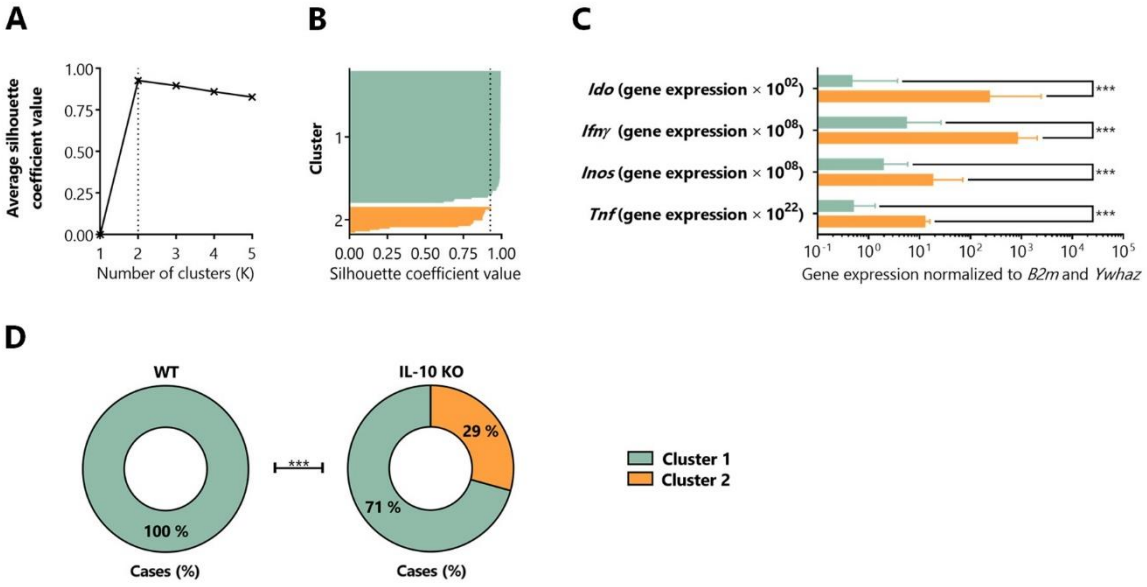

Figure 24. IL-10 KO mice were divided by a *k*-means clustering algorithm into 2 groups according to the colon inflammatory profile. A. Using the elbow method, the optimal number of clusters was determined. The dotted line depicts the k = 2 clusters. **B.** With k = 2, all mice had a silhouette coefficient value > 0 after the membership assignment. The dotted line depicts the average silhouette coefficient value for k = 2 clusters (0.93). **C.** Gene expression levels of *Ido*, *Ifnγ*, *Inos*, and *Tnf* normalized to *B2m* and *Ywhaz* in the colon of the animals from the distinct clusters. **D.** Proportion of WT and IL-10 KO mice in each cluster after the membership assignment. Data presented as median ± IQR of the values from four independent sets. $n_{WT\ CLUSTER\ 1}$ = 57; $n_{IL\text{-}10\ KO\ CLUSTER\ 1}$ = 41; $n_{IL\text{-}10\ KO\ CLUSTER\ 2}$ = 17. Statistical analysis was performed by a Mann-Whitney *U* test (**C**) or a Fisher's exact test (**D**). *** $p < 0.001$.

Interestingly, even after membership assignment, the gene expression levels of *Ido* and *Inos* remained increased in IL-10 KO mice assigned to the low inflammation cluster 1 (IC^{low}), when compared to WT mice. However, no longer differences were found in the gene expression levels of *Ifnγ* and *Tnf* between IL-10 KO IC^{low} and WT. The gene expression levels of all pro-inflammatory markers evaluated in the colon were raised in IL-10 KO mice assigned to the high inflammation cluster 2 (IC^{high}), when compared to IL-10 KO IC^{low} mice ([*Ido*: $\chi^2_{H(2)} = 50.19$, $p < 0.001$, $\eta^2 = 0.43$; WT IC^{low} *vs* IL-10 KO IC^{low}: $p = 0.009$, $r_u = 0.34$; IL-10 KO IC^{low} *vs* IL-10 KO IC^{high}: $p < 0.001$, $r_u = 0.78$]; [*Ifnγ*: $\chi^2_{H(2)} = 23.69$, $p < 0.001$, $\eta^2 = 0.19$; WT IC^{low} *vs* IL-10 KO IC^{low}: $p = 0.984$, $r_u = 0.09$; IL-10 KO IC^{low} *vs* IL-10 KO IC^{high}: $p < 0.001$, $r_u = 0.59$]; [*Inos*: $\chi^2_{H(2)} = 33.79$, $p < 0.001$, $\eta^2 = 0.28$; WT IC^{low} *vs* IL-10 KO IC^{low}: $p = 0.694$, $r_u = 0.10$; IL-10 KO IC^{low} *vs* IL-10 KO IC^{high}: $p < 0.001$, $r_u = 0.66$]; [*Tnf*: $\chi^2_{H(2)} = 36.39$,

$p < 0.001$, $\eta^2 = 0.31$; WT IC^{low} *vs* IL-10 KO IC^{low}: $p = 0.014$, $r_u = 0.29$; IL-10 KO IC^{low} *vs* IL-10 KO IC^{high}: $p < 0.001$, $r_u = 0.56$]; **Supplementary figure 7A-D**).

4.3.3 The colon inflammatory profile did not influence the behavior of IL-10 KO mice

After membership assignment, the behavioral performance of IL-10 KO IC^{low} and IL-10 KO IC^{high} mice was compared. The colon inflammatory profile did not impact the spatial reference memory during the learning phase of the BMT of IL-10 KO mice (latency to enter the target hole: $F_{(14, 448)} = 1.09$, $p = 0.362$, $\eta^2_p = 0.03$; total distance traveled in the arena: $F_{(14, 448)} = 1.56$, $p = 0.089$, $\eta^2_p = 0.05$; time spent in the target quadrant: $F_{(14, 448)} = 1.47$, $p = 0.117$, $\eta^2_p = 0.04$; **Supplementary figure 8A-C**). Additionally, the colon inflammatory profile did not impact the behavior of IL-10 KO mice during the probe trial of the BMT (total distance traveled in the arena: $t_{(32)} = 1.30$, $p = 0.203$, $d = 0.45$; latency to reach the former location of the target hole: $t_{(32)} = 0.48$, $p = 0.664$, $d = 0.16$; time spent in the target quadrant: $t_{(32)} = 0.75$, $p = 0.459$, $d = 0.27$; total number of nose pokes in the open holes: $t_{(32)} = 0.13$, $p = 0.894$, $d = 0.05$; percentage of nose pokes in the former location of the target hole: $t_{(32)} = 0.32$, $p = 0.755$, $d = 0.12$; **Supplementary figure 8D-H**). The analysis of the search strategies used by mice to find the location of the escape chamber in the BMT did not show any difference between IL-10 KO IC^{low} and IL-10 KO IC^{high} mice during the learning phase ($\chi^2_{(1)} < 0.01$, $p = 0.930$, $\phi_c < 0.01$; **Supplementary figure 9A**) nor the probe trial ($\chi^2_{(1)} < 0.01$, $p = 0.920$, $\phi_c = 0.02$; **Supplementary figure 9B**).

In the YMT, no differences were found between IL-10 KO IC^{low} and IL-10 KO IC^{high} mice (percentage of time in the novel arm: $U = 15.00$, $p = 0.849$, $r_u = 0.03$; total number of arm alternations: $U = 10.00$, $p = 0.346$, $r_u = 0.27$; **Supplementary figure 8I-J**). Regarding the NORT, the colon inflammatory profile also did not influence the behavior of IL-10 KO mice (total time of exploration: $U = 15.00$, $p = 0.849$, $r_u = 0.03$; percentage of exploration time spent in the novel object: $U = 13.00$, $p = 0.618$, $r_u = 0.12$; **Supplementary figure 8K-L**).

Moreover, the colon inflammatory profile did not impact the conditioning behavior during the CCFCT of IL-10 KO mice since no differences were found between clusters in this test (conditioning behavior through the 3 testing days: $F_{(4, 88)} = 0.58$, $p = 0.678$, $\eta^2_p = 0.03$; context discrimination index: $U = 38.00$, $p = 0.861$, $r_u = 0.02$; **Supplementary figure 8M-N**).

Lastly, the colon inflammatory profile did not impact the behavior of IL-10 KO mice in the OFT (total distance traveled: $t_{(55)} = 1.72$, $p = 0.091$, $d = 0.50$; average velocity: $t_{(34)} = 1.25$, $p = 0.222$, $d = 0.51$; percentage of distance traveled in the center of the arena: $t_{(55)} = 0.99$, $p = 0.326$, $d = 0.29$; time performing vertical exploration: $U = 78.00$, $p = 0.352$, $r_u = 0.15$; total number of rearings: $U = 84.00$, $p = 0.499$, $r_u = 0.11$; **Supplementary figure 8O-S**). Overall, these results indicate that the colon inflammatory profiles had no impact on the behavior of IL-10 KO mice.

4.4 Hippocampal structural plasticity characterization

The hippocampus harbors different forms of brain plasticity important for spatial reference memory (de Miranda *et al.*, 2017; Lisman *et al.*, 2017), which is impaired in the case of IL-10 KO mice, as mentioned in the aforementioned results. To better understand if IL-10 deficiency could affect the structural plasticity of the hippocampus, brains were processed for hippocampal stereological analysis by Giemsa staining and hippocampal 3-dimensional neuronal reconstruction and dendritic spine characterization by Golgi-Cox staining.

4.4.1 IL-10 KO mice showed decreased number of neurons and volumetric atrophy in the dorsal, but not in the ventral hippocampus

For the hippocampal structural analysis, the hippocampus was analyzed according to its main anatomical subregions: DG, CA1, and CA3. Each subregion was further delimited into three layers. In the DG, the ml, gcl, and pl were analyzed. In the case of CA1 and CA3, the so, pcl, and sr were examined. Hippocampal subregions were also divided accordingly to the dorsal-ventral axis (**Figure 25A**). Stereological estimations of number of neurons were performed in the hippocampal layers where the DG granule and CA1 and CA3 pyramidal neuronal somas are located (DG-gcl, CA1-pcl and CA3-pcl). Brains of IL-10 KO mice presented decreased number of neurons in all anatomical subregions evaluated in the DH (dDG-gcl: $t_{(22)} = 2.47$, $p = 0.022$, $d = 1.01$; dCA1-pcl: $t_{(22)} = 5.58$, $p < 0.001$, $d = 2.28$; dCA3-pcl: $t_{(22)} = 2.73$, $p = 0.012$, $d = 1.11$; **Figure 25B**), when compared to WT littermates. While in the VH, although IL-10 KO mice displayed reduction of the number of neurons in the vCA1-pcl ($t_{(22)} = 2.32$, $p = 0.030$, $d = 0.95$), no differences were detected in the vDG-gcl ($t_{(22)} = 0.37$, $p = 0.715$, $d = 0.15$), nor in the vCA3-pcl ($t_{(22)} = 0.93$, $p = 0.364$, $d = 0.38$; **Figure 25C**) between genotypes. After normalization of

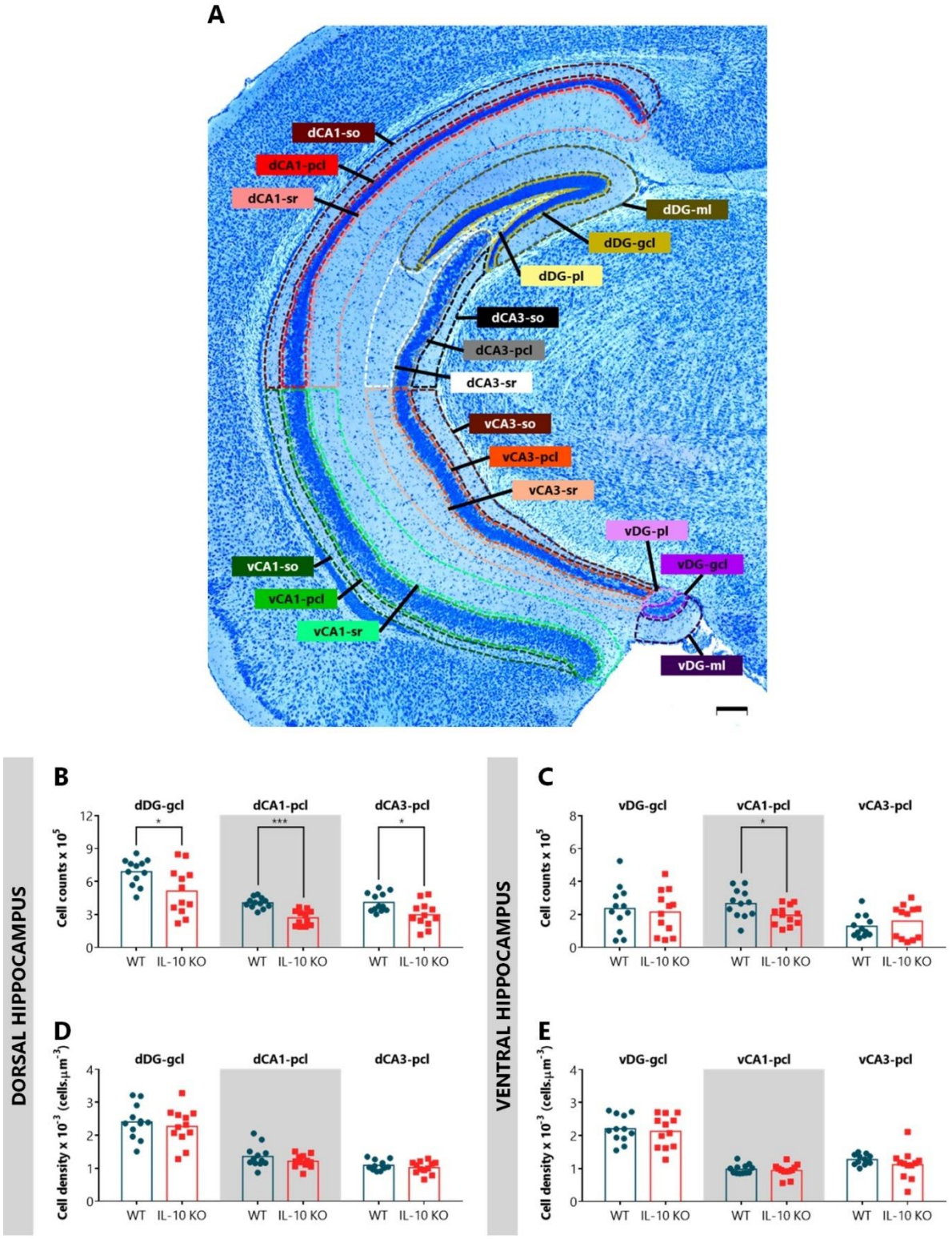

Figure 25. IL-10 absence led to a decreased number of neurons, but not neuron density in the dorsal hippocampus. **A.** Schematic representation of the anatomical hippocampal subregions. Scale bar = 200 µm. **B-C.** Stereological estimations of the number of neurons in the dorsal (**B**) and ventral (**C**) hippocampal main anatomical subregions DG, CA1, and CA3. **D-E.** Stereological estimations of the neuron density in the dorsal (**D**) and ventral (**E**) hippocampal main anatomical subregions DG, CA1, and CA3. Data presented as mean of the values from two independent sets. Each dot represents a brain hemisphere. dCA1 – dorsal *cornu ammonis* 1; dCA3 – dorsal *cornu ammonis* 3; dDG – dorsal dentate gyrus; gcl – granule cell layer; ml – molecular layer; pcl – pyramidal cell layer; pl – polymorph layer; so – *stratum oriens*; sr – *stratum radiatum*; vCA1 – ventral

cornu ammonis 1; vCA3 – ventral *cornu ammonis* 3; vDG – ventral dentate gyrus. n_{WT} = 12 (6 mice × 2 brain hemispheres); $n_{IL\text{-}10\ KO}$ = 12 (6 mice × 2 brain hemispheres). Statistical analysis was performed by a two-tailed independent samples *t*-test. * $p < 0.05$; *** $p < 0.001$.

the number of neurons to the volume of the respective subregion, it was observed that IL-10 absence did not affect the neuron density of any layer of the DH (dDG-gcl: $t_{(22)} = 0.63$, $p = 0.533$, $d = 0.26$; dCA1-pcl: $t_{(22)} = 1.34$, $p = 0.193$, $d = 0.55$; dCA3-pcl: $t_{(22)} = 0.97$, $p = 0.343$, $d = 0.40$; **Figure 25D**) or the VH (vDG-gcl: $t_{(22)} = 0.38$, $p = 0.707$, $d = 0.16$; vCA1-p cl: $t_{(22)} = 0.58$, $p = 0.568$, $d = 0.24$; vCA3-pcl: $t_{(22)} = 1.10$, $p = 0.283$, $d = 0.45$; **Figure 25E**).

Brains of IL-10 KO mice presented a total volume atrophy of the DG, CA1, and CA3 subregions of the DH (dDG: $t_{(22)} = 3.78$, $p = 0.001$, $d = 1.54$; dCA1: $t_{(22)} = 5.51$, $p < 0.001$, $d = 2.25$; dCA3: $t_{(22)} = 2.46$, $p = 0.023$, $d = 1.00$; **Figure 26A**), when compared to WT controls. Nonetheless, no differences were observed between genotypes in the VH of those anatomical hippocampal subregions (vDG: $t_{(22)} = 0.42$, $p = 0.678$, $d = 0.17$; vCA1: $t_{(22)} = 1.45$, $p = 0.160$, $d = 0.59$; vCA3: $t_{(22)} = 0.73$, $p = 0.471$, $d = 0.30$; **Figure 26B**). Specifically, within the dDG subregion, IL-10 deficiency led to a shrinkage of all its integrating layers (dDG-ml: $t_{(22)} = 3.97$, $p < 0.001$, $d = 1.62$; dDG-gcl: $t_{(22)} = 3.53$, $p = 0.002$, $d = 1.44$; dDG-pl: $t_{(22)} = 2.67$, $p = 0.014$, $d = 1.09$; **Figure 26C**). While this phenomenon was not present in the vDG, since there were no differences between genotypes in any vDG layer (vDG-ml: $t_{(22)} = 0.20$, $p = 0.841$, $d = 0.08$; vDG-gcl: $t_{(22)} = 0.30$, $p = 0.763$, $d = 0.13$; vDG-pl: $t_{(22)} = 0.95$, $p = 0.355$, $d = 0.39$; **Figure 26D**). Regarding the dCA1 subregion, brains of IL-10 KO mice showed decreased volume of all dCA1 constitutive layers (dCA1-so: $t_{(22)} = 6.14$, $p < 0.001$, $d = 2.51$; dCA1-pcl: $t_{(22)} = 5.51$, $p < 0.001$, $d = 2.25$; dCA1-sr: $t_{(22)} = 4.78$, $p < 0.001$, $d = 1.95$; **Figure 26E**), when compared to WT littermates. However, in the vCA1, IL-10 KO mice only had reduced volume of the vCA1-pcl ($t_{(22)} = 2.22$, $p = 0.037$, $d = 0.91$), while the other two vCA1 layers remained similar between genotypes (vCA1-so: $t_{(22)} = 1.31$, $p = 0.205$, $d = 0.53$; vCA1-sr: $t_{(22)} = 0.91$, $p = 0.373$, $d = 0.37$; **Figure 26F**). Concerning the dCA3 subregion, brains of IL-10 KO mice presented decreased volume of the dCA3-so ($t_{(22)} = 2.51$, $p = 0.020$, $d = 1.02$) and dCA3-pcl ($t_{(22)} = 2.92$, $p = 0.008$, $d = 1.19$) when compared to WT littermates, however no difference was detected between genotypes in the dCA3-sr ($t_{(22)} = 1.71$, $p = 0.101$, $d = 0.70$; **Figure 26G**). In the CA3 subregion of the VH, no differences were detected between genotypes in any layer (vCA3-so: $t_{(22)} = 0.17$, $p = 0.864$, $d = 0.07$; vCA3-pcl: $t_{(22)} = 1.32$, $p = 0.200$, $d = 0.54$; vCA3-sr: $t_{(22)} = 1.56$, $p = 0.132$, $d = 0.54$; **Figure 26H**). Overall, these results indicate that IL-10

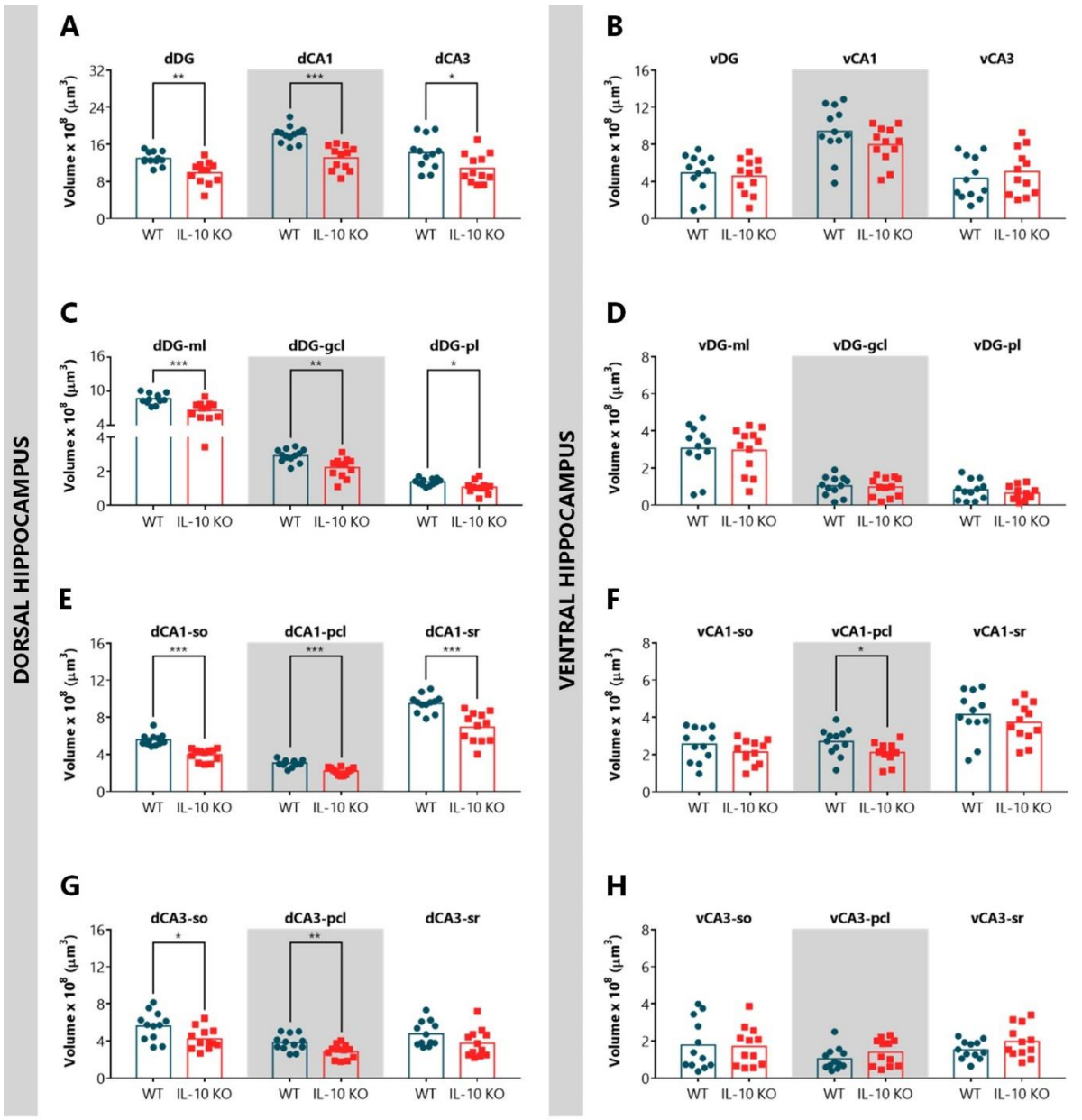

Figure 26. IL-10 absence led to a volumetric atrophy of the dorsal, but not of the ventral hippocampus. A-B. Stereological estimations of the volume of the total dorsal (**A**) and ventral (**B**) hippocampal main anatomical subregions DG, CA1, and CA3. **C-H**. The total volume of the dorsal (**C**) and ventral (**D**) DG, dorsal (**E**) and ventral (**F**) CA1, and dorsal (**G**) and ventral (**H**) CA3 subregions was calculated as the sum of the respective 3 layers. Data presented as mean of the values from two independent sets. Each dot represents a brain hemisphere. dCA1 – dorsal *cornu ammonis* 1; dCA3 – dorsal *cornu ammonis* 3; dDG – dorsal dentate gyrus; gcl – granule cell layer; ml – molecular layer; pcl – pyramidal cell layer; pl – polymorph layer; so – *stratum oriens*; sr – *stratum radiatum*; vCA1 – ventral *cornu ammonis* 1; vCA3 – ventral *cornu ammonis* 3; vDG – ventral dentate gyrus. n_{WT} = 12 (6 mice × 2 brain hemispheres); $n_{IL\text{-}10\ KO}$ = 12 (6 mice × 2 brain hemispheres). Statistical analysis was performed by a two-tailed independent samples *t*-test. * $p < 0.05$; ** $p < 0.01$; *** $p < 0.001$.

deficiency impaired the hippocampal structure by reducing the number of neurons and leading to volumetric atrophy of the DH, but not of the VH. In **Supplementary table 3**, the correlations between the variables of the hippocampal stereological analysis and other variables with statistically significant

differences between WT and IL-10 KO mice covered in this thesis were described.

4.4.2 IL-10 deficiency modulated the dendritic arborization and the dendritic spine dynamics of the hippocampal neurons

Dendrites are the largest portion of neurons that receive and process presynaptic inputs (Stuart and Spruston, 2015). Dendritic arborization is necessary for structural plasticity and suitable development of neuronal circuits. Variations in the dendritic arborization of the hippocampal neurons are known to modulate cognitive function and memory formation (Kasai *et al.*, 2010; Kulkarni and Firestein, 2012). The dendritic arborization of the granule neurons of the dDG and vDG subregions and pyramidal neurons of the CA1 and CA3 subregions were 3-dimensionally reconstructed by the Golgi-Cox staining method.

Concerning the dDG subregion (**Figure 27A**), a virtual representation of neurons of IL-10 KO mice and WT littermates are presented in **Figure 27B**. Neurons of mice lacking IL-10 exhibited shorter (total dendritic length: $t_{(70)} = 4.70$, $p < 0.001$, $d = 1.11$; **Figure 27C**) and less complex (dendritic ends: $t_{(70)} = 3.26$, $p = 0.002$, $d = 0.77$; **Figure 27D**) dendritic arborizations than their WT counterpart. A 3-dimensional version of the Sholl analysis of intersections also revealed that the arrangement of the dendrites throughout the distance from soma was strongly dependent on the genotype (genotype factor: $F_{(1, 70)} = 20.61$, $p < 0.001$, $\eta_p^2 = 0.23$; distance from soma factor: $F_{(29, 2030)} = 194.60$, $p < 0.001$, $\eta_p^2 = 0.74$; interaction: $F_{(29, 2030)} = 5.20$, $p < 0.001$, $\eta_p^2 = 0.07$; **Figure 27E**). Particularly, at a distance between 80 and 180 μm from the soma, a *post hoc* analysis showed that dDG neurons of IL-10 KO mice presented a less branched dendritic arborization than those of WT mice (80 μm: $p = 0.026$, $d = 0.66$; 90 μm: $p = 0.003$, $d = 0.82$; 100 μm: $p < 0.001$, $d = 0.94$; 110 μm: $p < 0.001$, $d = 0.92$; 120 μm: $p < 0.001$, $d = 0.75$; 130 μm: $p < 0.001$, $d = 0.69$; 140 μm: $p < 0.001$, $d = 0.71$; 150 μm: $p < 0.001$, $d = 0.76$; 160 μm: $p < 0.001$, $d = 0.76$; 170 μm: $p < 0.001$, $d = 0.71$; 180 μm: $p = 0.015$, $d = 0.68$).

The Golgi-Cox staining also allows the dendritic spine characterization. Dendritic spines are dynamic and specialized subcellular protrusions of the dendritic arborization where more than 90% of excitatory synapses occur within the CNS (Kirov, Sorra and Harris, 1999). The dendritic spine density directly indicates the number of excitatory synaptic inputs onto a particular dendritic segment, and their morphology indicates their maturity state (Berry and Nedivi, 2017).

On both proximal (PDS) and distal dendritic segments (DDS) to the neuronal soma, neurons within the dDG subregion of mice lacking IL-10 revealed higher dendritic spine densities than their WT

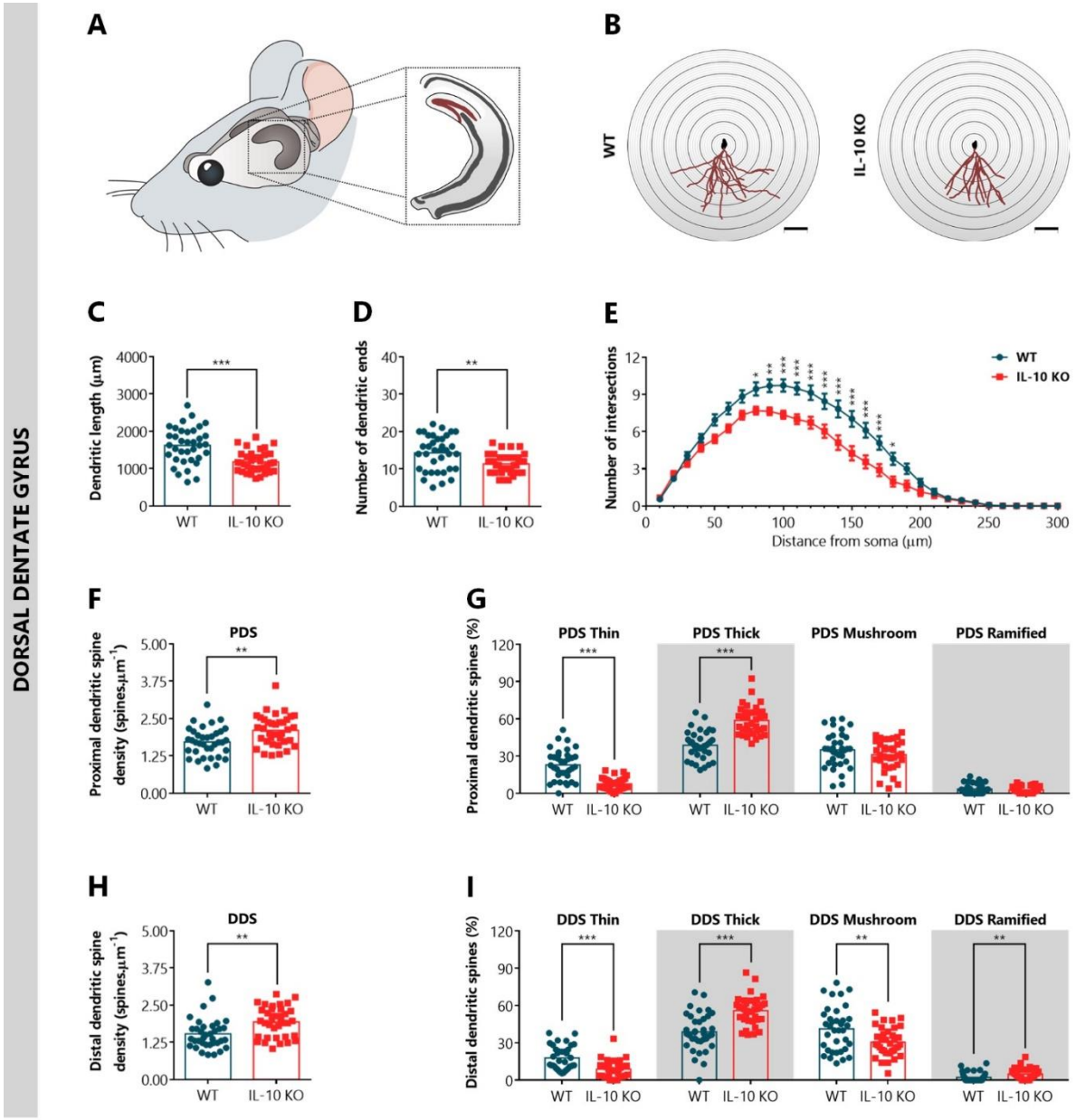

Figure 27. IL-10 absence impaired the dendritic arborization and modulated the dendritic spine dynamics of the dorsal dentate gyrus neurons. A. Schematic representation of the hippocampus location on the mice brain. The dorsal DG is highlighted in purple. **B.** Virtual representation of dorsal dentate gyrus granular neurons. The dendrites are highlighted in purple. **C.** Total dendritic length. **D.** Total number of dendritic ends. **E.** Rearrangement of the dendrites throughout the distance from soma (3-dimensional version of the Sholl analysis of intersections). **F.** Proximal dendritic spine density. **G.** Morphological classification of the proximal dendritic spines. **H.** Distal dendritic spine density. **I.** Morphological classification of the distal dendritic spines. Data presented as mean (**C-D**; **F-I**) or mean ± SEM (**E**) of the values from two independent sets. Each dot represents a neuron (**C-D**) or dendritic segment (**F-I**). DDS – distal dendritic segment; PDS – proximal dendritic segment. n_{WT} = 36 (6 mice × 6 neurons); $n_{IL\text{-}10\ KO}$ = 36 (6 mice × 6 neurons) (**C-E**); n_{WT} = 36 (2 mice × 6 neurons × 3 dendritic segments); $n_{IL\text{-}10\ KO}$ = 36 (2 mice × 6 neurons × 3 dendritic segments). Statistical analysis was performed by a two-tailed independent samples *t*-test (**C-D**; **F-I**) or a two-way repeated-measures ANOVA (**E**). * $p < 0.05$; ** $p < 0.01$; *** $p < 0.001$.

counterpart (PDS density: $t_{(70)} = 3.33$, $p = 0.001$, $d = 0.79$; DDS density: $t_{(70)} = 3.36$, $p = 0.001$, $d = 0.79$; **Figures 27F and 27H**). Also, IL-10 KO mice displayed a decreased proportion of immature thin

spines and an increase of thick spines, both on PDS and DDS (PDS thin: $t_{(70)} = 7.08$, $p < 0.001$, $d = 1.67$; DDS thin: $t_{(70)} = 4.63$, $p < 0.001$, $d = 1.09$; PDS thick: $t_{(70)} = 7.48$, $p < 0.001$, $d = 1.76$; DDS thick: $t_{(70)} = 5.41$, $p < 0.001$, $d = 1.27$). In contrast, IL-10 KO mice showed a reduction in the percentage of mature mushroom spines and an increase of specialized ramified spines on DDS, but not on PDS when compared to WT controls (PDS mushroom: $t_{(70)} = 1.31$, $p = 0.193$, $d = 0.31$; DDS mushroom: $t_{(70)} = 3.04$, $p = 0.001$, $d = 0.72$; PDS ramified: $t_{(70)} = 0.93$, $p = 0.358$, $d = 0.22$; DDS ramified: $t_{(70)} = 2.85$, $p = 0.006$, $d = 0.67$; **Figures 27G and 27I**).

In line with the dDG subregion, neurons from IL-10 KO mice in the vDG subregion (**Figures 28A and 28B**) presented shorter (total dendritic length: $t_{(70)} = 2.81$, $p = 0.006$, $d = 0.66$; **Figure 28C**) and less complex (dendritic ends: $t_{(70)} = 2.35$, $p = 0.022$, $d = 0.56$; **Figure 28D**) dendritic arborizations than those of WT mice. Moreover, the arrangement of the dendrites throughout the distance from soma was also highly dependent on the genotype (genotype factor: $F_{(1, 70)} = 8.88$, $p = 0.004$, $\eta_p^2 = 0.11$; distance from soma factor: $F_{(29, 2030)} = 184.80$, $p < 0.001$, $\eta_p^2 = 0.73$; interaction: $F_{(29, 2030)} = 2.46$, $p < 0.001$, $\eta_p^2 = 0.03$; **Figure 28E**). Specifically, at a distance between 100 and 130 μm from the soma, vDG neurons of IL-10 KO mice presented a less branched dendritic arborization than those of WT mice (100 μm: $p = 0.018$, $d = 0.76$; 110 μm: $p = 0.004$, $d = 0.79$; 120 μm: $p = 0.004$, $d = 0.68$; 130 μm: $p = 0.009$, $d = 0.54$).

IL-10 absence affected the dendritic spine dynamics of the vDG neurons by reducing the dendritic spine density on DDS of IL-10 KO neurons when compared to WT littermates (DDS density: $t_{(70)} = 2.51$, $p = 0.015$, $d = 0.59$; **Figure 28H**). However, this was not the case on PDS (PDS density: $t_{(70)} = 1.90$, $p = 0.062$, $d = 0.45$; **Figure 28F**). Both on PDS and DDS of the vDG neurons, IL-10 KO mice exhibited a decreased proportion of immature thin spines and an increase of thick and ramified spines than WT controls (PDS thin: $t_{(70)} = 3.27$, $p = 0.002$, $d = 0.77$; DDS thin: $t_{(70)} = 3.05$, $p = 0.003$, $d = 0.72$; PDS thick: $t_{(70)} = 3.23$, $p = 0.002$, $d = 0.76$; DDS thick: $t_{(70)} = 4.63$, $p < 0.001$, $d = 1.09$; PDS ramified: $t_{(70)} = 2.36$, $p = 0.021$, $d = 0.56$; DDS ramified: $t_{(70)} = 2.50$, $p = 0.015$, $d = 0.59$). Also, IL-10 absence reduced the percentage of mushroom spines on DDS, but not on PDS (PDS mushroom: $t_{(70)} = 1.35$, $p = 0.181$, $d = 0.32$; DDS mushroom: $t_{(70)} = 2.57$, $p = 0.012$, $d = 0.61$; **Figures 28G and 28I**).

Using Golgi-Cox staining, both apical and basal dendritic arborizations of the pyramidal neurons of the CA1 and CA3 subregions were evaluated. Concerning the apical side of CA1 neurons (**Figures 29A and 29B**), IL-10 deficiency led to an atrophy of the length (total dendritic length: $t_{(70)} = 2.56$, $p = 0.013$,

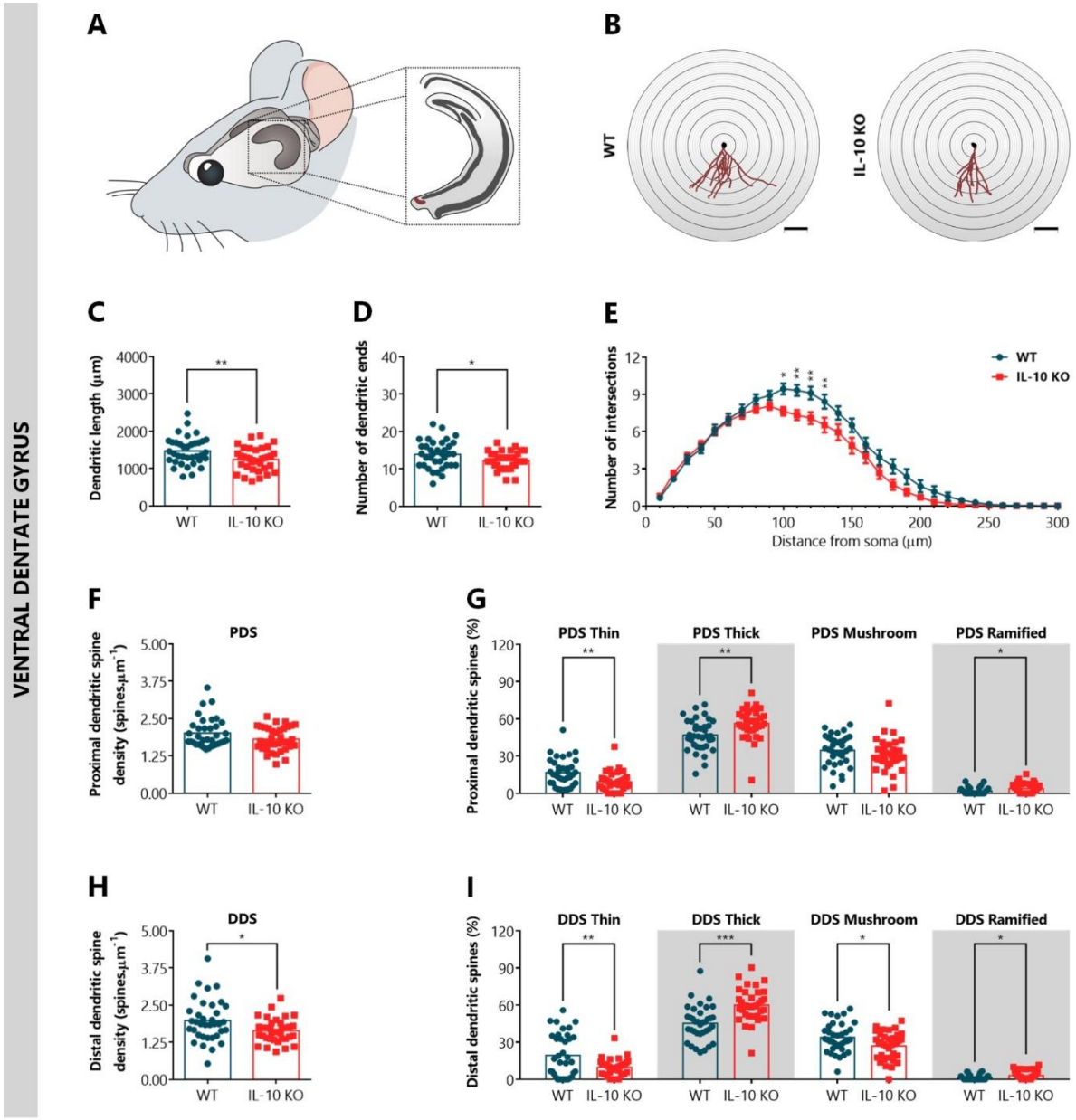

Figure 28. IL-10 absence impaired the dendritic arborization and modulated the dendritic spine dynamics of the ventral dentate gyrus neurons. A. Schematic representation of the hippocampus location on the mice brain. The ventral DG is highlighted in purple. **B.** Virtual representation of ventral dentate gyrus granular neurons. The dendrites are highlighted in purple. **C.** Total dendritic length. **D.** Total number of dendritic ends. **E.** Rearrangement of the dendrites throughout the distance from soma (3-dimensional version of the Sholl analysis of intersections). **F.** Proximal dendritic spine density. **G.** Morphological classification of the proximal dendritic spines. **H.** Distal dendritic spine density. **I.** Morphological classification of the distal dendritic spines. Data presented as mean (**C-D**; **F-I**) or mean ± SEM (**E**) of the values from two independent sets. Each dot represents a neuron (**C-D**) or dendritic segment (**F-I**). DDS – distal dendritic segment; PDS – proximal dendritic segment. n_{WT} = 36 (6 mice × 6 neurons); $n_{IL\text{-}10\ KO}$ = 36 (6 mice × 6 neurons) (**C-E**); n_{WT} = 36 (2 mice × 6 neurons × 3 dendritic segments); $n_{IL\text{-}10\ KO}$ = 36 (2 mice × 6 neurons × 3 dendritic segments). Statistical analysis was performed by a two-tailed independent samples *t*-test (**C-D**; **F-I**) or a two-way repeated-measures ANOVA (**E**). * $p < 0.05$; ** $p < 0.01$; *** $p < 0.001$.

$d = 0.60$; **Figures 29C**) and complexity of the apical dendritic arborization (dendritic ends: $t_{(70)} = 2.21$, $p = 0.031$, $d = 0.52$; **Figures 29D**). Additionally, IL-10 absence negatively impacted the arrangement of the

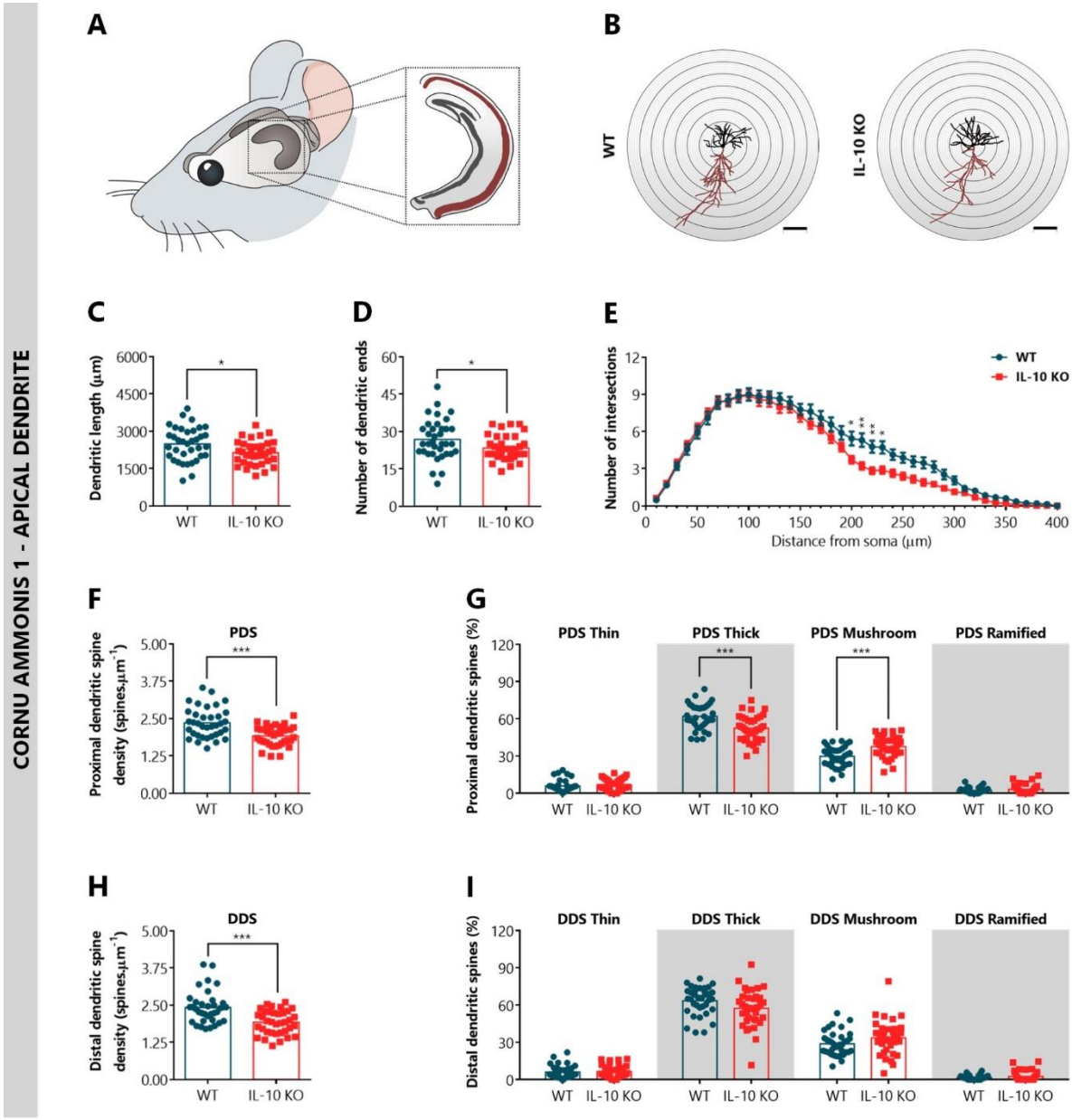

Figure 29. IL-10 absence impaired the dendritic arborization and modulated the dendritic spine dynamics of the apical dendrite of CA1 neurons. A. Schematic representation of the hippocampus location on the mice brain. The CA1 is highlighted in purple. **B.** Virtual representation of CA1 pyramidal neurons. The apical dendrite is highlighted in purple. **C.** Total dendritic length. **D.** Total number of dendritic ends. **E.** Rearrangement of the apical dendrite throughout the distance from soma (3-dimensional version of the Sholl analysis of intersections). **F.** Proximal dendritic spine density. **G.** Morphological classification of the proximal dendritic spines. **H.** Distal dendritic spine density. **I.** Morphological classification of the distal dendritic spines. Data presented as mean (**C-D**; **F-I**) or mean ± SEM (**E**) of the values from two independent sets. Each dot represents a neuron (**C-D**) or dendritic segment (**F-I**). DDS – distal dendritic segment; PDS – proximal dendritic segment. n_{WT} = 36 (6 mice × 6 neurons); $n_{IL\text{-}10\ KO}$ = 36 (6 mice × 6 neurons) (**C-E**); n_{WT} = 36 (2 mice × 6 neurons × 3 dendritic segments); $n_{IL\text{-}10\ KO}$ = 36 (2 mice × 6 neurons × 3 dendritic segments). Statistical analysis was performed by a two-tailed independent samples *t*-test (**C-D**; **F-I**) or a two-way repeated-measures ANOVA (**E**). * $p < 0.05$; ** $p < 0.01$; *** $p < 0.001$.

apical dendrite throughout the distance from soma (genotype factor: $F_{(1,\ 70)} = 5.98$, $p = 0.017$, $\eta_p^2 = 0.08$; distance from soma factor: $F_{(39,\ 2730)} = 182.40$, $p < 0.001$, $\eta_p^2 = 0.72$; interaction:

$F_{(39, 2730)} = 2.27$, $p < 0.001$, $\eta^2_p = 0.03$; **Figure 29E**). A *post hoc* evaluation of the Sholl analysis of intersections revealed a reduction of the apical dendritic branching at a distance between 200 and 230 μm from the soma of IL-10 KO neurons when compared to WT ones (200 μm: $p = 0.038$, $d = 0.63$; 210 μm: $p = 0.003$, $d = 0.79$; 220 μm: $p = 0.008$, $d = 0.82$; 230 μm: $p = 0.018$, $d = 0.74$).

IL-10 KO mice also presented a diminished dendritic spine density on both PDS and DDS of the apical dendrite of CA1 neurons when compared to their WT counterpart (PDS density: $t_{(70)} = 4.37$, $p < 0.001$, $d = 1.03$; DDS density: $t_{(70)} = 4.41$, $p < 0.001$, $d = 1.04$; **Figures 29F and 29H**). On PDS, IL-10 KO mice when compared to WT controls displayed a decrease in the proportion of thick spines and an increase in mushroom spines (PDS thick: $t_{(70)} = 3.92$, $p < 0.001$, $d = 0.92$; PDS mushroom: $t_{(70)} = 4.04$, $p < 0.001$, $d = 0.95$). These differences between genotypes were not present on DDS (DDS thick: $t_{(70)} = 1.96$, $p = 0.054$, $d = 0.46$; DDS mushroom: $t_{(70)} = 1.73$, $p = 0.087$, $d = 0.41$). Also, both on PDS and DDS, the genotype did not affect the proportion of thin and ramified spines in the apical dendrite of CA1 neurons (PDS thin: $t_{(70)} = 0.83$, $p = 0.407$, $d = 0.20$; DDS thin: $t_{(70)} = 0.41$, $p = 0.680$, $d = 0.10$; PDS ramified: $t_{(70)} = 1.04$, $p = 0.301$, $d = 0.25$; DDS ramified: $t_{(70)} = 1.05$, $p = 0.297$, $d = 0.25$; **Figures 29G and 29I**).

On the basal side of CA1 neurons (**Figures 30A and 30B**), the genotype did not impact the length (total dendritic length: $t_{(70)} = 0.77$, $p = 0.445$, $d = 0.18$; **Figure 30C**) nor the complexity (dendritic ends: $t_{(70)} = 0.05$, $p = 0.960$, $d = 0.01$; **Figure 30D**) of the basal dendritic arborization. Likewise, IL-10 absence did not impact the arrangement of the basal dendrites throughout the distance from soma (genotype factor: $F_{(1, 70)} = 1.10$, $p = 0.298$, $\eta^2_p = 0.02$; distance from soma factor: $F_{(19, 1330)} = 303.50$, $p < 0.001$, $\eta^2_p = 0.81$; interaction: $F_{(19, 1330)} = 1.40$, $p = 0.116$, $\eta^2_p = 0.02$; **Figure 30E**), although a *post hoc* analysis revealed that at a distance of 80 μm from the soma, IL-10 KO neurons presented increased basal dendritic branching comparing to WT littermates ($p = 0.046$, $d = 0.44$).

As for the apical side of CA1 neurons, in the basal side, IL-10 KO mice also presented a reduced dendritic spine density on both PDS and DDS when compared to WT littermates (PDS density: $t_{(70)} = 3.75$, $p < 0.001$, $d = 0.88$; DDS density: $t_{(70)} = 3.43$, $p = 0.001$, $d = 0.81$; **Figures 30F and 30H**). Both on PDS and DDS, IL-10 absence led to an increase in the proportion of specialized ramified spines in the basal dendrites of CA1 neurons (PDS ramified: $t_{(70)} = 3.35$, $p = 0.001$, $d = 0.79$; DDS ramified: $t_{(70)} = 2.87$, $p = 0.005$, $d = 0.68$). On DDS, IL-10 KO mice also demonstrated a reduction in the percentage of thick spines and an increase of mature mushroom spines when compared to WT controls

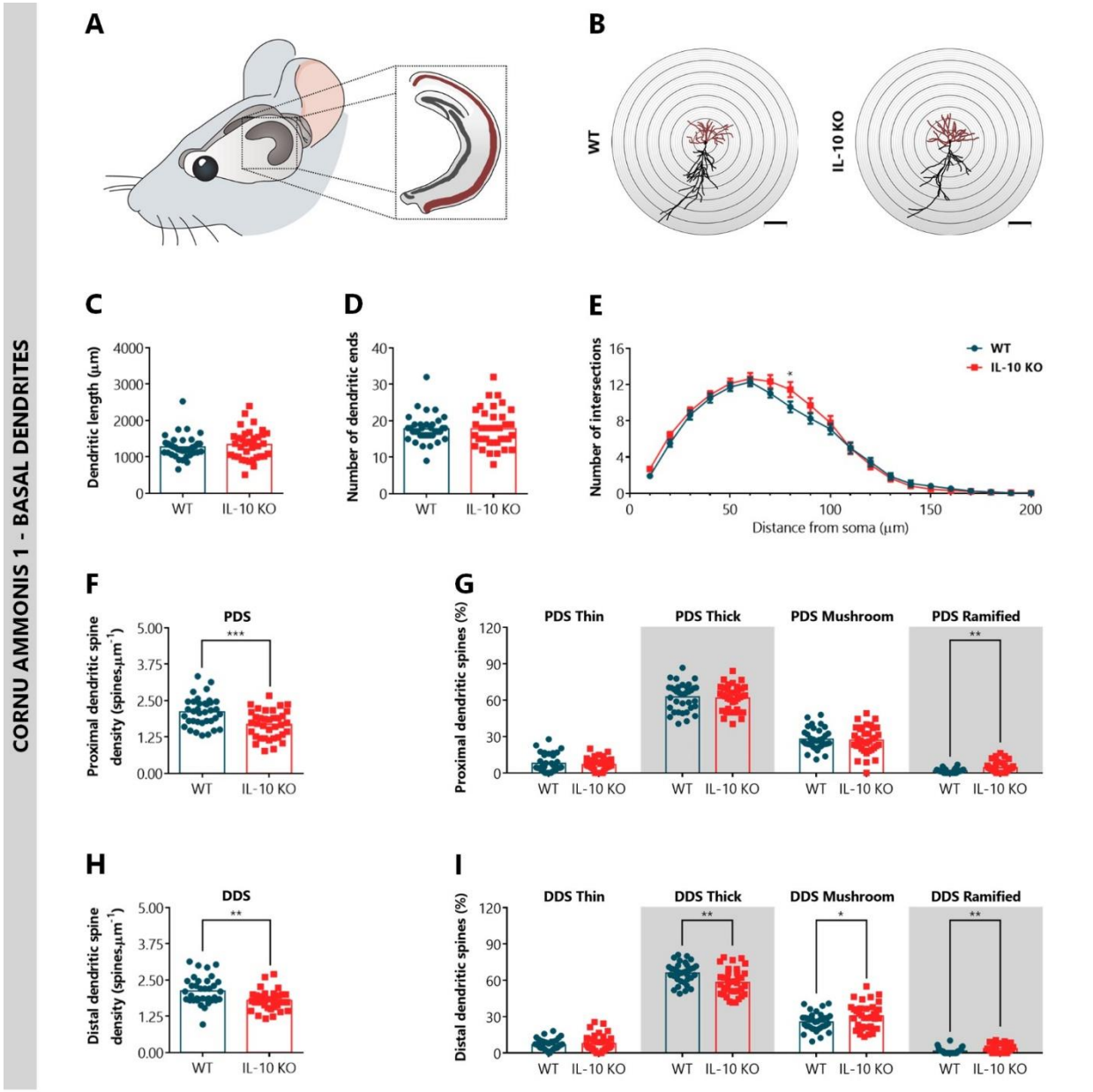

Figure 30. IL-10 absence did not impact the dendritic arborization but modulated the dendritic spine dynamics of the basal dendrites of CA1 neurons. A. Schematic representation of the hippocampus location on the mice brain. The CA1 is highlighted in purple. **B.** Virtual representation of CA1 pyramidal neurons. The basal dendrites are highlighted in purple. **C.** Total dendritic length. **D.** Total number of dendritic ends. **E.** Rearrangement of the basal dendrites throughout the distance from soma (3-dimensional version of the Sholl analysis of intersections). **F.** Proximal dendritic spine density. **G.** Morphological classification of the proximal dendritic spines. **H.** Distal dendritic spine density. **I.** Morphological classification of the distal dendritic spines. Data presented as mean (**C-D**; **F-I**) or mean ± SEM (**E**) of the values from two independent sets. Each dot represents a neuron (**C-D**) or dendritic segment (**F-I**). DDS – distal dendritic segment; PDS – proximal dendritic segment. n_{WT} = 36 (6 mice × 6 neurons); $n_{IL\text{-}10\ KO}$ = 36 (6 mice × 6 neurons) (**C-E**); n_{WT} = 36 (2 mice × 6 neurons × 3 dendritic segments); $n_{IL\text{-}10\ KO}$ = 36 (2 mice × 6 neurons × 3 dendritic segments). Statistical analysis was performed by a two-tailed independent samples *t*-test (**C-D**; **F-I**) or a two-way repeated-measures ANOVA (**E**). * $p < 0.05$; ** $p < 0.01$; *** $p < 0.001$.

(DDS thick: $t_{(70)} = 3.44$, $p = 0.001$, $d = 0.81$; DDS mushroom: $t_{(70)} = 2.28$, $p = 0.030$, $d = 0.54$). These differences between genotypes were not present on PDS (PDS thick: $t_{(70)} = 0.34$, $p = 0.735$, $d = 0.08$;

PDS mushroom: $t_{(70)} = 0.35$, $p = 0.724$, $d = 0.08$). Moreover, both on PDS and DDS, the genotype did not affect the proportion of immature thin spines in the basal dendrites of CA1 neurons (PDS thin: $t_{(70)} = 0.68$, $p = 0.498$, $d = 0.16$; DDS thin: $t_{(70)} = 0.68$, $p = 0.497$, $d = 0.16$; **Figures 30G and 30I**).

The pyramidal neurons of the CA3 subregions within the hippocampus were also evaluated. Concerning the apical side of CA3 neurons (**Figures 31A and 31B**), mice lacking IL-10 exhibited shorter (total dendritic length: $t_{(70)} = 3.23$, $p = 0.002$, $d = 0.76$; **Figure 31C**) and less complex (dendritic ends: $t_{(70)} = 2.39$, $p = 0.020$, $d = 0.56$; **Figure 31D**) apical dendritic arborizations than their WT counterpart. In addition, IL-10 KO mice showed a distinct arrangement of the apical dendrite throughout the distance from soma (genotype factor: $F_{(1, 70)} = 5.76$, p = 0.019, $\eta^2_p = 0.08$; distance from soma factor: $F_{(54, 3780)} = 93.18$, p < 0.001, $\eta^2_p = 0.57$; interaction: $F_{(54, 3780)} = 1.92$, p < 0.001, $\eta^2_p = 0.03$; **Figure 31E**). Specifically, at a distance of 360 μm from the soma, CA3 neurons of IL-10 KO mice presented a less branched apical dendritic arborization than those of WT mice ($p = 0.035$, $d = 0.67$).

IL-10 absence also affected the dendritic spine dynamics of the apical dendrite of CA3 neurons by reducing the dendritic spine density on both PDS and DDS of IL-10 KO neurons when compared to WT littermates (PDS density: $t_{(70)} = 3.34$, $p = 0.001$, $d = 0.79$; DDS density: $t_{(70)} = 5.24$, $p < 0.001$, $d = 1,24$; **Figures 31F and 31H**). On both PDS and DDS, IL-10 deficiency led to an increase in the proportion of thin spines (PDS thin: $t_{(70)} = 3.94$, $p < 0.001$, $d = 0.93$; DDS thin: $t_{(70)} = 2.92$, $p = 0.005$, $d = 0.69$). The percentage of thick spines was not affected by the genotypes both on PDS and DDS (PDS thick: $t_{(70)} = 0.05$, $p = 0.961$, $d = 0.01$; DDS thick: $t_{(70)} = 0.71$, $p = 0.483$, $d = 0.17$). IL-10 KO mice also displayed a decrease in the proportion of mature mushroom spines and an increase of specialized ramified spines on PDS, but not on DDS of the apical dendrite of CA3 neurons when compared to their WT counterpart (PDS mushroom: $t_{(70)} = 2.47$, $p = 0.016$, $d = 0.58$; DDS mushroom: $t_{(70)} = 0.92$, $p = 0.358$, $d = 0.22$; PDS ramified: $t_{(70)} = 2.87$, $p = 0.005$, $d = 0.68$; DDS ramified: $t_{(70)} = 1.67$, $p = 0.099$, $d = 0.39$; **Figures 31G and 31I**).

On the basal side of CA3 neurons (**Figures 32A and 32B**), IL-10 absence did not impact the length (total dendritic length: $t_{(70)} = 1.33$, $p = 0.189$, $d = 0.31$; **Figure 32C**) nor the complexity (dendritic ends: $t_{(70)} = 1.98$, $p = 0.052$, $d = 0.47$; **Figure 32D**) of the basal dendritic arborization. Moreover, the arrangement of the basal dendrites throughout the distance from soma was not impacted by the genotype (genotype factor: $F_{(1, 70)} = 0.92$, $p = 0.342$, $\eta^2_p = 0.01$; distance from soma factor: $F_{(29, 2030)} = 199.90$, $p < 0.001$, $\eta^2_p = 0.74$; interaction: $F_{(29, 2030)} = 1.94$, $p = 0.002$, $\eta^2_p = 0.03$; **Figure 32E**), although at

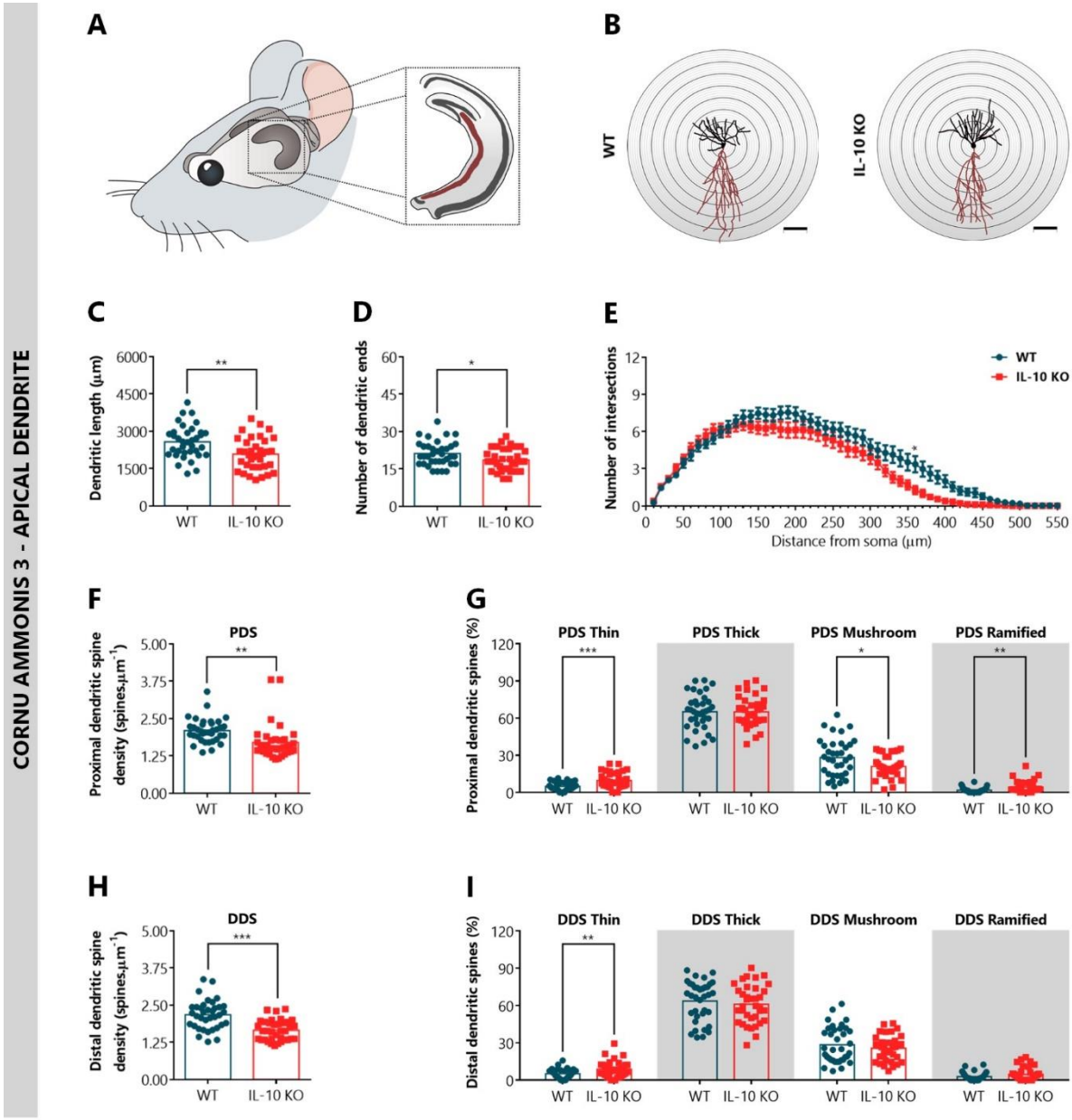

Figure 31. IL-10 absence impaired the dendritic arborization and modulated the dendritic spine dynamics of the apical dendrite of CA3 neurons. A. Schematic representation of the hippocampus location on the mice brain. The CA3 is highlighted in purple. **B.** Virtual representation of CA3 pyramidal neurons. The apical dendrite is highlighted in purple. **C.** Total dendritic length. **D.** Total number of dendritic ends. **E.** Rearrangement of the apical dendrite throughout the distance from soma (3-dimensional version of the Sholl analysis of intersections). **F.** Proximal dendritic spine density. **G.** Morphological classification of the proximal dendritic spines. **H.** Distal dendritic spine density. **I.** Morphological classification of the distal dendritic spines. Data presented as mean (**C-D**; **F-I**) or mean ± SEM (**E**) of the values from two independent sets. Each dot represents a neuron (**C-D**) or dendritic segment (**F-I**). DDS – distal dendritic segment; PDS – proximal dendritic segment. n_{WT} = 36 (6 mice × 6 neurons); $n_{IL\text{-}10\ KO}$ = 36 (6 mice × 6 neurons) (**C-E**); n_{WT} = 36 (2 mice × 6 neurons × 3 dendritic segments); $n_{IL\text{-}10\ KO}$ = 36 (2 mice × 6 neurons × 3 dendritic segments). Statistical analysis was performed by a two-tailed independent samples *t*-test (**C-D**; **F-I**) or a two-way repeated-measures ANOVA (**E**). * $p < 0.05$; ** $p < 0.01$; *** $p < 0.001$.

a distance of 90 µm from the soma, IL-10 KO neurons presented a decreased basal dendritic branching when compared to WT littermates ($p = 0.028$, $d = 0.49$).

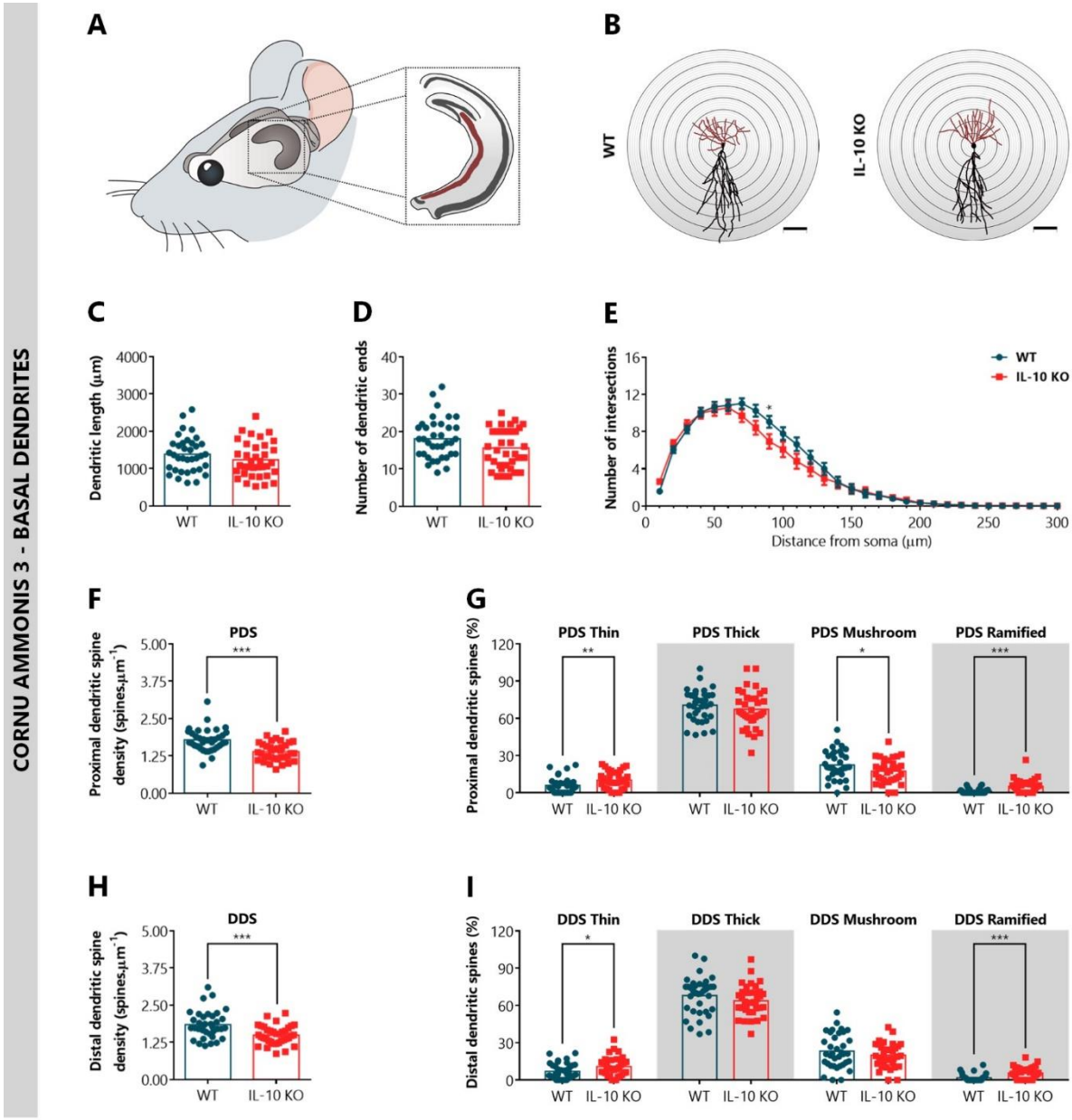

Figure 32. IL-10 absence did not impact the dendritic arborization but modulated the dendritic spine dynamics of the basal dendrites of CA3 neurons. A. Schematic representation of the hippocampus location on the mice brain. The CA3 is highlighted in purple. **B.** Virtual representation of CA3 pyramidal neurons. The basal dendrites are highlighted in purple. **C.** Total dendritic length. **D.** Total number of dendritic ends. **E.** Rearrangement of the basal dendrites throughout the distance from soma (3-dimensional version of the Sholl analysis of intersections). **F.** Proximal dendritic spine density. **G.** Morphological classification of the proximal dendritic spines. **H.** Distal dendritic spine density. **I.** Morphological classification of the distal dendritic spines. Data presented as mean (**C-D**; **F-I**) or mean ± SEM (**E**) of the values from two independent sets. Each dot represents a neuron (**C-D**) or dendritic segment (**F-I**). DDS – distal dendritic segment; PDS – proximal dendritic segment. n_{WT} = 36 (6 mice × 6 neurons); $n_{IL\text{-}10\ KO}$ = 36 (6 mice × 6 neurons) (**C-E**); n_{WT} = 36 (2 mice × 6 neurons × 3 dendritic segments); $n_{IL\text{-}10\ KO}$ = 36 (2 mice × 6 neurons × 3 dendritic segments). Statistical analysis was performed by a two-tailed independent samples *t*-test (**C-D**; **F-I**) or a two-way repeated-measures ANOVA (**E**). * $p < 0.05$; ** $p < 0.01$; *** $p < 0.001$.

Similarly to the apical dendritic arborization of CA3 neurons, in the basal side, IL-10 deficiency also led to a reduced dendritic spine density on both PDS and DDS (PDS density: $t_{(70)} = 4.84$, $p < 0.001$,

d = 1.14; DDS density: $t_{(70)}$ = 3.79, p < 0.001, d = 0.89; **Figures 32F and 32H**). Additionally, both on PDS and DDS, IL-10 KO mice displayed higher percentages of immature thin spines and specialized ramified spines than WT controls (PDS thin: $t_{(70)}$ = 2.87, p = 0.005, d = 0.68; DDS thin: $t_{(70)}$ = 2.30, p = 0.024, d = 0.54; PDS ramified: $t_{(70)}$ = 4.05, p < 0.001, d = 0.95; DDS ramified: $t_{(70)}$ = 4.07, p < 0.001, d = 0.96). In contrast, IL-10 KO mice presented a reduction in the percentage of mature mushroom spines on PDS, but not on DDS when compared to WT littermates (PDS mushroom: $t_{(70)}$ = 2.05, p = 0.044, d = 0.48; DDS mushroom: $t_{(70)}$ = 1.18, p = 0.242, d = 0.28). Both on PDS and DDS, the genotype did not affect the proportion of thick spines in the basal dendrites of CA3 neurons (PDS thick: $t_{(70)}$ = 1.02, p = 0.310, d = 0.24; DDS thick: $t_{(70)}$ = 1.31, p = 0.194, d = 0.31; **Figures 32G and 32I**). Overall, these results, summarized in **Table 12**, indicate that IL-10 deficiency modulated the dendritic arborization and the dendritic spine dynamics of the hippocampal neurons. In **Supplementary table 3**, the correlations between the variables of the hippocampal 3-dimensional neuronal reconstruction and dendritic spine characterization and other variables with statistically significant differences between WT and IL-10 KO mice covered in this thesis were described.

Table 12. Summary of the hippocampal 3-dimensional neuronal reconstruction and dendritic spine characterization results.

Hippocampal subregion		Dendritic length	Dendritic complexity	PDS					DDS				
				Density	Thin	Thick	Mushroom	Ramified	Density	Thin	Thick	Mushroom	Ramified
DG	*Dorsal*	↓	↓	↑	↓	↑	=	=	↑	↓	↑	↓	↑
	Ventral	↓	↓	=	↓	↑	=	↑	↓	↓	↑	↓	↑
CA1	*Apical dendrite*	↓	↓	↓	=	↓	↑	=	↓	=	=	=	=
	Basal dendrites	=	=	↓	=	=	=	↑	↓	=	↓	↑	↑
CA3	*Apical dendrite*	↓	↓	↓	↑	=	↓	↑	↓	↑	=	=	=
	Basal dendrites	=	=	↓	↑	=	↓	↑	↓	↑	=	=	↑

The symbols ↓, ↑, and = represent, respectively, statistically significant decrease, increase, and similarity of IL-10 KO mice when compared to WT littermate for $p < 0.05$.

4.5 Serum corticosterone levels characterization

Under basal conditions, IL-10 KO mice may present higher corticosterone levels (Smith *et al.*, 1999), a condition that is consistently reported to be associated with poor cognitive function both in humans and rodents (Ouanes and Popp, 2019). To better understand if alterations in corticosterone levels were correlated with the behavioral data, serum corticosterone levels were evaluated during the

diurnal nadir and the nocturnal zenith by ELISA.

4.5.1 IL-10 KO mice presented higher nadir serum corticosterone levels than WT mice

Serum corticosterone levels were higher in IL-10 KO mice than in WT littermates at nadir ($U = 1117.00$, $p < 0.001$, $r_U = 0.31$; **Figure 33A**). No differences between genotypes were revealed in the serum corticosterone levels at zenith ($t_{(44)} = 0.58$, $p = 0.567$, $d = 0.17$; **Figure 33B**). Moreover, at the end of the behavioral characterization, mice were also weighed. IL-10 KO mice revealed a lower body weight than the WT counterpart ($t_{(116)} = 3.79$, $p < 0.001$, $d = 0.70$; **Figure 33C**). In **Supplementary table 3**, the correlations between the variables of the serum corticosterone levels and other variables with statistically significant differences between WT and IL-10 KO mice covered in this thesis were described.

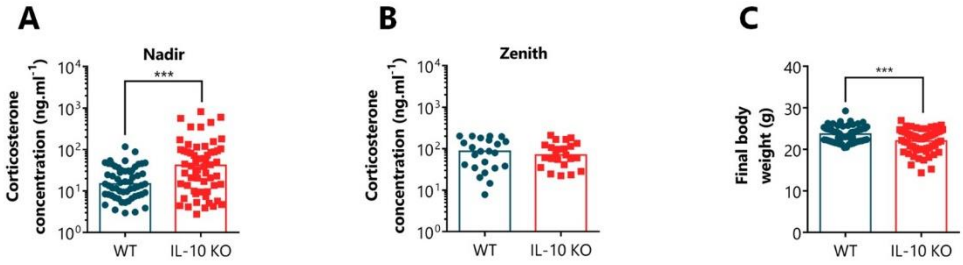

Figure 33. IL-10 absence increased the serum corticosterone levels at nadir, but not at zenith. A-B. Serum corticosterone concentration during the diurnal nadir (**A**) and the nocturnal zenith (**B**) after the behavioral assessment. **C.** Final body weight after the behavioral assessment. Data presented as median (**A**) or mean (**B-C**) of the values from four (**A**; **C**) or two (**B**) independent sets. Each dot represents an animal. $n_{WT} = 58$; $n_{IL\text{-}10\ KO} = 60$ (**A**; **C**); $n_{WT} = 23$; $n_{IL\text{-}10\ KO} = 23$ (**B**). Statistical analysis was performed by a Mann-Whitney *U* test (**A**) or a two-tailed independent samples *t*-test (**B-C**). *** $p < 0.001$.

4.6 Leukocyte profile characterization in the blood and lymph nodes

The current view is that leukocytes play modulatory roles in cognitive function (Kipnis *et al.*, 2004; Ziv *et al.*, 2006; Brynskikh *et al.*, 2008). To evaluate if modifications in the leukocyte profile induced by IL-10 deficiency were correlated with the cognitive data, flow cytometry analysis was used to characterize the percentage and the number of the main types of leukocytes in the blood and the ingLN and dcLN.

4.6.1 IL-10 absence affected the leukocyte profile in the blood

Concerning the major leukocyte populations of the innate immune system in the blood, IL-10 KO

mice presented a decrease in the percentage of eosinophils ($t_{(114)} = 3.28$, $p = 0.001$, $d = 0.61$; **Figure 34A**) and an increase in the percentage of neutrophils ($t_{(114)} = 3.41$, $p < 0.001$, $d = 0.63$; **Figure 34B**) within leukocytes, when compared to WT littermates. In contrast, IL-10 absence did not impact the percentage of monocytes within leukocytes ($U = 1617.50$, $p = 0.724$, $r_u = 0.03$; **Figure 34C**). The population of natural killer (NK) cells was subdivided according to the expression levels of Ly6C. Mature NK cells expressing high levels of Ly6C are reported to be resting cells, whereas NK cells expressing low levels of Ly6C are effector cells (Omi *et al.*, 2014). IL-10 KO mice showed a decrease in the percentage of both Ly6C^{high} ($t_{(114)} = 7.20$, $p < 0.001$, $d = 1.34$; **Figure 34D**) and Ly6C^{low} NK cells subsets ($U = 1015.00$, $p < 0.001$, $r_u = 0.34$; **Figure 34E**) within leukocytes, when compared to WT littermates. Regarding the major populations of the adaptive immune system in the blood, IL-10 KO mice

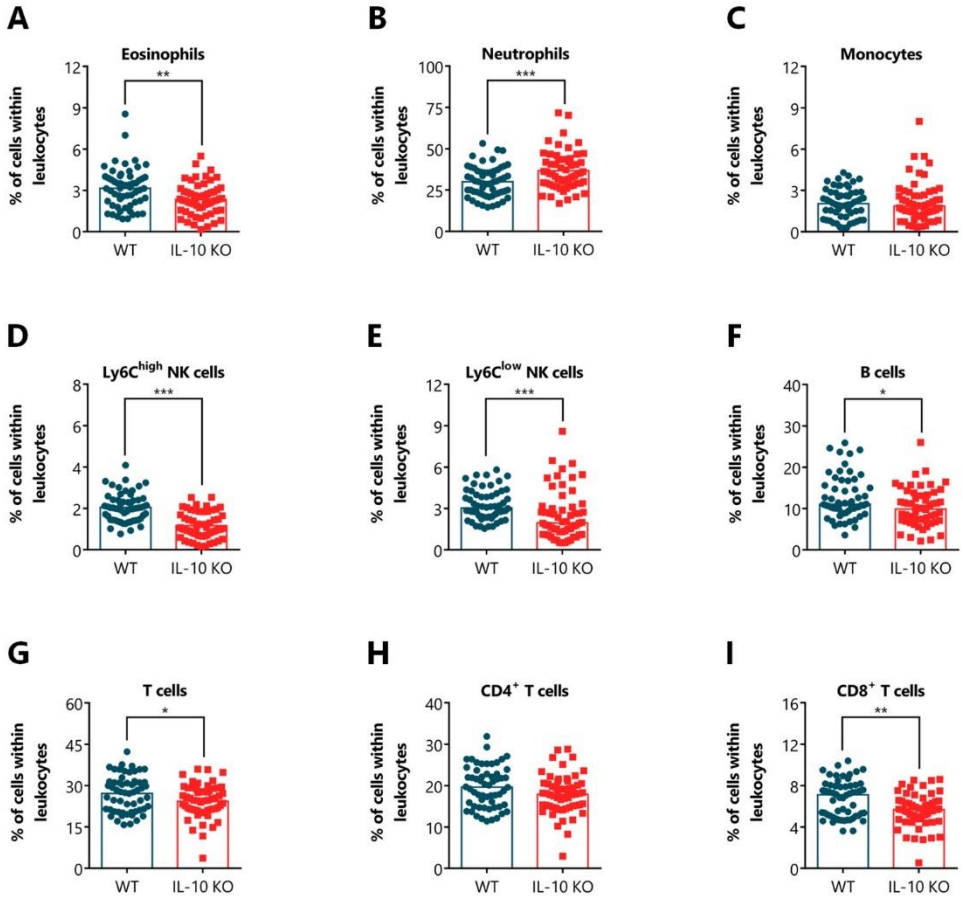

Figure 34. IL-10 absence impacted the percentage of the major leukocyte populations of the innate and adaptive immune systems in the blood. A-I. The percentage within leukocytes of eosinophils, neutrophils, monocytes, Ly6C^{high} and Ly6C^{low} NK cells, B cells, T cells, and both CD4$^+$ and CD8$^+$ T cells are shown. Data presented as mean (**A-B**; **D**; **G-H**) or median (**C**; **E-F**; **I**) of the values from four independent sets. Each dot represents an animal. $n_{WT} = 58$; $n_{IL\text{-}10\ KO} = 58$. Statistical analysis was performed by a two-tailed independent samples *t*-test (**A-B**; **D**; **G-H**) or a Mann-Whitney *U* test (**C**; **E-F**; **I**). * $p < 0.05$; ** $p < 0.01$; *** $p < 0.001$.

showed a decreased percentage of B cells (U = 1261.50, p = 0.020, r_u = 0.22; **Figure 34F**), T cells ($t_{(114)}$ = 2.41, p = 0.018, d = 0.45; **Figure 34G**), and CD8$^+$ T cells (U = 1171.50, p = 0.005, r_u = 0.26; **Figure 34I**) within leukocytes, when compared to WT littermates. In the percentage of CD4$^+$ T cells within leukocytes, no differences between genotypes were detected ($t_{(114)}$ = 1.91, p = 0.059, d = 1.36; **Figure 34H**). The number of circulating leukocytes per µL of blood was higher in IL-10 KO mice than in WT controls (U = 508.00, p = 0.026, r_u = 0.25; **Figure 35A**). Phenotypical analysis showed that only the number of neutrophils per µL of blood was higher in IL-10 KO mice that in WT littermates (U = 395.00, p = 0.002, r_u = 0.36; **Figure 35C**). No differences were observed between genotypes in the number of eosinophils (U = 700.00, p = 0.976, r_u < 0.01; **Figure 35B**), monocytes (U = 592.00, p = 0.242, r_u = 0.14; **Figure 35D**), both Ly6C^{high} (U = 545.00, p = 0.095, r_u = 0.19; **Figure 35E**) and Ly6C^{low} NK cells

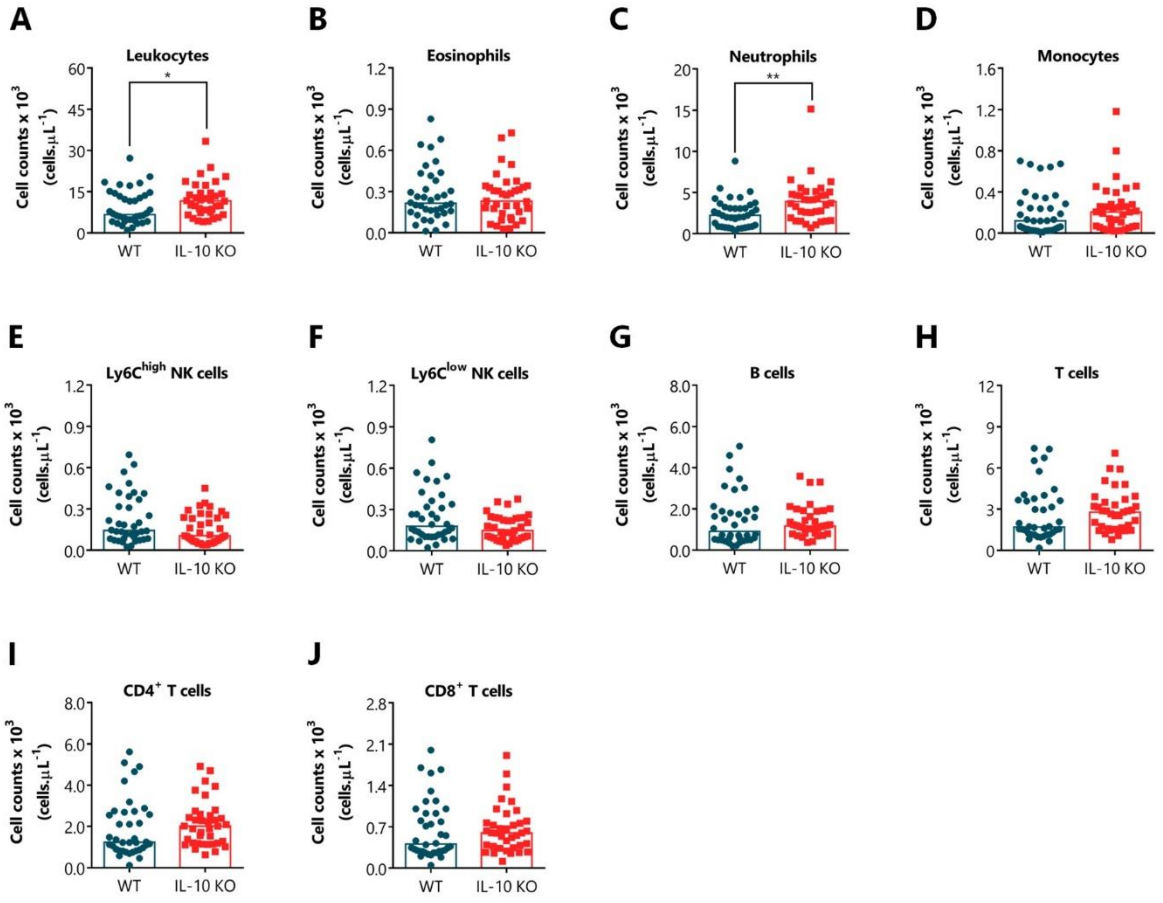

Figure 35. IL-10 absence impacted the number of neutrophils in the blood. A. The total number of leukocytes per µL of blood is presented. **B-J.** The number of eosinophils, neutrophils, monocytes, Ly6C^{high} and Ly6C^{low} NK cells, B cells, T cells, and both CD4$^+$ and CD8$^+$ T cells per µL of blood are also shown. Data presented as median of the values from three independent sets. Each dot represents an animal. n_{WT} = 38; $n_{IL\text{-}10\ KO}$ = 37. Statistical analysis was performed by a Mann-Whitney U test. * p < 0.05; ** p < 0.01.

(U = 539.00, p = 0.083, r_u = 0.20; **Figure 35F**), B cells (U = 612.00, p = 0.338, r_u = 0.11; **Figure 35G**), T cells (U = 587.00, p = 0.222, r_u = 0.14; **Figure 35H**), and both $CD4^+$ (U = 568.00, p = 0.154, r_u = 0.17; **Figure 35I**) and $CD8^+$ T cells (U = 632.00, p = 0.456, r_u = 0.09; **Figure 35J**) per µL of blood.

Aiming to understand if distinct B cell subsets were impacted by IL-10 absence and correlated with the cognitive data, the expression levels of the surface marker Ly6C, which is reported to be highly expressed in B cells with a plasma cell phenotype (Wrammert *et al.*, 2002; Tellier and Nutt, 2017), and the cell size were used to distinguish B cell subsets (**Figure 36A**). IL-10 absence did not affect the percentage of B cells expressing high levels of Ly6C ($FSC\text{-}A^{int}$, $Ly6C^{high}$: U = 1418.00, p = 0.190, r_u = 0.12; **Figure 36B**), nor the percentage of naïve B cells ($FSC\text{-}A^{low}$, $Ly6C^{low}$: U = 1326.00, p = 0.067, r_u = 0.17; **Figure 36C**). The percentage of large size B cells expressing low levels of Ly6C also remained similar between genotypes ($FSC\text{-}A^{high}$, $Ly6C^{low}$: $t_{(114)}$ = 0.77, p = 0.440, d = 0.14; **Figure 36D**).

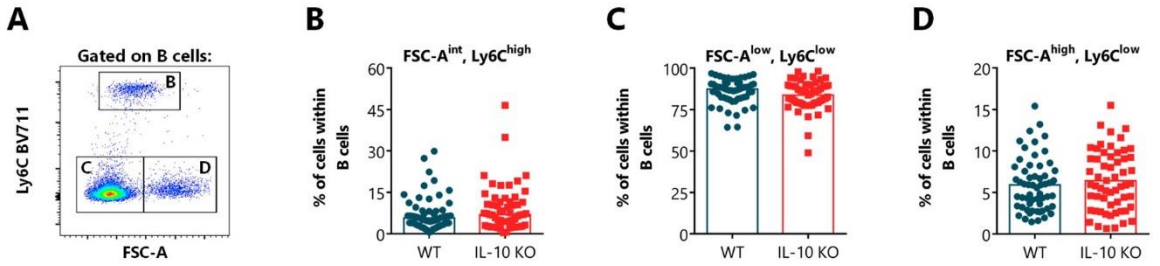

Figure 36. IL-10 absence did not impact the percentage of distinct B cell subsets in the blood. A. B cell subsets were characterized by the levels of Ly6C and further subdivided as $FSC\text{-}A^{low}$, and $FSC\text{-}A^{high}$ cells. **B-D.** The percentage of $FSC\text{-}A^{int}$, $Ly6C^{high}$ cells (**B**), $FSC\text{-}A^{low}$, $Ly6C^{low}$ cells (**C**), and $FSC\text{-}A^{high}$, $Ly6C^{low}$ cells (**D**) within B cells are shown. Data presented as median (**B-C**) or mean (**D**) of the values from four independent sets. Each dot represents an animal. n_{WT} = 58; $n_{IL\text{-}10\ KO}$ = 58. Statistical analysis was performed by a Mann-Whitney U test (**B-C**) or a two-tailed independent samples t-test (**D**).

To assess if alterations in distinct T cell subsets were induced by IL-10 deficiency and correlated with the behavioral performance, different cell compartments within $CD4^+$ and $CD8^+$ T cells were characterized. Within $CD4^+$ T cell (**Figure 37A**), the different compartments were distinguished by the expression levels of the surface markers CD44, which is highly expressed in CM and EM T cells, but not on the naïve counterparts (Baaten, Li and Bradley, 2010), and CD62L, which is highly expressed on naïve and CM T cells, but not on EM T cells (Sallusto, Geginat and Lanzavecchia, 2004). IL-10 absence did not affect the percentage of $CD4^+$ T cells with a naïve phenotype ($CD44^{low:int}$, $CD62L^{high}$: $t_{(114)}$ = 1.83, p = 0.070, d = 0.34; **Figure 37B**), nor the percentage of CM $CD4^+$ T cells ($CD44^{high}$, $CD62L^{high}$: U = 1413.50, p = 0.139, r_u = 0.14; **Figure 37C**). However, the percentage of $CD4^+$ T cells with lower

levels of CD44 and intermediate levels of CD62L were reduced ($CD44^{low:int}$, $CD62L^{int}$: $t_{(114)} = 4.00$, $p < 0.001$, $d = 0.74$; **Figure 37D**) and the percentage of EM $CD4^+$ T cells were increased ($CD44^{int:high}$, $CD62L^{low}$: $t_{(114)} = 6.09$, $p < 0.001$, $d = 1.13$; **Figure 37E**) in IL-10 KO mice when compared to WT controls. Within $CD8^+$ T cells (**Figure 38A**), the different compartments were analyzed by the expression levels of the surface markers CD62L and Ly6C, the latter being reported as a marker of memory $CD8^+$ T cells (Walunas *et al.*, 1995; Hänninen *et al.*, 2011). Blood of IL-10 KO mice showed an increased percentage of CM $CD8^+$ T cells ($Ly6C^{high}$, $CD62L^{high}$: $t_{(114)} = 3.16$, $p = 0.002$, $d = 0.59$; **Figure 38C**) and a decreased percentage of $CD8^+$ T cells expressing low levels of Ly6C and intermediate levels of CD62L ($Ly6C^{low}$, $CD62L^{int}$: $t_{(114)} = 2.63$, $p = 0.009$, $d = 0.49$; **Figure 38D**), when compared to WT littermates. The genotype did not influence the percentage of the remaining $CD8^+$ T cell subsets ($Ly6C^{low}$, $CD62L^{high}$: $t_{(114)} = 1.68$, $p = 0.095$, $d = 0.31$; $Ly6C^{high}$, $CD62L^{int}$: $t_{(114)} = 1.36$, $p = 0.176$, $d = 0.25$; $Ly6C^{low}$, $CD62L^{low}$: $U = 1396.50$, $p = 0.152$, $r_u = 0.13$; $Ly6C^{high}$, $CD62L^{low}$: $U = 1538.50$, $p = 0.524$, $r_u = 0.06$; **Figures 38B and 38E-G**). In **Supplementary table 3**, the correlations between the variables of the leukocyte profile characterization in the blood and other variables with statistically significant differences between WT and IL-10 KO mice covered in this thesis were described.

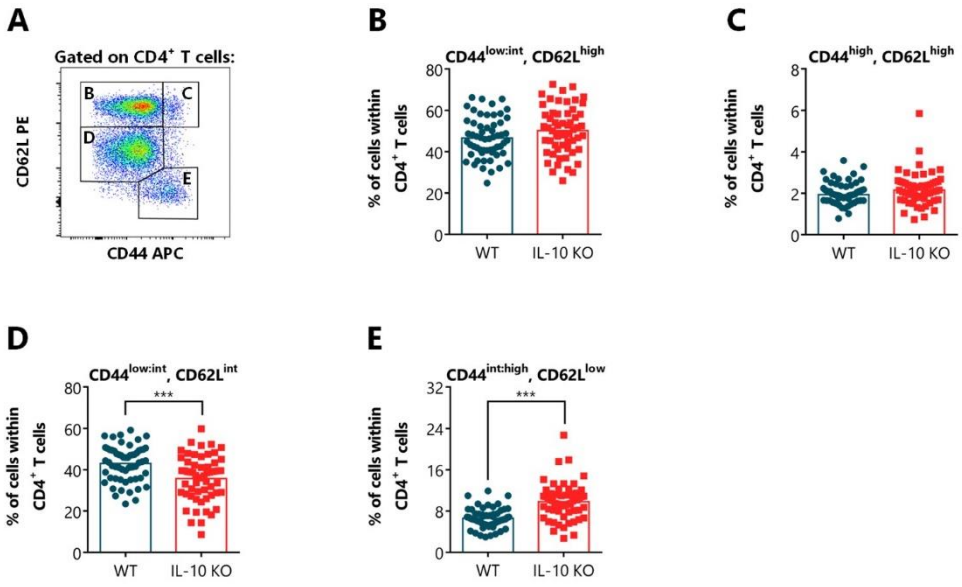

Figure 37. IL-10 absence impacted the percentage of distinct $CD4^+$ T cell subsets in the blood. A. $CD4^+$ T cell subsets were characterized by the levels of CD44 and CD62L. **B-E.** The percentage of $CD44^{low:int}$, $CD62L^{high}$ cells (**B**), $CD44^{high}$, $CD62L^{high}$ cells (**C**), $CD44^{low:int}$, $CD62L^{int}$ cells (**D**), and $CD44^{int:high}$, $CD62L^{low}$ cells (**E**) within $CD4^+$ T cells are shown. Data presented as mean (**B**; **D-E**) or median (**C**) or of the values from four independent sets. Each dot represents an animal. $n_{WT} = 58$; $n_{IL\text{-}10\ KO} = 58$. Statistical analysis was performed by a two-tailed independent samples *t*test (**B**; **D-E**) or a Mann-Whitney *U* test (**C**). *** $p < 0.001$.

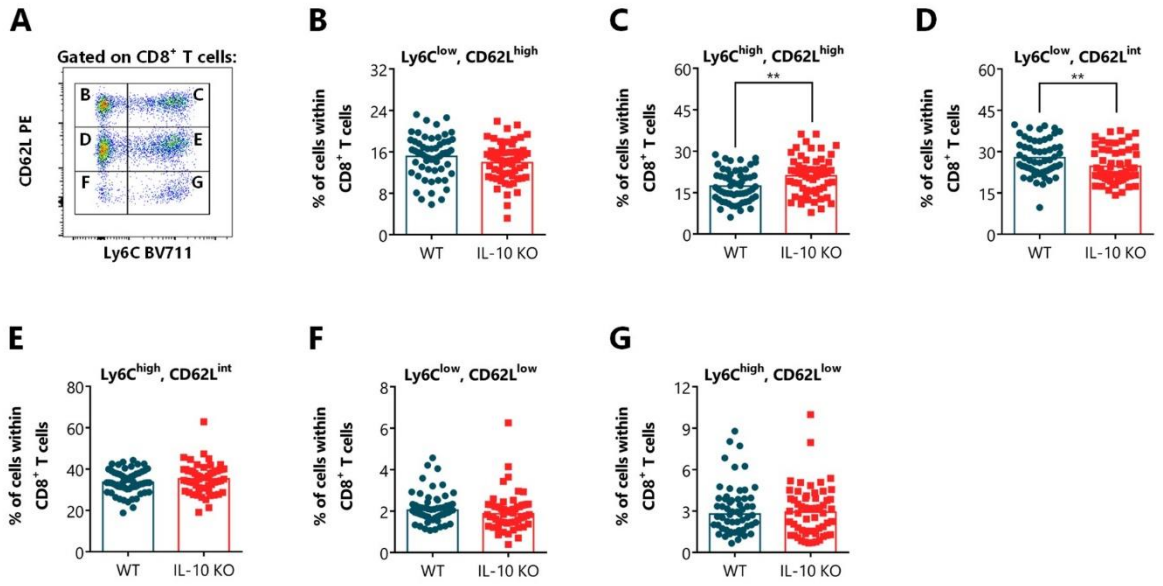

Figure 38. IL-10 absence impacted the percentage of distinct CD8$^+$ T cell subsets in the blood. A. CD8$^+$ T cell subsets were characterized by the levels of Ly6C and CD62L. **B-G.** The percentage of Ly6C^{low}, CD62L^{high} cells (**B**), Ly6C^{high}, CD62L^{high} cells (**C**), Ly6C^{low}, CD62L^{med} cells (**D**), Ly6C^{high}, CD62L^{med} cells (**E**), Ly6C^{low}, CD62L^{low} cells (**F**), and Ly6C^{high}, CD62L^{low} cells (**G**) within CD8$^+$ T cells are shown. Data presented as mean (**B-E**) or median (**F-G**) or of the values from four independent sets. Each dot represents an animal. n_{WT} = 58; $n_{IL\text{-}10\ KO}$ = 58. Statistical analysis was performed by a two-tailed independent samples *t*-test (**B-E**) or a Mann-Whitney *U* test (**F-G**). ** $p < 0.01$.

4.6.2 IL-10 deficiency impacted the leukocyte profile in the inguinal and deep cervical lymph nodes

The leukocyte profile was characterized in the dcLN, which drain the brain region (Kida, Pantazis and Weller, 1993), and in the ingLN, which play no role in the process of brain immune surveillance and were used as an internal control. Concerning the major leukocyte populations in the ingLN, IL-10 KO mice presented an increased percentage of B cells, a decreased percentage of T cells and CD4$^+$ T cells, and a similar percentage of CD8$^+$ T cells within leukocytes, when compared to WT littermates (B cells: $t_{(96)} = 3.54$, $p < 0.001$, $d = 0.71$; T cells: $t_{(96)} = 3.51$, $p < 0.001$, $d = 0.71$; CD4$^+$ T cells: $U = 703.00$, $p < 0.001$, $r_U = 0.36$; CD8$^+$ T cells: $t_{(96)} = 1.06$, $p = 0.292$, $d = 0.21$; **Figure 39A-D**). In contrast, in the dcLN, no differences were detected between genotypes in the percentage of B cells, T cells, CD4$^+$, and CD8$^+$ T cells within leukocytes (B cells: $t_{(96)} = 1.85$, $p = 0.067$, $d = 0.38$; T cells: $t_{(96)} = 1.25$, $p = 0.215$, $d = 0.25$; CD4$^+$ T cells: $U = 944.00$, $p = 0.070$, $r_U = 0.18$; CD8$^+$ T cells: $t_{(96)} = 0.34$, $p = 0.736$, $d = 0.07$; **Figures 39A-D**). The genotype did not influence the total number of leucocytes per ingLN ($U = 1177.50$, $p = 0.875$, $r_U = 0.02$), however, IL-10 KO mice presented an increased number of leukocytes in the dcLN, when compared to WT littermates ($U = 752.50$, $p = 0.001$, $r_U = 0.32$; **Figure 40A**).

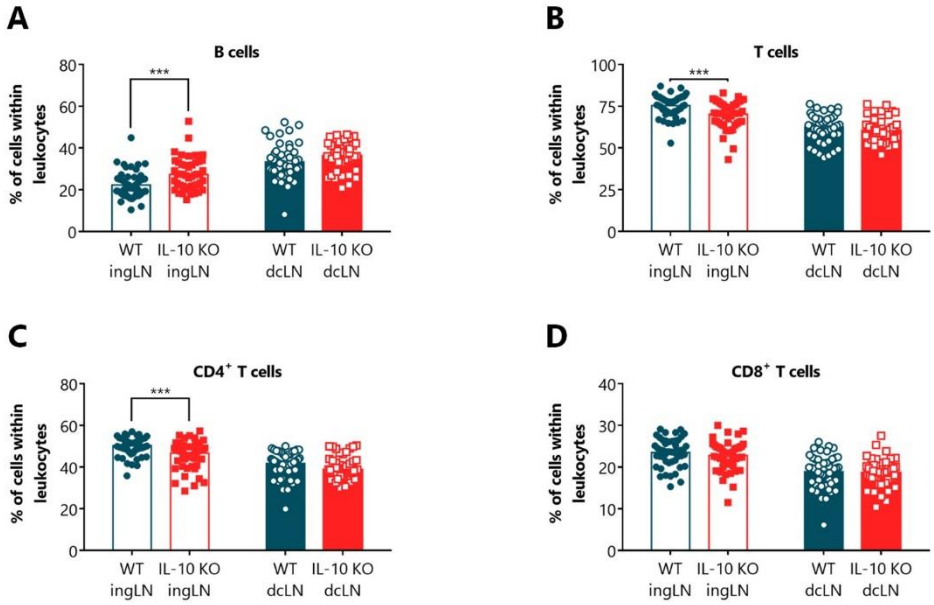

Figure 39. IL-10 absence impacted the percentage of the major leukocyte populations of the adaptive immune system in the inguinal, but not in the deep cervical lymph nodes. A-D. The percentage of B cells, T cells, and both $CD4^+$ and $CD8^+$ T cells within leukocytes are shown. Data presented as mean (**A-B**; **D**) or median (**C**) of the values from three independent sets. Each dot represents an animal. dcLN – deep cervical lymph nodes; ingLN – inguinal lymph nodes. n_{WT} = 50; $n_{IL\text{-}10\ KO}$ = 48. Statistical analysis was performed by a two-tailed independent samples *t*test (**A-B**; **D**) or a Mann-Whitney *U*test (**C**). *** $p < 0.001$.

Phenotypical analysis showed that IL-10 deficiency did not impact the numbers of B cells, T cells, $CD4^+$, and $CD8^+$ T cells in the ingLN (B cells: $U = 1016.00$, $p = 0.193$, $r_U = 0.13$; T cells: $U = 1071.0$, $p = 0.362$, $r_U = 0.09$; $CD4^+$ T cells: $U = 1034.00$, $p = 0.240$, $r_U = 0.12$; $CD8^+$ T cells: $U = 1125.5$, $p = 0.599$, $r_U = 0.05$; **Figure 40B-E**). Oppositely, IL-10 KO mice showed a higher number of all leukocyte types evaluated in the dcLN than WT controls (B cells: $U = 737.00$, $p < 0.001$, $r_U = 0.33$; T cells: $U = 765.0$, $p = 0.002$, $r_U = 0.31$; $CD4^+$ T cells: $U = 765.00$, $p = 0.002$, $r_U = 0.31$; $CD8^+$ T cells: $U = 763.00$, $p = 0.002$, $r_U = 0.31$; **Figure 40B-E).**

To assess if alterations in distinct T cell subsets were induced by IL-10 deficiency and correlated with the cognitive data, different cell compartments within $CD4^+$ and $CD8^+$ T cells were characterized. Within $CD4^+$ T cells (**Figure 41A**), IL-10 deficiency, in both the ingLN and dcLN, did not affect the percentage of cells with a naïve phenotype (ingLN - $CD44^{low:int}$, $CD62L^{high}$: $U = 1124.50$, $p = 0.594$, $r_U = 0.05$; dcLN - $CD44^{low:int}$, $CD62L^{high}$: $U = 1111.00$, $p = 0.530$, $r_U = 0.06$; **Figure 41B**) nor the percentage of EM $CD4^+$ T cells (ingLN - $CD44^{int:high}$, $CD62L^{low}$: $U = 1109.50$, $p = 0.523$, $r_U = 0.07$; dcLN - $CD44^{int:high}$, $CD62L^{low}$: $U = 1086.00$, $p = 0.421$, $r_U = 0.08$; **Figure 41C**). Within $CD8^+$ T cells (**Figure 42A**), the percentage of naïve cells was diminished in both the ingLN and dcLN of IL-10 KO mice when compared to

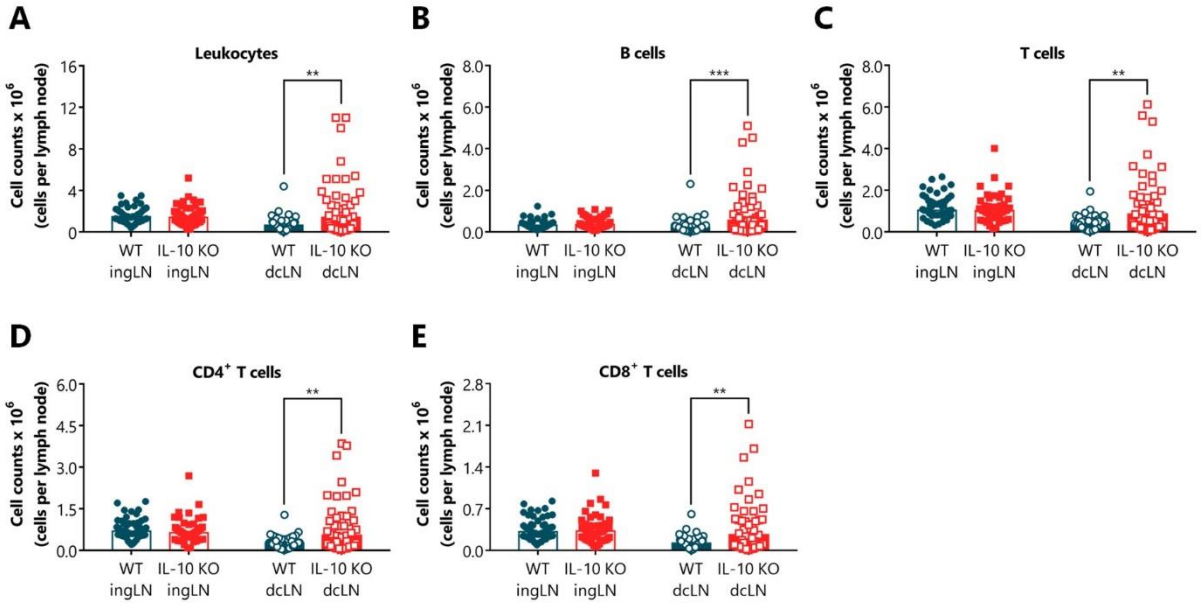

Figure 40. IL-10 absence impacted the number of leukocytes in the deep cervical, but not in the inguinal lymph nodes. I. The total number of leukocytes per lymph node is presented. **A-H.** The number of B cells, T cells, and both $CD4^+$ and $CD8^+$ T cells per lymph node are also shown. Data presented as median of the values from three independent sets. Each dot represents an animal. dcLN – deep cervical lymph nodes. ingLN – inguinal lymph nodes. $n_{WT} = 50$; $n_{IL\text{-}10\ KO} = 48$. Statistical analysis was performed by a Mann-Whitney *U* test. ** $p < 0.01$; *** $p < 0.001$.

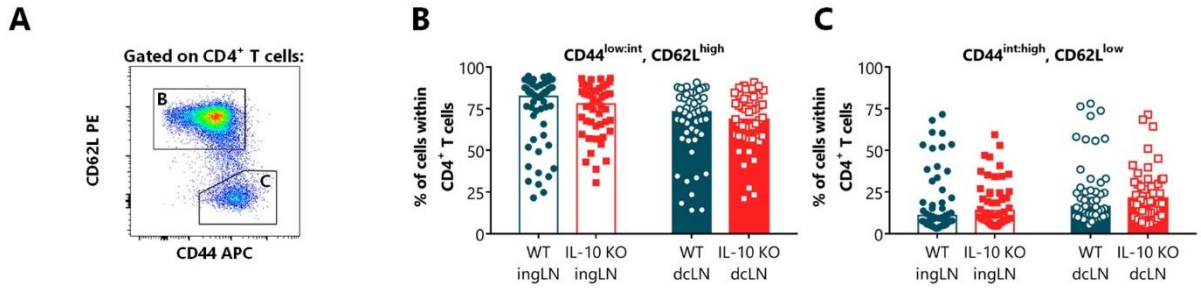

Figure 41. IL-10 absence did not impact the percentage of distinct $CD4^+$ T cell subsets in the inguinal and deep cervical lymph nodes. A. $CD4^+$ T cell subsets were characterized by the levels of CD44 and CD62L. **B-C.** The percentage of $CD44^{low:int}$, $CD62L^{high}$ cells (**B**), and $CD44^{int:high}$, $CD62L^{low}$ cells (**C**) within $CD4^+$ T cells are shown. Data presented as median of the values from three independent sets. Each dot represents an animal. dcLN – deep cervical lymph nodes; ingLN – inguinal lymph nodes. $n_{WT} = 50$; $n_{IL\text{-}10\ KO} = 48$. Statistical analysis was performed by a Mann-Whitney *U* test.

WT littermates (ingLN - $Ly6C^{low}$, $CD62L^{high}$: $t_{(96)} = 2.14$, $p = 0.035$, $d = 0.43$; dcLN - $Ly6C^{low}$, $CD62L^{high}$: $t_{(96)} = 2.54$, $p = 0.013$, $d = 0.51$; **Figure 42B**). IL-10 absence did not influence the percentage of the remaining $CD8^+$ T cell subsets in the lymph nodes (ingLN - $Ly6C^{high}$, $CD62L^{high}$: $U = 1007.00$, $p = 0.172$, $r_u = 0.14$; dcLN - $Ly6C^{high}$, $CD62L^{high}$: $U = 1151.50$, $p = 0.733$, $r_u = 0.03$; ingLN - $Ly6C^{low}$, $CD62L^{low}$: $U = 1180.00$, $p = 0.889$, $r_u = 0.01$; dcLN - $Ly6C^{low}$, $CD62L^{low}$: $U = 1063.50$, $p = 0.334$, $r_u = 0.10$; ingLN - $Ly6C^{high}$, $CD62L^{low}$: $U = 1066.50$, $p = 0.345$, $r_u = 0.10$; dcLN - $Ly6C^{high}$, $CD62L^{low}$:

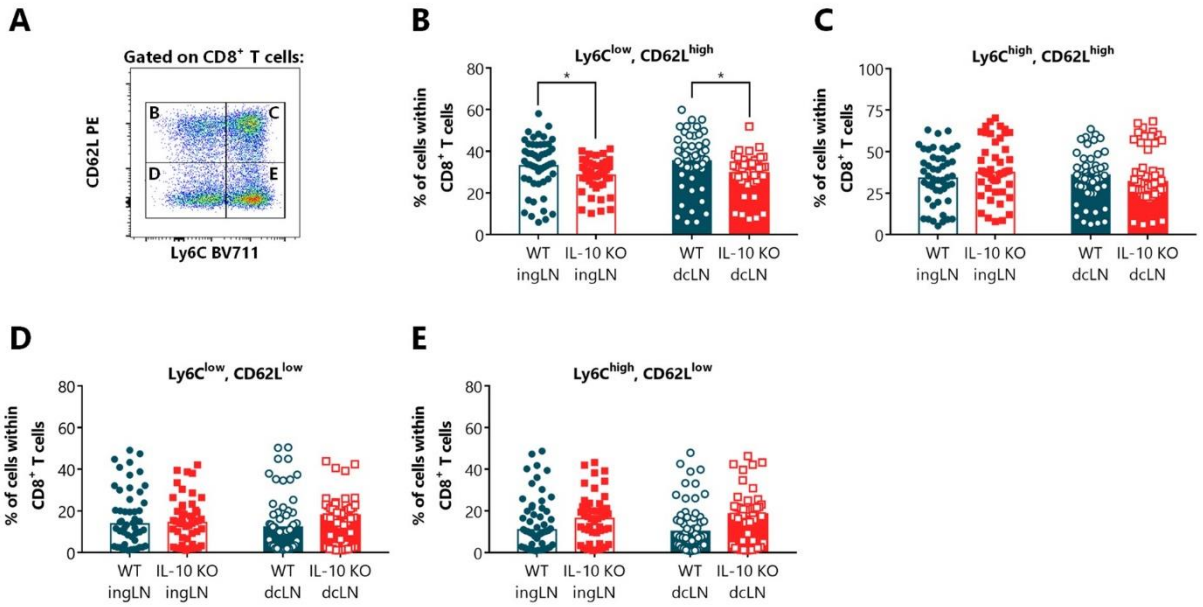

Figure 42. IL-10 absence impacted the percentage of naïve CD8⁺ T cells in the inguinal and deep cervical lymph nodes. **A.** CD8⁺ T cell subsets were characterized by the levels of Ly6C and CD62L. **B-E.** The percentage within CD8⁺ T cells of Ly6C^{low}, CD62L^{high} cells (**B**), Ly6C^{high}, CD62L^{high} cells (**C**), Ly6C^{low}, CD62L^{low} cells (**D**), and Ly6C^{high}, CD62L^{low} cells (**E**) are shown. Data presented as mean (**B**) or median (**C-E**) of the values from three independent sets. Each dot represents an animal. dcLN – deep cervical lymph nodes; ingLN – inguinal lymph nodes. n_{WT} = 50; $n_{IL\text{-}10\ KO}$ = 48. Statistical analysis was performed by a two-tailed independent samples *t*test (**B**) or a Mann-Whitney *U* test (**C-E**). * $p < 0.05$.

$U = 945.50$, $p = 0.071$, $r_U = 0.18$; **Figure 42C-E**). In **Supplementary table 3**, the correlations between the variables of the leukocyte profile characterization in the lymph nodes and other variables with statistically significant differences between WT and IL-10 KO mice covered in this thesis were described.

4.7 Gut microbiome depletion protocol optimization

As mentioned in the aforementioned results in *Part 1* of this thesis, IL-10 KO mice, when compared to WT littermates, presented cognitive impairments, which may be associated with alterations in hippocampal structural plasticity, in corticosterone levels, and in leukocyte profile in the blood and lymph nodes. In a striking display of trans-kingdom symbiosis, it is consistently reported that the gut microbiome may also cooperate with its host in the regulation of cognition through the gut-brain axis (Morais, Schreiber and Mazmanian, 2021). However, although it is known that IL-10 KO mice exhibit an altered gut microbiome in terms of microbial diversity and richness (Maharshak *et al.*, 2013; Singh *et al.*, 2016), the potential impact that the gut microbiome may have in the cognitive function of IL-10 KO mice remains a mystery. A way to test this association could be through gut microbiome modulation of IL-10 KO mice with the gut bacterial community of WT mice and, subsequently, assess if this modulation can

reverse the cognitive impairments of IL-10 KO mice. The first step in the gut microbiome modulation of IL-10 KO mice is the depletion of the pre-existing gut microbiome, so that the gut can later be recolonized with the microbiome of interest from WT mice. In *Part 2* of this thesis, aiming to optimize an effective protocol for gut microbiome depletion, a 10-day treatment with a daily oral gavage of an antibiotic cocktail was tested in both IL-10 KO and WT mice. This treatment was selected for testing as it is reported to result in a 10-fold reduction in *16S* DNA in stool pellets without dehydration of mice, and accompanied by anatomic, histologic, and immunologic changes characteristic of germ-free mice (Hill *et al.*, 2010; Kennedy, King and Baldridge, 2018).

4.7.1 The 10-day antibiotic treatment by oral gavage had no impact on animal welfare

To evaluate if the antibiotic treatment by oral gavage had a negative impact on animal welfare of IL-10 KO and WT mice, body weight was monitored daily in mice submitted to the antibiotic treatment and in age- and genotype-matched controls. Both IL-10 KO and WT mice receiving the antibiotic cocktail displayed similar body weight to the control counterparts in each day of treatment (time factor: $F_{(30, 380)} = 2.60$, $p = 0.005$, $\eta^2_p = 0.06$, $\eta^2_p = 0.13$; group factor: $F_{(3, 38)} = 0.56$, $p = 0.644$, $\eta^2_p = 0.04$; interaction: $F_{(30, 380)} = 3.56$, $p < 0.001$, $\eta^2_p = 0.22$; **Figure 43**). Moreover, treated mice exhibited no overt signs of sickness or distress, thus assuring the safety of the protocol used.

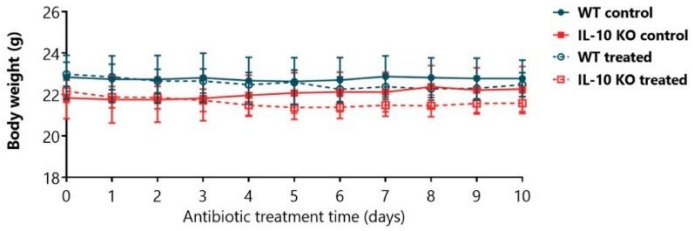

Figure 43. The 10-day antibiotic treatment by oral gavage had no impact on animal body weight. Both control and treated mice were weighed daily during the 10-day antibiotic treatment. Data presented as mean ± SEM of the values from two independent sets. $n_{WT\ control} = 6$; $n_{IL\text{-}10\ KO\ control} = 6$; $n_{WT\ treated} = 15$; $n_{IL\text{-}10\ KO\ treated} = 15$. Statistical analysis was performed by a two-way repeated-measures ANOVA.

4.7.2 Antibiotics did not deplete cultivable bacteria in the feces after 10 days of treatment

Throughout the 10-day antibiotic treatment, the effectiveness of the gut microbiome depletion was evaluated by CFUs quantification in aerobic and anaerobic conditions. On set 1, CFUs were assessed

on days 3, 7, and 10 of the antibiotic treatment, as fecal samples from day 0 were unutilized due to experimental error. The number of both aerobic and anaerobic CFUs changed during antibiotic treatment (aerobic CFUs: $\chi^2_{F(5)} = 44.90$, $p < 0.001$, $W = 0.23$; anaerobic CFUs: $\chi^2_{F(5)} = 29.08$, $p < 0.001$, $W = 0.18$; **Figure 44A-B**). However, the number of CFUs did not decrease as expected, since a *post hoc* analysis revealed that in both aerobic and anaerobic conditions, mice after 10 days of treatment displayed a higher number of CFUs than on day 3 of treatment (WT - aerobic CFUs: $p < 0.001$, $r_u = 0.84$; IL-10 KO - aerobic CFUs: $p < 0.001$, $r_u = 0.84$; WT - anaerobic CFUs: $p < 0.001$, $r_u = 0.84$; IL-10 KO - anaerobic CFUs: $p = 0.022$, $r_u = 0.70$). Considering the experimental problems of set 1 that did not allow to quantify the number of CFUs on day 0, set 2 was performed. On set 2, CFUs were also assessed on day 1 of the treatment to evaluate the impact of the antibiotic administration at an early time point. As in set 1, on set 2 the antibiotic treatment also affected the number of both aerobic and anaerobic CFUs (aerobic CFUs: $\chi^2_{F(10)} = 17.11$, $p = 0.047$, $W = 0.03$; anaerobic CFUs: $\chi^2_{F(8)} = 17.00$, $p = 0.017$, $W = 0.30$; **Figure 44C-D**). However, in this case, a *post hoc* analysis did not reveal any differences in the number of CFUs over time, when compared to day 0.

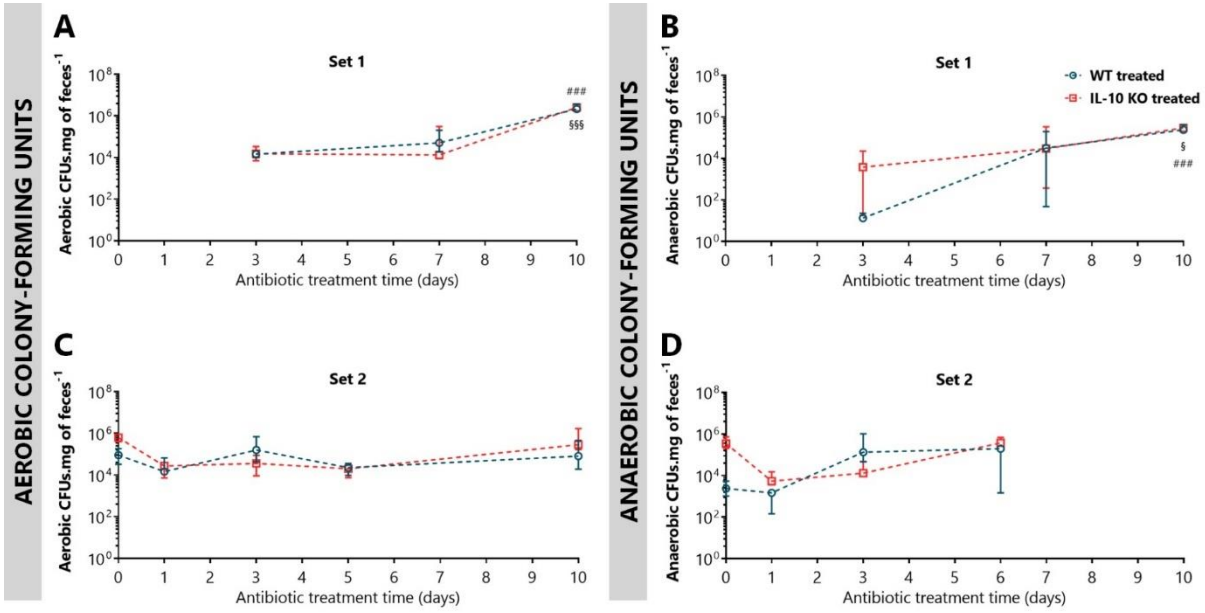

Figure 44. Antibiotics did not deplete cultivable aerobic and anaerobic bacteria in the feces after 10 days of treatment. A-B. On set 1, CFUs were assessed on days 3, 7, and 10 of the 10-day antibiotic treatment independently in aerobic (**A**) and anaerobic conditions (**B**). **C-D.** On set 2, CFUs were assessed on days 0, 1, 3, 5, and 10 of the 10-day antibiotic treatment in aerobic conditions (**C**), and independently on days 0, 1, 3, and 6 in anaerobic conditions (**D**). CFUs qualification was normalized for feces weight. Data presented as median ± IQR. CFUs – colony forming units. $n_{WT\ treated} = 12$; $n_{IL\text{-}10\ KO\ treated} = 12$ (**A-B**); $n_{WT\ treated} = 3$; $n_{IL\text{-}10\ KO\ treated} = 3$ (**C-D**). Statistical analysis was performed by a Friedman's test. * $p < 0.05$; *** $p < 0.001$. # $WT_{treated\ day\ 3}$ *vs* $WT_{treated\ day\ 7;\ 10}$; § IL-10 $KO_{treated\ day\ 3}$ *vs* IL-10 $KO_{treated\ day\ 7;\ 10}$.

4.7.3 Antibiotics effectively reduced the gene expression levels of the *16s* bacterial marker in the feces after 3 days of treatment

To confirm the effectiveness of the gut microbiome depletion throughout the antibiotic treatment, the total load of bacterial DNA in fecal pellets was also assessed through the gene expression levels of the *16s* bacterial marker by qRT-PCR. Since feces also contain murine host cells that have been shed (Watson *et al.*, 2009), the *Mpigr* gene was used to normalize the amount of *16s* present in the fecal pellets. On set 1, the antibiotic treatment significantly affected the gene expression levels of the *16s* bacterial marker throughout treatment time (*16s*: $\chi^2_{H(5)} = 33.38$, $p < 0.001$, $\eta^2 = 0.77$; **Figure 45A**). In fact, after only 3 days of antibiotic treatment, both IL-10 KO mice and WT littermates had already markedly reduced gene expression levels of *16s* in their feces relatively to day 0 (WT - day 3: $p < 0.001$, $r_U = 0.90$; IL-10 KO day 3: $p < 0.001$, $r_U = 0.90$). At day 7 of treatment, the gene expression levels of *16s* remained lower than those of day 0 in both genotypes (WT - day 7: $p = 0.011$, $r_U = 0.88$; IL-10 KO - day 7: $p = 0.008$, $r_U = 0.88$). To assess if antibiotic treatment led to fungal overgrowth, gene expression levels of the *Its2* fungal marker were evaluated. During antibiotic treatment, on set 1, no differences in *Its2* gene expression levels were detected in relation to day 0 (*Its2*: $\chi^2_{H(5)} = 3.31$, $p = 0.097$, $\eta^2 = 0.05$; **Figure 45B**). Overall, these results indicate that after 3 days of antibiotic treatment the total load of fecal bacterial DNA was diminished, without fungal overgrowth.

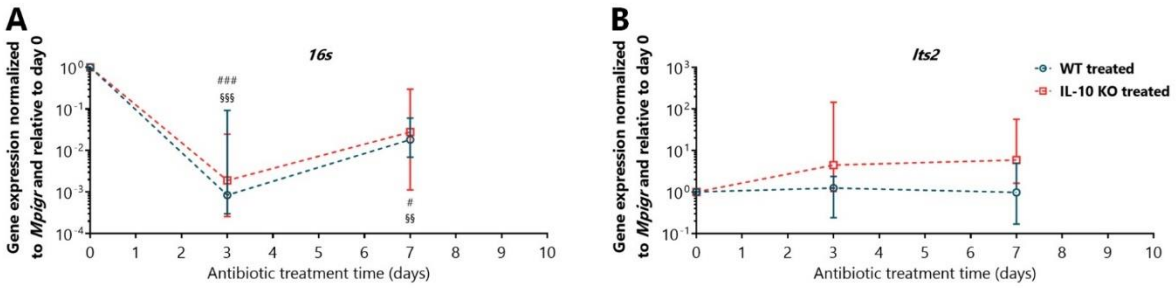

Figure 45. Antibiotics effectively reduced the gene expression levels of *16s* in the feces after 3 days of treatment. A-B. Gene expression levels of *16s* (**A**) and *Its2* (**B**) in the feces were assessed on days 0, 3, and 7 of the 10-day antibiotic treatment. Bacterial and fungal marker gene expression was quantified through qRT-PCR and normalized to the gene expression levels of *Mpigr* reference gene. Data presented as median ± IQR of the values from set 1. $n_{WT\ treated\ day\ 0} = 8$; $n_{WT\ treated\ day\ 3} = 5$; $n_{WT\ treated\ day\ 7} = 8$; $n_{IL\text{-}10\ KO\ treated\ day\ 0} = 8$; $n_{IL\text{-}10\ KO\ treated\ day\ 3} = 6$; $n_{IL\text{-}10\ KO\ treated\ day\ 7} = 8$. Statistical analysis was performed by a Kruskal-Wallis *H* test. * $p < 0.05$; ** $p < 0.01$; *** $p < 0.001$. # $WT_{treated\ day\ 0}$ *vs* $WT_{treated\ day\ 3;\ 7}$; § IL-10 $KO_{treated\ day\ 0}$ *vs* IL-10 $KO_{treated\ day\ 3;\ 7}$.

CHAPTER 5

DISCUSSION

CHAPTER 5 – **DISCUSSION**

In the last decades, it has been established that immune system homeostasis is crucial for cognitive abilities. So far, it is recognized that T cell absence and increased levels of pro-inflammatory cytokines are associated with impaired cognition (Baier *et al.*, 2009; Derecki *et al.*, 2010; Huang and Sheng, 2010; Monteiro *et al.*, 2015; Brombacher *et al.*, 2017). In contrast, anti-inflammatory cytokines, such as IL-10, have been poorly studied in the context of cognitive function. Recent studies, however, have shown that this anti-inflammatory cytokine might have important implications for cognitive processes (Xiu *et al.*, 2016; Jung *et al.*, 2019; Zhang *et al.*, 2020). Considering not only that IL-10 absence may affect cognitive abilities (Zhang *et al.*, 2020), but also that the effect of this anti-inflammatory cytokine in the CNS can be gender-specific (Mesquita *et al.*, 2008), it becomes vital to further decipher the role of IL-10 in the cognitive function of female mice and the potential mechanisms underlying its action.

In *Part 1* of this thesis, the effect of IL-10 absence in cognitive function was investigated in young--adult female BALB/c IL-10 KO and WT littermate mice submitted to a cognitive behavioral characterization. Herein, IL-10 absence was identified as a modulator of the hippocampal-dependent spatial reference memory in the BMT, as female IL-10 KO mice, mainly during the metestrus and diestrus phases of the estrous cycle, showed an impaired cognitive performance when compared to WT littermates. The detrimental properties of IL-10 deficiency in the cognitive function of female mice were restricted to the hippocampal-dependent spatial reference memory, as no differences were found in spatial and recognition short-term memory nor in spatial and non-spatial associative memory between IL-10 KO mice and WT littermates. In the OFT, IL-10 absence led to general and vertical exploration deficits but did not affect locomotor nor anxious-like behavior. To examine if the variables obtained by the behavioral characterization could classify the mice genotype, SVM models were used. This supervised machine learning method had classification accuracies of up to 89.3%, indicating that the mice genotype (WT *vs* IL-10 KO) can be classified through behavioral variables related to cognitive function. To analyze the impact of the colon inflammatory profile on behavioral data, the gene expression levels of pro-inflammatory markers were assessed by qRT-PCR. IL-10 absence led to increased gene expression levels of the pro-inflammatory markers *Ido*, *Ifnγ*, *Inos*, and *Tnf* in the colon. However, the results suggested that within IL-10 KO mice, the colon inflammatory profile did not influence their cognitive behavior.

Considering the hippocampal-dependent cognitive deficits observed in IL-10 KO mice, it was hypothesized that IL-10 deficiency could be affecting the structural plasticity of the hippocampus. The results revealed that IL-10 absence decreased the number of neurons and led to volumetric atrophy of

the DH, but not of the VH. Additionally, IL-10 deficiency modulated the dendritic spine dynamics by increasing the dendritic spine density in the dDG and reducing the dendritic spine density in the vDG, CA1, and CA3 subregions. Throughout the hippocampus, the neuronal dendrites of IL-10 KO mice displayed higher percentages of specialized ramified spines than WT controls. IL-10 absence also negatively affected the dendritic arborization of dDG and vDG granule neurons and CA1 and CA3 pyramidal neurons, which are known to support learning and memory (Espino, Gómez and Durán, 2020).

To better understand if IL-10 deficiency produced HPA axis activation alterations, serum corticosterone levels were assessed. IL-10 absence has led to higher levels of corticosterone at nadir, as previously reported (Smith *et al.*, 1999), but not at zenith, indicating a potential role of IL-10 in corticosterone circadian rhythm modulation.

Given the key roles of leukocytes in several brain functions (Kipnis *et al.*, 2004; Ziv *et al.*, 2006; Brynskikh *et al.*, 2008), it was hypothesized that modifications in the leukocyte profile could be induced by IL-10 deficiency. In the blood, flow cytometry analysis showed that IL-10 absence increased the total number and the percentage of neutrophils and decreased the percentage of eosinophils, natural-killer cells, B cells, and T cells. Additionally, in the blood, IL-10 deficiency increased the percentage of EM $CD4^+$ T cells and CM $CD8^+$ T cells. IL-10 absence also increased the total number of leukocytes in the dcLN, suggesting an increased cell recruitment to the lymphatic system of the brain.

In *Part 2* of this thesis, we aimed to characterize the potential impact that the gut microbiome modulation may have in the cognitive function of IL-10 KO mice. For that, a protocol for gut microbiome depletion was optimized through an antibiotic treatment. The results revealed that after 3 days of treatment, antibiotics reduced the gene expression levels of *16s* in the feces without fungal overgrowth, providing an initial step to explore the role of the gut microbiome in the cognition of IL-10 KO mice.

5.1 IL-10 absence as a modulator of cognitive function

In *Part 1* of this thesis, the central hypothesis was that IL-10 absence might modulate the cognitive abilities of female mice. To test this hypothesis, IL-10 KO mice and WT littermates were submitted to distinct behavioral tests to assess cognitive function. Of the several cognitive tests assessed, IL-10 absence selectively impaired the cognitive performance of mice in the BMT. Conceptually, this cognitive test is a hippocampal-dependent task for spatial learning and memory where mice learn the relationship between visual cues in the surrounding environment and a fixed escape chamber located in the target hole (Matthew, 2018). Rodents with hippocampal damage showed

impaired performance in the BMT (Fox *et al.*, 1998), supporting the involvement of the hippocampus in this test.

Our results revealed that during the learning phase of the BMT both genotypes were able to successfully learn the location of the target hole. However, in the probe trial, which was performed to assess spatial memory retrieval (Gawel *et al.*, 2019), IL-10 KO mice presented deficits in hippocampal--dependent spatial reference memory, as they had decreased poking behavior in the target hole, took longer to find its location, and spent less time in its vicinity than WT littermates. These results are supported by recent evidence indicating that reduced IL-10 expression in mice also led to cognitive deficits in the MWMT (Zhang *et al.*, 2020), which is another test to evaluate hippocampal-dependent spatial reference memory (Rogers *et al.*, 2017).

Additionally, the results of the classification of the paths taken by mice to find the location of the escape chamber revealed that IL-10 KO mice performed less hippocampal-dependent strategies (characterized by an immediate displacement or approach to the target hole) and more freezing, (specifically in the periphery of the BMT arena) than the WT littermates both during the learning phase and the probe trial. This data reinforced that the spatial orientation and navigation of IL-10 KO mice were compromised, indicating that IL-10 absence impacted the cognitive behavior. However, this classification of the paths taken by mice to find the location of the escape chamber into search strategies was done manually. Even with the researcher blind to the genotype during the analysis, manual classification of search strategies is prone to researcher bias, calling for a more objective method of data analysis. In future studies using the BMT in IL-10 KO mice, a supervised machine learning algorithm for unbiased BMT search strategy classification (Illouz *et al.*, 2016) should be adopted to overcome this issue.

During the learning phase of the BMT, the search strategy classification revealed a phenotype of cognitive impairment in IL-10 KO mice when compared to WT littermates, however, when looking at the variable of latency to enter the target hole in the same trials, this phenotype was not evident. This is explained by the fact that throughout the BMT, when mice found the position of the target hole, they did not always enter to the escape chamber, remaining in the vicinity of the target hole for the remaining time of the trial. Since this behavior may be associated with a lack of motivation to enter the escape chamber, future adaptations to the BMT protocol should be considered. One of them could be using the cued version of the BMT after performing the typical spatial version of this test. In the cue version, a visible cue is placed directly behind the target hole. The position of the target hole, and subsequently the location of the cue, varies from trial to trial. This version of BMT does not require hippocampal but rather striatum function, as mice need to associate the cue with the location of the target hole (Gawel *et al.*, 2019). Given

the critical role of the striatum in motivation (Liljeholm and O'Doherty, 2012), this protocol adaptation might help to assess variations in motivation to enter the target hole. Importantly, two other adaptations to the BMT protocol should also be considered: (1) the performance of a second probe trial 7 or 10 days after the end of the learning phase to evaluate long-term memory retrieval; and (2) the introduction of reverse learning trials to assess the cognitive flexibility of IL-10 KO mice, as reviewed elsewhere (Gawel *et al.*, 2019).

To our knowledge, the role of IL-10 in short-term memory was never addressed. In this thesis, the YMT and the NORT were used to respectively evaluate spatial and recognition short-term memory, which are cognitive abilities that involve the hippocampus (Broadbent *et al.*, 2010; Kraeuter, Guest and Sarnyai, 2019). Regarding the YMT, it was observed that IL-10 absence did not impact spatial short-term memory, however, IL-10 KO mice explored less the YMT arena than WT controls, as shown by the lower number of arm alternations during the testing trial. This result demonstrated that IL-10 deficiency may impact exploratory behaviors. In the same line, a study already demonstrated that IL-10 administration by itself was able to induce increased motor activity and exploration of mice (Harvey *et al.*, 2006), opening novel horizons to a direct role of this anti-inflammatory cytokine in exploration.

Still considering the YMT, it was observed that the mean percentage of time that WT mice explored the novel arm was close to the cut-off value that indicates a random exploration of the novel arm (33.3%). Since this phenomenon may have masked the spatial short-term memory phenotype in this test, a protocol adaptation should also be considered. In this thesis, a 2-trial YMT protocol was used to evaluate the spatial short-term memory of IL-10 KO mice. However, a single-trial spontaneous alternations protocol could also be performed in the same apparatus (Kraeuter, Guest and Sarnyai, 2019). In this version of the YMT, mice are placed in the center of the YMT arena with the 3 arms available for exploration. A spontaneous alternation is contemplated when mice visit the 3 arms of the arena sequentially without repetition – for instance, from arm A to arm B, and arm B to arm C. Incorrect entries occur when mice repeat a visit to the first arm after having visited the second arm – for instance, from arm A to arm B, and arm B to arm A (Sultana, Ogundele and Lee, 2019). Mice with a good working memory remember the arms of the YMT apparatus that were already visited and show a tendency to enter a less recently visited arm, thus increasing the number of spontaneous alternations performed (Kraeuter, Guest and Sarnyai, 2019).

The impact of IL-10 deficiency in short-term recognition memory was assessed using the NORT. In this test, although the percentage of exploration time spent in the novel object did not achieve a statistically significant difference between genotypes, there was a trend supported by a medium effect

size for IL-10 KO mice to spend less time exploring the novel object than the WT littermates. Actually, IL-10 KO mice had a percentage of exploration time spent in the novel object close to the cut-off for a random time in the novel object (50%), indicating that an exploration towards the novel object rather than the familiar one, might be reduced in IL-10 KO mice. Considering that this cognitive task was only successfully performed in one behavioral set, a novel set using IL-10 KO mice in the same conditions is required to confirm our hypothesis and understand the impact of IL-10 absence in short-term recognition memory.

The last test performed to assess the cognitive function of IL-10 KO mice was the CCFCT. In this test, the Pavlovian conditioned response of mice after the CS-US pairings was measured in two independent evaluations. In the first evaluation, the freezing behavior, which is the typical species--specific response to fear, was considered as the only conditioned response (Curzon, Rustay and Browman, 2009). With this analysis settings, the results demonstrate that, although right after conditioning, IL-10 KO mice exhibited longer times of freezing behavior than WT mice, no differences between genotypes were observed in the remaining trials. Nevertheless, during the first manual evaluation of the CCFCT, we observed that a series of conditioned responses besides freezing seem to emerge after the CS-US pairings in IL-10 KO and WT mice. Among them, tail rattle, vigorous grooming, vivid tremor, and intense jumping were noticed after the CS-US pairings, but not before conditioning. Tail rattle for instance has long been reported as a territorial behavior that occurs in response to threats or fear (Haber and Simmel, 1976), thus the CS-US pairings may have triggered the presence of this behavior during the CCFCT in our animal model. The second evaluation of the CCFCT was conducted considering freezing and these emerging behaviors as the conditioned response. With these analysis settings, the results demonstrate that IL-10 deficiency did not affect the conditioned response in any trial. Specifically, in the context probe, both genotypes associated the US to the spatial context in which they were placed (Context A), thus indicating that IL-10 absence did not impact spatial associative memory, a hippocampal-dependent cognitive ability that relies mainly in the DH function (Curzon, Rustay and Browman, 2009). In the cue probe, it was also revealed that after placing mice in a novel context (Context B), both genotypes associated the presence of the CS to the US. This result revealed that IL-10 deficiency did not impact non-spatial associative memory, which depends in the integrity of extrahippocampal memory circuits, mainly involving the amygdala (Curzon, Rustay and Browman, 2009).

The OFT was performed in all behavioral sets to control for locomotion, general and vertical exploration, and anxious-like behavior (Prut and Belzung, 2003). The results demonstrated that IL-10 KO mice presented general and vertical exploration deficits but did not present locomotor alterations nor

signs of anxious-like behavior when compared to the WT littermates. The general exploration, which was assessed by the distance traveled in the OFT, presented statistically significant correlations with features of the other behavior tests, namely a negative correlation with the latency to reach the target hole on probe trial of the BMT and positive correlations with the time spent in the target quadrant on probe trial of the BMT and the total number of arm alternations in the YMT. Regarding the BMT, these correlations raise doubts about whether general exploration deficits induced by IL-10 deficiency might have affected the behavioral performance of IL-10 KO mice. However, during the BMT no differences were detected between genotypes in the distance traveled in the BMT arena nor in the total number of nose pokes performed in the open holes, which indicates that there are no alterations in the exploratory behaviors mediated by IL-10 absence in the BMT that could have impacted the cognitive behavior.

Concerning the vertical exploration in the OFT, our results showed that IL-10 KO mice performed less rearings that lasted less time than the WT littermates. However, a study described the opposite phenotype: implying that IL-10 KO mice showed an increased number and duration of rearings (Mesquita *et al.*, 2008). This opposite result could be explained by the fact that the authors used WT non-littermate mice as control, which was not the case in this thesis. These opposite results demonstrate the importance of using littermate controls in research to minimize genetic variability (Holmdahl and Malissen, 2012) and to increase the reproducibility of results.

After the cognitive behavioral characterization, the question that persisted was whether the overall behavior variables analyzed could classify the mice genotype (WT *vs* IL-10 KO) using supervised machine learning techniques. To answer this question, SVM models were trained with the behavioral variables of each of the 4 sets performed in this thesis. SVM models perform a binary classification of a data set (Mountrakis, Im and Ogole, 2011; Nayak, Naik and Behera, 2015), which in this case translated into the classification of the mice genotype (WT *vs* IL-10 KO) based on their performance in each set. Since a large number of variables is generated in each set, in this thesis, a GA was developed from scratch to decrease the number of variables to be considered, and thus reduce the phenomenon that is known as the curse of dimensionality (Bellman, 1957). This GA when combined with the SVM model allowed to obtain the combination of behavioral variables within a set that best classified the mice genotype. To our knowledge, this is the first time that GA-SVM models are being used in this context.

On set 1 + set 2, the behavioral variables obtained in the OFT and BMT were used to classify the mice genotype. The SVM model alone led to a classification accuracy of 70.6%, proving that the behavior of IL-10 KO and WT mice on set 1 + set 2 was in fact distinct. Using the GA, 3 variables (total distance traveled in the OFT, latency to reach the target hole for the first time, and the number of pokes in the

target hole on the probe trial of the BMT) were selected as the combination of behavioral variables that best classified the mice genotype, increasing the classification accuracy to 75.0%. Of note, in each of the 3 behavioral variables selected by the GA, it was previously observed through inferential statistical tests that the behavior of the IL-10 KO mice was different from that of the WT mice. This evidence demonstrated that, in this case, the use of inferential statistical tests or GA-SVM models reached the same conclusion. On set 3, in contrast, this phenomenon did not occur. In this set, the GA selected 5 variables (the number of arm alternations in the YMT, the time exploring the novel object in the NORT, and the time of conditioned behaviors in the context probe, novel context, and cue probe of the CCFCT) as the feature combination that generates the best classification accuracy. However, of these 5 variables, only one (the number of arm alternations in the YMT) previously presented statistically significant differences between IL-10 KO and WT mice. This proves that GA-SVM models have a greater sensitivity than the commonly used inferential statistics tests to detect small differences between genotypes that would otherwise not be considered. By using these variables, on set 3, the mice genotype was classified with an accuracy of 89.3%. On set 4, even after the GA selection, the classification accuracy only reached 60.0%. This can be explained by the reduced sample size that was used in this set ($n_{WT} = 8$; $n_{IL\text{-}10\ KO} = 12$) and that may not have been enough to train the SVM model properly. Overall, these results revealed that the mice genotype (WT *vs* IL-10 KO) can be classified through behavioral variables related to cognitive function, thus indicating that the cognitive behavior of IL-10 KO mice is in fact distinct from that of the WT littermates. The use of GA-SVM models in this context also proved to be a potentially complementary approach to inferential statistical tests given its sensitivity.

5.2 Confounders that may be associated with the cognition of IL-10 KO female mice

Considering the reports indicating that the effect of IL-10 in the modulation of animal behaviors could be gender-specific (Mesquita *et al.*, 2008) and the preliminary data from our laboratory in male IL-10 KO mice supporting the protective role of this anti-inflammatory cytokine in cognitive abilities, in this thesis, we assessed the role of IL-10 absence in the cognitive function of female mice. The preliminary data from our laboratory had shown that IL-10 absence impaired the hippocampal-dependent memory in the BMT but not in other cognitive tasks of male mice. Additionally, IL-10 KO male mice presented reduced dendritic arborization of DG neurons, and alterations in the leukocyte profile in the blood and lymph nodes when compared to the WT littermates (unpublished data). In this thesis, using IL-10 KO female mice in the same conditions, we observed the same phenotypes regarding the cognitive

behavior and the remaining variables of hippocampal structural plasticity and leukocyte profile, thus indicating that, in our animal model, IL-10 absence may be affecting both genders in the same way.

The use of female animals in neuroscience research is however a rare practice, as females are often neglected. One of the major reasons for the exclusion of female animals from behavioral testing is the hormonal fluctuation that occurs during the estrous cycle, as they could potentially affect animal behavior, and affect data interpretation (Meziane *et al.*, 2007). In this thesis, to analyze the impact of the estrous cycle on behavioral data, for each behavioral testing day, female mice were divided, as previously proposed (Chari *et al.*, 2020). Our results revealed that in the majority of the behavioral variables analyzed, the estrous cycle did not impact the behavioral performance of both IL-10 KO and WT mice. However, although the sample size was small, the search strategy classification during the BMT revealed that IL-10 KO mice found to be in metestrus and diestrus had a worst hippocampal-dependent memory than the WT controls found to be in the same phases of the estrous cycle. In contrast, this phenomenon was not present in the proestrus and estrus phases, as both genotypes during these estrous cycle phases performed similar percentages of hippocampal-dependent strategies. Interestingly, IL-10 KO mice presented a worst cognitive function during metestrus and diestrus, which are the period where female mice do not present acceptance to males and decrease exploratory and social behaviors (Lohmiller, Swing and Hanson, 2019; Chari *et al.*, 2020). Several reports showed that during metestrus and diestrus, female mice have higher levels of progesterone and lower levels of estrogen (Lohmiller, Swing and Hanson, 2019), and it was already stated that estrogen alters inflammatory mediators by reducing the release of pro-inflammatory cytokines and increasing IL-10 levels (Dimayuga *et al.*, 2005; Shiversa *et al.*, 2015). This leads to the theory that during metestrus and diestrus the combined deficiency of IL-10 and the lower levels of estrogen may be increasing the levels of pro-inflammatory cytokines which in turn are negatively influencing the cognitive function of IL-10 KO mice. Together, these results provide evidence that the role of IL-10 absence in cognition may be dependent on hormonal fluctuation that occurs during the estrous cycle and the immunomodulatory properties of estrogen.

In previous studies, it was revealed that mice with lower IL-10 expression demonstrated increased signs of depressive-like behavior, alongside with impaired spatial learning and memory in the MWMT, when compared to WT littermates (Zhang *et al.*, 2020), and female mice lacking IL-10 presented increased signs of depressive- and anxious-like behavior when compared to the non-littermate WT controls (Mesquita *et al.*, 2008). This evidence raised the question of whether mood may influence the cognitive profile of IL-10 KO mice. In our animal model, the forced swim test and the tail suspension test, which are the commonly used tests to evaluate depressive-like behavior (Cryan, Mombereau and Vassout, 2005;

Yankelevitch-Yahav *et al.*, 2015), were also performed in our laboratory. It was found that IL-10 KO mice showed no changes in depressive-like signs when compared to WT littermate controls (data not shown). Moreover, preliminary data from our laboratory also showed that female mice lacking IL-10 did not present alteration in anxious-like behavior (unpublished data), since IL-10 KO mice and WT littermates behave similar in the elevated-plus maze test and in the light/dark box test, which are the frequently used tests to assess anxious-like behavior (Walf and Frye, 2007; Arranta, Schramm-Sapytab and Kuhn, 2013). Together these results demonstrate that the cognitive deficits of IL-10 KO mice are most likely not associated with mood alterations.

Another potential confounding factor that should be considered when assessing the cognitive profile of young-adult IL-10 KO mice, is their early postnatal neurodevelopment. It is known that IL-10 KO mice generated by the crossing of heterozygous C57BL/6 mice for IL-10 absence have postnatal growth impairments, which become evident from 3 weeks of age onwards (Kühn *et al.*, 1993) and might subsequently affect their early postnatal neurodevelopment. This phenomenon raised the question of whether the cognitive impairment of BALB/c IL-10 KO mice when compared to the WT littermates, is present since the postnatal period or only reveals itself in adulthood. To start addressing this question, in our laboratory, a protocol of developmental milestones was carried out as previously described (Lim *et al.*, 2008). This protocol included the performance of a diverse and well-described range of tests that evaluate different neurologic parameters such as motor coordination, spatial and auditory reflexes, and strength development. Preliminary data from our laboratory, from postnatal day 1 to postnatal day 21, did not reveal any developmental difference between IL-10 KO and WT mice (unpublished data). Truly, during this postnatal period, mice have not yet been weaned and, therefore, are still in the presence of exogenous IL-10 from the heterozygous mothers that can pass through lactation (Madsen *et al.*, 2002; Brenmoehl *et al.*, 2018). In this way, from postnatal day 1 to postnatal day 21, IL-10 KO mice have access to some IL-10, which leads to the theory that possible postnatal neurodevelopment differences induced by IL-10 deficiency might only appear after weaning. Even so, in the future, to eliminate possible negative impacts that IL-10 absence may have on postnatal neurodevelopment, the employment of IL-10 tissue- and time-specific (conditioned) KO mice, for instance by the use of a Cre transgenic line (Hofker and van Deursen, 2002), is of utmost importance. Using this type of IL-10 conditioned KO mice it will be possible to create transgenic mice that have an early postnatal period expressing endogenous IL-10 in a similar way to WT controls, which eliminates possible bias in the early postnatal neurodevelopment between genotypes. During adulthood, the expression of IL-10 might then be silenced allowing the study of the impact in cognition of the absence of this anti-inflammatory cytokine only later in life.

It is consistently reported that the ablation of IL-10 signaling may enhance pro-inflammatory responses, as reviewed elsewhere (Iyer and Cheng, 2012). For that reason, several authors argue that the processes mediated by IL-10 absence in animal behaviors could be a consequence of this modulatory effect in the production of pro-inflammatory cytokines, namely IL-1β, INF-γ, and TNF, rather than a direct effect of IL-10 absence itself (Moore *et al.*, 2001; Harvey *et al.*, 2006; Mesquita *et al.*, 2008). In fact, increased levels of pro-inflammatory cytokines are associated with cognitive deficits and the absence of these molecules increases the cognitive abilities of mice (Baier *et al.*, 2009; Derecki *et al.*, 2010; Huang and Sheng, 2010; Monteiro *et al.*, 2015; Brombacher *et al.*, 2017). This raises the question of whether the cognitive deficits observed in IL-10 KO mice are a functional behavioral outcome meditated directly by IL-10 absence or indirectly by a possible increase in the levels of pro-inflammatory cytokines. In our animal model, a way to attempt to establish a direct link between IL-10 and cognition could be through the exogenous IL-10 administration both in the CNS and in the periphery of IL-10 KO mice and evaluate if this can revert the detrimental effects of IL-10 absence in cognitive function. Additionally, it is important to evaluate how pro-inflammatory cytokine levels change during these procedures, to decipher possible relationships between the levels of different cytokines and the cognitive behavior of IL-10 KO mice.

5.3 Linking colon inflammation, gut microbiome and cognitive function in IL-10 KO mice

IBD is an idiopathic chronic inflammatory disorder of the gut, most commonly affecting the terminal colon and the perianal region, with serious acute and chronic complications (Keubler *et al.*, 2015). Although the IBD etiology remains largely unknown, it involves a complex interaction between genetics, environmental and microbial factors, and immune responses (Zhang and Li, 2014). Several studies revealed that patients with IBD have impaired cognitive and psychomotor function compared to healthy controls, especially in processing speed, mental perceptive abilities, and complex operative thinking (Langenberg *et al.*, 2017; Fan *et al.*, 2019; Tadin-Hadjina *et al.*, 2019). Additionally, systemic inflammation in IBD patients was significantly correlated with their cognitive impairment (Langenberg *et al.*, 2017). Regarding our IL-10 KO animal model, it is described that IL-10 absence can lead to spontaneous development of IBD and increase colon inflammation (Keubler *et al.*, 2015). In this thesis, our results support this evidence showing that IL-10 KO mice exhibit increased gene expression levels of the pro-inflammatory markers *Ido*, *Ifnγ*, *Inos*, and *Tnf* in the colon, when compared to the WT littermates. This raised the question of whether the colon inflammation profile of IL-10 KO mice was associated with their behavioral performance. Correlation analysis revealed that increased levels of some

pro-inflammatory markers were negatively associated with exploratory behavior variables but were not associated with the cognitive ones. Specifically, it was found that *Ido* gene expression correlates negatively with the number of arm alternations in the YMT and the total distance traveled in the OFT and *Inos* gene expression also correlates negatively with the total distance traveled in the OFT. To further analyze the impact of the colon inflammatory profile in the behavior data, a *k*-means clustering algorithm was used to cluster mice according to the expression levels of pro-inflammatory markers in the colon. This algorithm allowed the separation of IL-10 KO mice into two clusters: one with low gene expression levels of pro-inflammatory markers and another with increased levels. Our results demonstrated that, in all behavioral variables analyzed, IL-10 KO mice with low or high gene expression levels of pro-inflammatory markers behaved similarly, thus indicating that the colon inflammatory profile had no impact on the behavior of IL-10 KO mice.

One of the consequences of IBD is the misbalanced gut microbiome or dysbiosis (Keubler *et al.*, 2015). Different studies have studied the gut microbiome of IBD patients and revealed that this disease may lead to: (1) reduced gut microbiome biodiversity (Joossens *et al.*, 2011); decreased gut microbiome stability throughout time (Andoh *et al.*, 2011); and (3) reduction in *Firmicutes* and *Bacteroidetes* in the gut microbiome – which are the predominant phyla in healthy controls (Martinez *et al.*, 2008). This phenomenon of dysbiosis also occurs in IL-10 KO mice, as the absence of IL-10 has been reported to decrease the diversity and richness of the gut microbiome (Maharshak *et al.*, 2013; Singh *et al.*, 2016). Since it is known that the gut microbiome may cooperate with the host in the regulation of cognition through the gut-brain axis (Morais, Schreiber and Mazmanian, 2021), the hypothesis that emerged was whether alterations in the gut microbiome of IL-10 KO mice could be associated with their cognitive profile. The *16S* ribosomal RNA sequencing of the gut microbiome allows the assessment of alterations in the frequency of certain bacterial populations and its potential association with the behavioral performance of IL-10-KO mice. In our laboratory this procedure is already being carried out.

Another way to test the association between alterations in gut microbiome and cognitive profile of IL-10 KO mice, is through gut microbiome modulation and assess if this modulation reverse the cognitive impairments of IL-10 KO mice. In *Part 2* of this thesis, we aimed to optimize an effective protocol for gut microbiome depletion, since it is the first step in the process of gut microbiome modulation. For that, a 10-day treatment with a daily oral gavage of an antibiotic cocktail was tested. Our results revealed that the treatment by oral gavage had no impact on animal welfare, which is in agreement with data reported by other authors who used this protocol (Hill *et al.*, 2010; Kennedy, King and Baldridge, 2018). To test the effectiveness of the protocol, quantification of fecal CFUs was performed throughout time.

This technique revealed that the number of CFUs, both in aerobic and anaerobic conditions, did not decrease as expected, indicating that the antibiotic treatment might not be working properly in our animal model. However, taking into consideration that the majority of the bacteria within the gut microbiota is not cultivable in laboratory conditions (Lagkouvardos, Overmann and Clavel, 2017) and to confirm these results with another technique, the gene expression levels of the *16s* bacterial marker in fecal pellets were measured throughout time. Our results revealed that after 3 days of antibiotic treatment the total load of fecal bacterial DNA was diminished an average of 10^3 times when compared to day 0 in both WT and KO genotypes. Additionally, during this protocol the gene expression levels of the *Its2* fungal marker remained similar throughout time, thus indicating that the antibiotic treatment did not lead to fungal overgrowth. These results are in line with that reported by other authors (Hill *et al.*, 2010; Kennedy, King and Baldridge, 2018), providing a solid gut microbiome depletion of both IL-10 KO and WT mice. Subsequently, we plan to recolonize the gastrointestinal tract of IL-10 KO mice with the gut microbiome from WT mice after the third day of antibiotic treatment, and access if gut microbiome modulation of IL-10 KO mice is able to revert their cognitive impairments.

5.4 Alterations in the structural plasticity of the hippocampus induced by IL-10 absence

As previously indicated, The cognitive behavior characterization revealed that IL-10 absence selectively impaired the cognitive performance of mice in the BMT, which is a task highly dependent on hippocampal function (Matthew, 2018). Actually, the hippocampus harbors different forms of brain plasticity important for the encoding, storage, and retrieval of memories (de Miranda *et al.*, 2017; Lisman *et al.*, 2017). Our data from the hippocampal stereological analysis revealed that IL-10 absence decreased the number of neurons and led to a volumetric atrophy in the majority of the integrating layers of the DH, but not of the VH. While the DH has been shown to participate mainly in exploratory behaviors and spatial memory (as is the case of the BMT), the VH integrates brain circuits responsible for emotional responses (Saper, Scammell and Lu, 2005; Dong and Swanson, 2006; Nollet *et al.*, 2011; Mahan and Ressler, 2012; Hartley *et al.*, 2014; Strange *et al.*, 2014). Together, these results support that IL-10 absence had a dorsal-ventral axis specificity in the hippocampus, as both behaviorally and histologically, IL-10 KO mice presented alterations dependent on the DH, but not on the VH. Additionally, the lower volume of the DH might explain the cognitive outcome of IL-10 KO mice in the BMT, as a decreased hippocampal volume has often been associated with the impairment of several cognitive abilities in the past (Petten, 2004; Vijayakumar and Vijayakumar, 2012).

One of the key components of the structural plasticity of the hippocampus is the complexity of the dendritic arborization of hippocampal neurons. For instance, it is known that learning increases the dendritic arborization of recently generated neurons in the hippocampus (Espino, Gómez and Durán, 2020) and patients with autism spectrum disorder or schizophrenia present hippocampal neurons with a reduced dendritic arborization (Kolomeets, Orlovskaya and Uranova, 2007; Kulkarni and Firestein, 2012). Our results from the 3-dimensional neuronal reconstruction of hippocampal neurons revealed that IL-10 absence negatively affected the dendritic arborization of dDG and vDG granule neurons. The correlation analysis also showed that an increased complexity of the dendritic arborization of DG hippocampal neurons was positively associated with variables of the cognitive behavior. In particular, the number of dendritic ends of the neurons in the dDG subregion positively correlated with the percentage of pokes in the target hole of the probe trial of the BMT, and the number of dendritic ends of the neurons in the vDG subregion was positively linked with the time spent in the target quadrant on probe trial of the BMT. Our results also demonstrated that the apical dendrites of CA1 and CA3 pyramidal neurons were smaller and less complex in IL-10 KO mice when compared with WT controls. However, no differences were detected between genotypes in the basal dendrites of these neurons. It is known that apical and basal dendrites of hippocampal pyramidal neurons differ in various properties, including size, geometry, electrical conduction, and responsiveness to neurotrophic factors. Additionally, the dendritic arborization of the apical and basal dendrites are differentially regulated by guidance molecules (Polleux, Morrow and Ghosh, 2000; Arikkath, 2012; Wu, Fujishima and Kengaku, 2015). This information leads to the hypothesis that the action of IL-10 absence in the modulation of the dendritic arborization of pyramidal neurons in the hippocampus might also be distinct between apical and basal dendrites. Together, these data indicate that IL-10 absence had a detrimental effect in the dendritic arborization of hippocampal neurons and that this structural alteration may have impacted the cognitive outcome of IL-10 KO mice. To our knowledge, this is the first time that IL-10 absence was linked to adverse alterations in neuronal morphology *in vivo*, however in primary cultures of cortical neurons a report showed that blockade of IL-10 with neutralizing antibodies also markedly decreased neurite outgrowth and IL-10 administration promoted it (H. Chen *et al.*, 2016).

In a study, IL-10 administration increased the dendritic spines density of cortical neurons, and IL-10 neutralizing antibodies decreased this phenomenon (H. Chen *et al.*, 2016), which confirmed the protective role of IL-10 in this hippocampal plasticity process. Similarly, through Golgi-Cox staining in our animal model, it was observed that IL-10 deficiency led to a reduced dendritic spine density in the vDG, CA1, and CA3 subregions. Several studies have already reported that a lower dendritic spine density in

hippocampal neurons is associated with a worst cognitive performance (Moser, Trommald and Andersen, 1994; Conrad et al., 2012; Eilam-Stock et al., 2012). Thus, this information suggests that the cognitive impairment of IL-10 KO mice might be a behavioral outcome generated by the reduced dendritic spine density in these hippocampal neurons. However, IL-10 absence did not affect all hippocampal subregions in the same way, as oppositely to what would be expected, it was detected an increased dendritic spine density in the dDG of IL-10 KO mice when compared to the WT controls. We hypothesized that this phenomenon may have occurred as a local compensatory mechanism for the sharp decrease in the number of neurons, volumetric atrophy, and reduction in dendritic arborization that was found in dDG of IL-10 KO mice so that the functional integrity of this region could be maintained.

Throughout the hippocampus, the neuronal dendrites of IL-10 KO mice consistently displayed a higher percentage of specialized ramified spines than WT controls. Ramified spines are described as the dendritic spines with the highest maturity state (Harris, Jensen and Tsao, 1992; Risher *et al.*, 2014; Maiti *et al.*, 2015). These specialized structures are closer to the upper limits of synaptic size and strength and therefore have little range for plastic strengthening (Nimchinsky, Sabatini and Svoboda, 2002; Halbach, 2009; Berry and Nedivi, 2017). In IL-10 KO mice, this increased percentage of ramified spines might thus indicate an overall reduced hippocampal plasticity to the formation and/or development of novel dendritic spines.

In the hippocampus, alterations in the dendritic spine dynamics are commonly associated with LTP or LTD modifications (Matsuzaki *et al.*, 2004; Bosch and Hayashi, 2012; Frankfurt and Luine, 2015). This phenomenon raised the question of whether IL-10 absence, in addition to impair the hippocampal structural plasticity processes already described, also plays a role in the modulation of LTP or LTD. Until now, it is known that IL-10 administration is capable to abrogate the reduction of LTP in rats caused by LPS injection (Lynch *et al.*, 2004). However, under basal conditions, an association between IL-10 absence and LTP or LTD modifications has not yet been confirmed. In the future, this issue can be assessed by extracellular field electrophysiological recording in the hippocampus of IL-10 KO mice. Additionally, the hippocampal levels of BDNF, which plays a critical role not only in the increase of synaptic plasticity (Heldt *et al.*, 2007; Ron-Harel *et al.*, 2008; Derecki *et al.*, 2010) but also of hippocampal neurogenesis (Numakawa, Odaka and Adachi, 2017; Ferreira *et al.*, 2018), should also be assessed, as it is known that the exogenous administration of BDNF in rodents upregulates the expression of IL-10 in several conditions (Xu *et al.*, 2010, 2017).

The central role of the hippocampus in learning and memories requires another hippocampal plasticity process, which is the ongoing neurogenesis in the SGZ of the hippocampal DG, as it is

described that its pharmacological arrest results in long-term emotional and cognitive impairments (Shors *et al.*, 2001; Mateus-Pinheiro *et al.*, 2013). In the subventricular zone (the second consensual cytogenic niche), IL-10 reduces the differentiation of NSCs into new neurons and, therefore, decreases neurogenesis (Perez-Asensio *et al.*, 2013; Pereira *et al.*, 2015). However, the role of IL-10 in the hippocampal neurogenesis remains to be addressed. Currently, in our laboratory, immunofluorescence for neurogenic markers in hippocampal slices of IL-10 KO and WT mice is being conducted to start to unravel this question.

5.5 The circadian rhythm of corticosterone in the absence of IL-10

Some evidence has shown that IL-10 absence can lead to HPA axis hyperactivation (Smith *et al.*, 1999), which is recognized as a mechanism associated with impairments in cognitive function (Ouanes and Popp, 2019) and hippocampal plasticity processes (Alfarez *et al.*, 2009). Our results demonstrated that under basal conditions, IL-10 KO mice showed increased serum corticosterone levels at nadir, but not at zenith when compared to the WT littermates. This data indicates that IL-10 absence might be impacting the circadian rhythm of corticosterone by causing sustained increased serum corticosterone levels. Several findings strongly suggest that IL-10 exerts a negative regulation on corticosterone production by down-regulating the enzymes responsible for its biosynthesis in the adrenal glands (Koldzic-Zivanovic *et al.*, 2006). Thus, the increased serum corticosterone levels present in IL-10 KO animals could be explained by the lack the down-regulation of corticosterone production mediated by IL-10.

Several studies have documented that prolonged, increased exposure to glucocorticoids may have long-lasting adverse effects on cognitive behavior, due to functionally and, over time, structurally promote brain alterations (Foy *et al.*, 1987; Starkman *et al.*, 1992; Bodnoff *et al.*, 1995; Brown, 2009). Brain areas important in cognitive functioning, like the hippocampus, are rich in glucocorticoid receptors and are therefore particularly vulnerable to high levels of corticosterone. Specifically, prolonged increased serum corticosterone levels can impair hippocampal LTP and decreases hippocampal synaptic plasticity (Foy *et al.*, 1987; Bodnoff *et al.*, 1995). Our results indicated that the nadir serum corticosterone levels do not correlate with the variables of the cognitive behavioral performance. However, it was observed that mice with increased nadir serum corticosterone levels were associated with a smaller dendritic arborization of the apical dendrite of CA3 hippocampal neurons, which gave a first clue that the effect of IL-10 absence in hippocampal plasticity processes might be mediated by a direct action of corticosterone.

5.6 IL-10 absence interconnects the immune system to cognitive function

Given the key roles of leukocytes in several brain functions (Kipnis *et al.*, 2004; Ziv *et al.*, 2006; Brynskikh *et al.*, 2008) and to further explore the interconnected mechanisms between the immune system and cognition, it was hypothesized that leukocyte profile alterations induced by IL-10 deficiency could be correlated with their cognitive behavior. Our results suggest that IL-10 absence led to leukocyte profile alterations both in blood and in lymph nodes, namely in the dcLN, which drain the brain region (Kida, Pantazis and Weller, 1993).

In the blood, flow cytometry analysis showed that IL-10 absence increased the total number and the percentage of neutrophils within leukocytes. Neutrophils are one of the main leukocytes involved in the initiation of inflammatory responses and the primary mediators of the innate immune defense against most bacteria and fungi (Malech, DeLeo and Quinn, 2014). During inflammatory responses, neutrophils can be rapidly mobilized from the circulation into damaged tissues, while the supply of neutrophils in the blood is at the same time replenished by their recruitment from the bone marrow to the vasculature (Rosales *et al.*, 2017). Interestingly, our results revealed that a higher percentage of neutrophils within leukocytes in the blood correlated positively with the increased expression levels of pro-inflammatory markers, specifically *Ido* and *Tnf*, in the colon, demonstrating that the increased percentage of neutrophils in IL-10 KO animals could be an immune response to the context of colon inflammation. In fact, several studies have already demonstrated that IL-10 is necessary to prevent exacerbated neutrophil recruitment, since after infection with microorganisms, IL-10 KO mice showed increased recruitment of neutrophils, whereas mice with overexpressing IL-10 had decreased neutrophil recruitment to the infection location (Sun *et al.*, 2009; Andrade *et al.*, 2013; Peñaloza *et al.*, 2015).

Aside from their crucial role in inflammatory responses, increased blood neutrophils have also been associated with cognitive deficits. A report revealed that there is an accumulation of neutrophils before the onset of cognitive deficits in a mice model of Alzheimer's disease, suggesting that neutrophils may play a role in the induction of cognitive decline in this pathology (Zenaro *et al.*, 2015). Additionally, a human study also found that an elevated neutrophil/leukocyte ratio was associated with an increased risk of cognitive impairments in aged individuals (Liu *et al.*, 2020). In our animal, although no correlation was found between the number and percentage of neutrophils within leukocytes and the cognitive behavior variables, the association between the increased neutrophils in IL-10 KO mice and their cognitive impairment should be studied further in the future.

A mechanism that could be associated with the increased number and percentage of neutrophils

within leukocytes found in IL-10 KO mice may be the HPA axis hyperactivation. It is known that glucocorticoids are one of the factors that promote neutrophil maturation in the bone marrow and their mobilization into the vasculature. This is one of the reasons why the response to excessive glucocorticoids leads to neutrophilia (Cavalcanti *et al.*, 2006, 2007; Ronchetti *et al.*, 2018). Curiously, our results from the correlation analysis also revealed that the increased number and percentage of neutrophils within leukocytes was positively correlated to the corticosterone serum levels at nadir, which was increased in IL-10 KO mice, as previously described.

A positive correlation between the total number of leukocytes in the blood and the corticosterone serum levels at nadir was also found. However, while IL-10 KO mice presented an increased total number of leukocytes in the blood when compared to the WT controls, this is mainly attributed to the alteration in the number of neutrophils, as no differences were found between genotypes in the remaining leukocyte types analyzed (eosinophils, $Ly6C^{high}$ and $Ly6C^{low}$ NK cells, B cells, T cells, and both $CD4^+$ and $CD8^+$ T cells).

Besides the increased percentage of neutrophils within leukocytes in IL-10 KO mice, it was also observed that the proportion of blood eosinophils, $Ly6C^{high}$ and $Ly6C^{low}$ NK cells, B cells, T cells, and $CD8^+$ T cells within leukocytes was reduced in IL-10 KO mice when compared to the WT littermates. Additionally, although does not achieve a statistically significance between genotypes, there is also a trend supported by a high effect size for IL-10 KO mice to have a decreased percentage of $CD4^+$ T cells in the blood. Because the number of circulating cells of all these leukocyte types in the blood is similar between genotypes, we hypothesized that the reduced proportion of these leukocyte types in the blood of IL-10 KO mice might be due only to a mathematical implication of the increased proportion of neutrophils. However, it should be noted that some of these leukocyte types have already been associated with cognitive impairments in different contexts, and so they should not be disregarded. For instance, the protective role of B cells and T cells in the cognitive function is constantly supported by several studies describing that: (1) mice lacking both B cells and T cells present spatial memory impairments that are reverted after immune system restoration with T cells (Kipnis *et al.*, 2004; Brynskikh *et al.*, 2008; Ron-Harel *et al.*, 2008); (2) a better cognitive performance of healthy aged individuals is associated with higher numbers of B cells (Serre-Miranda *et al.*, 2015); and (3) training in cognitive tasks leads to an accumulation of T cells and IL-4-producing $CD4^+$ T cells in the meninges (Derecki *et al.*, 2010; Brombacher *et al.*, 2017).

Since cytokines are key protagonists in the development, survival, differentiation, and proliferation of lymphocytes (Schluns and Lefrançois, 2003; Raphael *et al.*, 2015; Vazqueza, Catalan-Dibene and Zlotnik, 2015), we subsequently aimed to decipher if alterations in both B cells and T cells subsets were

promoted by IL-10 absence. Regarding B cells, no differences were observed between IL-10 KO and WT mice in the distinct subsets analyzed. However, when looking at T cells it was observed that IL-10 deficiency reduced the percentage of both $CD44^{low:int}$, $CD62L^{int}$, $CD4^+$ T cells, and $Ly6C^{low}$, $CD62L^{int}$, $CD8^+$ T cells and increased the percentage of both EM $CD4^+$ T cells and CM $CD8^+$ T cells. Importantly, a lower percentage of EM $CD4^+$ T cells in the blood were found to be correlated with a higher latency for mice to reach the target hole for the first time in the probe trial of the BMT. Also in aged individuals, the same phenomenon was already observed, since lower numbers of EM $CD4^+$ T cells in the blood not only were associated with a better cognitive function but also were found to be predictors of executive function and memory, even when considering factors known to influence cognitive performance, such as age, gender, education, and mood (Serre-Miranda *et al.*, 2015). Together this data support that the elevated EM $CD4^+$ T cells found in IL-10 KO mice may have a detrimental effect in their cognitive function. Additionally, because EM $CD4^+$ T cells are the major cytokine producers among T cells (Okada *et al.*, 2008), and considering that pro-inflammatory cytokines were already reported to have a detrimental effect on cognitive function (Huang and Sheng, 2010; Monteiro *et al.*, 2015; Serre-Miranda *et al.*, 2020), the association found between higher EM $CD4^+$ T cells and impaired cognitive function of IL-10 KO mice may be related to a more pro-inflammatory profile that needs to be further elucidated.

A diverse repertoire of leukocytes has been described within CNS borders (Hickey, 2001), which are ultimately responsible for the brain immune surveillance and subsequently drain to dcLN (Aspelund *et al.*, 2015; Louveau *et al.*, 2015). Flow cytometry analysis revealed that IL-10 absence selectively increased the total number of leukocytes in the dcLN, which is a feature of local lymphadenopathy (Mohseni *et al.*, 2014). Additionally, the phenotypical analysis also showed that all leukocyte types assessed (B cells, T cells, and both $CD4^+$ and $CD8^+$ T cells) were elevated in terms of leukocyte number in the dcLN of IL-10 KO mice when compared to the WT littermates. However, the proportion between leukocytes remained similar between genotypes. Interestingly, this phenomenon did not happen to lymph nodes that play no role in the process of brain immune surveillance, as both IL-10 KO and WT mice presented a similar total number of leukocytes in the ingLN. Also, in both dcLN and ingLN, IL-10 absence reduced the percentage of naïve $CD8^+$ T cells and did not impact the percentage of the remaining T cell subsets evaluated. Together, this information indicated that IL-10 KO mice have an increased number of leukocytes (of all leukocyte types evaluated) in the dcLN, which might suggest an increased cell recruitment to the lymphatic system of the brain. Additionally, since no differences between genotypes were detected in the number of leukocytes in ingLN, this mechanism may be unique in the vicinity of the

brain and may not happen in other regions. To our knowledge, current literature lacks to answer what is the significant relevance of an increased number of leukocytes in the dcLN in the context of cognitive impairment, and subsequently what is the role of IL-10 absence in this interconnection. However, it is known that increased levels of pro-inflammatory cytokines might exert a negative effect in lymphadenopathy (Ohshima *et al.*, 2000), which unravels the determinant role of cytokines in this condition. Given the critical role of the IL-10 absence in cognitive function and to further explore the interconnected mechanisms between the immune system and cognition, in the future, further studies in IL-10 KO and WT mice involving leukocyte and inflammatory profile not only in the dcLN but also in the meninges and CSF should be considered to help decipher processes mediated by IL-10 absence in the leukocyte recruitment to the dcLN.

CHAPTER 6

CONCLUDING REMARKS

CHAPTER 6 – CONCLUDING REMARKS

This thesis contributed to increasing the knowledge of the interplay between the immune system and the CNS since it is the first report describing the role of IL-10 absence in the modulation of cognitive function and the mechanisms underlying this association. Our results identified IL-10 absence as deleterious to cognitive function, specifically the hippocampal-dependent spatial reference memory of female mice found to be in the metestrus and diestrus phases of the estrous cycle. Importantly, it was observed that the genotype of IL-10 KO mice and WT littermates can be computationally classified with high accuracies by support vector machine models using behavioral variables related to cognitive function. We had hypothesized that the cognitive impairments mediated by IL-10 absence could be associated with alterations in several mechanisms, including the colon inflammatory profile, hippocampal plasticity processes, HPA axis activation, leukocyte profile in the blood and lymph nodes, and gut microbiome. Our results demonstrate that IL-10 absence led to increased gene expression levels of pro-inflammatory markers in the colon, however, although several further studies are needed to confirm these results, it was observed that the cognitive function of IL-10 KO mice was not impacted by the colon inflammatory profile. According to the cognitive behavioral alterations, we described IL-10 absence as having a negative impact in hippocampal structural plasticity processes, being able to decrease the number of neurons and the volume of the DH, reduce the complexity of the dendritic arborization of hippocampal neurons and modulate the dendritic spines dynamics throughout the hippocampus. Interestingly, alterations in the hippocampal structural plasticity processes induced by IL-10 deficiency were correlated with a worst cognitive performance and HPA axis hyperactivation. Although the increased serum corticosterone levels at nadir found in IL-10 KO mice did not correlate with their cognitive function *per se*, they were positively correlated with increased blood neutrophils, which is a condition that may play a role in the induction of cognitive decline. Additionally, it was reported that the absence of IL-10 led to an increase in the percentage of EM $CD4^+$ T cells, which is an alteration in the leukocyte profile that was previously associated with cognitive impairments in other studies. We also identified IL-10 KO mice as having a higher number of leukocytes in the dcLN, suggesting an increased cell recruitment to the lymphatic system of the brain that needs further clarification. Lastly, we optimized a protocol for gut microbiome depletion. Our results revealed that after 3 days of treatment, antibiotics reduced the gene expression levels of *16s* in the feces without fungal overgrowth, providing an initial step to explore the role of the gut microbiome in the cognition of IL-10 KO mice. Together, these results unraveled the role of IL-10 absence in cognitive function and highlighted mechanisms that could be important contributors to the development of novel IL-10-based therapies for cognitive impairments.

CHAPTER 7

REFERENCES

CHAPTER 7 – **REFERENCES**

Adolphs, R. (2001) 'The neurobiology of social cognition', *Current Opinion in Neurobiology*, 11(1), pp. 231–239.

Aggleton, J. *et al.* (2010) 'Hippocampal-anterior thalamic pathways for memory: Uncovering a network of direct and indirect actions', *European Journal of Neuroscience*, 31(12), pp. 2292–2307.

Al-Aidroos, N., Said, C. and Turk-Browne, N. (2012) 'Top-down attention switches coupling between low-level and high-level areas of human visual cortex', *Proceedings of the National Academy of Sciences of the United States of America*, 109(36), pp. 14675–14680.

Al-Qazzaz, N. *et al.* (2014) 'Cognitive impairment and memory dysfunction after a stroke diagnosis: A post-stroke memory assessment', *Neuropsychiatric Disease and Treatment*, 10(1), pp. 1677–1691.

Alam, M. *et al.* (2018) 'Adult neurogenesis conserves hippocampal memory capacity', *Journal of Neuroscience*, 38(31), pp. 6854–6863.

Alfarez, D. *et al.* (2009) 'Corticosterone reduces dendritic complexity in developing hippocampal CA1 neurons', *Hippocampus*, 19(9), pp. 828–836.

Ali, S., Begum, T. and Reza, F. (2018) 'Hormonal influences on cognitive function', *Malaysian Journal of Medical Sciences*, 25(4), pp. 31–41.

Andersen, P., Bliss, T. and Skrede, K. (1971) 'Lamellar organization of hippocampal excitatory pathways', *Experimental Brain Research*, 13(2), pp. 222–238.

Andoh, A. *et al.* (2011) 'Comparison of the fecal microbiota profiles between ulcerative colitis and Crohn's disease using terminal restriction fragment length polymorphism analysis', *Journal of Gastroenterology*, 46(4), pp. 479–486.

Andrade, E. *et al.* (2013) 'TLR2-Induced IL-10 Production Impairs Neutrophil Recruitment to Infected Tissues during Neonatal Bacterial Sepsis', *The Journal of Immunology*, 191(9), pp. 4759–4768.

Arikkath, J. (2012) 'Molecular mechanisms of dendrite morphogenesis', *Frontiers in Cellular Neuroscience*, 6(1), pp. 1–14.

Arimoto, T. *et al.* (2007) 'Interleukin-10 protects against inflammation-mediated degeneration of dopaminergic neurons in substantia nigra', *Neurobiology of Aging*, 28(6), pp. 894–906.

Arlt, S. (2013) 'Non-Alzheimer's disease–related memory impairment and dementia', *Dialogues in Clinical Neuroscience*, 15(4), pp. 465–473.

Arranta, A., Schramm-Sapytab, N. and Kuhn, C. (2013) 'Use of the light/dark test for anxiety in adult and adolescent male rats', *Behavioural Brain Research*, 1(256), pp. 119–127.

Aspelund, A. *et al.* (2015) 'A dural lymphatic vascular system that drains brain interstitial fluid and macromolecules', *Journal of Experimental Medicine*, 212(7), pp. 991–999.

Atallah, H., Rudy, J. and O'Reilly, R. (2008) 'The role of the dorsal striatum and dorsal hippocampus in probabilistic and deterministic odor discrimination tasks', *Learning and Memory*, 15(5), pp. 294–298.

Atkinson, R. and Shiffrin, R. (1968) 'Human Memory: A proposed system and its control processes', *The Psychology of Learning and Motivation*, 2(5), pp. 89–195.

Baaten, B., Li, C. and Bradley, L. (2010) 'Multifaceted regulation of T cells by CD44', *Communicative and Integrative Biology*, 3(6), pp. 508–512.

Babcock, H. (1930) 'An experiment in the measurement of mental deterioration', *Archives of Psychology*, 1(117), pp. 1–105.

Bacyinski, A. *et al.* (2017) 'The paravascular pathway for brain waste clearance: Current understanding, significance and controversy', *Frontiers in Neuroanatomy*, 11(101), pp. 1–8.

Baddeley, A. (2000) 'The episodic buffer: a new component of working memory?', *Trends in Cognitive Sciences*, 4(11), pp. 417–423.

Baddeley, A. and Hitch, G. (1974) 'Working memory', *Psychology of Learning and Motivation*, 8(1), pp. 47–89.

Baier, P. *et al.* (2009) 'Impaired hippocampus-dependent and -independent learning in IL-6 deficient mice', *Behavioural Brain Research*, 200(1), pp. 192–196.

Balasingam, V. and Yong, V. (1996) 'Attenuation of astroglial reactivity by interleukin-10', *Journal of Neuroscience*, 16(9), pp. 2945–2955.

Balschun, D. *et al.* (2004) 'Interleukin-6: a cytokine to forget', *The FASEB Journal*, 18(14), pp. 1788–1790.

Banks, W., Kastin, A. and Broadwell, R. (1995) 'Passage of cytokines across the Blood-Brain Barrier', *Recent Progress in Neuroimmunomodulation*, 2(1), pp. 241–248.

Bannerman, D. *et al.* (2002) 'Double dissociation of function within the hippocampus: Spatial memory and hyponeophagia', *Behavioral Neuroscience*, 116(5), pp. 884–901.

Bear, M. and Malenka, R. (1994) 'Synaptic plasticity: LTP and LTD', *Current Opinion in Neurobiology*, 4(3), pp. 389–399.

Beaudoin, C. and Beauchamp, M. (2020) 'Social cognition', *Handbook of Clinical Neurology*, 173(1), pp. 255–264.

Bellman, R. (1957) 'Dynamic Programming', *Princeton University Press*, 1(1), pp. 1–501.

Benjafield, J., Kingstone, A. and Smilek, D. (2010) 'Cognition', *Oxford University Press*, 4(1), pp. 1–528.

Berdugo-Vega, G. *et al.* (2020) 'Increasing neurogenesis refines hippocampal activity rejuvenating navigational learning strategies and contextual memory throughout life', *Nature Communications*, 11(1), pp. 1–12.

Berkan, T. *et al.* (1986) 'A protocol for papanicolaou staining of cytologic specimens following flow analysis', *Cytometry*, 7(1), pp. 101–103.

Berry, K. and Nedivi, E. (2017) 'Spine Dynamics: Are They All the Same?', *Neuron*, 96(1), pp. 43–55.

Bevins, R. and Besheer, J. (2006) 'Object recognition in rats and mice: A one-trial non-matching-to-sample learning task to study "recognition memory"', *Nature Protocols*, 1(3), pp. 1306–1311.

Bialuk, I., Jakubów, P. and Winnicka, M. (2019) 'Significance of IL-6 Deficiency in Recognition Memory in Young Adult and Aged Mice', *Behavior Genetics*, 49(4), pp. 415–423.

Bird, C. (2017) 'The role of the hippocampus in recognition memory', *Cortex*, 93(1), pp. 155–165.

Bluthé, R. *et al.* (1999) 'Central injection of IL-10 antagonizes the behavioural effects of lipopolysaccharide in rats', *Psychoneuroendocrinology*, 24(3), pp. 301–311.

Bodnoff, S. *et al.* (1995) 'Enduring effects of chronic corticosterone treatment on spatial learning, synaptic plasticity, and hippocampal neuropathology in young and mid-aged rats', *Journal of Neuroscience*, 15(1), pp. 61–69.

Bolkan, S. *et al.* (2017) 'Thalamic projections sustain prefrontal activity during working memory maintenance', *Nature Neuroscience*, 20(7), pp. 987–996.

Bonzano, S. *et al.* (2018) 'Neuron-Astroglia Cell Fate Decision in the Adult Mouse Hippocampal Neurogenic Niche Is Cell-Intrinsically Controlled by COUP-TFI In Vivo', *Cell Reports*, 24(2), pp. 329–341.

Bosch, M. and Hayashi, Y. (2012) 'Structural plasticity of dendritic spines', *Current Opinion in Neurobiology*, 22(3), pp. 383–388.

Boxel-Dezaire, A. *et al.* (1999) 'Decreased interleukin-10 and increased interleukin- 12p40 mRNA are associated with disease activity and characterize different disease stages in multiple sclerosis', *Annals of Neurology*, 45(6), pp. 695–703.

Brem, A., Ran, K. and Pascual-Leone, A. (2013) 'Learning and memory', *Handbook of Clinical Neurology*, 116(1), pp. 693–737.

Brenmoehl, J. *et al.* (2018) 'Cytokines in milk and the role of TGF-beta', *Best Practice and Research: Clinical Endocrinology and Metabolism*, 32(1), pp. 47–56.

Brewin, C. (2014) 'Episodic memory, perceptual memory, and their interaction: foundations for a theory of posttraumatic stress disorder', *Psychological bulletin*, 140(1), pp. 69–97.

Broadbent, N. *et al.* (2010) 'Object recognition memory and the rodent hippocampus', *Learning and Memory*, 17(1), pp. 5–11.

Brody, D. and Holtzman, D. (2006) 'Morris water maze search strategy analysis in PDAPP mice before and after experimental traumatic brain injury', *Experimental Neurology*, 197(2), pp. 330–340.

Brombacher, T. *et al.* (2017) 'IL-13–Mediated Regulation of Learning and Memory', *The Journal of Immunology*, 198(7), pp. 2681–2688.

Brown, E. (2009) 'Effects of glucocorticoids on mood, memory, and the hippocampus: Treatment and preventive therapy', *Annals of the New York Academy of Sciences*, 1179(1), pp. 41–55.

Brynskikh, A. *et al.* (2008) 'Adaptive immunity affects learning behavior in mice', *Brain, Behavior, and Immunity*, 22(6), pp. 861–869.

Bucchieri, F. *et al.* (2015) 'Lymphatic vessels of the dura mater: A new discovery?', *Journal of Anatomy*, 227(5), pp. 702–703.

Burkholder, T. *et al.* (2012) 'Health Evaluation of Experimental Laboratory Mice', *Current protocols in mouse biology*, 2(1), pp. 145–165.

Byers, S. *et al.* (2012) 'Mouse estrous cycle identification tool and images', *PLoS ONE*, 7(4), pp. 1–5.

Camina, E. and Güell, F. (2017) 'The neuroanatomical, neurophysiological and psychological basis of memory: Current models and their origins', *Frontiers in Pharmacology*, 8(438), pp. 1–16.

Carrithers, M. *et al.* (2002) 'Role of genetic background in P selectin-dependent immune surveillance of the central nervous system', *Journal of Neuroimmunology*, 129(1), pp. 51–57.

Castelhano-Carlos, M. *et al.* (2010) 'Identification methods in newborn C57BL/6 mice: A developmental and behavioural evaluation', *Laboratory Animals*, 44(2), pp. 88–103.

Cavalcanti, D. *et al.* (2006) 'Adrenal deficiency alters mechanisms of neutrophil mobilization', *Molecular and Cellular Endocrinology*, 249(1–2), pp. 32–39.

Cavalcanti, D. *et al.* (2007) 'Endogenous glucocorticoids control neutrophil mobilization from bone marrow to blood and tissues in non-inflammatory conditions', *British Journal of Pharmacology*, 152(8), pp. 1291–1300.

Chari, T. *et al.* (2020) 'The Stage of the Estrus Cycle Is Critical for Interpretation of Female Mouse Social Interaction Behavior', *Frontiers in Behavioral Neuroscience*, 14(113), pp. 1–9.

Chavant, F. *et al.* (2011) 'Memory disorders associated with consumption of drugs: Updating through a case/noncase study in the French PharmacoVigilance Database', *British Journal of Clinical Pharmacology*, 72(6), pp. 898–904.

Chen, H. *et al.* (2016) 'IL-10 Promotes Neurite Outgrowth and Synapse Formation in Cultured Cortical Neurons after the Oxygen-Glucose Deprivation via JAK1/STAT3 Pathway', *Scientific Reports*, 6(1), pp. 1–16.

Chen, M. *et al.* (2016) 'Tattooing various combinations of ears, tail, and toes to identify mice reliably and permanently', *Journal of the American Association for Laboratory Animal Science*, 55(2), pp. 189–198.

Chia-Chen, L. *et al.* (2013) 'Apolipoprotein E and Alzheimer disease: risk, mechanisms, and therapy', *Nature Reviews Neuroscience*, 9(2), pp. 106–118.

Cohen, J. (1988) 'Statistical Power Analysis for the Behavioral Sciences', *Lawrence Erlbaum Associates*, 2(1), pp. 1–579.

Cohen, J. *et al.* (2002) 'Applied Multiple Regression/Correlation Analysis for the Behavioral Sciences', *Lawrence Erlbaum Associates*, 3(1), pp. 1–703.

Conrad, C. *et al.* (2012) 'Chronic Stress and a Cyclic Regimen of Estradiol Administration Separately Facilitate Spatial Memory: Relationship with CA1 Spine Density and Dendritic Complexity', *Behavioral Neuroscience*, 126(1), pp. 142–156.

Correa, S. *et al.* (2007) 'Cytokines and the immune-neuroendocrine network: What did we learn from infection and autoimmunity?', *Cytokine and Growth Factor Reviews*, 18(1–2), pp. 125–134.

Craver, C. (2003) 'The making of a memory mechanism', *Journal of the History of Biology*, 36(1), pp. 153–195.

Cryan, J., Mombereau, C. and Vassout, A. (2005) 'The tail suspension test as a model for assessing antidepressant activity: Review of pharmacological and genetic studies in mice', *Neuroscience and Biobehavioral Reviews*, 29(1), pp. 571–625.

Cua, D. *et al.* (2001) 'Central Nervous System Expression of IL-10 Inhibits Autoimmune Encephalomyelitis', *The Journal of Immunology*, 166(1), pp. 602–608.

Curtis, C. and D'Esposito, M. (2003) 'Persistent activity in the prefrontal cortex during working memory', *Trends in Cognitive Sciences*, 7(9), pp. 415–423.

Curzon, P., Rustay, N. and Browman, K. (2009) 'Cued and Contextual Fear Conditioning for Rodents', *Methods of Behavior Analysis in Neuroscience*, 2(2), pp. 19–37.

Daneman, R. and Prat, A. (2015) 'The blood–brain barrier', *Cold Spring Harbor Laboratory Press*, 7(1), pp. 1–23.

Davis, A., Maney, D. and Maerz, J. (2008) 'The use of leukocyte profiles to measure stress in vertebrates: A review for ecologists', *Functional Ecology*, 22(5), pp. 760–772.

Deane, R. *et al.* (2003) 'RAGE mediates amyloid-β peptide transport across the blood-brain barrier and accumulation in brain', *Nature Medicine*, 9(7), pp. 907–913.

Deng, W., Aimone, J. and Gage, F. (2010) 'New neurons and new memories: how does adult hippocampal neurogenesis affect learning and memory?', *Nature Reviews Neuroscience*, 11(5), pp. 339–350.

Derecki, N. *et al.* (2010) 'Regulation of learning and memory by meningeal immunity: A key role for IL-4', *Journal of Experimental Medicine*, 207(5), pp. 1067–1080.

Deutsch, V. *et al.* (2007) 'Sustained leukocyte count during rising cortisol level', *Acta Haematologica*, 118(2), pp. 73–76.

Diamond, A. (2013) 'Executive functions', *Annual Review of Psychology*, 64(1), pp. 135–168.

Diamond, B. *et al.* (2008) 'Relationships between information processing, depression, fatigue and cognition in multiple sclerosis', *Archives of Clinical Neuropsychology*, 23(2), pp. 189–199.

Dickerson, B. and Eichenbaum, H. (2010) 'The episodic memory system: Neurocircuitry and disorders', *Neuropsychopharmacology*, 35(1), pp. 86–104.

Dimayuga, F. *et al.* (2005) 'Estrogen and brain inflammation: Effects on microglial expression of MHC, costimulatory molecules and cytokines', *Journal of Neuroimmunology*, 161(1–2), pp. 123–136.

Dong, H. and Swanson, L. (2006) 'Projections from bed nuclei of the stria terminalis, anteromedial area: Cerebral hemisphere integration of neuroendocrine, autonomic, and behavioral aspects of energy balance', *Journal of Comparative Neurology*, 494(1), pp. 142–178.

Dupont, S. *et al.* (2001) 'Delayed verbal memory retrieval: A functional MRI study in epileptic patients with structural lesions of the left medial temporal lobe', *NeuroImage*, 14(5), pp. 995–1003.

Eilam-Stock, T. *et al.* (2012) 'Bisphenol-A Impairs Memory and Reduces Dendritic Spine Density in Adult Male Rats', *Behavioral Neuroscience*, 126(1), pp. 175–185.

Engelhardt, B. and Ransohoff, R. (2005) 'The ins and outs of T-lymphocyte trafficking to the CNS: Anatomical sites and molecular mechanisms', *Trends in Immunology*, 26(9), pp. 485–495.

Espino, L., Gómez, A. and Durán, D. (2020) 'Cognitive training increases dendritic arborization in the dorsal hippocampal CA1 and CA3 neurons of female and male Long–Evans rats', *Synapse*, 74(4), pp. 1–14.

Fan, W. *et al.* (2019) 'Aberrant brain function in active-stage ulcerative colitis patients: A resting-state functional MRI study', *Frontiers in Human Neuroscience*, 13(1), pp. 1–10.

Felix-Ortiz, A. and Tye, K. (2014) 'Amygdala inputs to the ventral hippocampus bidirectionally modulate social behavior', *Journal of Neuroscience*, 34(2), pp. 586–595.

Femenía, T. *et al.* (2012) 'Dysfunctional hippocampal activity affects emotion and cognition in mood disorders', *Brain Research*, 1476(1), pp. 58–70.

Ferreira, F. *et al.* (2018) 'Brain-derived neurotrophic factor (BDNF) role in cannabinoid-mediated neurogenesis', *Frontiers in Cellular Neuroscience*, 12(1), pp. 1–16.

Ferreira, V. *et al.* (2019) 'Cytokines and Interferons: Types and Functions', *Autoantibodies and Cytokines*, 4(1), pp. 65–87.

Fiorentino, D., Bond, M. and Mosmann, T. (1989) 'Two types of mouse T helper cell: IV. Th2 clones secrete a factor that inhibits cytokine production by Th1 clones', *Journal of Experimental Medicine*, 170(6), pp. 2081–2095.

Fischer, H., Bonifas, U. and Reichmann, G. (2000) 'Phenotype and Functions of Brain Dendritic Cells Emerging During Chronic Infection of Mice with Toxoplasma gondii', *The Journal of Immunology*, 164(9), pp. 4826–4834.

Fischer, J. and Hammerschmidt, K. (2011) 'Ultrasonic vocalizations in mouse models for speech and socio-cognitive disorders: Insights into the evolution of vocal communication', *Genes, Brain and Behavior*, 10(1), pp. 17–27.

Fisher, G., Chacon, M. and Chaffee, D. (2019) 'Theories of cognitive aging and work', *Academic Press*, 1(1), pp. 17–45.

Flach, P., Hernández-Orallo, J. and Ferri, C. (2011) 'A coherent interpretation of AUC as a measure of aggregated classification performance', *Proceedings of the 28th International Conference on Machine Learning, ICML 2011*, 1(1), pp. 657–664.

Flores, Á. *et al.* (2018) 'Lost in translation: how to upgrade fear memory research', *Molecular Psychiatry*, 23(11), pp. 2122–2132.

Fong, S. *et al.* (2014) 'Towards enhancement of performance of K-means clustering using nature-inspired optimization algorithms', *Scientific World Journal*, 2014(1), pp. 1–16.

Fonseca, J., Ferreira, J. and Pavão-Martins, I. (2017) 'Cognitive performance in aphasia due to stroke: A systematic review', *International Journal on Disability and Human Development*, 16(2), pp. 127–139.

Fox, G. *et al.* (1998) 'Effect of traumatic brain injury on mouse spatial and nonspatial learning in the Barnes circular maze', *Journal of Neurotrauma*, 15(12), pp. 1037–1046.

Foy, M. *et al.* (1987) 'Behavioral stress impairs long-term potentiation in rodent hippocampus', *Behavioral and Neural Biology*, 48(1), pp. 138–149.

Franco, R. *et al.* (2007) 'The emergence of neurotransmitters as immune modulators', *Trends in Immunology*, 28(9), pp. 400–407.

Frankfurt, M. and Luine, V. (2015) 'The evolving role of dendritic spines and memory: Interaction(s) with estradiol', *Hormones and Behavior*, 74(1), pp. 28–36.

Galic, M., Riazi, K. and Pittman, Q. (2012) 'Cytokines and brain excitability', *Frontiers in Neuroendocrinology*, 33(1), pp. 116–125.

Gareau, M. (2016) 'Cognitive Function and the Microbiome', *International Review of Neurobiology*, 131(1), pp. 227–246.

Gawel, K. *et al.* (2019) 'Assessment of spatial learning and memory in the Barnes maze task in rodents—methodological consideration', *Naunyn-Schmiedeberg's Archives of Pharmacology*, 392(1), pp. 1–18.

Gazzaniga, M. *et al.* (2013) 'Psychological Science', *W. W. Norton & Company*, 3(1), pp. 1–936.

George, A. *et al.* (2004) 'Wallerian degeneration after crush or chronic constriction injury of rodent sciatic nerve is associated with a depletion of endoneurial interleukin-10 protein', *Experimental Neurology*, 188(1), pp. 187–191.

Gibb, R. and Kolb, B. (1998) 'A method for vibratome sectioning of Golgi-Cox stained whole rat brain', *Journal of Neuroscience Methods*, 79(1), pp. 1–4.

Goldman, J. *et al.* (2012) 'Clinical differences among mild cognitive impairment subtypes in Parkinson's disease', *Movement Disorders*, 27(9), pp. 1129–1136.

Goldmann, J. *et al.* (2006) 'T cells traffic from brain to cervical lymph nodes via the cribroid plate and the nasal mucosa', *Journal of Leukocyte Biology*, 80(4), pp. 797–801.

Gonzalez, S., Alvarez, V. and Nelson, E. (2019) 'Do Gross and Fine Motor Skills Differentially Contribute to Language Outcomes? A Systematic Review', *Frontiers in Psychology*, 10(1), pp. 1–16.

Grigorenko, E., Mambrino, E. and Preiss, D. (2012) 'Writing: A mosaic of new perspectives', *Psychology Press*, 1(1), pp. 1–505.

Gundersen, H. *et al.* (1988) 'Some new, simple and efficient stereological methods and their use in pathological research and diagnosis', *APMIS*, 96(5), pp. 379–394.

Haber, S. and Simmel, E. (1976) 'Tail rattling and agonistic behavior in mice: Coincidental or causal?', *Bulletin of the Psychonomic Society*, 7(1), pp. 84–86.

Hafting, T. *et al.* (2005) 'Microstructure of a spatial map in the entorhinal cortex', *Nature*, 436(7052), pp. 801–806.

Halbach, O. (2009) 'Structure and function of dendritic spines within the hippocampus', *Annals of Anatomy*, 191(6), pp. 518–531.

Hänninen, A. *et al.* (2011) 'Ly6C supports preferential homing of central memory CD8+ T cells into lymph nodes', *European Journal of Immunology*, 41(3), pp. 634–644.

Harris, K., Jensen, F. and Tsao, B. (1992) 'Three-dimensional structure of dendritic spines and synapses in rat hippocampus (CA1) at postnatal day 15 and adult ages: Implications for the maturation of synaptic physiology and long-term potentiation', *Journal of Neuroscience*, 12(7), pp. 2685–2705.

Hart, D. and Fabre, J. (1981) 'Demonstration and characterization of ia-positive dendritic cells in the interstitial connective tissues of rat heart and other tissues, but not brain', *Journal of Experimental Medicine*, 154(2), pp. 347–361.

Hartley, T. *et al.* (2014) 'Space in the brain: How the hippocampal formation supports spatial cognition', *Philosophical Transactions of the Royal Society B: Biological Sciences*, 369(1635), pp. 1–18.

Harvey, D. *et al.* (2006) 'Interleukin-10 (IL-10) but not Lipopolysaccharide (LPS) produces increased motor activity and abnormal exploratory patterns while impairing spatial learning in Balb/c mice', *Physiology and Behavior*, 87(5), pp. 842–847.

Harvey, P. (2019) 'Domains of cognition and their assessment', *Dialogues in Clinical Neuroscience*, 21(3), pp. 227–237.

Haworth, J. *et al.* (2016) 'Measuring Information Processing Speed in Mild Cognitive Impairment: Clinical Versus Research Dichotomy', *Journal of Alzheimer's Disease*, 51(1), pp. 263–275.

Heldt, S. *et al.* (2007) 'Hippocampus-specific deletion of BDNF in adult mice impairs spatial memory and extinction of aversive memories', *Molecular Psychiatry*, 12(7), pp. 656–670.

Herz, J., Johnson, K. and McGavern, D. (2015) 'Therapeutic antiviral T cells noncytopathically clear persistently infected microglia after conversion into antigen-presenting cells', *Journal of Experimental Medicine*, 212(8), pp. 1153–1169.

Hesse, D. *et al.* (2011) 'Disease protection and interleukin-10 induction by endogenous interferon-β in multiple sclerosis?', *European Journal of Neurology*, 18(2), pp. 266–272.

Hickey, W. (1999) 'Leukocyte traffic in the central nervous system: the participants and their roles', *Seminars in Immunology*, 11(1), pp. 125–137.

Hickey, W. (2001) 'Basic principles of immunological surveillance of the normal central nervous system', *Glia*, 36(2), pp. 118–124.

Hill, D. *et al.* (2010) 'Metagenomic analyses reveal antibiotic-induced temporal and spatial changes in intestinal microbiota with associated alterations in immune cell homeostasis', *Mucosal Immunology*, 3(2), pp. 148–158.

Hofker, M. and van Deursen, J. (2002) 'Transgenic Mouse Methods and Protocols', *Transgenic Mouse Methods and Protocols*, 693(1), p. 1.27.

Holland, J. (1975) 'Adaptation in Natural and Artificial Systems: An Introductory Analysis with Applications to Biology, Control and Artificial Intelligence', *MIT Press*, 55(1), pp. 1–228.

Holmdahl, R. and Malissen, B. (2012) 'The need for littermate controls', *European Journal of Immunology*, 42(1), pp. 45–47.

Howes, A., Gabryšová, L. and O'Garra, A. (2014) 'Role of IL-10 and the IL-10 Receptor in Immune Responses', *Reference Module in Biomedical Sciences*, 1(1), pp. 1–11.

Huang, Y. *et al.* (2018) 'Repopulated microglia are solely derived from the proliferation of residual microglia after acute depletion', *Nature Neuroscience*, 21(4), pp. 530–540.

Huang, Z. and Sheng, G. (2010) 'Interleukin-1β with learning and memory', *Neuroscience Bulletin*, 26(6), pp. 455–468.

Huemer, M. (1999) 'The Problem of Memory Knowledge', *Pacific Phylosophical Quarterly*, 80(1), pp. 346–357.

Iliff, J. *et al.* (2012) 'A paravascular pathway facilitates CSF flow through the brain parenchyma and the clearance of interstitial solutes, including amyloid β', *Science Translational Medicine*, 4(147), pp. 1–11.

Illouz, T. *et al.* (2016) 'Unbiased classification of spatial strategies in the Barnes maze', *Bioinformatics*, 32(21), pp. 3314–3320.

Iyer, S. and Cheng, G. (2012) 'Role of interleukin 10 transcriptional regulation in inflammation and autoimmune disease', *Critical Reviews in Immunology*, 32(1), pp. 23–63.

Jameison, K. and Dinan, T. (2001) 'Glucocorticoids and cognitive function: From physiology to pathophysiology', *Human Psychopharmacology*, 16(4), pp. 293–302.

Janda, E., Boi, L. and Carta, A. (2018) 'Microglial phagocytosis and its regulation: A therapeutic target in parkinson's disease?', *Frontiers in Molecular Neuroscience*, 11(1), pp. 1–8.

Johanson, C. and Johanson, N. (2018) 'Choroid Plexus Blood-CSF Barrier: Major Player in Brain Disease Modeling and Neuromedicine', *Journal of Neurology & Neuromedicine*, 3(4), pp. 39–58.

Jonathan, G. *et al.* (2011) 'Traumatic stress is linked to a deficit in associative episodic memory', *Journal of Traumatic Stress*, 24(3), pp. 260–267.

Joossens, M. *et al.* (2011) 'Dysbiosis of the faecal microbiota in patients with Crohn's disease and their unaffected relatives', *Gut*, 60(5), pp. 631–637.

Jung, Y. *et al.* (2019) 'Relationships among stress, emotional intelligence, cognitive intelligence, and cytokines', *Medicine*, 98(18), pp. 1–9.

Kaminski, M. *et al.* (2012) 'Migration of monocytes after intracerebral injection at entorhinal cortex lesion site', *Journal of Leukocyte Biology*, 92(1), pp. 31–39.

Kane, M. and Engle, R. (2002) 'The role of prefrontal cortex in working-memory capacity, executive attention, and general fluid intelligence: An individual-differences perspective', *Psychonomic Bulletin and Review*, 9(4), pp. 637–671.

Kapaki, E. *et al.* (2005) 'The diagnostic value of tau protein, β-amyloid (1-42) and their ratio for the discrimination of alcohol-related cognitive disorders from Alzheimer's disease in the early stages', *International Journal of Geriatric Psychiatry*, 20(8), pp. 722–729.

Karman, J. *et al.* (2004) 'Initiation of Immune Responses in Brain Is Promoted by Local Dendritic Cells', *The Journal of Immunology*, 173(4), pp. 2353–2361.

Kasai, H. *et al.* (2010) 'Structural dynamics of dendritic spines in memory and cognition', *Trends in Neurosciences*, 33(3), pp. 121–129.

Kempermann, G., Song, H. and Gage, F. (2015) 'Neurogenesis in the adult hippocampus', *Cold Spring Harbor Perspectives in Biology*, 7(9), pp. 1–14.

Kendall, M. and Smith, B. (1939) 'The problem of m rankings', *The Annals of Mathematical Statistics*, 10(3), pp. 275–287.

Kennedy, E., King, K. and Baldridge, M. (2018) 'Mouse microbiota models: Comparing germ-free mice and antibiotics treatment as tools for modifying gut bacteria', *Frontiers in Physiology*, 9(1534), pp. 1–16.

Keubler, L. *et al.* (2015) 'A multihit model: Colitis lessons from the interleukin-10-deficient mouse', *Inflammatory Bowel Diseases*, 21(8), pp. 1967–1975.

Keuker, J., Vollmann-Honsdorf, G. and Fuchs, E. (2001) 'How to use the optical fractionator: An example based on the estimation of neurons in the hippocampal CA1 and CA3 regions of tree shrews', *Brain Research Protocols*, 7(3), pp. 211–221.

Kida, S., Pantazis, A. and Weller, R. (1993) 'CSF drains directly from the subarachnoid space into nasal lymphatics in the rat. Anatomy, histology and immunological significance', *Neuropathology and Applied Neurobiology*, 19(6), pp. 480–488.

Kim, I. *et al.* (2002) 'Interferon γ Induces Retrograde Dendritic Retraction and Inhibits Synapse Formation', *Journal of Neuroscience*, 22(11), pp. 4530–4539.

Kim, J. and Jung, M. (2006) 'Neural circuits and mechanisms involved in Pavlovian fear conditioning: A critical review', *Neuroscience and Biobehavioral Reviews*, 30(2), pp. 188–202.

Kipnis, J. *et al.* (2004) 'T cell deficiency leads to cognitive dysfunction: Implications for therapeutic vaccination for schizophrenia and other psychiatric conditions', *Proceedings of the National Academy of Sciences of the United States of America*, 101(21), pp. 8180–8185.

Kipnis, J. *et al.* (2008) 'Immunity and cognition: what do age-related dementia, HIV-dementia and "chemo-brain" have in common?', *Trends in Immunology*, 29(10), pp. 455–463.

Kipnis, J., Gadani, S. and Derecki, N. (2012) 'Pro-cognitive properties of T cells', *Nature Reviews Neuroscience*, 12(9), pp. 663–669.

Kirov, S., Sorra, K. and Harris, K. (1999) 'Slices have more synapses than perfusion-fixed hippocampus from both young and mature rats', *Journal of Neuroscience*, 19(8), pp. 2876–2886.

Kitraki, E. *et al.* (2016) 'Effects of pre- and post-natal exposure to bisphenol A on the stress system', *Endocrine Disruptors*, 4(1), pp. 1–13.

Kiyota, T. *et al.* (2012) 'AAV serotype 2/1-mediated gene delivery of anti-inflammatory interleukin-10 enhances neurogenesis and cognitive function in APPPS1 mice', *Gene Therapy*, 19(7), pp. 724–733.

Knowles, E., David, A. and Reichenberg, A. (2010) 'Processing Speed Deficits in Schizophrenia: Reexamining the Evidence', *American Journal of Psychiatry*, 167(1), pp. 828–835.

Kocoska-Maras, L. *et al.* (2013) 'Cognitive function in association with sex hormones in postmenopausal women', *Gynecological Endocrinology*, 29(1), pp. 59–62.

Kolb, B. and Whishaw, I. (2003) 'Fundamentals of Human Neuropsychology', *Worth Publishers*, 1(1), pp. 1–764.

Koldzic-Zivanovic, N. *et al.* (2006) 'Regulation of adrenal glucocorticoid synthesis by interleukin-10: A preponderance of IL-10 receptor in the adrenal zona fasciculata', *Brain, Behavior, and Immunity*, 20(5), pp. 460–468.

Kolomeets, N., Orlovskaya, D. and Uranova, N. (2007) 'Decreased numerical density of CA3 hippocampal mossy fiber synapses in schizophrenia', *Synapse*, 61(8), pp. 615–621.

Kostulas, N. *et al.* (2002) 'Dendritic cells are present in ischemic brain after permanent middle cerebral artery occlusion in the rat', *Stroke*, 33(4), pp. 1129–1134.

Kraeuter, A., Guest, P. and Sarnyai, Z. (2019) 'The Y-Maze for Assessment of Spatial Working and Reference Memory in Mice', *Methods in Molecular Biology*, 1916(1), pp. 105–111.

Krueger, J. *et al.* (1994) 'Sleep, Microbes and Cytokines', *Neuroimmunomodulation*, 1(1), pp. 100–109.

Kühn, R. *et al.* (1993) 'Interleukin-10-deficient mice develop chronic enterocolitis', *Cell*, 75(2), pp. 263–274.

Kulkarni, V. and Firestein, B. (2012) 'The dendritic tree and brain disorders', *Molecular and Cellular Neuroscience*, 50(1), pp. 10–20.

Langenberg, D. *et al.* (2017) 'Cognitive impairment in Crohn's disease is associated with systemic inflammation, symptom burden and sleep disturbance', *United European Gastroenterology Journal*, 5(4), pp. 579–587.

Lebow, M. and Chen, A. (2016) 'Overshadowed by the amygdala: The bed nucleus of the stria terminalis emerges as key to psychiatric disorders', *Molecular Psychiatry*, 21(4), pp. 450–463.

Ledeboer, A. *et al.* (2002) 'Expression and regulation of interleukin-10 and interleukin-10 receptor in rat astroglial and microglial cells', *European Journal of Neuroscience*, 16(7), pp. 1175–1185.

Leger, M. *et al.* (2013) 'Object recognition test in mice', *Nature Protocols*, 8(12), pp. 2531–2537.

Lezak, M. *et al.* (2004) 'Neuropsychological assessment', *Oxford University Press*, 1(4), pp. 1–1029.

Liljeholm, M. and O'Doherty, J. (2012) 'Contributions of the striatum to learning, motivation, and performance: an associative account', *Trends in Cognitive Sciences*, 16(9), pp. 467–475.

Lim, M. *et al.* (2008) 'Regardless of genotype, offspring of VIP deficient female mice exhibit developmental delays and deficits in social behavior', *International Journal of Developmental Neuroscience*, 26(5), pp. 423–434.

Linkenauger, S. *et al.* (2012) 'A Perceptual-Motor Deficit Predicts Social and Communicative Impairments in Individuals With Autism Spectrum Disorders', *Autism Research*, 5(5), pp. 352–362.

Lisman, J. *et al.* (2017) 'Viewpoints: How the hippocampus contributes to memory, navigation and cognition', *Nature Neuroscience*, 20(11), pp. 1434–1447.

Liu, J. *et al.* (2020) 'Elevated blood neutrophil to lymphocyte ratio in older adults with cognitive impairment', *Archives of Gerontology and Geriatrics*, 88(104041), pp. 1–6.

Liu, X. and Carter, A. (2018) 'Ventral hippocampal inputs preferentially drive corticocortical neurons in the infralimbic prefrontal cortex', *Journal of Neuroscience*, 38(33), pp. 7351–7363.

Livak, K. and Schmittgen, T. D. (2001) 'Analysis of relative gene expression data using real-time quantitative PCR and the 2-ΔΔCT method', *Methods*, 25(4), pp. 402–408.

Lobo-Silva, D. *et al.* (2016) 'Balancing the immune response in the brain: IL-10 and its regulation', *Journal of Neuroinflammation*, 13(1), pp. 1–10.

Lohmiller, J., Swing, S. and Hanson, M. (2019) 'Reproduction and breeding', *The Laboratory Rat*, 1(6), pp. 157–179.

Lopez-Rojas, J. and Kreutz, M. (2016) 'Mature granule cells of the dentate gyrus-Passive bystanders or principal performers in hippocampal function?', *Neuroscience and Biobehavioral Reviews*, 64(1), pp. 167–174.

Louveau, A. *et al.* (2015) 'Structural and functional features of central nervous system lymphatic vessels', *Nature*, 523(7560), pp. 337–341.

Louveau, A., Harris, T. H. and Kipnis, J. (2015) 'Revisiting the Mechanisms of CNS Immune Privilege', *Trends in Immunology*, 36(10), pp. 569–577.

Lynch, A. *et al.* (2004) 'Lipopolysaccharide-induced increase in signalling in hippocampus is abrogated by IL-10 - A role for IL-1β?', *Journal of Neurochemistry*, 88(3), pp. 635–646.

Lyra, N. *et al.* (2021) 'Pro-inflammatory interleukin-6 signaling links cognitive impairments and peripheral metabolic alterations in Alzheimer's disease', *Translational Psychiatry*. Springer US, 11(1).

Mackenzie-Graham, A. *et al.* (2004) 'A multimodal, multidimensional atlas of the C57BL/6J mouse brain', *Journal of Anatomy*, 204(2), pp. 93–102.

Madsen, K. *et al.* (2002) 'Normal breast milk limits the development of colitis in IL-10-deficient mice', *Inflammatory Bowel Diseases*, 8(6), pp. 390–398.

Mahan, A. and Ressler, K. (2012) 'Fear Conditioning, Synaptic Plasticity, and the Amygdala: Implications for Posttraumatic Stress Disorder', *Trends in Neurosciences*, 35(1), pp. 24–35.

Maharshak, N. *et al.* (2013) 'Altered enteric microbiota ecology in interleukin 10-deficient mice during development and progression of intestinal inflammation', *Gut Microbes*, 4(4), pp. 316–324.

Maiti, P. *et al.* (2015) 'Molecular regulation of dendritic spine dynamics and their potential impact on synaptic plasticity and neurological diseases', *Neuroscience and Biobehavioral Reviews*, 59(101), pp. 208–237.

Malech, H., DeLeo, F. and Quinn, M. (2014) 'The Role of Neutrophils in the Immune System: An Overview', *Methods in Molecular Biology*, 1124(1), pp. 3–10.

Marin, I. and Kipnis, J. (2013) 'Learning and memory... and the immune system', *Learning and Memory*, 20(10), pp. 601–606.

Martinez, C. *et al.* (2008) 'Unstable composition of the fecal microbiota in ulcerative colitis during clinical remission', *American Journal of Gastroenterology*, 103(3), pp. 643–648.

Mateus-Pinheiro, A. *et al.* (2013) 'Sustained remission from depressive-like behavior depends on hippocampal neurogenesis', *Translational psychiatry*, 3(1), pp. 1–9.

Matsuzaki, M. *et al.* (2004) 'Structural basis of long-term potentiation in single dendritic spines', *Nature*, 429(6993), pp. 761–766.

Matthew, W. (2018) 'Barnes Maze Procedure for Spatial Learning and Memory in Mice', *Bio-protocol*, 8(5), pp. 139–148.

McBain, C. and Fisahn, A. (2001) 'Interneurons unbound', *Nature Reviews Neuroscience*, 2(1), pp. 11–23.

Mesquita, A. *et al.* (2008) 'IL-10 modulates depressive-like behavior', *Journal of Psychiatric Research*, 43(2), pp. 89–97.

Da Mesquita, S. *et al.* (2018) 'Functional aspects of meningeal lymphatics in ageing and Alzheimer's disease', *Nature*. Springer US, 560(7717), pp. 185–191.

Mesulam, M. M. (2000) 'Principles of Behavioral and Cognitive Neurology', *Oxford University Press*, 2(1), pp. 1–577.

Meziane, H. *et al.* (2007) 'Estrous cycle effects on behavior of C57BL/6J and BALB/cByJ female mice: Implications for phenotyping strategies', *Genes, Brain and Behavior*, 6(2), pp. 192–200.

Michalos, A. (2014) 'Encyclopedia of quality of life and well-being research', *Dordrecht: Springer Netherlands*, 1(1), pp. 1077–1079.

de Miranda, A. *et al.* (2017) 'Hippocampal adult neurogenesis: Does the immune system matter?', *Journal of the Neurological Sciences*, 372(1), pp. 482–495.

Mohseni, S. *et al.* (2014) 'Peripheral lymphadenopathy: Approach and diagnostic tools', *Iranian Journal of Medical Sciences*, 39(2), pp. 158–170.

Monteiro, S. *et al.* (2015) 'Absence of IFNγ promotes hippocampal plasticity and enhances cognitive performance', *Translational Psychiatry*, 6(707), pp. 1–8.

Moore, K. *et al.* (2001) 'Interleukin-10 and the Interleukin-10 Receptor', *Molecular and Cellular Biology*, 1(1), pp. 683–765.

Morais, L., Schreiber, H. and Mazmanian, S. (2021) 'The gut microbiota–brain axis in behaviour and brain disorders', *Nature Reviews Microbiology*, 19(4), pp. 241–255.

Morris, R. (1984) 'Developments of a water-maze procedure for studying spatial learning in the rat', *Journal of Neuroscience Methods*, 11(1), pp. 47–60.

Moser, E., Kropff, E. and Moser, M. (2008) 'Place cells, grid cells, and the brain's spatial representation system', *Annual Review of Neuroscience*, 31(1), pp. 69–89.

Moser, M. *et al.* (1995) 'Spatial learning with a minislab in the dorsal hippocampus', *Proceedings of the National Academy of Sciences of the United States of America*, 92(21), pp. 9697–9701.

Moser, M., Trommald, M. and Andersen, P. (1994) 'An increase in dendritic spine density on hippocampal CA1 pyramidal cells following spatial learning in adult rats suggests the formation of new synapses', *Proceedings of the National Academy of Sciences of the United States of America*, 91(26), pp. 12673–12675.

Mountrakis, G., Im, J. and Ogole, C. (2011) 'Support vector machines in remote sensing: A review', *ISPRS Journal of Photogrammetry and Remote Sensing*, 66(3), pp. 247–259.

Murray, P. (2006) 'Understanding and exploiting the endogenous interleukin-10/STAT3-mediated anti-inflammatory response', *Current Opinion in Pharmacology*, 6(4), pp. 379–386.

Nadeau, S. (2008) 'The thalamus and working memory', *Journal of the International Neuropsychological Society*, 14(5), pp. 900–901.

Nayak, J., Naik, B. and Behera, H. (2015) 'A Comprehensive Survey on Support Vector Machine in Data Mining Tasks: Applications & Challenges', *International Journal of Database Theory and Application*, 8(1), pp. 169–186.

Neves, G., Cooke, S. and Bliss, T. (2008) 'Synaptic plasticity, memory and the hippocampus: A neural network approach to causality', *Nature Reviews Neuroscience*, 9(1), pp. 65–75.

Nimchinsky, E., Sabatini, B. and Svoboda, K. (2002) 'Structure and function of dendritic spines', *Annual Review of Physiology*, 64(1), pp. 313–353.

Nollet, M. *et al.* (2011) 'Activation of orexin neurons in dorsomedial/perifornical hypothalamus and antidepressant reversal in a rodent model of depression', *Neuropharmacology*, 61(1–2), pp. 336–346.

Norden, D. *et al.* (2014) 'TGFβ produced by IL-10 redirected astrocytes attenuates microglial activation', *Glia*, 62(6), pp. 881–895.

Numakawa, T., Odaka, H. and Adachi, N. (2017) 'Actions of brain-derived neurotrophic factor and glucocorticoid stress in neurogenesis', *International Journal of Molecular Sciences*, 18(11), pp. 1–15.

Nyuyki, K. *et al.* (2018) 'Altered brain excitability and increased anxiety in mice with experimental colitis: Consideration of hyperalgesia and sex differences', *Frontiers in Behavioral Neuroscience*, 12(58), pp. 1–11.

O'Keefe, J., Dostrovsky, J. and J. O'Keefe, J. (1971) 'Short Communications The hippocampus as a spatial map. Preliminary evidence from unit activity in the freely-moving rat', *Brain Research*, 34(1), pp. 171–175.

Ogawa, H. *et al.* (2003) 'Expression of multiple mRNA species for choline acetyltransferase in human T-lymphocytes', *Life Sciences*, 72(18–19), pp. 2127–2130.

Ohshima, K. *et al.* (2000) 'Cytoplasmic cytokines in lymphoproliferative disorders: Multiple cytokine production in angioimmunoblastic lymphadenopathy with dysproteinemia', *Leukemia and Lymphoma*, 38(5–6), pp. 541–545.

Okada, R. *et al.* (2008) 'Phenotypic classification of human CD4+ T cell subsets and their differentiation', *International Immunology*, 20(9), pp. 1189–1199.

Omi, A. *et al.* (2014) 'Mature resting Ly6Chigh natural killer cells can be reactivated by IL-15', *European Journal of Immunology*, 44(9), pp. 2638–2647.

Ouanes, S. and Popp, J. (2019) 'High Cortisol and the Risk of Dementia and Alzheimer's Disease: A Review of the Literature', *Frontiers in Aging Neuroscience*, 11(1), pp. 1–11.

Pacheco, R. *et al.* (2006) 'Glutamate Released by Dendritic Cells as a Novel Modulator of T Cell Activation', *The Journal of Immunology*, 177(10), pp. 6695–6704.

Packard, M. and Knowlton, B. (2002) 'Learning and memory functions of the basal ganglia', *Annual Review of Neuroscience*, 25(1), pp. 563–593.

Pantzar, A. *et al.* (2014) 'Cognitive deficits in unipolar old-age depression: A population-based study', *Psychological Medicine*, 44(5), pp. 937–947.

Papadopoulos, Z., Herz, J. and Kipnis, J. (2020) 'Meningeal Lymphatics: From Anatomy to Central Nervous System Immune Surveillance', *The Journal of Immunology*, 204(2), pp. 286–293.

Parker, N. *et al.* (2019) 'Anatomy of the Nervous System', *National Institutes of Health*, 1(1), pp. 1–6.

Peñaloza, H. *et al.* (2015) 'Interleukin-10 plays a key role in the modulation of neutrophils recruitment and lung inflammation during infection by Streptococcus pneumoniae', *Immunology*, 146(1), pp. 100–112.

Pereira, L. *et al.* (2015) 'IL-10 regulates adult neurogenesis by modulating ERK and STAT3 activity', *Frontiers in Cellular Neuroscience*, 9(1), pp. 1–9.

Perez-Asensio, F. *et al.* (2013) 'Interleukin-10 regulates progenitor differentiation and modulates neurogenesis in adult brain', *Journal of Cell Science*, 126(18), pp. 4208–4219.

Petersen, S. and Posner, M. (2012) 'The Attention System of the Human Brain: 20 Years After', *Annual review of neuroscience*, 35(1), pp. 73–89.

Petten, C. (2004) 'Relationship between hippocampal volume and memory ability in healthy individuals across the lifespan: Review and meta-analysis', *Neuropsychologia*, 42(1), pp. 1394–1413.

Pohlack, S. *et al.* (2014) 'Bigger is better! Hippocampal volume and declarative memory performance in healthy young men', *Brain Structure and Function*, 219(1), pp. 255–267.

Polleux, F., Morrow, T. and Ghosh, A. (2000) 'Semaphorin 3A is a chemoattractant for cortical apical dendrites', *Nature*, 404(6778), pp. 567–573.

Portfors, C. and Perkel, D. (2014) 'The role of ultrasonic vocalizations in mouse communication', *Current Opinion in Neurobiology*, 28(1), pp. 115–120.

Posner, M. (2011) 'Attention in a social world', *Oxford University Press*, 1(1), pp. 1–224.

Prut, L. and Belzung, C. (2003) 'The open field as a paradigm to measure the effects of drugs on anxiety-like behaviors: A review', *European Journal of Pharmacology*, 463(1), pp. 3–33.

Ransohoff, R., Kivisäkk, P. and Kidd, G. (2003) 'Three or more routes for leukocyte migration into the central nervous system', *Nature Reviews Immunology*, 3(7), pp. 569–581.

Raphael, I. *et al.* (2015) 'T cell subsets and their signature cytokines in autoimmune and inflammatory diseases', *Cytokine*, 74(1), pp. 5–17.

Richwine, A. *et al.* (2009) 'Cognitive deficits in interleukin-10-deficient mice after peripheral injection of lipopolysaccharide', *Brain, Behavior, and Immunity*, 23(6), pp. 794–802.

Risher, W. *et al.* (2014) 'Rapid golgi analysis method for efficient and unbiased classification of dendritic spines', *PLoS ONE*, 9(9), pp. 1–8.

Robertson, S. *et al.* (2019) 'Comparison of Co-housing and Littermate Methods for Microbiota Standardization in Mouse Models', *Cell Reports*, 27(6), pp. 1910–1919.

Roediger, H. and Karpicke, J. (2005) 'Learning and Memory', *Encyclopedia of Social Measurement*, 1(1), pp. 479–486.

Rogers, J. *et al.* (2017) 'Search strategy selection in the Morris water maze indicates allocentric map formation during learning that underpins spatial memory formation', *Neurobiology of Learning and Memory*, 139(1), pp. 37–49.

Ron-Harel, N. *et al.* (2008) 'Age-dependent spatial memory loss can be partially restored by immune activation', *Rejuvenation Research*, 11(5), pp. 903–913.

Ronchetti, S. *et al.* (2018) 'How glucocorticoids affect the neutrophil life', *International Journal of Molecular Sciences*, 19(12), pp. 1–12.

Roozendaal, B., McEwen, B. and Chattarji, S. (2009) 'Stress, memory and the amygdala', *Nature Reviews Neuroscience*, 10(6), pp. 423–433.

Rosales, C. *et al.* (2017) 'Neutrophils: Their role in innate and adaptive immunity', *Journal of Immunology Research*, 2017(1), pp. 2–4.

Rosenbaum, D., Carlson, R. and Gilmore, R. (2001) 'Acquisition of intellectual and perceptual-motor skills', *Annual review psychology*, 52(1), pp. 453–470.

Rousseeuw, P. (1987) 'Silhouettes: A graphical aid to the interpretation and validation of cluster analysis', *Journal of Computational and Applied Mathematics*, 20(1), pp. 53–65.

Rubin, D., Shaker, A. and Levin, M. (2012) 'Chronic intestinal inflammation: Inflammatory bowel disease and colitis-associated colon cancer', *Frontiers in Immunology*, 3(1), pp. 1–10.

Sachdev, P. *et al.* (2014) 'Classifying neurocognitive disorders: The DSM-5 approach', *Nature Reviews Neurology*, 10(11), pp. 634–642.

Sah, P., Sun, Y. and Gooch, H. (2020) 'Fear conditioning and the basolateral amygdala', *F1000Research*, 9(53), pp. 1–8.

Sallusto, F., Geginat, J. and Lanzavecchia, A. (2004) 'Central memory and effector memory T cell subsets: Function, generation, and maintenance', *Annual Review of Immunology*, 22(1), pp. 745–763.

Salthouse, T. (1996) 'The Processing-Speed Theory of Adult Age Differences in Cognition', *Psychological Review*, 103(3), pp. 403–428.

Saper, C., Scammell, T. and Lu, J. (2005) 'Hypothalamic regulation of sleep and circadian rhythms', *Nature*, 437(7063), pp. 1257–1263.

Saraiva, M. and O'Garra, A. (2010) 'The regulation of IL-10 production by immune cells', *Nature Reviews Immunology*, 10(3), pp. 170–181.

Schaefer, J. *et al.* (2013) 'The global cognitive impairment in schizophrenia: Consistent over decades and around the world', *Schizophrenia Research*, 150(1), pp. 42–50.

Scheinin, T. *et al.* (2003) 'Validation of the interleukin-10 knockout mouse model of colitis: Antitumour necrosis factor-antibodies suppress the progression of colitis', *Clinical and Experimental Immunology*, 133(1), pp. 38–43.

Schetters, S. *et al.* (2018) 'Neuroinflammation: Microglia and T cells get ready to tango', *Frontiers in Immunology*, 8(1905), pp. 1–11.

Schluns, K. and Lefrançois, L. (2003) 'Cytokine control of memory T-cell development and survival', *Nature Reviews Immunology*, 3(4), pp. 269–279.

Schwartz, M. and Shechter, R. (2010) 'Protective autoimmunity functions by intracranial immunosurveillance to support the mind: The missing link between health and disease', *Molecular Psychiatry*, 15(4), pp. 342–354.

Seibenhener, M. and Wooten, M. (2015) 'Use of the open field maze to measure locomotor and anxiety-like behavior in mice', *Journal of Visualized Experiments*, 52434(1), pp. 1–6.

Serre-Miranda, C. *et al.* (2015) 'Effector memory CD4+ T cells are associated with cognitive performance in a senior population', *Neurology: Neuroimmunology and NeuroInflammation*, 2(1), pp. 1–8.

Serre-Miranda, C. *et al.* (2020) 'Cognition Is Associated With Peripheral Immune Molecules in Healthy Older Adults: A Cross-Sectional Study', *Frontiers in Immunology*, 11(2045), pp. 1–10.

Shiversa, K. *et al.* (2015) 'Estrogen alters baseline and inflammatory-induced cytokine levels independent from hypothalamic–pituitary–adrenal axis activity', *Cytokine*, 72(2), pp. 121–129.

Sholl, D. (1956) 'The measurable parameters of the cerebral cortex and their significance in its organization', *Progress in neurobiology*, 2(1), pp. 324–333.

Shors, T. *et al.* (2001) 'Neurogenesis in the adult is involved in the formation of trace memories', *Nature*, 414(6866), pp. 1–6.

Simola, N. (2015) 'Rat Ultrasonic Vocalizations and Behavioral Neuropharmacology: From the Screening of Drugs to the Study of Disease', *Current Neuropharmacology*, 13(2), pp. 164–179.

Singh, V. *et al.* (2016) 'Inhibition of Interleukin-10 Signaling Induces Microbiota-Dependent Chronic Colitis in Apolipoprotein E Deficient Mice', *Inflammatory Bowel Diseases*, 22(4), pp. 841–852.

Sira, C. and Mateer, C. (2014) 'Executive Function', *Encyclopedia of the Neurological Sciences*, 2(1), pp. 239–242.

Small, G. (2002) 'What we need to know about age related memory loss', *British Medical Journal*, 324(7352), pp. 1502–1505.

Small, S. *et al.* (2012) 'A pathophysiological framework of hippocampal dysfunction in ageing and disease', *Nature Reviews Neuroscience*, 12(10), pp. 585–601.

Smith, E. *et al.* (1999) 'IL-10 as a mediator in the HPA axis and brain', *Journal of Neuroimmunology*, 100(1), pp. 140–148.

Starkman, M. *et al.* (1992) 'Hippocampal formation volume, memory dysfunction, and cortisol levels in patients with Cushing's syndrome', *Biological Psychiatry*, 32(9), pp. 756–765.

Steinke, J. *et al.* (2004) 'Functional Analysis of −571 IL-10 Promoter Polymorphism Reveals a Repressor Element Controlled by Sp1', *The Journal of Immunology*, 173(5), pp. 3215–3222.

Stout, J. *et al.* (2011) 'Neurocognitive Signs in Prodromal Huntington Disease', *Neuropsychology*, 25(1), pp. 1–14.

Strange, B. *et al.* (2014) 'Functional organization of the hippocampal longitudinal axis', *Nature Reviews Neuroscience*, 15(10), pp. 655–669.

Strominger, N., Demarest, R. and Laemle, L. (2012) 'Meninges, Ventricles, and Cerebrospinal Fluid', *Noback's Human Nervous System*, 5(1), pp. 91–101.

Stuart, G. and Spruston, N. (2015) 'Dendritic integration: 60 years of progress', *Nature Neuroscience*, 18(12), pp. 1713–1721.

Stulemeijer, M. *et al.* (2010) 'How mild traumatic brain injury may affect declarative memory performance in the post-acute stage', *Journal of Neurotrauma*, 27(9), pp. 1585–1595.

Sturlan, S. *et al.* (2001) 'Interleukin-10-deficient mice and inflammatory bowel disease associated cancer development', *Carcinogenesis*, 22(4), pp. 665–671.

Sturman, O., Germain, P. and Bohacek, J. (2018) 'Exploratory rearing: a context- and stress-sensitive behavior recorded in the open-field test', *Stress*, 21(5), pp. 443–452.

Suk-yu, Y., Ang, L. and Kwok-Fai, S. (2015) 'Involvement of Adult Hippocampal Neurogenesis in Learning and Forgetting', *Neural Plasticity*, 2015(1), pp. 1–13.

Sultana, R., Ogundele, O. and Lee, C. (2019) 'Contrasting characteristic behaviours among common laboratory mouse strains', *Royal Society Open Science*, 6(1), pp. 1–15.

Sun, L. *et al.* (2009) 'Effect of IL-10 on neutrophil recruitment and survival after Pseudomonas aeruginosa challenge', *American Journal of Respiratory Cell and Molecular Biology*, 41(1), pp. 76–84.

Sweeney, P. and Yang, Y. (2015) 'An excitatory ventral hippocampus to lateral septum circuit that suppresses feeding', *Nature Communications*, 6(1), pp. 1–11.

Tadin-Hadjina, I. *et al.* (2019) 'Impaired neurocognitive and psychomotor performance in patients with inflammatory bowel disease', *Scientific Reports*, 9(1), pp. 1–13.

Tancredi, V. *et al.* (2000) 'The inhibitory effects of interleukin-6 on synaptic plasticity in the rat hippocampus are associated with an inhibition of mitogen-activated protein kinase ERK', *Journal of Neurochemistry*, 75(2), pp. 634–643.

Taube, J. (2007) 'The head direction signal: Origins and sensory-motor integration', *Annual Review of Neuroscience*, 30(1), pp. 181–207.

Tellier, J. and Nutt, S. (2017) 'Standing out from the crowd: How to identify plasma cells', *European Journal of Immunology*, 47(8), pp. 1276–1279.

Testar, J. (2019) 'Cytokines: Introduction', *British Society of Immunology*, 1(1), pp. 1–2.

Tronel, S. *et al.* (2010) 'Spatial learning sculpts the dendritic arbor of adult-born hippocampal neurons', *Proceedings of the National Academy of Sciences of the United States of America*, 107(17), pp. 7963–7968.

Vazqueza, M., Catalan-Dibene, J. and Zlotnik, A. (2015) 'B cells responses and cytokine production are regulated by their immune microenvironment', *Cytokine*, 74(2), pp. 318–326.

Vijayakumar, A. and Vijayakumar, A. (2012) 'Comparison of Hippocampal Volume in Dementia Subtypes', *ISRN Radiology*, 2013(174524), pp. 1–5.

Virji-Babul, N. *et al.* (2006) 'Perceptual-motor deficits in children with Down syndrome: Implications for intervention', *Down Syndrome Research and Practice*, 10(2), pp. 74–82.

Walf, A. and Frye, C. (2007) 'The use of the elevated plus maze as an assay of anxiety-related behavior in rodents', *Nature Protocols*, 2(2), pp. 322–328.

Walsh, J. *et al.* (2014) 'Regulatory T cells in central nervous system injury: A double- edged sword', *Journal of Immunology*, 193(10), pp. 5013–5022.

Walunas, T. *et al.* (1995) 'Ly-6C is a marker of memory CD8+ T cells', *The Journal of Immunology*, 155(4), pp. 1873–1883.

Wang, J., John, Y. and Barbas, H. (2021) 'Pathways for contextual memory: The primate hippocampal pathway to anterior cingulate cortex', *Cerebral Cortex*, 31(3), pp. 1807–1826.

Watson, A. *et al.* (2009) 'Mechanisms of epithelial cell shedding in the mammalian intestine and maintenance of barrier function', *Annals of the New York Academy of Sciences*, 1165(1), pp. 135–142.

West, M., Slomianka, L. and Gundersen, H. (1991) 'Unbiased stereological estimation of the total number of neurons in the subdivisions of the rat hippocampus using the optical fractionator', *The Anatomical Record*, 231(4), pp. 482–497.

Wichers, M. and Maes, M. (2002) 'The psychoneuroimmuno-pathophysiology of cytokine-induced depression in humans', *International Journal of Neuropsychopharmacology*, 5(4), pp. 375–388.

Wilson, D. *et al.* (2011) 'Compromised verbal episodic memory with intact visual and procedural memory during pregnancy', *Journal of Clinical and Experimental Neuropsychology*, 33(6), pp. 680–691.

Wiltgen, B. *et al.* (2004) 'New circuits for old memories: The role of the neocortex in consolidation', *Neuron*, 44(1), pp. 101–108.

Witter, M. (1993) 'Organization of the entorhinal-hippocampal system: A review of current anatomical data', *Hippocampus*, 3(1), pp. 33–44.

Wolf, S. *et al.* (2009) 'CD4-Positive T Lymphocytes Provide a Neuroimmunological Link in the Control of Adult Hippocampal Neurogenesis', *The Journal of Immunology*, 182(7), pp. 3979–3984.

Wrammert, J. *et al.* (2002) 'Ly6C expression differentiates plasma cells from other B cell subsets in mice', *European Journal of Immunology*, 32(1), pp. 97–103.

Wu, Y., Fujishima, K. and Kengaku, M. (2015) 'Differentiation of apical and basal dendrites in pyramidal cells and granule cells in dissociated hippocampal cultures', *PLoS ONE*, 10(2), pp. 1–16.

Wyss, J. and Groen, T. (1992) 'Connections Between the Retrosplenial Cortex and the Hippocampal Formation in the Rat: A Review', *Hippocampus*, 2(1), pp. 1–12.

Xiu, M. *et al.* (2016) 'Contribution of IL-10 and its -592 A/C polymorphism to cognitive functions in first-episode drug-naive schizophrenia', *Brain, Behavior, and Immunity*, 57(1), pp. 116–124.

Xu, D. *et al.* (2017) 'Brain-derived neurotrophic factor reduces inflammation and hippocampal apoptosis in experimental Streptococcus pneumoniae meningitis', *Journal of Neuroinflammation*, 14(1), pp. 1–13.

Xu, G. *et al.* (2010) 'Effects of brain-derived neurotrophic factor on local inflammation in experimental stroke of rat', *Mediators of Inflammation*, 2010(372423), pp. 1–10.

Yang, L. *et al.* (2021) 'Depression-like Behavior Associated with E/I imbalance of mPFC and Amygdala without TRPC Channels in mice of Knockout IL-10 from Microglia', *Brain Behavior and Immunity*, 1(1), pp. 1–35.

Yang, Y., Lu, J. and Zuo, Y. (2018) 'Changes of Synaptic Structures Associated with Learning, Memory and Diseases', *Brain Science Advances*, 4(2), pp. 99–117.

Yankelevitch-Yahav, R. *et al.* (2015) 'The forced swim test as a model of depressive-like behavior', *Journal of Visualized Experiments*, 97(52587), pp. 1–7.

Yin, J. *et al.* (2011) 'Deficits in spatial learning and memory is associated with hippocampal volume loss in aged apolipoprotein e4 mice', *Journal of Alzheimer's Disease*, 27(1), pp. 89–98.

Zenaro, E. *et al.* (2015) 'Neutrophils promote Alzheimer's disease-like pathology and cognitive decline via LFA-1 integrin', *Nature Medicine*, 21(8), pp. 880–886.

Zhang, H. *et al.* (2020) 'A1 astrocytes contribute to murine depression-like behavior and cognitive dysfunction, which can be alleviated by IL-10 or fluorocitrate treatment', *Journal of Neuroinflammation*, 17(1), pp. 1–13.

Zhang, Y. and Li, Y. (2014) 'Inflammatory bowel disease: Pathogenesis', *World Journal of Gastroenterology*, 20(1), pp. 91–99.

Zhao, M. *et al.* (2011) 'Feature selection and parameter optimization for support vector machines: A new approach based on genetic algorithm with feature chromosomes', *Expert Systems with Applications*, 38(5), pp. 5197–5204.

Zhao, Z. *et al.* (2015) 'Central role for PICALM in amyloid–β blood–brain barrier transcytosis and clearance', *Nature Neuroscience*, 18(7), pp. 978–987.

Zhou, Z. *et al.* (2009) 'Interleukin-10 provides direct trophic support to neurons', *Journal of Neurochemistry*, 110(5), pp. 1617–1627.

Ziv, Y. *et al.* (2006) 'Immune cells contribute to the maintenance of neurogenesis and spatial learning abilities in adulthood', *Nature Neuroscience*, 9(2), pp. 268–275.

Zlokovic, B. (2012) 'Neurovascular pathways to neurodegeneration in Alzheimer's disease and other disorders Berislav', *Nature Reviews Neuroscience*, 12(12), pp. 723–738.

CHAPTER 8

ANNEXES

Annex 1: Custom-written MATLAB codes

Unsupervised machine learning: an algorithm for data clustering

```
%% k-means clustering algorithm

data = colon_inflammatory_marker_genes;

rng default

% Request the maximum K value to test

max_k = input('What is the maximum K value you want to test? ');

if max_k > size(data,1)
    disp('The maximum K value must be smaller than or equal to the number of rows in your data
matrix.');
else
    if max_k ~= round(max_k)
        disp('The maximum K value must be an integer.');
    else
        if max_k <= 1
        disp('The maximum K value must be greater than or equal to 2.');
        else
            disp('The maximum K value inserted was successfully accepted.');

            % Find the best K value

            sk = zeros(100,max_k);

            for i = 1:100
                for k = 2:max_k
                    IDX = kmeans(data,k);
                    s = silhouette(data, IDX);
                    sk(i,k) = mean(s);
                end
            end

            msk = mean(sk,1);
            [~,I] = max(msk);
            best_k = I;

            disp(['K values from 2 to ',num2str(max_k),' were tested. The best K value is
',num2str(best_k),'.']);

            % K-means clustering with the best K

            IDX = kmeans(data,best_k);

            % Find the assigned cluster

            assigned_cluster = IDX;

            disp(['For K = ',num2str(best_k),', the assigned clustering results should be
assessed on "assigned_cluster" data matrix.']);

            % Find the silhouette values

            silhouette_values = silhouette(data,assigned_cluster);
            average_silhouette_value = mean(silhouette_values);

            disp(['For K = ',num2str(best_k),', the average silhouette value is
',num2str(average_silhouette_value),'. The individual silhouette values are shown in the
"silhouette_values" data matrix.']);
        end
    end
end
```

```
%% Genetic algorithm + Support vector machine

% Data matrix processing

groups = behavior_data(:,1);
data = behavior_data(:,2:max(size(behavior_data,2)));

rng default

% Request the feature selection parameter values for the genetic algorithm

disp('Feature selection parameter values for the genetic algorithm:')

population_size = input('1. What is the population size you want to test? ');
generations = input('2. How many generations do you want to create? ');
tau_input = input('3. What percentage of the population of feature combinations do you intend
to keep between generations? ');
upsilon_input = input('4. What percentage of the population of feature combinations do you
intend to create by crossover in each generation? ');
delta_input = input('5. What percentage of feature mutation you want to test in each mutated
individual feature combination? ');

disp('The feature selection parameter values for the genetic algorithm were successfully
accepted.');

% Generate the initial population of random feature combinations

tic

population = (randi([0,1],population_size,size(data,2)));

error = zeros(population_size,1);

for g = 1:generations

    disp(['Starting generation = ',num2str(g),'.']);

    for i = 1:population_size
        while sum(population(i,:)) == 0
            population(i,:) = (randi([0,1],1,size(data,2)));
        end
    end

    % Perform the classification assignment

    for i = 1:population_size
        alfa = population(i,:);
        beta = find(alfa == 1);
        svmmodel = fitcsvm(data(:,beta),groups);
        cvmodel = crossval(svmmodel);
        error(i) = kfoldLoss(cvmodel);
    end

    % Keep the elite population of feature combinations between generations

    [rank_error,spot_alfa] = sort(error);

    tau_percentage = tau_input/100;
    elite = population(spot_alfa(1:tau_percentage*population_size),:);

    % Create the crossover population of feature combinations in each generation

    sigma = population(spot_alfa(find(rank_error < 0.5)),:);
    sigma_error = rank_error(find(rank_error < 0.5));

    upsilon_percentage = upsilon_input/100;

    upsilon = zeros(1,size(data,2));
    upsilon_sigma = zeros(upsilon_percentage*population_size,size(data,2));

    for u = 1:round(upsilon_percentage*population_size)
        sigma_5 = randi([1,size(sigma,1)],1,5);
        sigma_5_beta = sigma(sigma_5,:);
        sigma_5_error = sigma_error(sigma_5);
```

```
        [~,best_2_rank] = mink(sigma_5_error,2);
        sigma_couple = sigma_5_beta(best_2_rank,:);
        lambda = randi([0,1],1,size(data,2));
        for k = 1:size(data,2)
            if lambda(k) == 0
                upsilon(k) = sigma_couple(1,k);
            else
                upsilon(k) = sigma_couple(2,k);
            end
        end
        upsilon_sigma(u,:) = upsilon;
    end

    % Create the mutated population of feature combinations in each generation

    gamma_input = 100 - tau_input - upsilon_input;
    gamma_percentage = 1 - tau_percentage - upsilon_percentage;

    delta_percentage = delta_input/100;

    gamma_sigma = zeros(gamma_percentage*population_size,size(sigma,2));

    for i = 1:round(gamma_percentage*population_size)
        no_gamma_rank = randi(size(sigma,1));
        no_gamma_beta = sigma(no_gamma_rank,:);
        gamma_beta = randperm(size(population,2),round((delta_percentage/100)*size(data,2)));
        gamma = no_gamma_beta;
        for u = 1:length(gamma_beta)
            if gamma(gamma_beta(u)) == 1
               gamma(gamma_beta(u)) = 0;
            else
                gamma(gamma_beta(u)) = 1;
            end
        end
        gamma_sigma(i,:) = gamma;
    end

    population = [elite; upsilon_sigma; gamma_sigma];
end

[rank_error,spot_alfa] = sort(error);

% Select the best individual feature combination for classification assignment

best_combination = population(spot_alfa(1),:);
best_combination_error = rank_error(1);

disp(['For a population = ',num2str(population_size),', a number of generations =
',num2str(generations),', a percentage of elite individual feature combinations per generation
= ',num2str(tau_input),'%, a percentage of crossover individual feature combinations per
generation = ',num2str(upsilon_input),'%, a percentage of mutated individual feature
combinations per generation = ',num2str(gamma_input),'% (with ',num2str(delta_input),'% of
feature mutation per mutated individual feature combination), the best feature combination for
classification assignment can be found in the "best_combination" data matrix. With this
feature combination, the classification assignment error is
',num2str(best_combination_error),'.']);

% Find the elapsed time

elapsed_time = toc;
```

Annex 2: Supplementary figures

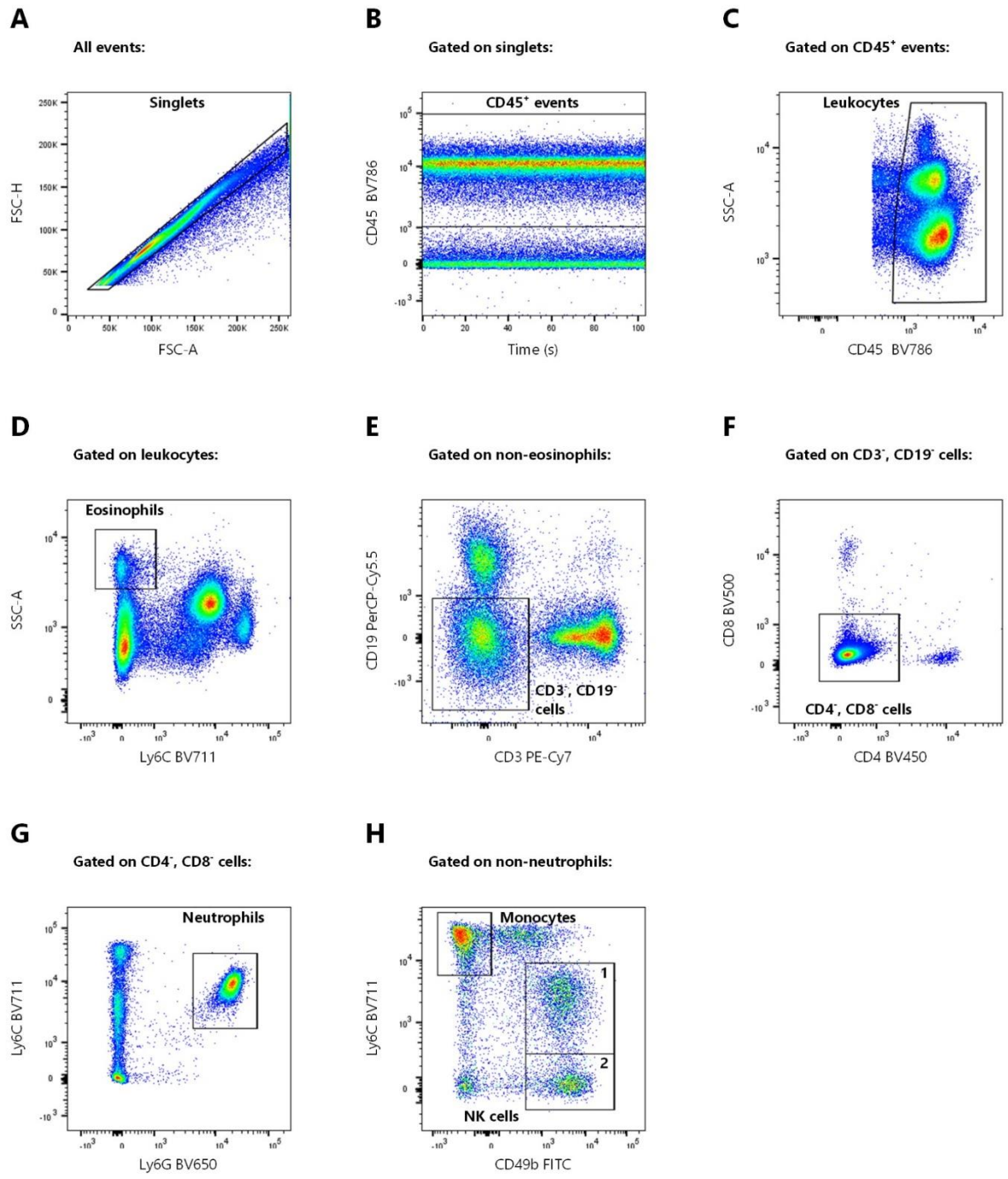

Supplementary figure 1. Gating strategy used to assess the percentage of the major populations of the innate immune system in the blood. A. The analysis was initiated by the selection of singlets. **B.** All $CD45^+$ events were selected over time. **C.** Leukocytes were defined by excluding debris. **D.** Within leukocytes, eosinophils were defined as $Ly6C^-$ and $SSC\text{-}A^{high}$ cells. **E.** After excluding eosinophils, $CD3^-$, $CD19^-$ cells were selected. **F.** $CD4^-$, $CD8^-$ cells were then gated. **G.** Within $CD4^-$, $CD8^-$ cells, neutrophils were defined as $Ly6G^+$, $Ly6C^{high}$ cells. **H.** After excluding neutrophils, NK cells were subdivided as $Ly6C^{high}$ (**1**) and $Ly6C^{low}$(**2**) cells, and monocytes were defined as $CD49b^-$, $Ly6C^{high}$ cells.

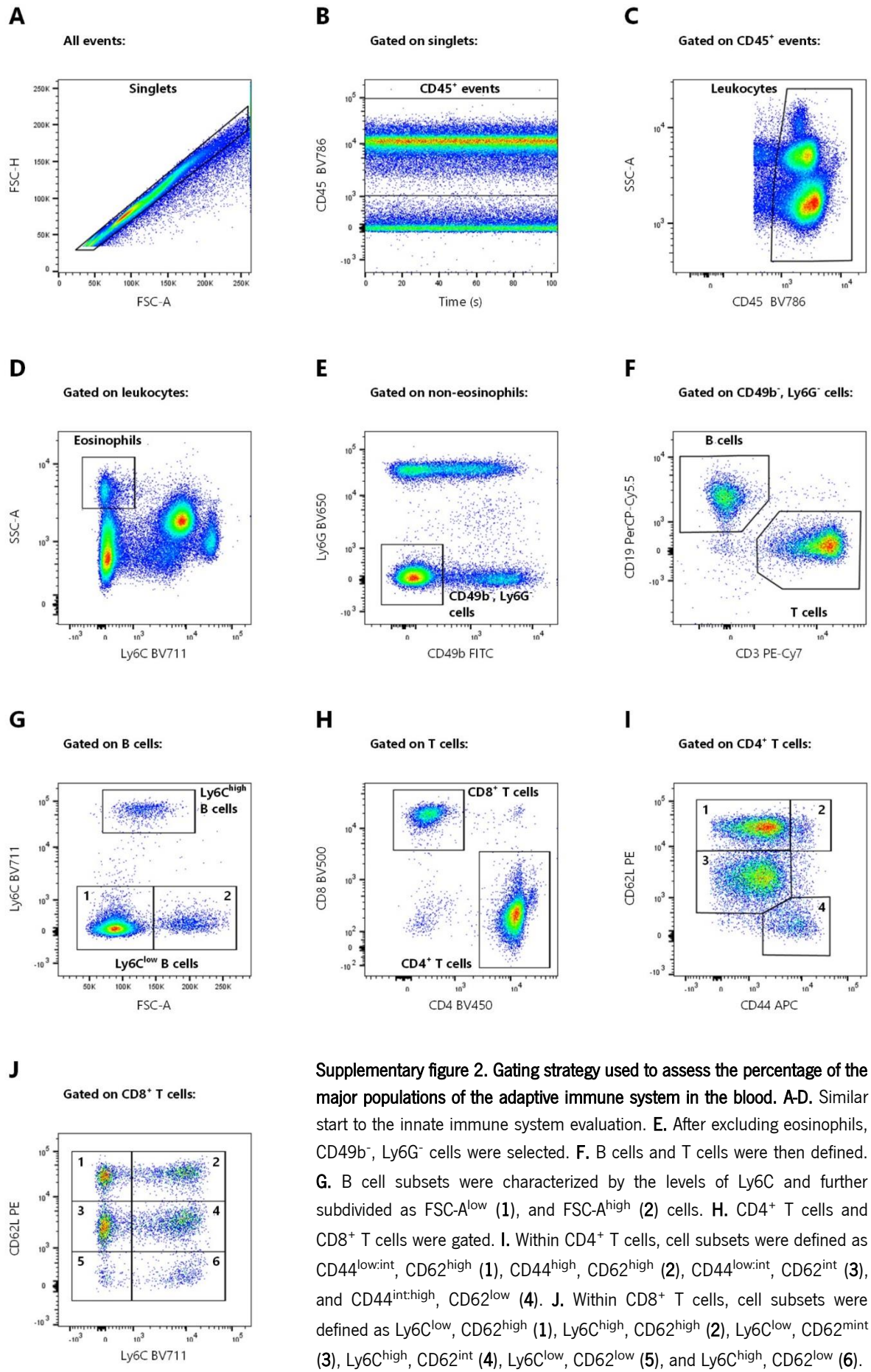

Supplementary figure 2. Gating strategy used to assess the percentage of the major populations of the adaptive immune system in the blood. A-D. Similar start to the innate immune system evaluation. **E.** After excluding eosinophils, CD49b$^-$, Ly6G$^-$ cells were selected. **F.** B cells and T cells were then defined. **G.** B cell subsets were characterized by the levels of Ly6C and further subdivided as FSC-A^{low} (**1**), and FSC-A^{high} (**2**) cells. **H.** CD4$^+$ T cells and CD8$^+$ T cells were gated. **I.** Within CD4$^+$ T cells, cell subsets were defined as CD44$^{low:int}$, CD62^{high} (**1**), CD44^{high}, CD62^{high} (**2**), CD44$^{low:int}$, CD62^{int} (**3**), and CD44$^{int:high}$, CD62^{low} (**4**). **J.** Within CD8$^+$ T cells, cell subsets were defined as Ly6C^{low}, CD62^{high} (**1**), Ly6C^{high}, CD62^{high} (**2**), Ly6C^{low}, CD62^{mint} (**3**), Ly6C^{high}, CD62^{int} (**4**), Ly6C^{low}, CD62^{low} (**5**), and Ly6C^{high}, CD62^{low} (**6**).

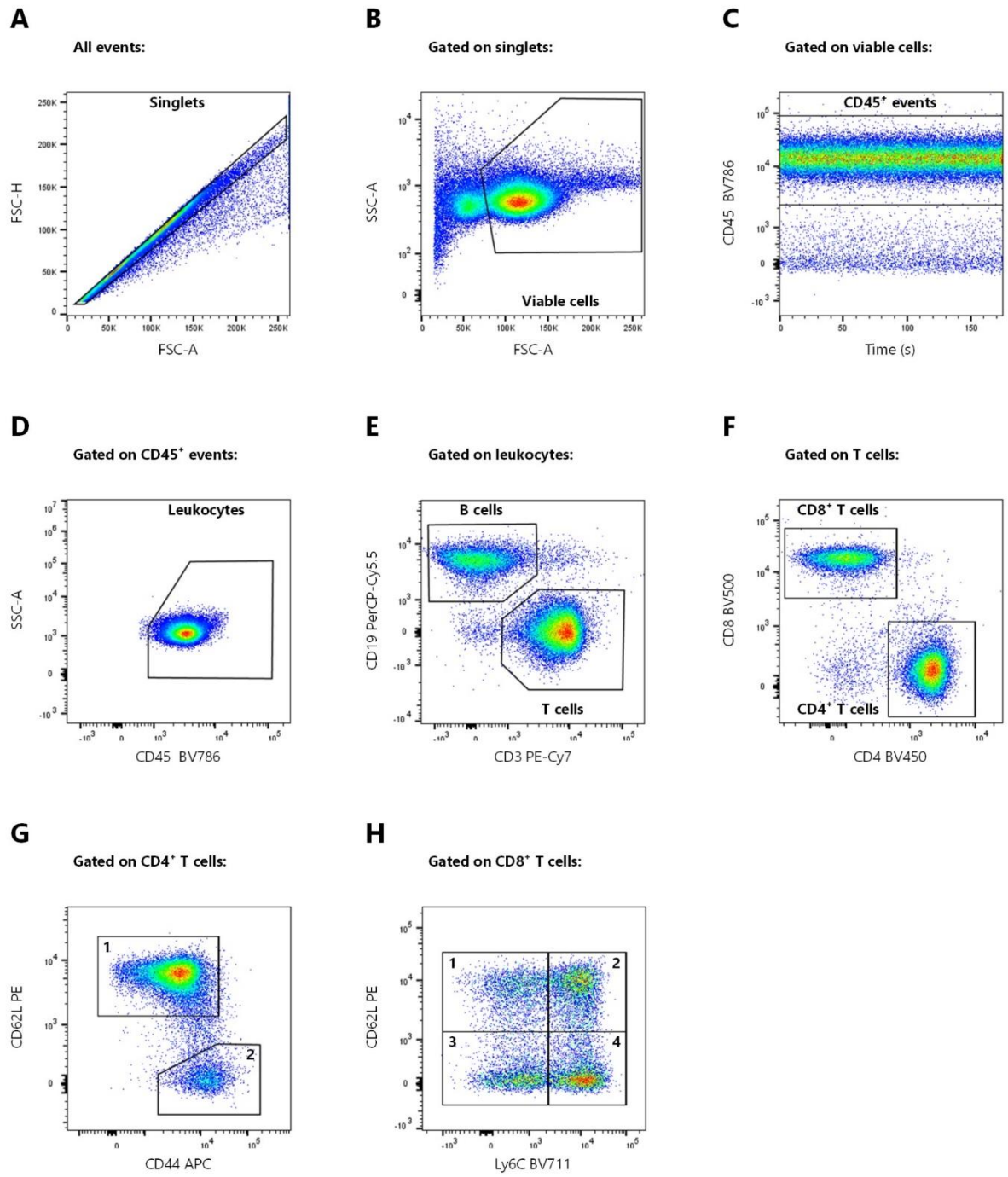

Supplementary figure 3. Gating strategy used to assess the percentage of the major populations of the adaptive immune system in both inguinal and deep cervical lymph nodes. A. The analysis was initiated by the selection of singlets. **B.** Viable cells were gated based on their size and complexity. **C.** All $CD45^+$ events were selected over time. **D.** Leukocytes were defined by excluding debris. **E.** B cells and T cells were then gated. **F.** $CD4^+$ T cells and $CD8^+$ T cells were gated. **I.** Within $CD4^+$ T cells, cell subsets were defined as $CD44^{low:int}$, $CD62^{high}$ (**1**), and $CD44^{int:high}$, $CD62^{low}$ (**2**). **J.** Within $CD8^+$ T cells, cell subsets were defined as $Ly6C^{low}$, $CD62^{high}$ (**1**), $Ly6C^{high}$, $CD62^{high}$ (**2**), $Ly6C^{low}$, $CD62^{low}$ (**3**), and $Ly6C^{high}$, $CD62^{low}$ (**4**).

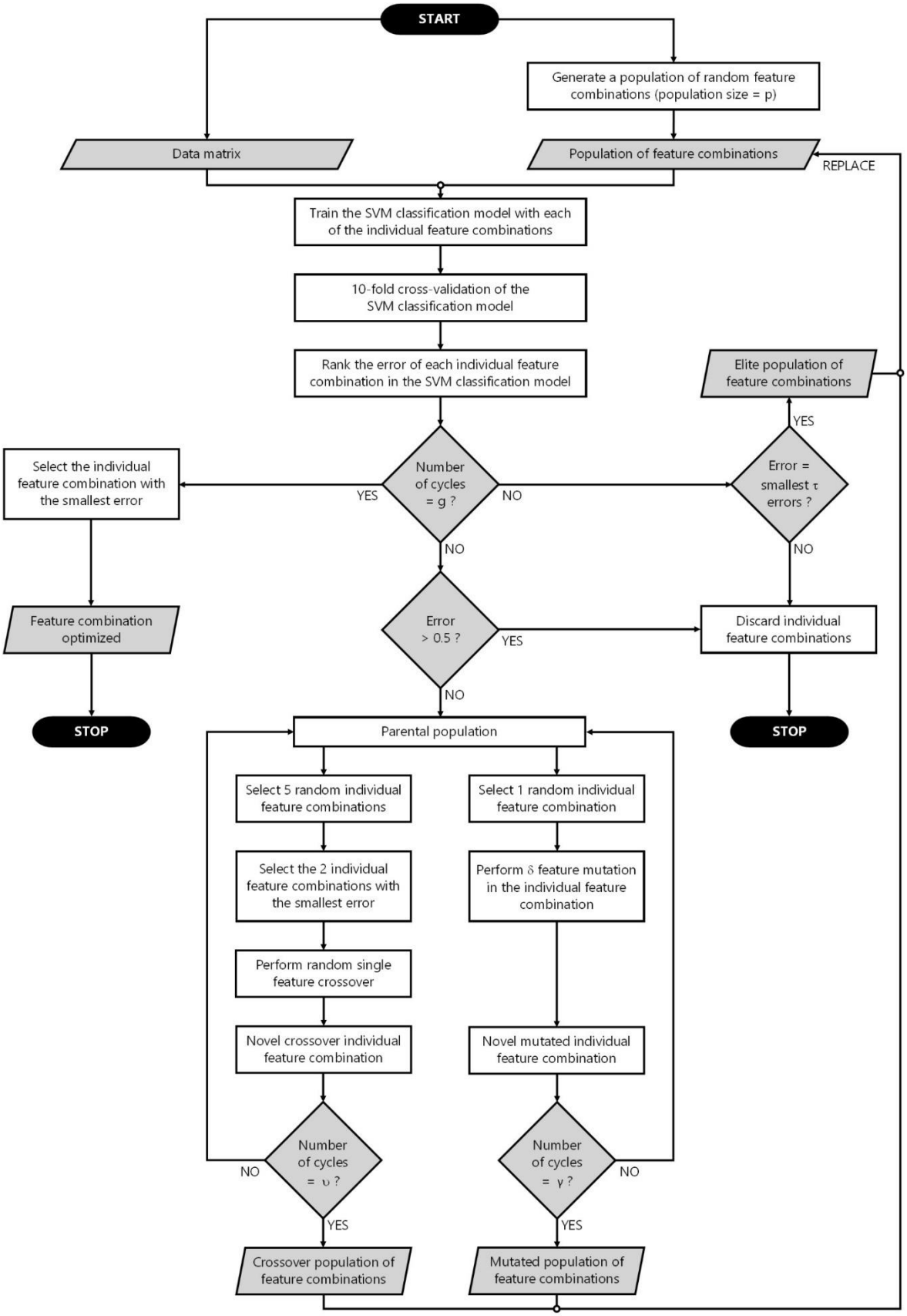

Supplementary figure 4. Flowchart depicting the architectural concept of the GA-SVM model. To find the individual with the optimized feature combination was used: p = 500; g = 50; τ = 5 (1%); υ = 375 (75%); γ = 120 (24%); δ = 10%.

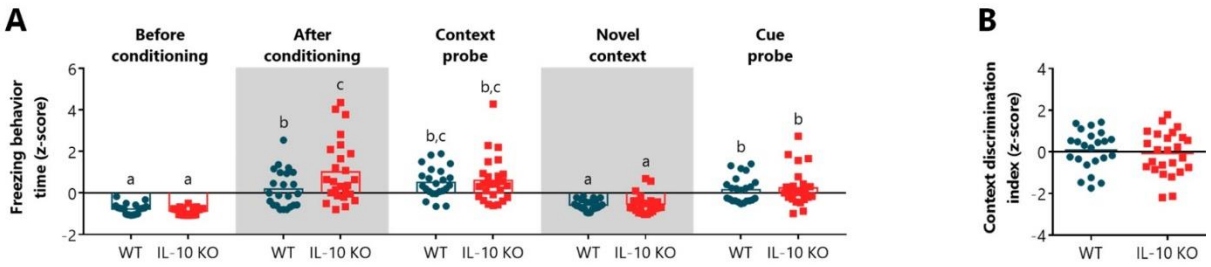

Supplementary figure 5. IL-10 absence did not impact spatial and non-spatial associative memory as assessed by the freezing behavior time. A. Time that mice spent performing freezing behavior in each of the trials of the contextual and cued fear conditioning test. **B.** Context discrimination index considering the time that mice spent performing freezing behavior in the context probe and in the novel context trials. Data presented as mean of z-scores of the values from two independent sets. Each dot represents an animal. $n_{WT} = 23$; $n_{IL\text{-}10\ KO} = 25$. Statistical analysis was performed by a two-way repeated-measures ANOVA (**A**) or a two-tailed independent samples *t*test (**B**). Distinct and equal letters denote, respectively, statistically and non-statistically significant differences for $p < 0.05$ ("a" is significantly different from "b" and "c"; "b" is significantly different from "c").

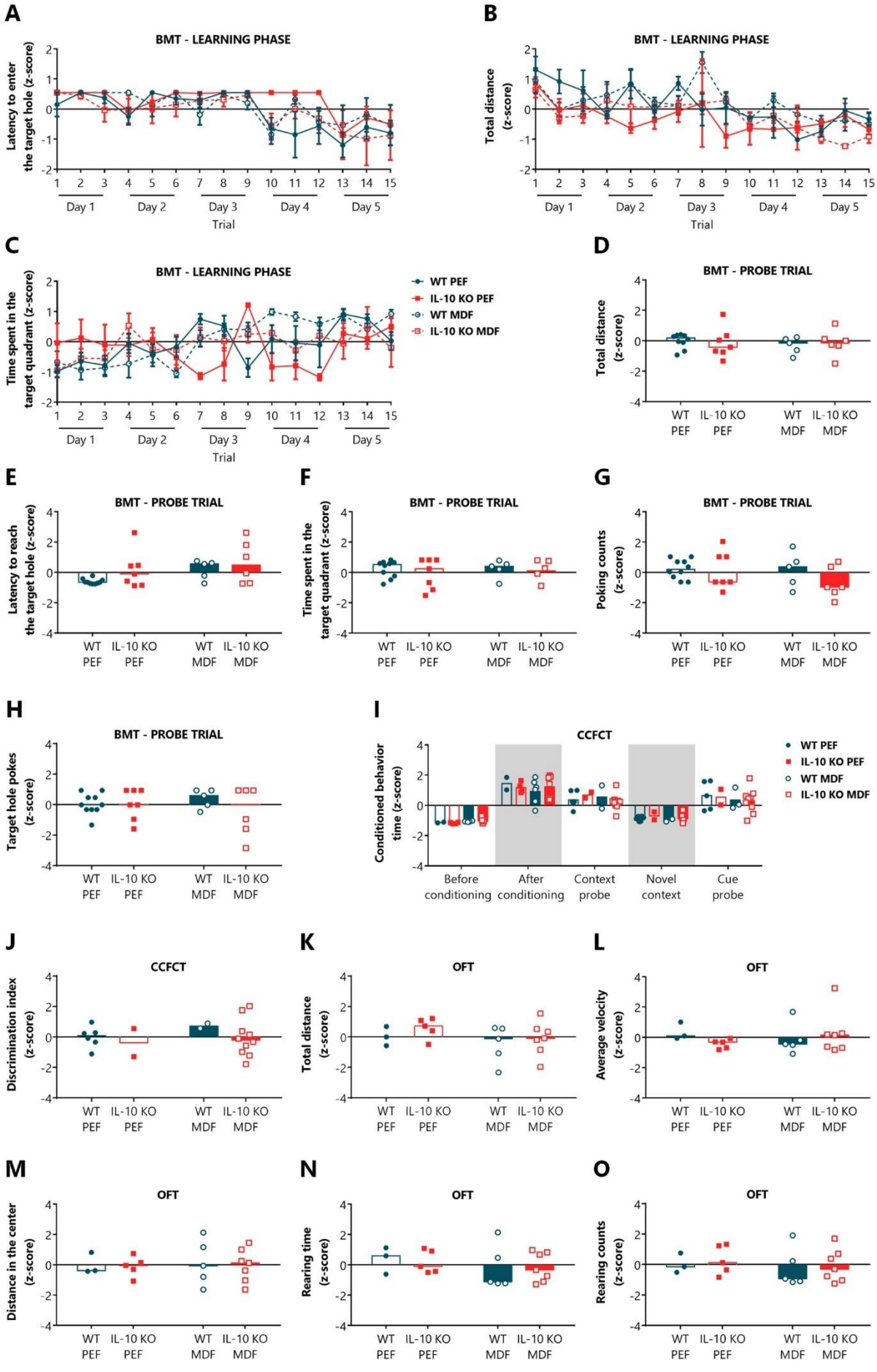
A
BMT - LEARNING PHASE
Latency to enter the target hole (z-score)
Day 1
Day 2
Day 3
Day 4
Day 5
Trial
B
BMT - LEARNING PHASE
Total distance (z-score)
C
BMT - LEARNING PHASE
Time spent in the target quadrant (z-score)
WT PEF
IL-10 KO PEF
WT MDF
IL-10 KO MDF
D
BMT - PROBE TRIAL
Total distance (z-score)
E
BMT - PROBE TRIAL
Latency to reach the target hole (z-score)
F
BMT - PROBE TRIAL
Time spent in the target quadrant (z-score)
G
BMT - PROBE TRIAL
Poking counts (z-score)
H
BMT - PROBE TRIAL
Target hole pokes (z-score)
I
CCFCT
Conditioned behavior time (z-score)
Before conditioning
After conditioning
Context probe
Novel context
Cue probe
J
CCFCT
Discrimination index (z-score)
K
OFT
Total distance (z-score)
L
OFT
Average velocity (z-score)
M
OFT
Distance in the center (z-score)
N
OFT
Rearing time (z-score)
O
OFT
Rearing counts (z-score)

Supplementary figure 6. The estrous cycle did not influence the behavior performance of mice in the Barnes-maze test, in the contextual and cued fear conditioning test, and in the open-field test. A. Latency to enter the target hole during the learning phase of the BMT. **B.** Total distance traveled in the arena during the learning phase of the BMT. **C.** Time spent in the target quadrant during the learning phase of the BMT. **D.** Total distance traveled in the arena during the probe trial of the BMT. **E.** Latency to reach the former location of the target hole for the first time during the probe trial of the BMT. **F.** Time spent in the target quadrant during the probe trial of the BMT. **G.** Total number of nose pokes in the open holes during the probe trial of the BMT. **H.** Percentage of nose pokes in the former location of the target hole during the probe trial of the BMT. **I.** Time that mice spent performing conditioned behaviors in each of the trials of the CCFCT. **J.** Context discrimination index considering the time that mice spent performing conditioned behaviors in the context probe and in the novel context trials of the CCFCT. **K.** Total distance traveled in the OFT arena. **L.** Average velocity in the OFT. **M.** Percentage of distance traveled in the center of the OFT arena. **N.** Time performing vertical exploration (rearings) in the OFT. **O.** Total number of rearings in the OFT. Data presented as median of z-scores of the values from one set. Each dot represents an animal. BMT – Barnes-maze test; CCFCT – contextual and cued fear conditioning test; MDF – metestrus and diestrus females; OFT – open-field test; PEF – proestrus and estrous females. $n_{WT\ PEF}$ = 3-10; $n_{IL\text{-}10\ KO\ PEF}$ = 2-9; $n_{WT\ MDF}$ = 5-12; $n_{IL\text{-}10\ KO\ MDF}$ = 4-11 (**A-C**); $n_{WT\ PEF}$ = 10; $n_{IL\text{-}10\ KO\ PEF}$ = 7; $n_{WT\ MDF}$ = 5; $n_{IL\text{-}10\ KO\ MDF}$ = 6 (**D-H**); $n_{WT\ PEF}$ = 2-6; $n_{IL\text{-}10\ KO\ PEF}$ = 2-4; $n_{WT\ MDF}$ = 2-6; $n_{IL\text{-}10\ KO\ MDF}$ = 7-10 (**I-J**); $n_{WT\ PEF}$ = 3; $n_{IL\text{-}10\ KO\ PEF}$ = 5; $n_{WT\ MDF}$ = 5; $n_{IL\text{-}10\ KO\ MDF}$ = 7 (**K-O**). Statistical analysis was performed by a two-way ANOVA (**A-C**; **I**) or a Kruskal-Wallis *H* test (**D-H**; **J-O**).

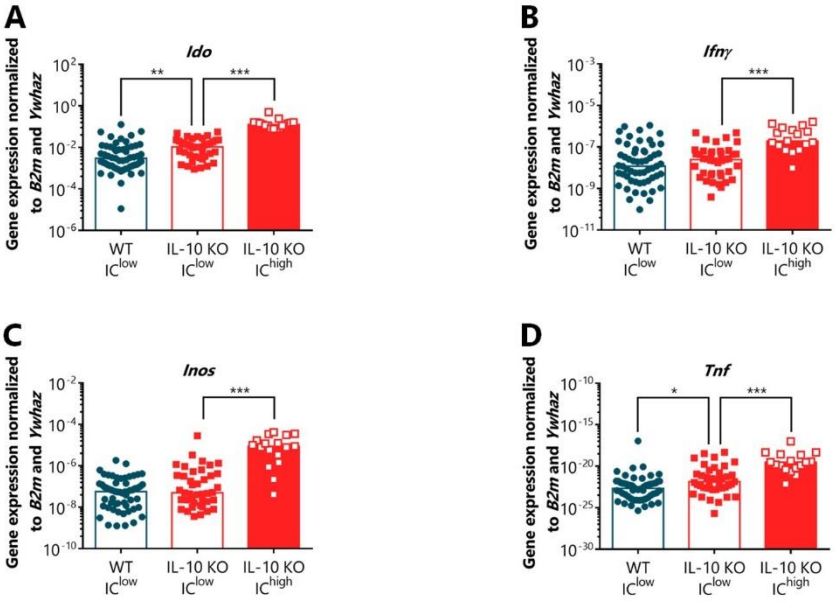

Supplementary figure 7. IL-10 absence led to increased gene expression levels of pro-inflammatory markers in the colon, even after *k*-means clustering. Gene expression levels of *Ido* (**A**), *Ifnγ* (**B**), *Inos* (**C**), and *Tnf* (**D**) in the colon. The gene expression levels of pro-inflammatory markers were quantified through qRT-PCR and normalized to the gene expression levels of *B2m* and *Ywhaz* reference genes. Data presented as median of the values from four independent sets. Each dot represents an animal. IC^{high} – high inflammation cluster; IC^{low} – low inflammation cluster. $n_{WT\ IC\ low}$ = 57; $n_{IL\text{-}10\ KO\ IC\ low}$ = 41; $n_{IL\text{-}10\ KO\ IC\ high}$ = 17. Statistical analysis was performed by a Kruskal-Wallis *H* test. * $p < 0.05$; ** $p < 0.01$; *** $p < 0.001$.

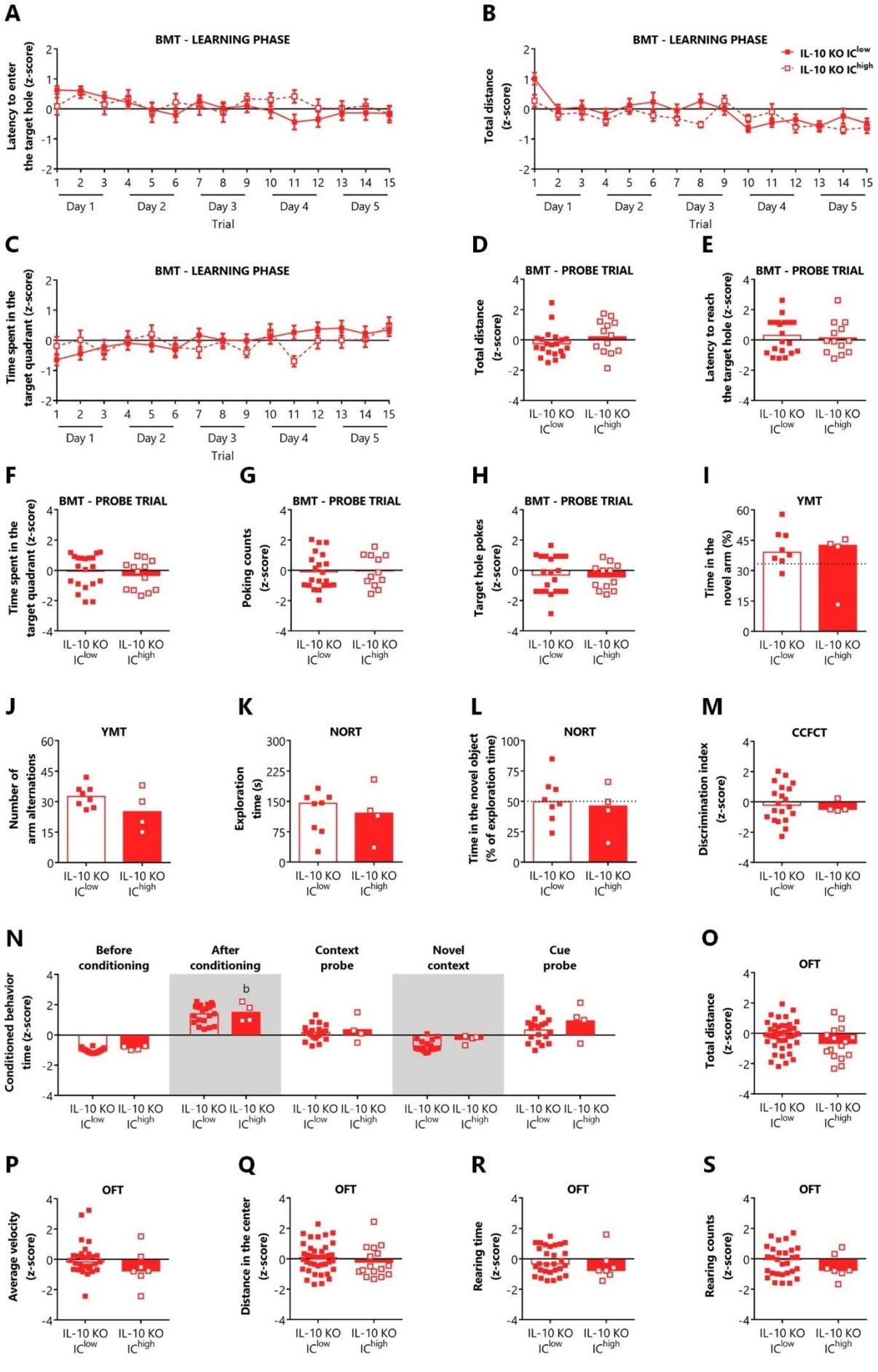
A
BMT - LEARNING PHASE
Latency to enter the target hole (z-score)
Day 1
Day 2
Day 3
Day 4
Day 5
Trial
B
BMT - LEARNING PHASE
IL-10 KO IC^low
IL-10 KO IC^high
Total distance (z-score)
Trial
C
BMT - LEARNING PHASE
Time spent in the target quadrant (z-score)
D
BMT - PROBE TRIAL
Total distance (z-score)
E
BMT - PROBE TRIAL
Latency to reach the target hole (z-score)
F
BMT - PROBE TRIAL
Time spent in the target quadrant (z-score)
G
BMT - PROBE TRIAL
Poking counts (z-score)
H
BMT - PROBE TRIAL
Target hole pokes (z-score)
I
YMT
Time in the novel arm (%)
J
YMT
Number of arm alternations
K
NORT
Exploration time (s)
L
NORT
Time in the novel object (% of exploration time)
M
CCFCT
Discrimination index (z-score)
N
Before conditioning
After conditioning
Context probe
Novel context
Cue probe
Conditioned behavior time (z-score)
b
O
OFT
Total distance (z-score)
P
OFT
Average velocity (z-score)
Q
OFT
Distance in the center (z-score)
R
OFT
Rearing time (z-score)
S
OFT
Rearing counts (z-score)
IL-10 KO IC^low
IL-10 KO IC^high

Supplementary figure 8. The colon inflammatory profile did not influence the behavior performance of IL-10 KO mice in the Barnes-maze test, in the Y-maze test, in the novel object recognition test, in the contextual and cued fear conditioning test, and in the open-field test. A. Latency to enter the target hole during the learning phase of the BMT. **B.** Total distance traveled in the arena during the learning phase of the BMT. **C.** Time spent in the target quadrant during the learning phase of the BMT. **D.** Total distance traveled in the arena during the probe trial of the BMT. **E.** Latency to reach the former location of the target hole for the first time during the probe trial of the BMT. **F.** Time spent in the target quadrant during the probe trial of the BMT. **G.** Total number of nose pokes in the open holes during the probe trial of the BMT. **H.** Percentage of nose pokes in the former location of the target hole during the probe trial of the BMT. **I.** Percentage of time in the novel arm of the YMT. The dotted line depicts the cut-off for a random time in the novel arm (33.3%). **J.** Total number of arm alternations in the YMT. **K.** Total time that mice spent exploring both objects in the NORT. **L.** Percentage of exploration time spent in the novel object of the NORT. The dotted line depicts the cut-off for a random time in the novel object (50%). **M.** Context discrimination index considering the time that mice spent performing conditioned behaviors in the context probe and in the novel context trials of the CCFCT. **N.** Time that mice spent performing conditioned behaviors in each of the trials of the CCFCT. **O.** Total distance traveled in the OFT arena. **P.** Average velocity in the OFT. **Q.** Percentage of distance traveled in the center of the OFT arena. **R.** Time performing vertical exploration (rearings) in the OFT. **S.** Total number of rearings in the OFT. Data presented as mean of z-scores of the values from two (**A-H**; **N**), three (**P**), or four (**O**; **Q**) independent sets, median of z-scores of the values from three independent sets (**R-S**), or median of the values from one set (**I-L**). Each dot represents an animal. BMT – Barnes-maze test; CCFCT – contextual and cued fear conditioning test; IC^{high} – high inflammation cluster; IC^{low} – low inflammation cluster; OFT – open-field test; NORT – novel object recognition test; YMT – Y-maze test. $n_{IL\text{-}10\ KO\ IC\ low}$ = 21; $n_{IL\text{-}10\ KO\ IC\ high}$ = 13 (**A-H**); $n_{IL\text{-}10\ KO\ IC\ low}$ = 8; $n_{IL\text{-}10\ KO\ IC\ high}$ = 4 (**I-L**); $n_{IL\text{-}10\ KO\ IC\ low}$ = 20; $n_{IL\text{-}10\ KO\ IC\ high}$ = 4 (**J-K**); $n_{IL\text{-}10\ KO\ IC\ low}$ = 41; $n_{IL\text{-}10\ KO\ IC\ high}$ = 16 (**O**; **Q**); $n_{IL\text{-}10\ KO\ IC\ low}$ = 29; $n_{IL\text{-}10\ KO\ IC\ high}$ = 7 (**Q**; **R-S**). Statistical analysis was performed by a two-way repeated-measures ANOVA (**A-C**; **N**), a two-tailed independent samples *t*-test (**D-H; O-Q**), or a Mann-Whitney *U* test (**I-M; R-S**).

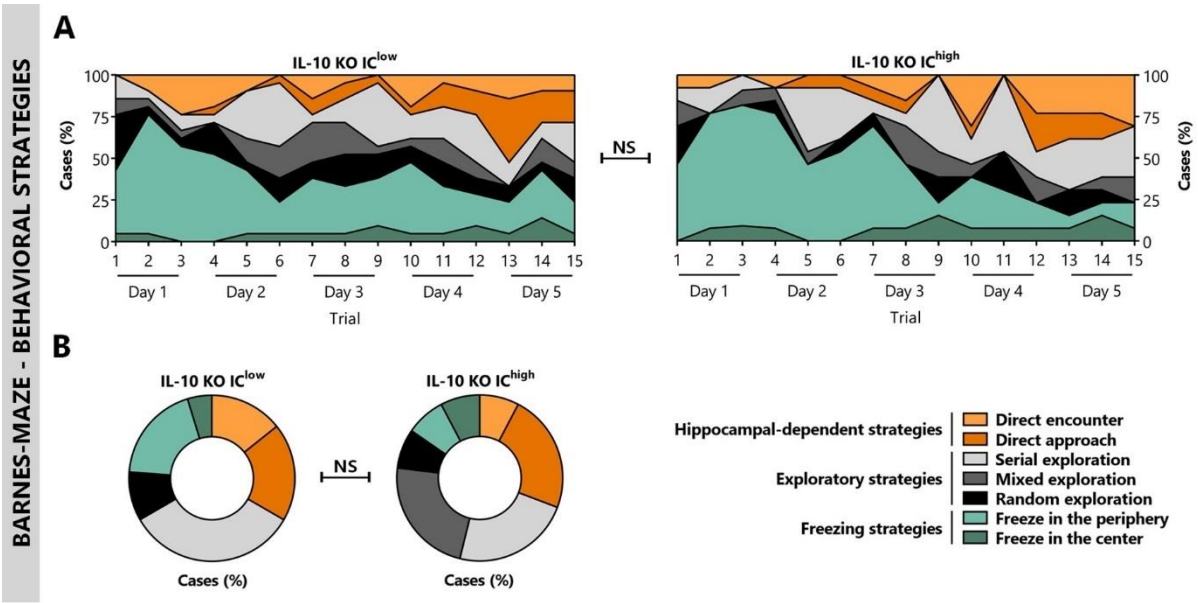

Supplementary figure 9. The colon inflammatory profile did not influence the strategies used by IL-10 KO mice to find the location of the escape chamber in the Barnes-maze test. A. Search strategies performed during the learning phase. **B.** Search strategies adopted during the probe trial. Data presented as the percentage of cases from two independent sets. IC^{high} – high inflammation cluster; IC^{low} – low inflammation cluster; NS – non-statistical significance. $n_{IL\text{-}10\ KO\ IC\ low}$ = 21; $n_{IL\text{-}10\ KO\ IC\ high}$ = 13. Statistical analysis was performed by a Cochran-Armitage χ^2 test for trend.

Annex 3: Supplementary tables

Supplementary table 1. Descriptive statistics of the variables analyzed in WT and IL-10 KO mice.

	Feature	Assume normal distribution?	WT			IL-10 KO		
			Sample size	Measure of central tendency	Measure of dispersion	Sample size	Measure of central tendency	Measure of dispersion
BMT	*Latency to reach the target hole (z-score)*	Yes	35	-0.24	0.14	35	0.24	0.18
	Total distance (z-score)	No	35	0.10	0.98	35	-0.26	1.10
	Time spent in the target quadrant (z-score)	Yes	35	0.28	0.11	35	-0.28	0.20
	Poking counts (z-score)	Yes	35	0.09	0.15	35	-0.09	0.19
	% of pokes in the target hole (z-score)	Yes	35	0.31	0.13	35	-0.31	0.19
YMT	*Time in the novel arm (%)*	Yes	15	37.47	1.68	13	39.28	2.97
	Number of arm alternations	Yes	15	39.73	1.03	13	30.46	2.04
NOR	*Exploration time (s)*	Yes	15	144.6	10.05	13	126.3	15.54
	Time in the novel object (% of exploration time)	Yes	15	61.69	3.60	13	50.16	3.02
CCFCT	*Before conditioning (z-score of conditioning)*	Yes	23	-0.95	0.03	25	-1.01	0.03
	After conditioning (z-score of conditioning)	Yes	23	1.06	0.18	25	1.45	0.12
	Context probe (z-score of conditioning)	Yes	23	0.17	0.17	25	0.21	0.11
	Novel context (z-score of conditioning)	Yes	23	-0.80	0.04	25	-0.65	0.08
	Cue probe (z-score of conditioning)	Yes	23	0.04	0.16	25	0.44	0.16
	Context discrimination index (z-score of conditioning)	Yes	23	0.13	0.18	25	-0.12	0.22
OFT	*Total distance (z-score)*	Yes	58	0.31	0.12	60	-0.31	0.13
	Average velocity (z-score)	Yes	38	0.11	0.14	38	-0.11	0.18
	% of distance in the center (z-score)	Yes	58	0.02	0.13	60	-0.02	0.13
	Rearing time (z-score)	Yes	38	0.23	0.17	38	-0.23	0.15
	Rearing counts (z-score)	Yes	38	0.25	0.16	38	-0.25	0.15
	Nadir corticosterone concentration (ng.ml^{-1})	No	58	14.79	22.93	60	41.49	82.77
	Zenith corticosterone concentration (ng.ml^{-1})	Yes	23	97.62	14.16	23	87.11	11.45
	Final body weight (g)	Yes	58	23.67	0.25	60	21.99	0.36
qRT-PCR	*Ido gene expression (normalized × 10^{3})*	No	57	3.00	8.89	58	17.65	75.25
	Ifnγ gene expression (normalized × 10^{8})	No	57	1.19	5.90	58	4.69	17.12
	Inos gene expression (normalized × 10^{8})	No	57	5.68	13.24	58	21.70	328.46
	Tnf gene expression (normalized × 10^{22})	No	57	0.22	1.00	58	6.23	204.50
Hippocampal stereological analysis	*Number of neurons in the dDG-gcl × 10^{5}*	Yes	12	6.89	0.35	12	5.13	0.62
	Number of neurons in the dCA1-pcl × 10^{5}	Yes	12	4.07	0.14	12	2.70	0.20
	Number of neurons in the dCA3-pcl × 10^{5}	Yes	12	4.11	0.25	12	2.98	0.33
	Number of neurons in the vDG-gcl × 10^{5}	Yes	12	2.35	0.40	12	2.15	0.38
	Number of neurons in the vCA1-pcl × 10^{5}	Yes	12	2.67	0.25	12	1.96	0.17
	Number of neurons in the vCA3-pcl × 10^{5}	Yes	12	1.28	0.19	12	1.61	0.29
	dDG-gcl neuron density × 10^{-3} (cells.μm^{-3})	Yes	12	2.41	0.15	12	2.27	0.16
	dCA1-pcl neuron density × 10^{-3} (cells.μm^{-3})	Yes	12	1.36	0.10	12	1.21	0.06
	dCA3-pcl neuron density × 10^{-3} (cells.μm^{-3})	Yes	12	1.09	0.04	12	1.02	0.05
	vDG-gcl neuron density × 10^{-3} (cells.μm^{-3})	Yes	12	2.21	0.12	12	2.13	0.14
	vCA1-pcl neuron density × 10^{-3} (cells.μm^{-3})	Yes	12	0.98	0.04	12	0.94	0.06
	vCA3-pcl neuron density × 10^{-3} (cells.μm^{-3})	Yes	12	1.27	0.04	12	1.12	0.13
	Total dDG volume × 10^{8} (μm^{3})	Yes	12	12.97	0.41	12	9.92	0.69
	Total dCA1 volume × 10^{8} (μm^{3})	Yes	12	18.15	0.53	12	13.12	0.74
	Total dCA3 volume × 10^{8} (μm^{3})	Yes	12	14.19	1.02	12	10.84	0.91
	Total vDG volume × 10^{8} (μm^{3})	Yes	12	4.92	0.61	12	4.58	0.54
	Total vCA1 volume × 10^{8} (μm^{3})	Yes	12	9.41	0.80	12	7.98	0.58
	Total vCA3 volume × 10^{8} (μm^{3})	Yes	12	4.35	0.66	12	5.06	0.72
	dDG-ml volume × 10^{8} (μm^{3})	Yes	12	8.69	0.26	12	6.64	0.44
	dDG-gcl volume × 10^{8} (μm^{3})	Yes	12	2.91	0.11	12	2.21	0.16
	dDG-pl volume × 10^{8} (μm^{3})	Yes	12	1.38	0.06	12	1.07	0.10
	vDG-ml volume × 10^{8} (μm^{3})	Yes	12	3.06	0.37	12	2.96	0.35
	vDG-gcl volume × 10^{8} (μm^{3})	Yes	12	1.04	0.15	12	0.97	0.15
	vDG-pl volume × 10^{8} (μm^{3})	Yes	12	0.82	0.15	12	0.65	0.11
	dCA1-so volume × 10^{8} (μm^{3})	Yes	12	5.58	0.18	12	3.96	0.19
	dCA1-pcl volume × 10^{8} (μm^{3})	Yes	12	3.07	0.11	12	2.22	0.11

The measures of central tendency and dispersion are presented as mean ± SEM when normal distribution was assumed, and median ± IQR when normal distribution was not assumed.

Supplementary table 1. Continuation.

	Feature	Assume normal distribution?	WT			IL-10 KO		
			Sample size	Measure of central tendency	Measure of dispersion	Sample size	Measure of central tendency	Measure of dispersion
Hippocampal stereological analysis	*dCA1-sr volume × 10^8 (μm^3)*	Yes	12	9.50	0.27	12	6.34	0.46
	vCA1-so volume × 10^8 (μm^3)	Yes	12	2.56	0.26	12	2.14	0.18
	vCA1-pcl volume × 10^8 (μm^3)	Yes	12	2.70	0.21	12	2.11	0.16
	vCA1-sr volume × 10^8 (μm^3)	Yes	12	4.15	0.36	12	3.73	0.29
	dCA3-so volume × 10^8 (μm^3)	Yes	12	5.62	0.44	12	4.24	0.33
	dCA3-pcl volume × 10^8 (μm^3)	Yes	12	3.81	0.25	12	2.84	0.22
	dCA3-sr volume × 10^8 (μm^3)	Yes	12	4.76	0.39	12	3.76	0.44
	vCA3-so volume × 10^8 (μm^3)	Yes	12	1.78	0.39	12	1.70	0.30
	vCA3-pcl volume × 10^8 (μm^3)	Yes	12	1.04	0.17	12	1.40	0.20
	vCA3-sr volume × 10^8 (μm^3)	Yes	12	1.52	0.14	12	1.97	0.25
Neuronal reconstruction and dendritic spine characterization	*dDG dendritic length (μm)*	Yes	36	1622	81	36	1179	47
	dDG dendritic ends	Yes	36	14.28	0.79	36	11.33	0.44
	dDG proximal dendritic spines.μm^{-1}	Yes	36	1.72	0.08	36	2.11	0.09
	dDG % of thin proximal dendritic spines	Yes	36	22.87	2.01	36	7.61	0.79
	dDG % of thick proximal dendritic spines	Yes	36	38.68	1.87	36	58.68	1.91
	dDG % of mushroom proximal dendritic spines	Yes	36	35.00	2.31	36	31.02	1.96
	dDG % of ramified proximal dendritic spines	Yes	36	3.45	0.66	36	2.70	0.48
	dDG distal dendritic spine spines.μm^{-1}	Yes	36	1.53	0.09	36	1.94	0.08
	dDG % of thin distal dendritic spines	Yes	36	17.85	1.58	36	8.84	1.14
	dDG % of thick distal dendritic spines	Yes	36	38.76	2.51	36	55.84	1.91
	dDG % of mushroom distal dendritic spines	Yes	36	41.22	2.99	36	30.45	1.91
	dDG % of ramified distal dendritic spines	Yes	36	2.18	0.61	36	4.88	0.72
	vDG dendritic length (μm)	Yes	36	1472	62	36	1244	52
	vDG dendritic ends	Yes	36	13.89	0.61	36	12.19	0.39
	vDG proximal dendritic spines.μm^{-1}	Yes	36	2.01	0.08	36	1.81	0.07
	vDG % of thin proximal dendritic spines	Yes	36	16.59	1.85	36	9.27	1.26
	vDG % of thick proximal dendritic spines	Yes	36	46.90	2.10	36	56.28	1.99
	vDG % of mushroom proximal dendritic spines	Yes	36	34.60	2.03	36	30.63	2.12
	vDG % of ramified proximal dendritic spines	Yes	36	1.91	0.46	36	3.82	0.67
	vDG distal dendritic spine spines.μm^{-1}	Yes	36	1.98	0.12	36	1.64	0.07
	vDG % of thin distal dendritic spines	Yes	36	19.39	2.94	36	9.83	1.10
	vDG % of thick distal dendritic spines	Yes	36	45.28	2.34	36	60.05	2.18
	vDG % of mushroom distal dendritic spines	Yes	36	33.88	1.95	36	26.99	1.83
	vDG % of ramified distal dendritic spines	Yes	36	1.46	0.37	36	3.13	0.56
	CA1 apical dendritic length (μm)	Yes	36	2486	112	36	2133	79
	CA1 apical dendritic ends	Yes	36	26.83	1.35	36	23.33	0.83
	CA1 apical proximal dendritic spines.μm^{-1}	Yes	36	2.36	0.08	36	1.92	0.06
	CA1 apical % of thin proximal dendritic spines	Yes	36	5.85	0.79	36	6.77	0.77
	CA1 apical % of thick proximal dendritic spines	Yes	36	62.01	1.72	36	52.54	1.70
	CA1 apical % of mushroom proximal dendritic spines	Yes	36	29.83	1.32	36	37.60	1.40
	CA1 apical % of ramified proximal dendritic spines	Yes	36	2.31	0.38	36	3.09	0.64
	CA1 apical distal dendritic spine spines.μm^{-1}	Yes	36	2.42	0.09	36	1.92	0.07
	CA1 apical % of thin distal dendritic spines	Yes	36	6.07	0.85	36	6.56	0.82
	CA1 apical % of thick distal dendritic spines	Yes	36	63.42	1.89	36	57.32	2.48
	CA1 apical % of mushroom distal dendritic spines	Yes	36	28.79	1.61	36	33.62	2.28
	CA1 apical % of ramified distal dendritic spines	Yes	36	1.73	0.32	36	2.50	0.67
	CA1 basal dendritic length (μm)	Yes	36	1272	54	36	1339	68
	CA1 basal dendritic ends	Yes	36	17.75	0.64	36	17.81	0.89
	CA1 basal proximal dendritic spines.μm^{-1}	Yes	36	2.11	0.08	36	1.68	0.08
	CA1 basal % of thin proximal dendritic spines	Yes	36	7.88	1.23	36	6.85	0.87
	CA1 basal % of thick proximal dendritic spines	Yes	36	62.68	1.86	36	61.81	1.74
	CA1 basal % of mushroom proximal dendritic spines	Yes	36	27.82	1.42	36	27.00	1.83
	CA1 basal % of ramified proximal dendritic spines	Yes	36	1.62	0.29	36	4.33	0.76
	CA1 basal distal dendritic spine spines.μm^{-1}	Yes	36	2.13	0.08	36	1.80	0.06
	CA1 basal % of thin distal dendritic spines	Yes	36	6.80	0.73	36	7.73	1.16
	CA1 basal % of thick distal dendritic spines	Yes	36	65.98	1.38	36	58.23	1.78
	CA1 basal % of mushroom distal dendritic spines	Yes	36	25.62	1.22	36	30.42	1.73
	CA1 basal % of ramified distal dendritic spines	Yes	36	1.60	0.39	36	3.62	0.58
	CA3 apical dendritic length (μm)	Yes	36	2575	109	36	2080	107

The measures of central tendency and dispersion are presented as mean ± SEM when normal distribution was assumed, and median ± IQR when normal distribution was not assumed.

Supplementary table 1. Continuation.

	Feature	Assume normal distribution?	WT			IL-10 KO		
			Sample size	Measure of central tendency	Measure of dispersion	Sample size	Measure of central tendency	Measure of dispersion
Neuronal reconstruction and dendritic spine characterization	*CA3 apical dendritic ends*	Yes	36	21.14	0.81	36	18.53	0.73
	CA3 apical proximal dendritic spines.μm^{-1}	Yes	36	2.10	0.07	36	1.70	0.10
	CA3 apical % of thin proximal dendritic spines	Yes	36	4.97	0.56	36	9.71	1.06
	CA3 apical % of thick proximal dendritic spines	Yes	36	65.16	2.38	36	65.01	2.05
	CA3 apical % of mushroom proximal dendritic spines	Yes	36	28.14	2.51	36	21.01	1.43
	CA3 apical % of ramified proximal dendritic spines	Yes	36	1.74	0.36	36	4.27	0.81
	CA3 apical distal dendritic spine spines.μm^{-1}	Yes	36	2.18	0.08	36	1.66	0.06
	CA3 apical % of thin distal dendritic spines	Yes	36	5.15	0.63	36	8.76	1.06
	CA3 apical % of thick distal dendritic spines	Yes	36	63.64	2.70	36	61.02	2.55
	CA3 apical % of mushroom distal dendritic spines	Yes	36	28.40	2.41	36	25.68	1.69
	CA3 apical % of ramified distal dendritic spines	Yes	36	2.81	0.53	36	4.55	0.89
	CA3 basal dendritic length (μm)	Yes	36	1384	80	36	1235	78
	CA3 basal dendritic ends	Yes	36	18.08	0.91	36	15.61	0.86
	CA3 basal proximal dendritic spines.μm^{-1}	Yes	36	1.78	0.06	36	1.39	0.05
	CA3 basal % of thin proximal dendritic spines	Yes	36	5.83	1.04	36	10.20	1.11
	CA3 basal % of thick proximal dendritic spines	Yes	36	70.49	2.09	36	67.17	2.48
	CA3 basal % of mushroom proximal dendritic spines	Yes	36	25.45	1.86	36	17.49	1.54
	CA3 basal % of ramified proximal dendritic spines	Yes	36	1.23	0.33	36	5.14	0.91
	CA3 basal distal dendritic spine spines.μm^{-1}	Yes	36	1.84	0.08	36	1.49	0.05
	CA3 basal % of thin distal dendritic spines	Yes	36	7.01	1.04	36	10.74	1.25
	CA3 basal % of thick distal dendritic spines	Yes	36	67.96	2.51	36	63.72	2.04
	CA3 basal % of mushroom distal dendritic spines	Yes	36	23.26	2.29	36	19.96	1.61
	CA3 basal % of ramified distal dendritic spines	Yes	36	1.78	0.48	36	5.58	0.80
Blood leukocyte profile	*Number of eosinophils × 10^3 (cells.μL^{-1})*	No	38	0.21	0.24	37	0.23	0.21
	% of eosinophils	Yes	58	3.16	0.19	58	2.36	0.15
	Number of neutrophils × 10^3 (cells.μL^{-1})	No	38	2.24	2.43	37	3.91	2.91
	% of neutrophils	Yes	58	30.04	1.22	58	36.68	1.52
	Number of monocytes × 10^3 (cells.μL^{-1})	No	38	0.12	0.28	37	0.21	0.23
	% of monocytes	No	58	2.04	1.76	58	1.87	1.50
	Number of Ly6C^{high} NK cells × 10^3 (cells.μL^{-1})	No	38	0.14	0.29	37	0.11	0.18
	% of Ly6C^{high} NK cells	Yes	58	2.05	0.09	58	1.17	0.08
	Number of Ly6C^{low} NK cells × 10^3 (cells.μL^{-1})	No	38	0.18	0.24	37	0.15	0.15
	% of Ly6C^{low} NK cells	No	58	3.04	1.63	58	1.96	2.00
	Number of B cells × 10^3 (cells.μL^{-1})	No	38	0.91	1.42	37	1.17	1.08
	% of B cells	No	58	11.05	6.90	58	9.87	5.97
	% of FSC-A^{int}, Ly6C^{high}, B cells	No	58	5.71	4.96	58	6.96	8.36
	% of FSC-A^{low}, Ly6C^{low}, B cells	No	58	87.35	8.83	58	83.70	10.60
	% of FSC-A^{high}, Ly6C^{low}, B cells	Yes	58	5.92	0.42	58	6.41	0.47
	Number of T cells × 10^3 (cells.μL^{-1})	No	38	1.70	2.52	37	2.78	2.04
	% of T cells	Yes	58	27.15	0.86	58	24.33	0.79
	Number of CD4$^+$ T cells × 10^3 (cells.μL^{-1})	No	38	1.24	1.84	37	2.01	1.38
	% of CD4$^+$ T cells	Yes	58	19.62	0.65	58	17.90	0.62
	% of CD44$^{low:int}$, CD62L^{high}, CD4$^+$ T cells	Yes	58	46.58	1.29	58	50.18	1.50
	% of CD44^{high}, CD62L^{high}, CD4$^+$ T cells	No	58	1.94	0.68	58	2.16	0.80
	% of CD44$^{low:int}$, CD62L^{int}, CD4$^+$ T cells	Yes	58	43.05	1.13	58	35.75	1.43
	% of CD44$^{int:high}$, CD62L^{low}, CD4$^+$ T cells	Yes	58	6.60	0.25	58	9.81	0.46
	Number of CD8$^+$ T cells × 10^3 (cells.μL^{-1})	No	38	0.41	0.66	37	0.60	0.42
	% of CD8$^+$ T cells	No	58	7.12	2.98	58	5.68	1.75
	% of Ly6C^{low}, CD62L^{high}, CD8$^+$ T cells	Yes	58	15.12	0.53	58	13.90	0.49
	% of Ly6C^{high}, CD62L^{high}, CD8$^+$ T cells	Yes	58	17.37	0.75	58	21.10	0.91
	% of Ly6C^{low}, CD62L^{int}, CD8$^+$ T cells	Yes	58	27.80	0.85	58	24.69	0.82
	% of Ly6C^{high}, CD62L^{int}, CD8$^+$ T cells	Yes	58	33.66	0.76	58	35.28	0.92
	% of Ly6C^{low}, CD62L^{low}, CD8$^+$ T cells	No	58	2.04	0.67	58	1.87	0.85
	% of Ly6C^{high}, CD62L^{low}, CD8$^+$ T cells	No	58	2.79	2.09	58	2.92	2.42
	Number of leukocytes × 10^3 (cells.μL^{-1})	No	38	6.70	9.49	37	11.67	7.01
LNLP	*Number of ingLN B cells × 10^6*	No	50	0.32	0.26	48	0.36	0.39
	Number of dcLN B cells × 10^6		50	0.21	0.25	48	0.54	1.18
	% of ingLN B cells	Yes	50	22.28	0.90	48	27.31	1.10

The measures of central tendency and dispersion are presented as mean ± SEM when normal distribution was assumed, and median ± IQR when normal distribution was not assumed.

Supplementary table 1. Continuation.

	Feature	Assume normal distribution?	WT			IL-10 KO		
			Sample size	Measure of central tendency	Measure of dispersion	Sample size	Measure of central tendency	Measure of dispersion
Lymph node leukocyte profile	*% of dcLN B cells*	Yes	50	33.34	1.18	48	36.17	0.96
	Number of ingLN T cells × 10^6	No	50	1.03	0.67	48	1.02	0.65
	Number of dcLN T cells × 10^6		50	0.40	0.35	48	0.83	1.54
	% of ingLN T cells	Yes	50	75.42	0.91	48	70.20	1.18
	% of dcLN T cells		50	62.37	1.16	48	60.44	1.01
	Number of ingLN $CD4^+$ T cells × 10^6	No	50	0.69	0.45	48	0.64	0.39
	Number of dcLN $CD4^+$ T cells × 10^6		50	0.27	0.24	48	0.53	1.07
	% of ingLN $CD4^+$ T cells	No	50	50.25	5.45	48	46.65	8.50
	% of dcLN $CD4^+$ T cells		50	41.75	7.20	48	38.70	7.25
	% of ingLN $CD44^{low,int}$, $CD62L^{high}$, $CD4^+$ T cells	No	50	82.30	29.39	48	77.75	20.95
	% of dcLN $CD44^{low,int}$, $CD62L^{high}$, $CD4^+$ T cells		50	73.10	25.03	48	68.35	23.40
	% of ingLN $CD44^{int,high}$, $CD62L^{low}$, $CD4^+$ T cells	No	50	10.90	25.03	48	13.85	16.97
	% of dcLN $CD44^{int,high}$, $CD62L^{low}$, $CD4^+$ T cells		50	16.30	17.50	48	21.15	18.17
	Number of ingLN $CD8^+$ T cells × 10^6	No	50	0.31	0.21	48	0.33	0.24
	Number of dcLN $CD8^+$ T cells × 10^6		50	0.12	0.11	48	0.26	0.46
	% of ingLN $CD8^+$ T cells	Yes	50	23.48	0.47	48	22.75	0.50
	% of dcLN $CD8^+$ T cells		50	18.86	0.55	48	18.61	0.48
	% of ingLN $Ly6C^{low}$, $CD62L^{high}$, $CD8^+$ T cells	Yes	50	33.07	1.79	48	28.53	1.11
	% of dcLN $Ly6C^{low}$, $CD62L^{high}$, $CD8^+$ T cells		50	35.35	1.89	48	29.45	1.33
	% of ingLN $Ly6C^{high}$, $CD62L^{high}$, $CD8^+$ T cells	No	50	34.05	20.85	48	37.50	26.22
	% of dcLN $Ly6C^{high}$, $CD62L^{high}$, $CD8^+$ T cells		50	35.85	15.40	48	31.65	27.17
	% of ingLN $Ly6C^{low}$, $CD62L^{low}$, $CD8^+$ T cells	No	50	13.75	22.70	48	14.40	16.88
	% of dcLN $Ly6C^{low}$, $CD62L^{low}$, $CD8^+$ T cells		50	12.25	16.99	48	12.75	18.20
	% of ingLN $Ly6C^{high}$, $CD62L^{low}$, $CD8^+$ T cells	No	50	10.85	17.99	48	16.35	16.29
	% of dcLN $Ly6C^{high}$, $CD62L^{low}$, $CD8^+$ T cells		50	10.12	14.27	48	18.35	17.22
	Number of ingLN leukocytes × 10^6	No	50	1.48	1.09	48	0.66	0.65
	Number of dcLN leukocytes × 10^6		50	1.40	1.02	48	1.40	2.92

The measures of central tendency and dispersion are presented as mean ± SEM when normal distribution was assumed, and median ± IQR when normal distribution was not assumed.

Supplementary table 2. Descriptive statistics of the variables analyzed in the gut microbiome depletion protocol.

Feature		Assume normal distribution?	WT control			IL-10 KO control			WT treated			IL-10 KO treated		
			Sample size	Measure of central tendency	Measure of dispersion	Sample size	Measure of central tendency	Measure of dispersion	Sample size	Measure of central tendency	Measure of dispersion	Sample size	Measure of central tendency	Measure of dispersion
Body weight (g)	*Day 0*	Yes	6	22.8	1.1	6	21.8	1.0	15	23.0	0.6	15	22.2	0.5
	Day 1		6	22.7	1.1	6	21.8	1.1	15	22.9	0.6	15	21.9	0.5
	Day 2		6	22.7	1.2	6	21.8	1.1	15	22.7	0.6	15	21.9	0.5
	Day 3		6	22.8	1.2	6	21.8	1.1	15	22.7	0.6	15	21.7	0.5
	Day 4		6	22.6	1.1	6	22.0	1.0	15	22.5	0.6	15	21.5	0.5
	Day 5		6	22.6	1.1	6	22.1	1.0	15	22.6	0.6	15	21.4	0.6
	Day 6		6	22.7	1.1	6	22.1	1.0	15	22.3	0.6	15	21.4	0.5
	Day 7		6	22.9	1.0	6	22.1	1.0	15	22.4	0.6	15	21.5	0.5
	Day 8		6	22.8	1.0	6	22.4	1.0	15	22.3	0.6	15	21.5	0.5
	Day 9		6	22.8	1.0	6	22.2	1.1	15	22.3	0.6	15	21.6	0.5
	Day 10		6	22.8	0.9	6	22.3	1.1	15	22.5	0.6	15	21.6	0.5
SET 1: *Aerobic CFUS.mg of feces^{-1} × 10^{-4}*	*Day 3*	No	-	-	-	-	-	-	12	1.45	0.82	12	1.52	2.68
	Day 7		-	-	-	-	-	-	12	5.0	18.4	12	1.3	30.1
	Day 10		-	-	-	-	-	-	12	213	171	12	252	92
SET 1: *Anaerobic CFUS.mg of feces^{-1} × 10^{-4}*	*Day 3*	No	-	-	-	-	-	-	12	0.01	0.01	12	0.38	2.26
	Day 7		-	-	-	-	-	-	12	3.2	19.8	12	3.0	33.4
	Day 10		-	-	-	-	-	-	12	24.1	22.1	12	29.5	18.0
SET 2: *Aerobic CFUS.mg of feces^{-1} × 10^{-4}*	*Day 0*	No	-	-	-	-	-	-	3	9.0	15.1	3	62.5	33.2
	Day 1		-	-	-	-	-	-	3	1.46	5.23	3	2.73	3.13
	Day 3		-	-	-	-	-	-	3	15.8	65.5	3	3.59	7.86
	Day 5		-	-	-	-	-	-	3	2.26	2.66	3	1.97	2.55
	Day 10		-	-	-	-	-	-	3	8.1	43.2	3	29	151
SET 2: *Anaerobic CFUS.mg of feces^{-1} × 10^{-4}*	*Day 0*	No	-	-	-	-	-	-	3	0.24	0.44	3	34.8	52.3
	Day 1		-	-	-	-	-	-	3	0.15	0.16	3	0.54	1.14
	Day 3		-	-	-	-	-	-	3	13.3	97.2	3	1.30	3.55
	Day 7		-	-	-	-	-	-	3	19.6	24.6	3	37.2	40.0
16s gene expression (normalized and relative to day 0) × 10^{2}	*Day 0*	No	-	-	-	-	-	-	8	100	0	8	100	0
	Day 3								5	0.08	9.17	6	0.19	2.44
	Day 7		-	-	-	-	-	-	8	1.82	5.34	8	2.8	29.9
Its2 gene expression (normalized and relative to day 0)	*Day 0*	No	-	-	-	-	-	-	8	1	0	8	1	0
	Day 3								5	1.25	2.12	6	4	144
	Day 7		-	-	-	-	-	-	8	0.98	4.76	8	5.9	54.9

The measures of central tendency and dispersion are presented as mean ± SEM when normal distribution was assumed, and median ± IQR when normal distribution was not assumed.

Supplementary table 3. Correlation table of variables with statistically significant differences between WT and IL-10 KO mice.

	Feature	Sample size	BMT			YMT	OFT		
			Latency target hole	Time target quadrant	% pokes target hole	Arm alternations	Total distance	Rearing time	Rearing counts
Sample size			70	70	69	28	117	76	76
BMT	*Latency to reach the target hole*	70		**$p < 0.001$**	$p = 0.078$	-	**$p = 0.029$**	$p = 0.375$	$p = 0.445$
	Time spent in the target quadrant	70	$s = -0.525$		**$p < 0.001$**	-	**$p = 0.028$**	$p = 0.762$	$p = 0.770$
	% of pokes in the target hole	69	$r = -0.213$	$s = 0.456$		-	$p = 0.286$	$p = 0.608$	$p = 0.702$
YMT Number of arm alternations		28	-	-	-		**$p = 0.045$**	$p = 0.843$	$p = 0.483$
OFT	*Total distance*	117	$r = -0.262$	$s = 0.265$	$r = 0.131$	$r = 0.381$		**$p < 0.001$**	**$p < 0.001$**
	Rearing time	76	$s = -0.174$	$s = 0.060$	$s = -0.101$	$s = 0.039$	$s = 0.642$		**$p < 0.001$**
	Rearing counts	76	$s = -0.150$	$s = 0.058$	$s = -0.076$	$s = 0.138$	$s = 0.616$	$s = 0.942$	
Nadir corticosterone concentration		118	$s = 0.016$	$s = -0.041$	$s = -0.138$	$s = 0.123$	$s = -0.069$	$s = -0.039$	$s = -0.061$
Final body weight		118	$r = -0.071$	$s = 0.213$	$r = 0.104$	$r = 0.486$	$r = 0.307$	$s = 0.220$	$s = 0.151$
qRT-PCR	*Ido gene expression*	115	$s = 0.136$	$s = -0.141$	$s = -0.229$	$s = -0.470$	$s = -0.281$	$s = -0.084$	$s = -0.123$
	Ifnγ gene expression	115	$s = 0.003$	$s = -0.056$	$s = -0.073$	$s = -0.378$	$s = -0.137$	$s = -0.005$	$s = -0.017$
	Inos gene expression	115	$s = 0.070$	$s = -0.062$	$s = -0.073$	$s = -0.108$	$s = -0.186$	$s = -0.076$	$s = -0.083$
	Tnf gene expression	115	$s = 0.025$	$s = -0.155$	$s = -0.189$	$s = -0.215$	$s = -0.130$	$s = -0.143$	$s = -0.152$
Hippocampal stereological analysis	*Number of neurons in the dDG-gcl*	12	$r = -0.457$	$s = 0.257$	$r = 0.575$	-	$r = -0.158$	$s = 0.029$	$s = 0.257$
	Number of neurons in the dCA1-pcl	12	$r = -0.678$	$s = -0.200$	$r = 0.757$	-	$r = 0.083$	$s = 0.086$	$s = 0.143$
	Number of neurons in the dCA3-pcl	12	$r = 0.013$	$s = -0.086$	$r = 0.172$	-	$r = -0.146$	$s = 0.086$	$s = 0.143$
	Number of neurons in the vCA1-pcl	12	$r = -0.680$	$s = 0.314$	$r = 0.768$	-	$r = 0.062$	$s = 0.429$	$s = 0.600$
	Total dDG volume	12	$r = -0.352$	$s = 0.493$	$r = 0.328$	-	$r = 0.001$	$s = 0.086$	$s = 0.200$
	Total dCA1 volume	12	$r = -0.705$	$s = 0.714$	$r = 0.539$	-	$r = -0.057$	$s = -0.486$	$s = -0.143$
	Total dCA3 volume	12	$r = 0.072$	$s = -0.029$	$r = -0.011$	-	$r = -0.163$	$s = -0.429$	$s = -0.314$
	dDG-ml volume	12	$r = -0.380$	$s = 0.600$	$r = 0.360$	-	$r = 0.016$	$s = 0.086$	$s = 0.200$
	dDG-gcl volume	12	$r = -0.340$	$s = 0.543$	$r = 0.250$	-	$r = -0.024$	$s = -0.143$	$s = -0.086$
	dDG-pl volume	12	$r = -0.273$	$s = 0.486$	$r = 0.336$	-	$r = 0.023$	$s = 0.086$	$s = 0.200$
	dCA1-so volume	12	$r = -0.759$	$s = 0.486$	$r = 0.687$	-	$r = -0.056$	$s = -0.486$	$s = -0.143$
	dCA1-pcl volume	12	$r = -0.567$	$s = 0.714$	$r = 0.366$	-	$r = -0.023$	$s = -0.486$	$s = -0.143$
	dCA1-sr volume	12	$r = -0.695$	$s = 0.714$	$r = 0.494$	-	$r = -0.066$	$s = -0.486$	$s = -0.143$
	vCA1-pcl volume	12	$r = -0.834$	$s = 0.257$	$r = 0.821$	-	$r = 0.311$	$s = 0.829$	$s = 0.829$
	dCA3-so volume	12	$r = -0.057$	$s = 0.257$	$r = 0.046$	-	$r = -0.119$	$s = -0.290$	$s = -0.232$
	dCA3-pcl volume	12	$r = -0.042$	$s = 0.143$	$r = 0.057$	-	$r = -0.040$	$s = -0.143$	$s = -0.143$
Neuronal reconstruction	*dDG dendritic length*	12	$r = 0.132$	$s = 0.257$	$r = 0.763$	-	$r = -0.281$	$s = -0.371$	$s = -0.371$
	dDG dendritic ends	12	$r = -0.040$	$s = 0.290$	$r = 0.883$	-	$r = -0.238$	$s = 0.029$	$s = 0.029$
	vDG dendritic length	13	$r = -0.090$	$s = 0.771$	$r = 0.589$	-	$r = -0.244$	$s = -0.143$	$s = -0.143$
	vDG dendritic ends	13	$r = -0.648$	$s = 0.899$	$r = 0.666$	-	$r = -0.136$	$s = -0.414$	$s = -0.414$
	CA1 apical dendritic length	12	$r = 0.049$	$s = -0.143$	$r = 0.656$	-	$r = 0.061$	$s = 0.029$	$s = 0.029$
	CA1 apical dendritic ends	12	$r = -0.647$	$s = 0.348$	$r = 0.725$	-	$r = 0.113$	$s = -0.029$	$s = -0.029$
	CA3 apical dendritic length	12	$r = 0.345$	$s = 0.143$	$r = 0.577$	-	$r = -0.157$	$s = -0.771$	$s = -0.771$
	CA3 apical dendritic ends	12	$r = -0.303$	$s = 0.029$	$r = 0.589$	-	$r = -0.151$	$s = 0.086$	$s = 0.086$
Blood leukocyte profile	*% of eosinophils*	116	$r = -0.109$	$s = 0.101$	$r = 0.065$	$r = 0.376$	$r = 0.226$	$s = 0.095$	$s = 0.084$
	Number of neutrophils	75	$s = 0.187$	$s = -0.110$	$s = -0.186$	$s = -0.270$	$s = -0.156$	$s = -0.011$	$s = -0.024$
	% of neutrophils	116	$s = 0.081$	$s = 0.108$	$s = 0.122$	$s = -0.112$	$s = -0.078$	$s = 0.064$	$s = 0.035$
	% of Ly6C^{high} NK cells	116	$r = -0.306$	$s = 0.219$	$r = 0.150$	$r = 0.593$	$r = 0.220$	$s = 0.094$	$s = 0.105$
	% of Ly6C^{low} NK cells	116	$s = -0.219$	$s = 0.172$	$s = 0.001$	$s = 0.637$	$s = 0.141$	$s = 0.175$	$s = 0.169$
	% of B cells	116	$s = -0.049$	$s = 0.045$	$s = -0.018$	$s = -0.207$	$s = 0.033$	$s = -0.004$	$s = -0.053$
	% of T cells	116	$r = -0.118$	$s = -0.096$	$r = -0.097$	$r = 0.195$	$r = 0.084$	$s = -0.073$	$s = -0.023$
	% of CD44$^{low;int}$, CD62L^{int} **(1)**, *CD4^{+} T cells*	116	$r = -0.313$	$s = 0.108$	$r = 0.080$	$r = 0.375$	$r = 0.192$	$s = 0.111$	$s = 0.083$
	% of CD44$^{int;high}$, CD62L^{low} **(2)**, *CD4^{+} T cells*	116	$s = 0.163$	$s = -0.141$	$s = -0.005$	$s = -0.579$	$s = -0.256$	$s = -0.059$	$s = -0.069$
	% of CD8^{+} T cells	116	$r = -0.176$	$s = -0.078$	$r = -0.067$	$r = 0.247$	$r = 0.110$	$s = -0.090$	$s = -0.059$
	% of Ly6C^{high}, CD62L^{high} **(3)**, *CD8^{+} T cells*	116	$r = 0.208$	$s = -0.070$	$r = 0.004$	$r = -0.333$	$r = -0.130$	$s = -0.098$	$s = -0.094$
	% of Ly6C^{low}, CD62L^{int} **(4)**, *CD8^{+} T cells*	116	$r = -0.180$	$s = 0.107$	$r = 0.021$	$r = 0.224$	$r = 0.132$	$s = 0.154$	$s = 0.145$
	Number of leukocytes	76	$s = 0.091$	$s = -0.142$	$s = -0.229$	$s = -0.422$	$s = -0.182$	$s = -0.079$	$s = -0.064$
Lymph nodes leukocyte profile	*Number of dcLN B cells*	98	$s = -0.016$	$s = -0.029$	$s = -0.047$	$s = -0.483$	$s = -0.223$	$s = -0.030$	$s = -0.055$
	% of ingLN B cells	98	$r = 0.279$	$s = -0.134$	$r = -0.270$	$r = -0.318$	$r = -0.203$	$s = -0.071$	$s = -0.123$
	Number of dcLN T cells	98	$s = -0.051$	$s = -0.042$	$s = -0.098$	$s = -0.467$	$s = -0.208$	$s = -0.046$	$s = -0.079$
	% of ingLN T cells	98	$s = -0.170$	$s = 0.131$	$s = 0.085$	$s = 0.392$	$s = 0.249$	$s = 0.089$	$s = 0.144$
	Number of dcLN CD4^{+} T cells	98	$s = -0.046$	$s = -0.031$	$s = -0.077$	$s = -0.450$	$s = -0.204$	$s = -0.023$	$s = -0.054$
	% of ingLN CD4^{+} T cells	98	$s = -0.063$	$s = 0.123$	$s = 0.052$	$s = 0.324$	$s = 0.209$	$s = 0.041$	$s = 0.093$
	Number of dcLN CD8^{+} T cells	98	$s = -0.056$	$s = -0.055$	$s = -0.109$	$s = -0.466$	$s = -0.220$	$s = -0.025$	$s = -0.056$
	% of ingLN Ly6C^{low}, CD62L^{high} **(5)**, *CD8^{+} T cells*	98	$r = -0.059$	$s = -0.083$	$r = -0.013$	$r = 0.380$	$r = 0.126$	$s = 0.137$	$s = 0.118$
	% of dcLN Ly6C^{low}, CD62L^{high} **(6)**, *CD8^{+} T cells*	98	$s = 0.044$	$s = -0.058$	$s = 0.062$	$s = 0.609$	$s = 0.057$	$s = 0.104$	$s = 0.066$
	Number of dcLN leukocytes	98	$s = -0.032$	$s = -0.033$	$s = -0.071$	$s = -0.453$	$s = -0.208$	$s = -0.053$	$s = -0.082$

The *r* and *s* coefficients are shown in white and the *p*-values in grey. Statistical significance ($p < 0.05$) is highlighted in bold.

Supplementary table 3. Continuation.

	Feature	Sample size	Nadir corticosterone concentration	Final body weight	qRT-PCR				HSA
					Ido gene expression	*Ifnγ* gene expression	*Inos* gene expression	*Tnf* gene expression	dDG-gcl neurons
	Sample size		118	118	115	115	115	115	12
BMT	*Latency to reach the target hole*	70	$p = 0.894$	$p = 0.559$	$p = 0.270$	$p = 0.979$	$p = 0.572$	$p = 0.842$	$p = 0.362$
BMT	*Time spent in the target quadrant*	70	$p = 0.736$	$p = 0.077$	$p = 0.250$	$p = 0.651$	$p = 0.614$	$p = 0.207$	$p = 0.658$
BMT	*% of pokes in the target hole*	69	$p = 0.257$	$p = 0.394$	$p = 0.063$	$p = 0.558$	$p = 0.558$	$p = 0.126$	$p = 0.233$
	YMT Number of arm alternations	28	$p = 0.533$	**$p = 0.009$**	**$p = 0.013$**	$p = 0.052$	$p = 0.592$	$p = 0.282$	-
OFT	*Total distance*	117	$p = 0.462$	**$p = 0.001$**	**$p = 0.002$**	$p = 0.146$	**$p = 0.048$**	$p = 0.166$	$p = 0.623$
OFT	*Rearing time*	76	$p = 0.738$	$p = 0.056$	$p = 0.478$	$p = 0.969$	$p = 0.522$	$p = 0.227$	$p > 0.999$
OFT	*Rearing counts*	76	$p = 0.599$	$p = 0.194$	$p = 0.299$	$p = 0.887$	$p = 0.485$	$p = 0.199$	$p = 0.658$
	Nadir corticosterone concentration	118		$p = 0.303$	$p = 0.759$	$p = 0.507$	$p = 0.324$	**$p = 0.006$**	$p = 0.366$
	Final body weight	118	$s = -0.096$		**$p < 0.001$**	**$p = 0.019$**	**$p = 0.001$**	**$p < 0.001$**	$p = 0.502$
qRT-PCR	*Ido gene expression*	115	$s = 0.029$	$s = -0.375$		**$p < 0.001$**	**$p < 0.001$**	**$p < 0.001$**	$p = 0.766$
qRT-PCR	*Ifnγ gene expression*	115	$s = 0.063$	$s = -0.218$	$s = 0.654$		**$p < 0.001$**	$p = 0.114$	$p = 0.939$
qRT-PCR	*Inos gene expression*	115	$s = 0.093$	$s = -0.300$	$s = 0.704$	$s = 0.748$		**$p < 0.001$**	$p = 0.835$
qRT-PCR	*Tnf gene expression*	115	$s = 0.257$	$s = -0.358$	$s = 0.395$	$s = 0.148$	$s = 0.389$		$p = 0.766$
Hippocampal stereological analysis	*Number of neurons in the dDG-gcl*	12	$s = 0.287$	$r = -0.215$	$s = 0.098$	$s = -0.028$	$s = 0.070$	$s = 0.098$	
Hippocampal stereological analysis	*Number of neurons in the dCA1-pcl*	12	$s = 0.063$	$r = 0.039$	$s = -0.182$	$s = -0.308$	$s = -0.350$	$s = -0.126$	$r = 0.858$
Hippocampal stereological analysis	*Number of neurons in the dCA3-pcl*	12	$s = -0.095$	$r = -0.129$	$s = 0.126$	$s = 0.130$	$s = -0.067$	$s = -0.004$	$r = 0.787$
Hippocampal stereological analysis	*Number of neurons in the vCA1-pcl*	12	$s = 0.545$	$r = -0.128$	$s = -0.084$	$s = -0.189$	$s = 0.028$	$s = -0.133$	$r = 0.642$
Hippocampal stereological analysis	*Total dDG volume*	12	$s = -0.193$	$r = 0.219$	$s = -0.032$	$s = 0.102$	$s = -0.266$	$s = -0.301$	$r = 0.730$
Hippocampal stereological analysis	*Total dCA1 volume*	12	$s = -0.161$	$r = 0.283$	$s = -0.210$	$s = -0.133$	$s = -0.448$	$s = -0.406$	$r = 0.644$
Hippocampal stereological analysis	*Total dCA3 volume*	12	$s = -0.168$	$r = 0.013$	$s = 0.238$	$s = 0.336$	$s = -0.007$	$s = 0.007$	$r = 0.581$
Hippocampal stereological analysis	*dDG-ml volume*	12	$s = -0.168$	$r = 0.239$	$s = -0.119$	$s = 0.001$	$s = -0.343$	$s = -0.364$	$r = 0.744$
Hippocampal stereological analysis	*dDG-gcl volume*	12	$s = -0.245$	$r = 0.137$	$s = -0.042$	$s = 0.049$	$s = -0.231$	$s = -0.154$	$r = 0.736$
Hippocampal stereological analysis	*dDG-pl volume*	12	$s = -0.147$	$r = 0.281$	$s = -0.189$	$s = 0.021$	$s = -0.343$	$s = -0.371$	$r = 0.550$
Hippocampal stereological analysis	*dCA1-so volume*	12	$s = -0.133$	$r = 0.328$	$s = -0.259$	$s = -0.196$	$s = -0.510$	$s = -0.441$	$r = 0.542$
Hippocampal stereological analysis	*dCA1-pcl volume*	12	$s = -0.175$	$r = 0.327$	$s = -0.028$	$s = 0.070$	$s = -0.287$	$s = -0.308$	$r = 0.580$
Hippocampal stereological analysis	*dCA1-sr volume*	12	$s = -0.203$	$r = 0.239$	$s = -0.210$	$s = -0.126$	$s = -0.431$	$s = -0.343$	$r = 0.702$
Hippocampal stereological analysis	*vCA1-pcl volume*	12	$s = 0.308$	$r = 0.032$	$s = -0.573$	$s = -0.427$	$s = -0.371$	$s = -0.413$	$r = 0.530$
Hippocampal stereological analysis	*dCA3-so volume*	12	$s = -0.256$	$r = 0.154$	$s = 0.217$	$s = 0.312$	$s = -0.039$	$s = -0.116$	$r = 0.526$
Hippocampal stereological analysis	*dCA3-pcl volume*	12	$s = -0.189$	$r = -0.017$	$s = 0.119$	$s = 0.168$	$s = -0.070$	$s = -0.063$	$r = 0.619$
Neuronal reconstruction	*dDG dendritic length*	12	$s = -0.385$	$r = -0.100$	$s = 0.252$	$s = -0.280$	$s = -0.357$	$s = 0.294$	-
Neuronal reconstruction	*dDG dendritic ends*	12	$s = -0.273$	$r = -0.182$	$s = 0.200$	$s = -0.259$	$s = -0.371$	$s = 0.123$	-
Neuronal reconstruction	*vDG dendritic length*	13	$s = -0.358$	$r = 0.136$	$s = 0.047$	$s = -0.441$	$s = -0.394$	$s = 0.091$	-
Neuronal reconstruction	*vDG dendritic ends*	13	$s = -0.168$	$r = -0.209$	$s = 0.386$	$s = -0.295$	$s = -0.295$	$s = 0.165$	-
Neuronal reconstruction	*CA1 apical dendritic length*	12	$s = -0.042$	$r = -0.160$	$s = 0.049$	$s = -0.147$	$s = -0.308$	$s = 0.399$	-
Neuronal reconstruction	*CA1 apical dendritic ends*	12	$s = -0.007$	$r = -0.139$	$s = -0.168$	$s = 0.039$	$s = -0.028$	$s = 0.585$	-
Neuronal reconstruction	*CA3 apical dendritic length*	12	$s = -0.608$	$r = -0.111$	$s = 0.455$	$s = -0.392$	$s = -0.266$	$s = 0.112$	-
Neuronal reconstruction	*CA3 apical dendritic ends*	12	$s = -0.007$	$r = 0.321$	$s = -0.533$	$s = 0.119$	$s = 0.070$	$s = 0.375$	-
Blood leukocyte profile	*% of eosinophils*	116	$s = -0.305$	$r = 0.188$	$s = -0.211$	$s = -0.123$	$s = -0.179$	$s = -0.431$	$r = -0.264$
Blood leukocyte profile	*Number of neutrophils*	75	$s = 0.458$	$s = -0.365$	$s = 0.084$	$s = 0.165$	$s = 0.003$	$s = 0.197$	$s = -0.029$
Blood leukocyte profile	*% of neutrophils*	116	$s = 0.210$	$s = -0.291$	$s = 0.242$	$s = 0.162$	$s = 0.159$	$s = 0.253$	$s = 0.769$
Blood leukocyte profile	*% of Ly6C^{high} NK cells*	116	$s = -0.071$	$r = 0.538$	$s = -0.526$	$s = -0.264$	$s = -0.306$	$s = -0.394$	$r = -0.421$
Blood leukocyte profile	*% of Ly6C^{low} NK cells*	116	$s = -0.175$	$s = -0.161$	$s = 0.089$	$s = -0.014$	$s = -0.053$	$s = 0.009$	$s = 0.595$
Blood leukocyte profile	*% of B cells*	116	$s = -0.100$	$s = 0.488$	$s = -0.329$	$s = -0.181$	$s = -0.170$	$s = -0.120$	$s = -0.578$
Blood leukocyte profile	*% of T cells*	116	$s = -0.040$	$r = 0.124$	$s = -0.094$	$s = -0.140$	$s = -0.107$	$s = -0.011$	$r = -0.566$
Blood leukocyte profile	*% of CD44$^{low:int}$, CD62L^{int}* **(1)**, *CD4^{+} T cells*	116	$s = -0.333$	$r = 0.168$	$s = 0.048$	$s = 0.007$	$s = -0.044$	$s = -0.040$	$r = 0.525$
Blood leukocyte profile	*% of CD44$^{int:high}$, CD62L^{low}* **(2)**, *CD4^{+} T cells*	116	$s = -0.080$	$s = -0.274$	$s = 0.389$	$s = 0.233$	$s = 0.193$	$s = 0.161$	$s = 0.434$
Blood leukocyte profile	*% of CD8^{+} T cells*	116	$s = -0.088$	$r = 0.093$	$s = -0.200$	$s = -0.270$	$s = -0.260$	$s = -0.045$	$r = -0.638$
Blood leukocyte profile	*% of Ly6C^{high}, CD62L^{high}* **(3)**, *CD8^{+} T cells*	116	$s = 0.235$	$r = 0.085$	$s = -0.136$	$s = 0.024$	$s = 0.044$	$s = -0.123$	$r = -0.794$
Blood leukocyte profile	*% of Ly6C^{low}, CD62L^{int}* **(4)**, *CD8^{+} T cells*	116	$s = -0.150$	$r = -0.259$	$s = 0.133$	$s = 0.095$	$s = 0.044$	$s = 0.061$	$r = 0.866$
Blood leukocyte profile	*Number of leukocytes*	76	$s = 0.416$	$s = -0.361$	$s = 0.032$	$s = 0.151$	$s = -0.031$	$s = 0.175$	$s = -0.371$
Lymph nodes leukocyte profile	*Number of dcLN B cells*	98	$s = -0.016$	$s = -0.531$	$s = 0.407$	$s = 0.279$	$s = 0.233$	$s = 0.180$	$s = 0.200$
Lymph nodes leukocyte profile	*% of ingLN B cells*	98	$s = -0.070$	$r = 0.070$	$s = 0.153$	$s = 0.068$	$s = 0.185$	$s = 0.019$	$r = 0.254$
Lymph nodes leukocyte profile	*Number of dcLN T cells*	98	$s = -0.019$	$s = -0.532$	$s = 0.341$	$s = 0.226$	$s = 0.155$	$s = 0.180$	$s = -0.257$
Lymph nodes leukocyte profile	*% of ingLN T cells*	98	$s = 0.083$	$s = -0.150$	$s = -0.167$	$s = -0.074$	$s = -0.179$	$s = -0.003$	$s = -0.143$
Lymph nodes leukocyte profile	*Number of dcLN CD4^{+} T cells*	98	$s = -0.020$	$s = -0.532$	$s = 0.343$	$s = 0.229$	$s = 0.154$	$s = 0.180$	$s = -0.257$
Lymph nodes leukocyte profile	*% of ingLN CD4^{+} T cells*	98	$s = -0.007$	$s = -0.110$	$s = -0.149$	$s = 0.032$	$s = -0.083$	$s = -0.099$	$s = -0.029$
Lymph nodes leukocyte profile	*Number of dcLN CD8^{+} T cells*	98	$s = -0.006$	$s = -0.543$	$s = 0.344$	$s = 0.213$	$s = 0.153$	$s = 0.191$	$s = -0.029$
Lymph nodes leukocyte profile	*% of ingLN Ly6C^{low}, CD62L^{high}* **(5)**, *CD8^{+} T cells*	98	$s = -0.027$	$r = 0.331$	$s = -0.331$	$s = -0.154$	$s = -0.135$	$s = -0.278$	$r = 0.118$
Lymph nodes leukocyte profile	*% of dcLN Ly6C^{low}, CD62L^{high}* **(6)**, *CD8^{+} T cells*	98	$s = 0.042$	$s = 0.415$	$s = -0.336$	$s = -0.185$	$s = -0.104$	$s = -0.253$	$s = 0.143$
Lymph nodes leukocyte profile	*Number of dcLN leukocytes*	98	$s = -0.022$	$s = -0.521$	$s = 0.361$	$s = 0.246$	$s = 0.180$	$s = 0.170$	$s = 0.200$

The *r* and *s* coefficients are shown in white and the *p*-values in grey. Statistical significance ($p < 0.05$) is highlighted in bold.

Supplementary table 3. Continuation.

	Feature	Sample size	Hippocampal stereological analysis						
			dCA1-pcl neurons	dCA3-pcl neurons	vCA1-pcl neurons	Total dDG volume	Total dCA1 volume	Total dCA3 volume	dDG-ml volume
Sample size			12	12	12	12	12	12	12
BMT	*Latency to reach the target hole*	70	$p = 0.139$	$p = 0.981$	$p = 0.137$	$p = 0.494$	$p = 0.118$	$p = 0.892$	$p = 0.458$
	Time spent in the target quadrant	70	$p = 0.714$	$p = 0.919$	$p = 0.564$	$p = 0.333$	$p = 0.136$	$p > 0.999$	$p = 0.242$
	% of pokes in the target hole	69	$p = 0.081$	$p = 0.745$	$p = 0.074$	$p = 0.525$	$p = 0.270$	$p = 0.984$	$p = 0.483$
YMT Number of arm alternations		28	-	-	-	-	-	-	-
OFT	*Total distance*	117	$p = 0.797$	$p = 0.651$	$p = 0.847$	$p = 0.998$	$p = 0.861$	$p = 0.614$	$p = 0.962$
	Rearing time	76	$p = 0.919$	$p = 0.919$	$p = 0.419$	$p = 0.919$	$p = 0.356$	$p = 0.419$	$p = 0.919$
	Rearing counts	76	$p = 0.803$	$p = 0.803$	$p = 0.242$	$p = 0.714$	$p = 0.803$	$p = 0.564$	$p = 0.714$
Nadir corticosterone concentration		118	$p = 0.851$	$p = 0.761$	$p = 0.071$	$p = 0.538$	$p = 0.619$	$p = 0.604$	$p = 0.604$
Final body weight		118	$p = 0.904$	$p = 0.689$	$p = 0.691$	$p = 0.494$	$p = 0.373$	$p = 0.969$	$p = 0.455$
qRT-PCR	*Ido gene expression*	115	$p = 0.573$	$p = 0.695$	$p = 0.800$	$p = 0.916$	$p = 0.514$	$p = 0.457$	$p = 0.716$
	Ifnγ gene expression	115	$p = 0.331$	$p = 0.687$	$p = 0.558$	$p = 0.754$	$p = 0.683$	$p = 0.287$	$p = 1.009$
	Inos gene expression	115	$p = 0.266$	$p = 0.829$	$p = 0.939$	$p = 0.394$	$p = 0.147$	$p = 0.991$	$p = 0.276$
	Tnf gene expression	115	$p = 0.700$	$p = 0.986$	$p = 0.683$	$p = 0.333$	$p = 0.193$	$p = 0.991$	$p = 0.246$
Hippocampal stereological analysis	*Number of neurons in the dDG-gcl*	12	**$p < 0.001$**	**$p = 0.002$**	**$p = 0.024$**	**$p = 0.007$**	**$p = 0.024$**	**$p = 0.048$**	**$p = 0.006$**
	Number of neurons in the dCA1-pcl	12		**$p = 0.007$**	**$p = 0.009$**	**$p = 0.008$**	**$p = 0.007$**	$p = 0.085$	**$p = 0.006$**
	Number of neurons in the dCA3-pcl	12	$r = 0.728$		$p = 0.300$	**$p = 0.002$**	**$p = 0.025$**	**$p < 0.001$**	**$p = 0.003$**
	Number of neurons in the vCA1-pcl	12	$r = 0.713$	$r = 0.327$		$p = 0.471$	$p = 0.457$	$p = 0.854$	$p = 0.428$
	Total dDG volume	12	$r = 0.722$	$r = 0.788$	$r = 0.230$		**$p < 0.001$**	**$p < 0.001$**	**$p < 0.001$**
	Total dCA1 volume	12	$r = 0.728$	$r = 0.639$	$r = 0.238$	$r = 0.920$		**$p = 0.003$**	**$p < 0.001$**
	Total dCA3 volume	12	$r = 0.518$	$r = 0.858$	$r = -0.060$	$r = 0.854$	$r = 0.776$		**$p = 0.001$**
	dDG-ml volume	12	$r = 0.738$	$r = 0.771$	$r = 0.253$	$r = 0.997$	$r = 0.930$	$r = 0.839$	
	dDG-gcl volume	12	$r = 0.728$	$r = 0.827$	$r = 0.222$	$r = 0.980$	$r = 0.893$	$r = 0.866$	$r = 0.965$
	dDG-pl volume	12	$r = 0.552$	$r = 0.707$	$r = 0.108$	$r = 0.950$	$r = 0.818$	$r = 0.807$	$r = 0.938$
	dCA1-so volume	12	$r = 0.675$	$r = 0.546$	$r = 0.209$	$r = 0.872$	$r = 0.979$	$r = 0.717$	$r = 0.887$
	dCA1-pcl volume	12	$r = 0.690$	$r = 0.691$	$r = 0.186$	$r = 0.921$	$r = 0.974$	$r = 0.807$	$r = 0.920$
	dCA1-sr volume	12	$r = 0.751$	$r = 0.660$	$r = 0.266$	$r = 0.921$	$r = 0.993$	$r = 0.778$	$r = 0.932$
	vCA1-pcl volume	12	$r = 0.642$	$r = 0.155$	$r = 0.879$	$r = 0.313$	$r = 0.305$	$r = -0.103$	$r = 0.334$
	dCA3-so volume	12	$r = 0.464$	$r = 0.814$	$r = -0.080$	$r = 0.842$	$r = 0.777$	$r = 0.965$	$r = 0.830$
	dCA3-pcl volume	12	$r = 0.595$	$r = 0.927$	$r = 0.054$	$r = 0.833$	$r = 0.718$	$r = 0.959$	$r = 0.811$
Neuronal reconstruction	*dDG dendritic length*	12	-	-	-	-	-	-	-
	dDG dendritic ends	12	-	-	-	-	-	-	-
	vDG dendritic length	13	-	-	-	-	-	-	-
	vDG dendritic ends	13	-	-	-	-	-	-	-
	CA1 apical dendritic length	12	-	-	-	-	-	-	-
	CA1 apical dendritic ends	12	-	-	-	-	-	-	-
	CA3 apical dendritic length	12	-	-	-	-	-	-	-
	CA3 apical dendritic ends	12	-	-	-	-	-	-	-
Blood leukocyte profile	*% of eosinophils*	116	$r = -0.102$	$r = -0.363$	$r = 0.266$	$r = -0.261$	$r = -0.292$	$r = -0.583$	$r = -0.290$
	Number of neutrophils	75	$s = 0.086$	$s = 0.086$	$s = -0.029$	$s = 0.143$	$s = -0.429$	$s = -0.371$	$s = 0.143$
	% of neutrophils	116	$s = 0.531$	$s = 0.483$	$s = 0.573$	$s = 0.130$	$s = 0.001$	$s = 0.182$	$s = 0.147$
	% of Ly6C^{high} NK cells	116	$r = -0.197$	$r = -0.083$	$r = -0.274$	$r = 0.111$	$r = 0.250$	$r = 0.125$	$r = 0.103$
	% of Ly6C^{low} NK cells	116	$s = 0.616$	$s = 0.421$	$s = 0.722$	$s = 0.526$	$s = 0.651$	$s = 0.266$	$s = 0.574$
	% of B cells	116	$s = -0.27$	$s = -0.225$	$s = -0.599$	$s = 0.095$	$s = 0.214$	$s = 0.021$	$s = 0.074$
	% of T cells	116	$r = -0.410$	$r = -0.175$	$r = -0.663$	$r = -0.250$	$r = -0.064$	$r = 0.081$	$r = -0.269$
	% of CD44$^{low;int}$, CD62L^{int} **(1)**, *CD4^{+} T cells*	116	$r = 0.787$	$r = 0.319$	$r = 0.555$	$r = 0.554$	$r = 0.576$	$r = 0.193$	$r = 0.560$
	% of CD44$^{int;high}$, CD62L^{low} **(2)**, *CD4^{+} T cells*	116	$s = 0.081$	$s = 0.044$	$s = 0.343$	$s = -0.181$	$s = -0.231$	$s = -0.158$	$s = -0.196$
	% of CD8^{+} T cells	116	$r = -0.429$	$r = -0.381$	$r = -0.647$	$r = -0.404$	$r = -0.177$	$r = -0.132$	$r = -0.406$
	% of Ly6C^{high}, CD62L^{high} **(3)**, *CD8^{+} T cells*	116	$r = -0.756$	$r = -0.557$	$r = -0.568$	$r = -0.632$	$r = -0.494$	$r = -0.329$	$r = -0.625$
	% of Ly6C^{low}, CD62L^{int} **(4)**, *CD8^{+} T cells*	116	$r = 0.767$	$r = 0.522$	$r = 0.666$	$r = 0.514$	$r = 0.419$	$r = 0.259$	$r = 0.534$
	Number of leukocytes	76	$s = -0.200$	$s = -0.200$	$s = -0.657$	$s = -0.143$	$s = -0.257$	$s = -0.143$	$s = -0.143$
Lymph nodes leukocyte profile	*Number of dcLN B cells*	98	$s = 0.257$	$s = -0.486$	$s = 0.714$	$s = -0.551$	$s = -0.371$	$s = -0.600$	$s = -0.371$
	% of ingLN B cells	98	$r = -0.060$	$r = 0.020$	$r = 0.365$	$r = -0.410$	$r = -0.663$	$r = -0.261$	$r = -0.437$
	Number of dcLN T cells	98	$s = -0.029$	$s = -0.771$	$s = 0.543$	$s = -0.783$	$s = -0.486$	$s = -0.600$	$s = -0.657$
	% of ingLN T cells	98	$s = 0.086$	$s = 0.371$	$s = -0.314$	$s = 0.493$	$s = 0.657$	$s = 0.257$	$s = 0.486$
	Number of dcLN CD4^{+} T cells	98	$s = -0.029$	$s = -0.771$	$s = 0.543$	$s = -0.783$	$s = -0.486$	$s = -0.600$	$s = -0.657$
	% of ingLN CD4^{+} T cells	98	$s = 0.086$	$s = 0.143$	$s = 0.029$	$s = 0.464$	$s = 0.771$	$s = -0.029$	$s = 0.543$
	Number of dcLN CD8^{+} T cells	98	$s = 0.086$	$s = -0.543$	$s = 0.486$	$s = -0.696$	$s = -0.600$	$s = -0.486$	$s = -0.600$
	% of ingLN Ly6C^{low}, CD62L^{high} **(5)**, *CD8^{+} T cells*	98	$r = 0.505$	$r = -0.101$	$r = 0.664$	$r = -0.419$	$r = -0.435$	$r = -0.407$	$r = -0.388$
	% of dcLN Ly6C^{low}, CD62L^{high} **(6)**, *CD8^{+} T cells*	98	$s = 0.371$	$s = 0.143$	$s = 0.086$	$s = -0.261$	$s = -0.314$	$s = 0.086$	$s = -0.200$
	Number of dcLN leukocytes	98	$s = 0.257$	$s = -0.486$	$s = 0.714$	$s = -0.551$	$s = -0.371$	$s = -0.600$	$s = -0.371$

The *r* and *s* coefficients are shown in white and the *p*-values in grey. Statistical significance ($p < 0.05$) is highlighted in bold.

Supplementary table 3. Continuation.

	Feature	Sample size	Hippocampal stereological analysis						
			dDG-gcl volume	dDG-pl volume	dCA1-so volume	dCA1-pcl volume	dCA1-sr volume	vCA1-pcl volume	dCA3-so volume
	Sample size		12	12	12	12	12	12	12
BMT	*Latency to reach the target hole*	70	$p = 0.510$	$p = 0.600$	$p = 0.080$	$p = 0.240$	$p = 0.125$	**$p = 0.039$**	$p = 0.915$
BMT	*Time spent in the target quadrant*	70	$p = 0.297$	$p = 0.356$	$p = 0.356$	$p = 0.136$	$p = 0.136$	$p = 0.658$	$p = 0.658$
BMT	*% of pokes in the target hole*	69	$p = 0.633$	$p = 0.515$	$p = 0.132$	$p = 0.476$	$p = 0.319$	**$p = 0.045$**	$p = 0.931$
	YMT Number of arm alternations	28	-	-	-	-	-	-	-
OFT	*Total distance*	117	$p = 0.942$	$p = 0.943$	$p = 0.863$	$p = 0.943$	$p = 0.838$	$p = 0.324$	$p = 0.713$
OFT	*Rearing time*	76	$p = 0.803$	$p = 0.919$	$p = 0.356$	$p = 0.356$	$p = 0.356$	$p = 0.058$	$p = 0.556$
OFT	*Rearing counts*	76	$p = 0.919$	$p = 0.714$	$p = 0.803$	$p = 0.803$	$p = 0.803$	$p = 0.058$	$p = 0.617$
	Nadir corticosterone concentration	118	$p = 0.443$	$p = 0.651$	$p = 0.683$	$p = 0.588$	$p = 0.516$	$p = 0.331$	$p = 0.413$
	Final body weight	118	$p = 0.671$	$p = 0.377$	$p = 0.298$	$p = 0.300$	$p = 0.454$	$p = 0.921$	$p = 0.633$
qRT-PCR	*Ido gene expression*	115	$p = 0.904$	$p = 0.558$	$p = 0.417$	$p = 0.939$	$p = 0.502$	$p = 0.056$	$p = 0.495$
qRT-PCR	*Ifnγ gene expression*	115	$p = 0.886$	$p = 0.956$	$p = 0.543$	$p = 0.835$	$p = 0.687$	$p = 0.169$	$p = 0.322$
qRT-PCR	*Inos gene expression*	115	$p = 0.471$	$p = 0.276$	$p = 0.094$	$p = 0.366$	$p = 0.159$	$p = 0.237$	$p = 0.899$
qRT-PCR	*Tnf gene expression*	115	$p = 0.635$	$p = 0.237$	$p = 0.154$	$p = 0.331$	$p = 0.268$	$p = 0.184$	$p = 0.711$
Hippocampal stereological analysis	*Number of neurons in the dDG-gcl*	12	**$p = 0.006$**	$p = 0.064$	$p = 0.068$	**$p = 0.048$**	**$p = 0.011$**	$p = 0.076$	$p = 0.079$
Hippocampal stereological analysis	*Number of neurons in the dCA1-pcl*	12	**$p = 0.007$**	$p = 0.063$	**$p = 0.016$**	**$p = 0.013$**	**$p = 0.005$**	**$p = 0.024$**	$p = 0.129$
Hippocampal stereological analysis	*Number of neurons in the dCA3-pcl*	12	**$p = 0.001$**	**$p = 0.010$**	$p = 0.067$	**$p = 0.013$**	**$p = 0.019$**	$p = 0.631$	**$p = 0.001$**
Hippocampal stereological analysis	*Number of neurons in the vCA1-pcl*	12	$p = 0.487$	$p = 0.738$	$p = 0.515$	$p = 0.563$	$p = 0.402$	**$p < 0.001$**	$p = 0.804$
Hippocampal stereological analysis	*Total dDG volume*	12	**$p < 0.001$**	**$p < 0.001$**	**$p < 0.001$**	**$p < 0.001$**	**$p < 0.001$**	$p = 0.322$	**$p = 0.001$**
Hippocampal stereological analysis	*Total dCA1 volume*	12	**$p < 0.001$**	**$p = 0.001$**	**$p < 0.001$**	**$p < 0.001$**	**$p < 0.001$**	$p = 0.335$	**$p = 0.003$**
Hippocampal stereological analysis	*Total dCA3 volume*	12	**$p < 0.001$**	**$p = 0.002$**	**$p = 0.009$**	**$p = 0.002$**	**$p = 0.003$**	$p = 0.750$	**$p < 0.001$**
Hippocampal stereological analysis	*dDG-ml volume*	12	**$p < 0.001$**	**$p < 0.001$**	**$p < 0.001$**	**$p < 0.001$**	**$p < 0.001$**	$p = 0.289$	**$p = 0.001$**
Hippocampal stereological analysis	*dDG-gcl volume*	12		**$p < 0.001$**	**$p = 0.001$**	**$p < 0.001$**	**$p < 0.001$**	$p = 0.364$	**$p = 0.001$**
Hippocampal stereological analysis	*dDG-pl volume*	12	$r = 0.910$		**$p = 0.002$**	**$p < 0.001$**	**$p = 0.002$**	$p = 0.452$	**$p = 0.001$**
Hippocampal stereological analysis	*dCA1-so volume*	12	$r = 0.817$	$r = 0.806$		**$p < 0.001$**	**$p < 0.001$**	$p = 0.348$	**$p = 0.008$**
Hippocampal stereological analysis	*dCA1-pcl volume*	12	$r = 0.912$	$r = 0.849$	$r = 0.948$		**$p < 0.001$**	$p = 0.464$	**$p = 0.001$**
Hippocampal stereological analysis	*dCA1-sr volume*	12	$r = 0.904$	$r = 0.792$	$r = 0.951$	$r = 0.956$		$p = 0.306$	**$p = 0.003$**
Hippocampal stereological analysis	*vCA1-pcl volume*	12	$r = 0.288$	$r = 0.240$	$r = 0.297$	$r = 0.234$	$r = 0.323$		$p = 0.721$
Hippocampal stereological analysis	*dCA3-so volume*	12	$r = 0.841$	$r = 0.811$	$r = 0.720$	$r = 0.821$	$r = 0.778$	$r = -0.115$	
Hippocampal stereological analysis	*dCA3-pcl volume*	12	$r = 0.875$	$r = 0.778$	$r = 0.637$	$r = 0.784$	$r = 0.726$	$r = -0.005$	$r = 0.930$
Neuronal reconstruction	*dDG dendritic length*	12	-	-	-	-	-	-	-
Neuronal reconstruction	*dDG dendritic ends*	12	-	-	-	-	-	-	-
Neuronal reconstruction	*vDG dendritic length*	13	-	-	-	-	-	-	-
Neuronal reconstruction	*vDG dendritic ends*	13	-	-	-	-	-	-	-
Neuronal reconstruction	*CA1 apical dendritic length*	12	-	-	-	-	-	-	-
Neuronal reconstruction	*CA1 apical dendritic ends*	12	-	-	-	-	-	-	-
Neuronal reconstruction	*CA3 apical dendritic length*	12	-	-	-	-	-	-	-
Neuronal reconstruction	*CA3 apical dendritic ends*	12	-	-	-	-	-	-	-
Blood leukocyte profile	*% of eosinophils*	116	$r = -0.202$	$r = -0.177$	$r = -0.286$	$r = -0.213$	$r = -0.311$	$r = 0.421$	$r = -0.546$
Blood leukocyte profile	*Number of neutrophils*	75	$s = -0.029$	$s = 0.143$	$s = -0.429$	$s = -0.429$	$s = -0.429$	$s = 0.257$	$s = -0.232$
Blood leukocyte profile	*% of neutrophils*	116	$s = 0.238$	$s = 0.168$	$s = 0.021$	$s = -0.098$	$s = 0.049$	$s = 0.580$	$s = 0.021$
Blood leukocyte profile	*% of $Ly6C^{high}$ NK cells*	116	$r = 0.062$	$r = 0.254$	$r = 0.347$	$r = 0.377$	$r = 0.157$	$r = -0.228$	$r = 0.256$
Blood leukocyte profile	*% of $Ly6C^{low}$ NK cells*	116	$s = 0.511$	$s = 0.354$	$s = 0.630$	$s = 0.574$	$s = 0.663$	$s = 0.550$	$s = 0.333$
Blood leukocyte profile	*% of B cells*	116	$s = 0.042$	$s = 0.032$	$s = 0.200$	$s = 0.301$	$s = 0.175$	$s = -0.578$	$s = 0.144$
Blood leukocyte profile	*% of T cells*	116	$r = -0.209$	$r = -0.229$	$r = -0.031$	$r = 0.022$	$r = -0.104$	$r = -0.794$	$r = 0.113$
Blood leukocyte profile	*% of $CD44^{low;int}$, $CD62L^{int}$* **(1)**, *$CD4^+$ T cells*	116	$r = 0.569$	$r = 0.445$	$r = 0.548$	$r = 0.523$	$r = 0.590$	$r = 0.702$	$r = 0.143$
Blood leukocyte profile	*% of $CD44^{int;high}$, $CD62L^{low}$* **(2)**, *$CD4^+$ T cells*	116	$s = -0.046$	$s = -0.182$	$s = -0.270$	$s = -0.249$	$s = -0.165$	$s = 0.287$	$s = -0.263$
Blood leukocyte profile	*% of $CD8^+$ T cells*	116	$r = -0.398$	$r = -0.373$	$r = -0.092$	$r = -0.145$	$r = -0.229$	$r = -0.720$	$r = -0.109$
Blood leukocyte profile	*% of $Ly6C^{high}$, $CD62L^{high}$* **(3)**, *$CD8^+$ T cells*	116	$r = -0.686$	$r = -0.492$	$r = -0.370$	$r = -0.455$	$r = -0.560$	$r = -0.642$	$r = -0.293$
Blood leukocyte profile	*% of $Ly6C^{low}$, $CD62L^{int}$* **(4)**, *$CD8^+$ T cells*	116	$r = 0.539$	$r = 0.308$	$r = 0.292$	$r = 0.346$	$r = 0.500$	$r = 0.660$	$r = 0.233$
Blood leukocyte profile	*Number of leukocytes*	76	$s = -0.029$	$s = -0.143$	$s = -0.257$	$s = -0.257$	$s = -0.257$	$s = -0.543$	$s = -0.116$
Lymph nodes leukocyte profile	*Number of dcLN B cells*	98	$s = -0.600$	$s = -0.257$	$s = -0.257$	$s = -0.657$	$s = -0.371$	$s = 0.314$	$s = -0.486$
Lymph nodes leukocyte profile	*% of ingLN B cells*	98	$r = -0.452$	$r = -0.241$	$r = -0.543$	$r = -0.751$	$r = -0.673$	$r = 0.062$	$r = -0.400$
Lymph nodes leukocyte profile	*Number of dcLN T cells*	98	$s = -0.829$	$s = -0.543$	$s = -0.429$	$s = -0.771$	$s = -0.486$	$s = 0.143$	$s = -0.486$
Lymph nodes leukocyte profile	*% of ingLN T cells*	98	$s = 0.600$	$s = 0.257$	$s = 0.600$	$s = 0.714$	$s = 0.657$	$s = 0.143$	$s = 0.200$
Lymph nodes leukocyte profile	*Number of dcLN $CD4^+$ T cells*	98	$s = -0.829$	$s = -0.543$	$s = -0.429$	$s = -0.771$	$s = -0.486$	$s = 0.143$	$s = -0.486$
Lymph nodes leukocyte profile	*% of ingLN $CD4^+$ T cells*	98	$s = 0.600$	$s = 0.257$	$s = 0.657$	$s = 0.771$	$s = 0.771$	$s = 0.314$	$s = 0.029$
Lymph nodes leukocyte profile	*Number of dcLN $CD8^+$ T cells*	98	$s = -0.771$	$s = -0.429$	$s = -0.486$	$s = -0.829$	$s = -0.600$	$s = 0.086$	$s = -0.429$
Lymph nodes leukocyte profile	*% of ingLN $Ly6C^{low}$, $CD62L^{high}$* **(5)**, *$CD8^+$ T cells*	98	$r = -0.559$	$r = -0.278$	$r = -0.178$	$r = -0.582$	$r = -0.510$	$r = 0.423$	$r = -0.488$
Lymph nodes leukocyte profile	*% of dcLN $Ly6C^{low}$, $CD62L^{high}$* **(6)**, *$CD8^+$ T cells*	98	$s = -0.371$	$s = 0.029$	$s = -0.086$	$s = -0.543$	$s = -0.314$	$s = 0.143$	$s = 0.029$
Lymph nodes leukocyte profile	*Number of dcLN leukocytes*	98	$s = -0.600$	$s = -0.257$	$s = -0.257$	$s = -0.657$	$s = -0.371$	$s = 0.314$	$s = -0.486$

The *r* and *s* coefficients are shown in white and the *p*-values in grey. Statistical significance ($p < 0.05$) is highlighted in bold.

Supplementary table 3. Continuation.

	Feature	Sample size	HSA	Neuronal reconstruction					
			dCA3-pcl volume	dDG dendritic length	dDG dendritic ends	vDG dendritic length	vDG dendritic ends	CA1 apical dendritic length	CA1 apical dendritic ends
Sample size			12	12	12	13	13	12	12
BMT	*Latency to reach the target hole*	70	$p = 0.937$	$p = 0.804$	$p = 0.941$	$p = 0.865$	$p = 0.164$	$p = 0.926$	$p = 0.165$
	Time spent in the target quadrant	70	$p = 0.803$	$p = 0.658$	$p = 0.600$	$p = 0.103$	**$p = 0.028$**	$p = 0.803$	$p = 0.511$
	% of pokes in the target hole	69	$p = 0.915$	$p = 0.078$	**$p = 0.020$**	$p = 0.219$	$p = 0.149$	$p = 0.157$	$p = 0.103$
YMT Number of arm alternations		28	-	-	-	-	-	-	-
OFT	*Total distance*	117	$p = 0.901$	$p = 0.377$	$p = 0.457$	$p = 0.422$	$p = 0.658$	$p = 0.850$	$p = 0.726$
	Rearing time	76	$p = 0.803$	$p = 0.497$	$p > 0.999$	$p = 0.783$	$p = 0.327$	$p > 0.999$	$p > 0.999$
	Rearing counts	76	$p = 0.803$	$p = 0.497$	$p > 0.999$	$p = 0.783$	$p = 0.327$	$p > 0.999$	$p > 0.999$
Nadir corticosterone concentration		118	$p = 0.558$	$p = 0.218$	$p = 0.381$	$p = 0.225$	$p = 0.575$	$p = 0.904$	$p = 0.978$
Final body weight		118	$p = 0.959$	$p = 0.757$	$p = 0.571$	$p = 0.658$	$p = 0.493$	$p = 0.619$	$p = 0.667$
qRT-PCR	*Ido gene expression*	115	$p = 0.716$	$p = 0.430$	$p = 0.531$	$p = 0.881$	$p = 0.193$	$p = 0.886$	$p = 0.592$
	Ifnγ gene expression	115	$p = 0.604$	$p = 0.379$	$p = 0.407$	$p = 0.130$	$p = 0.321$	$p = 0.651$	$p = 0.908$
	Inos gene expression	115	$p = 0.835$	$p = 0.256$	$p = 0.229$	$p = 0.179$	$p = 0.321$	$p = 0.331$	$p = 0.926$
	Tnf gene expression	115	$p = 0.851$	$p = 0.355$	$p = 0.704$	$p = 0.767$	$p = 0.587$	$p = 0.201$	**$p = 0.049$**
Hippocampal stereological analysis	*Number of neurons in the dDG-gcl*	12	**$p = 0.032$**	-	-	-	-	-	-
	Number of neurons in the dCA1-pcl	12	**$p = 0.041$**	-	-	-	-	-	-
	Number of neurons in the dCA3-pcl	12	**$p < 0.001$**	-	-	-	-	-	-
	Number of neurons in the vCA1-pcl	12	$p = 0.869$	-	-	-	-	-	-
	Total dDG volume	12	**$p = 0.001$**	-	-	-	-	-	-
	Total dCA1 volume	12	**$p = 0.008$**	-	-	-	-	-	-
	Total dCA3 volume	12	**$p < 0.001$**	-	-	-	-	-	-
	dDG-ml volume	12	**$p = 0.001$**	-	-	-	-	-	-
	dDG-gcl volume	12	**$p < 0.001$**	-	-	-	-	-	-
	dDG-pl volume	12	**$p = 0.003$**	-	-	-	-	-	-
	dCA1-so volume	12	**$p = 0.026$**	-	-	-	-	-	-
	dCA1-pcl volume	12	**$p = 0.003$**	-	-	-	-	-	-
	dCA1-sr volume	12	**$p = 0.008$**	-	-	-	-	-	-
	vCA1-pcl volume	12	$p = 0.989$	-	-	-	-	-	-
	dCA3-so volume	12	**$p < 0.001$**	-	-	-	-	-	-
	dCA3-pcl volume	12		-	-	-	-	-	-
Neuronal reconstruction	*dDG dendritic length*	12	-		**$p < 0.001$**	**$p = 0.002$**	**$p = 0.018$**	**$p = 0.002$**	$p = 0.090$
	dDG dendritic ends	12	-	$r = 0.951$		**$p < 0.001$**	**$p = 0.002$**	**$p = 0.002$**	$p = 0.118$
	vDG dendritic length	13	-	$r = 0.800$	$r = 0.855$		**$p = 0.001$**	**$p = 0.013$**	$p = 0.170$
	vDG dendritic ends	13	-	$r = 0.665$	$r = 0.803$	$r = 0.787$		$p = 0.061$	$p = 0.216$
	CA1 apical dendritic length	12	-	$r = 0.818$	$r = 0.815$	$r = 0.687$	$r = 0.555$		**$p = 0.006$**
	CA1 apical dendritic ends	12	-	$r = 0.534$	$r = 0.499$	$r = 0.424$	$r = 0.386$	$r = 0.740$	
	CA3 apical dendritic length	12	-	$r = 0.807$	$r = 0.745$	$r = 0.690$	$r = 0.646$	$r = 0.584$	$r = 0.214$
	CA3 apical dendritic ends	12	-	$r = 0.206$	$r = 0.067$	$r = 0.013$	$r = -0.199$	$r = 0.030$	$r = 0.328$
Blood leukocyte profile	*% of eosinophils*	116	$r = -0.428$	$r = -0.022$	$r = -0.047$	$r = -0.174$	$r = -0.225$	$r = 0.184$	$r = 0.505$
	Number of neutrophils	75	$s = -0.086$	$s = -0.143$	$s = 0.486$	$s = -0.107$	$s = 0.036$	$s = -0.257$	$s = -0.657$
	% of neutrophils	116	$s = 0.252$	$s = -0.427$	$s = -0.305$	$s = -0.416$	$s = -0.190$	$s = -0.503$	$s = -0.529$
	% of $Ly6C^{high}$ NK cells	116	$r = 0.095$	$r = -0.037$	$r = -0.082$	$r = 0.255$	$r = -0.003$	$r = -0.087$	$r = 0.134$
	% of $Ly6C^{low}$ NK cells	116	$s = 0.375$	$s = 0.417$	$s = 0.407$	$s = 0.317$	$s = 0.484$	$s = 0.158$	$s = 0.246$
	% of B cells	116	$s = -0.011$	$s = -0.116$	$s = -0.242$	$s = -0.011$	$s = -0.494$	$s = -0.179$	$s = -0.014$
	% of T cells	116	$r = 0.003$	$r = 0.425$	$r = 0.345$	$r = 0.325$	$r = 0.423$	$r = 0.413$	$r = 0.319$
	% of $CD44^{low;int}$, $CD62L^{int}$ **(1)**, *$CD4^+$ T cells*	116	$r = 0.253$	$r = 0.504$	$r = 0.569$	$r = 0.751$	$r = 0.496$	$r = 0.276$	$r = 0.132$
	% of $CD44^{int;high}$, $CD62L^{low}$ **(2)**, *$CD4^+$ T cells*	116	$s = -0.088$	$s = -0.126$	$s = 0.039$	$s = -0.174$	$s = -0.041$	$s = -0.196$	$s = -0.294$
	% of $CD8^+$ T cells	116	$r = -0.219$	$r = 0.378$	$r = 0.327$	$r = 0.372$	$r = 0.466$	$r = 0.400$	$r = 0.209$
	% of $Ly6C^{high}$, $CD62L^{high}$ **(3)**, *$CD8^+$ T cells*	116	$r = -0.430$	$r = -0.643$	$r = -0.706$	$r = -0.628$	$r = -0.559$	$r = -0.442$	$r = -0.317$
	% of $Ly6C^{low}$, $CD62L^{int}$ **(4)**, *$CD8^+$ T cells*	116	$r = 0.361$	$r = 0.687$	$r = 0.772$	$r = 0.570$	$r = 0.640$	$r = 0.599$	$r = 0.452$
	Number of leukocytes	76	$s = -0.086$	$s = 0.812$	$s = 0.696$	$s = 0.703$	$s = 0.945$	$s = 0.348$	$s = 0.145$
Lymph nodes leukocyte profile	*Number of dcLN B cells*	98	$s = -0.600$	$s = -0.429$	$s = -0.464$	$s = -0.943$	$s = -0.812$	$s = 0.143$	$s = 0.203$
	% of ingLN B cells	98	$r = -0.401$	$r = -0.494$	$r = -0.655$	$r = -0.624$	$r = -0.589$	$r = -0.525$	$r = -0.007$
	Number of dcLN T cells	98	$s = -0.829$	$s = -0.371$	$s = -0.406$	$s = -0.886$	$s = -0.812$	$s = 0.257$	$s = 0.058$
	% of ingLN T cells	98	$s = 0.429$	$s = 0.543$	$s = 0.522$	$s = 0.486$	$s = 0.638$	$s = 0.429$	$s = 0.145$
	Number of dcLN $CD4^+$ T cells	98	$s = -0.829$	$s = -0.371$	$s = -0.406$	$s = -0.886$	$s = -0.812$	$s = 0.257$	$s = 0.058$
	% of ingLN $CD4^+$ T cells	98	$s = 0.257$	$s = 0.886$	$s = 0.841$	$s = 0.371$	$s = 0.551$	$s = 0.600$	$s = 0.203$
	Number of dcLN $CD8^+$ T cells	98	$s = -0.657$	$s = -0.371$	$s = -0.406$	$s = -0.886$	$s = -0.812$	$s = 0.257$	$s = 0.058$
	% of ingLN $Ly6C^{low}$, $CD62L^{high}$ **(5)**, *$CD8^+$ T cells*	98	$r = -0.461$	$r = -0.962$	$r = -0.965$	$r = -0.589$	$r = -0.360$	$r = -0.556$	$r = -0.351$
	% of dcLN $Ly6C^{low}$, $CD62L^{high}$ **(6)**, *$CD8^+$ T cells*	98	$s = -0.086$	$s = -0.886$	$s = -0.928$	$s = -0.429$	$s = -0.493$	$s = -0.886$	$s = -0.464$
	Number of dcLN leukocytes	98	$s = -0.600$	$s = -0.371$	$s = -0.406$	$s = -0.886$	$s = -0.812$	$s = 0.257$	$s = 0.058$

The *r* and *s* coefficients are shown in white and the *p*-values in grey. Statistical significance ($p < 0.05$) is highlighted in bold.

Supplementary table 3. Continuation.

	Feature	Sample size	Neuronal reconstruction		Blood leukocyte profile				
			CA3 apical dendritic length	CA3 apical dendritic ends	% eosinophils	Number neutrophils	% neutrophils	% Ly6C^{high} NK cells	% Ly6C^{low} NK cells
	Sample size		12	12	116	75	116	116	116
BMT	*Latency to reach the target hole*	70	$p = 0.503$	$p = 0.560$	$p = 0.375$	$p = 0.349$	$p = 0.512$	**$p = 0.011$**	$p = 0.073$
	Time spent in the target quadrant	70	$p = 0.803$	$p > 0.999$	$p = 0.414$	$p = 0.584$	$p = 0.381$	$p = 0.073$	$p = 0.162$
	% of pokes in the target hole	69	$p = 0.230$	$p = 0.218$	$p = 0.603$	$p = 0.353$	$p = 0.327$	$p = 0.225$	$p = 0.991$
	YMT Number of arm alternations	28	-	-	**$p = 0.049$**	$p = 0.164$	$p = 0.569$	**$p = 0.001$**	**$p < 0.001$**
OFT	*Total distance*	117	$p = 0.626$	$p = 0.640$	**$p = 0.015$**	$p = 0.182$	$p = 0.408$	**$p = 0.018$**	$p = 0.131$
	Rearing time	76	$p = 0.103$	$p = 0.919$	$p = 0.419$	$p = 0.927$	$p = 0.586$	$p = 0.425$	$p = 0.132$
	Rearing counts	76	$p = 0.103$	$p = 0.919$	$p = 0.475$	$p = 0.838$	$p = 0.767$	$p = 0.369$	$p = 0.148$
	Nadir corticosterone concentration	118	**$p = 0.040$**	$p = 0.978$	**$p = 0.001$**	**$p < 0.001$**	**$p = 0.024$**	$p = 0.447$	$p = 0.061$
	Final body weight	118	$p = 0.731$	$p = 0.309$	**$p = 0.043$**	**$p = 0.001$**	**$p = 0.002$**	**$p < 0.001$**	$p = 0.085$
qRT-PCR	*Ido gene expression*	115	$p = 0.140$	$p = 0.075$	**$p = 0.025$**	$p = 0.485$	**$p = 0.010$**	**$p < 0.001$**	$p = 0.346$
	Ifnγ gene expression	115	$p = 0.210$	$p = 0.711$	$p = 0.196$	$p = 0.166$	$p = 0.087$	**$p = 0.005$**	$p = 0.886$
	Inos gene expression	115	$p = 0.404$	$p = 0.830$	$p = 0.058$	$p = 0.978$	$p = 0.093$	**$p = 0.001$**	$p = 0.575$
	Tnf gene expression	115	$p = 0.733$	$p = 0.228$	**$p < 0.001$**	$p = 0.098$	**$p = 0.007$**	**$p < 0.001$**	$p = 0.928$
Hippocampal stereological analysis	*Number of neurons in the dDG-gcl*	12	-	-	$p = 0.407$	$p > 0.999$	**$p = 0.005$**	$p = 0.173$	**$p = 0.044$**
	Number of neurons in the dCA1-pcl	12	-	-	$p = 0.753$	$p = 0.919$	$p = 0.079$	$p = 0.539$	**$p = 0.036$**
	Number of neurons in the dCA3-pcl	12	-	-	$p = 0.246$	$p = 0.919$	$p = 0.113$	$p = 0.797$	$p = 0.173$
	Number of neurons in the vCA1-pcl	12	-	-	$p = 0.404$	$p > 0.999$	$p = 0.056$	$p = 0.389$	**$p = 0.010$**
	Total dDG volume	12	-	-	$p = 0.412$	$p = 0.803$	$p = 0.687$	$p = 0.731$	$p = 0.081$
	Total dCA1 volume	12	-	-	$p = 0.357$	$p = 0.419$	$p = 1.009$	$p = 0.432$	**$p = 0.025$**
	Total dCA3 volume	12	-	-	**$p = 0.047$**	$p = 0.497$	$p = 0.573$	$p = 0.698$	$p = 0.400$
	dDG-ml volume	12	-	-	$p = 0.360$	$p = 0.803$	$p = 0.651$	$p = 0.750$	$p = 0.054$
	dDG-gcl volume	12	-	-	$p = 0.530$	$p > 0.999$	$p = 0.457$	$p = 0.849$	$p = 0.092$
	dDG-pl volume	12	-	-	$p = 0.582$	$p = 0.803$	$p = 0.604$	$p = 0.426$	$p = 0.258$
	dCA1-so volume	12	-	-	$p = 0.368$	$p = 0.419$	$p = 0.956$	$p = 0.269$	**$p = 0.031$**
	dCA1-pcl volume	12	-	-	$p = 0.506$	$p = 0.419$	$p = 0.766$	$p = 0.227$	$p = 0.054$
	dCA1-sr volume	12	-	-	$p = 0.325$	$p = 0.419$	$p = 0.881$	$p = 0.627$	**$p = 0.022$**
	vCA1-pcl volume	12	-	-	$p = 0.173$	$p = 0.658$	$p = 0.052$	$p = 0.476$	$p = 0.067$
	dCA3-so volume	12	-	-	$p = 0.066$	$p = 0.617$	$p = 0.951$	$p = 0.421$	$p = 0.287$
	dCA3-pcl volume	12	-	-	$p = 0.165$	$p = 0.919$	$p = 0.430$	$p = 0.769$	$p = 0.229$
Neuronal reconstruction	*dDG dendritic length*	12	**$p = 0.003$**	$p = 0.544$	$p = 0.945$	$p = 0.803$	$p = 0.169$	$p = 0.909$	$p = 0.178$
	dDG dendritic ends	12	**$p = 0.008$**	$p = 0.844$	$p = 0.886$	$p = 0.356$	$p = 0.327$	$p = 0.800$	$p = 0.189$
	vDG dendritic length	13	**$p = 0.013$**	$p = 0.968$	$p = 0.570$	$p = 0.840$	$p = 0.155$	$p = 0.401$	$p = 0.288$
	vDG dendritic ends	13	**$p = 0.023$**	$p = 0.536$	$p = 0.461$	$p = 0.951$	$p = 0.525$	$p = 0.991$	$p = 0.095$
	CA1 apical dendritic length	12	**$p = 0.046$**	$p = 0.927$	$p = 0.566$	$p = 0.658$	$p = 0.099$	$p = 0.788$	$p = 0.623$
	CA1 apical dendritic ends	12	$p = 0.503$	$p = 0.297$	$p = 0.094$	$p = 0.175$	$p = 0.078$	$p = 0.678$	$p = 0.438$
	CA3 apical dendritic length	12		$p = 0.691$	$p = 0.189$	$p = 0.242$	$p = 0.134$	$p = 0.662$	$p = 0.178$
	CA3 apical dendritic ends	12	$r = -0.128$		**$p = 0.006$**	$p = 0.497$	$p = 0.252$	**$p = 0.023$**	$p = 0.676$
Blood leukocyte profile	*% of eosinophils*	116	$r = -0.407$	$r = 0.738$		**$p = 0.049$**	$p = 0.055$	**$p = 0.010$**	**$p = 0.001$**
	Number of neutrophils	75	$s = -0.600$	$s = -0.371$	$s = -0.319$		**$p < 0.001$**	**$p = 0.011$**	**$p < 0.001$**
	% of neutrophils	116	$s = -0.462$	$s = -0.354$	$s = -0.178$	$s = 0.525$		**$p < 0.001$**	$p = 0.540$
	% of Ly6C^{high} NK cells	116	$r = -0.141$	$r = 0.646$	$r = 0.239$	$s = -0.292$	$s = -0.594$		$p = 0.079$
	% of Ly6C^{low} NK cells	116	$s = 0.417$	$s = 0.134$	$s = 0.292$	$s = -0.448$	$s = 0.057$	$s = 0.164$	
	% of B cells	116	$s = -0.144$	$s = 0.299$	$s = -0.139$	$s = -0.243$	$s = -0.630$	$s = 0.499$	$s = -0.378$
	% of T cells	116	$r = 0.735$	$r = -0.240$	$r = -0.061$	$s = -0.354$	$s = -0.754$	$r = 0.326$	$s = -0.106$
	% of CD44$^{low:int}$, CD62L^{int} **(1)**, *CD4^{+} T cells*	116	$r = 0.541$	$r = -0.076$	$r = 0.231$	$s = -0.398$	$s = -0.071$	$r = 0.233$	$s = 0.653$
	% of CD44$^{int:high}$, CD62L^{low} **(2)**, *CD4^{+} T cells*	116	$s = -0.406$	$s = -0.165$	$s = 0.121$	$s = 0.223$	$s = 0.460$	$s = -0.544$	$s = 0.047$
	% of CD8^{+} T cells	116	$r = 0.744$	$r = -0.302$	$r = -0.082$	$s = -0.351$	$s = -0.697$	$r = 0.367$	$s = 0.055$
	% of Ly6C^{high}, CD62L^{high} **(3)**, *CD8^{+} T cells*	116	$r = -0.632$	$r = 0.141$	$r = -0.110$	$s = 0.343$	$s = -0.108$	$r = 0.033$	$s = -0.703$
	% of Ly6C^{low}, CD62L^{int} **(4)**, *CD8^{+} T cells*	116	$r = 0.608$	$r = -0.248$	$r = -0.032$	$s = -0.267$	$s = 0.200$	$r = -0.198$	$s = 0.607$
	Number of leukocytes	76	$s = 0.493$	$s = 0.377$	$s = -0.289$	$s = 0.896$	$s = 0.169$	$s = -0.078$	$s = -0.284$
Lymph nodes leukocyte profile	*Number of dcLN B cells*	98	$s = -0.486$	$s = 0.314$	$s = 0.097$	$s = 0.023$	$s = 0.349$	$s = -0.552$	$s = 0.246$
	% of ingLN B cells	98	$r = -0.766$	$r = 0.279$	$r = 0.268$	$s = 0.051$	$s = 0.043$	$r = -0.209$	$s = -0.398$
	Number of dcLN T cells	98	$s = -0.429$	$s = 0.086$	$s = 0.078$	$s = 0.012$	$s = 0.290$	$s = -0.529$	$s = 0.273$
	% of ingLN T cells	98	$s = 0.371$	$s = -0.200$	$s = -0.261$	$s = -0.045$	$s = -0.060$	$s = 0.211$	$s = 0.357$
	Number of dcLN CD4^{+} T cells	98	$s = -0.429$	$s = 0.086$	$s = 0.079$	$s = 0.005$	$s = 0.302$	$s = -0.54$	$s = 0.275$
	% of ingLN CD4^{+} T cells	98	$s = 0.771$	$s = 0.257$	$s = -0.110$	$s = -0.060$	$s = -0.090$	$s = 0.194$	$s = 0.286$
	Number of dcLN CD8^{+} T cells	98	$s = -0.429$	$s = 0.086$	$s = 0.040$	$s = 0.035$	$s = 0.295$	$s = -0.514$	$s = 0.272$
	% of ingLN Ly6C^{low}, CD62L^{high} **(5)**, *CD8^{+} T cells*	98	$r = -0.810$	$r = -0.636$	$r = 0.081$	$s = -0.259$	$s = -0.369$	$r = 0.372$	$s = -0.371$
	% of dcLN Ly6C^{low}, CD62L^{high} **(6)**, *CD8^{+} T cells*	98	$s = -0.714$	$s = -0.314$	$s = -0.005$	$s = -0.139$	$s = -0.296$	$s = 0.414$	$s = -0.338$
	Number of dcLN leukocytes	98	$s = -0.429$	$s = 0.086$	$s = 0.102$	$s = 0.013$	$s = 0.314$	$s = -0.534$	$s = 0.264$

The *r* and *s* coefficients are shown in white and the *p*-values in grey. Statistical significance ($p < 0.05$) is highlighted in bold.

Supplementary table 3. Continuation.

	Feature	Sample size	Blood leukocyte profile						
			% B cells	% T cells	% (1) $CD4^+$ T cells	% (2) $CD4^+$ T cells	% $CD8^+$ T cells	% (3) $CD8^+$ T cells	% (4) $CD8^+$ T cells
Sample size			116	116	116	116	116	116	116
BMT	*Latency to reach the target hole*	70	$p = 0.693$	$p = 0.338$	**$p = 0.009$**	$p = 0.185$	$p = 0.151$	$p = 0.089$	$p = 0.142$
	Time spent in the target quadrant	70	$p = 0.715$	$p = 0.436$	$p = 0.379$	$p = 0.253$	$p = 0.528$	$p = 0.573$	$p = 0.385$
	% of pokes in the target hole	69	$p = 0.888$	$p = 0.436$	$p = 0.518$	$p = 0.969$	$p = 0.592$	$p = 0.977$	$p = 0.863$
YMT Number of arm alternations		28	$p = 0.291$	$p = 0.321$	**$p = 0.049$**	**$p = 0.001$**	$p = 0.205$	$p = 0.084$	$p = 0.253$
OFT	*Total distance*	117	$p = 0.729$	$p = 0.369$	**$p = 0.039$**	**$p = 0.006$**	$p = 0.241$	$p = 0.165$	$p = 0.159$
	Rearing time	76	$p = 0.976$	$p = 0.536$	$p = 0.345$	$p = 0.615$	$p = 0.444$	$p = 0.401$	$p = 0.187$
	Rearing counts	76	$p = 0.653$	$p = 0.843$	$p = 0.477$	$p = 0.558$	$p = 0.615$	$p = 0.420$	$p = 0.216$
Nadir corticosterone concentration		118	$p = 0.286$	$p = 0.668$	**$p < 0.001$**	$p = 0.394$	$p = 0.346$	**$p = 0.011$**	$p = 0.109$
Final body weight		118	**$p < 0.001$**	$p = 0.184$	$p = 0.071$	**$p = 0.003$**	$p = 0.322$	$p = 0.366$	**$p = 0.005$**
qRT-PCR	*Ido gene expression*	115	**$p < 0.001$**	$p = 0.321$	$p = 0.610$	**$p < 0.001$**	**$p = 0.034$**	$p = 0.150$	$p = 0.161$
	Ifnγ gene expression	115	$p = 0.055$	$p = 0.138$	$p = 0.944$	**$p = 0.013$**	**$p = 0.004$**	$p = 0.804$	$p = 0.314$
	Inos gene expression	115	$p = 0.071$	$p = 0.257$	$p = 0.643$	**$p = 0.040$**	**$p = 0.005$**	$p = 0.640$	$p = 0.643$
	Tnf gene expression	115	$p = 0.204$	$p = 0.907$	$p = 0.672$	$p = 0.088$	$p = 0.636$	$p = 0.193$	$p = 0.523$
Hippocampal stereological analysis	*Number of neurons in the dDG-gcl*	12	$p = 0.051$	$p = 0.055$	$p = 0.080$	$p = 0.159$	**$p = 0.026$**	**$p = 0.002$**	**$p < 0.001$**
	Number of neurons in the dCA1-pcl	12	$p = 0.387$	$p = 0.186$	**$p = 0.002$**	$p = 0.804$	$p = 0.164$	**$p = 0.004$**	**$p = 0.004$**
	Number of neurons in the dCA3-pcl	12	$p = 0.479$	$p = 0.586$	$p = 0.312$	$p = 0.892$	$p = 0.222$	$p = 0.060$	$p = 0.081$
	Number of neurons in the vCA1-pcl	12	**$p = 0.042$**	**$p = 0.019$**	$p = 0.061$	$p = 0.272$	**$p = 0.023$**	$p = 0.054$	**$p = 0.018$**
	Total dDG volume	12	$p = 0.769$	$p = 0.433$	$p = 0.062$	$p = 0.561$	$p = 0.193$	**$p = 0.028$**	$p = 0.087$
	Total dCA1 volume	12	$p = 0.502$	$p = 0.844$	**$p = 0.049$**	$p = 0.460$	$p = 0.582$	$p = 0.102$	$p = 0.175$
	Total dCA3 volume	12	$p = 0.951$	$p = 0.803$	$p = 0.547$	$p = 0.614$	$p = 0.682$	$p = 0.296$	$p = 0.416$
	dDG-ml volume	12	$p = 0.822$	$p = 0.398$	$p = 0.058$	$p = 0.531$	$p = 0.191$	**$p = 0.030$**	$p = 0.074$
	dDG-gcl volume	12	$p = 0.899$	$p = 0.514$	$p = 0.054$	$p = 0.881$	$p = 0.200$	**$p = 0.014$**	$p = 0.071$
	dDG-pl volume	12	$p = 0.926$	$p = 0.475$	$p = 0.147$	$p = 0.561$	$p = 0.232$	$p = 0.104$	$p = 0.330$
	dCA1-so volume	12	$p = 0.531$	$p = 0.923$	$p = 0.065$	$p = 0.387$	$p = 0.777$	$p = 0.236$	$p = 0.358$
	dCA1-pcl volume	12	$p = 0.339$	$p = 0.945$	$p = 0.081$	$p = 0.425$	$p = 0.653$	$p = 0.137$	$p = 0.271$
	dCA1-sr volume	12	$p = 0.581$	$p = 0.747$	**$p = 0.043$**	$p = 0.596$	$p = 0.474$	$p = 0.058$	$p = 0.098$
	vCA1-pcl volume	12	$p = 0.051$	**$p = 0.002$**	**$p = 0.011$**	$p = 0.362$	**$p = 0.008$**	**$p = 0.024$**	**$p = 0.020$**
	dCA3-so volume	12	$p = 0.653$	$p = 0.727$	$p = 0.658$	$p = 0.398$	$p = 0.737$	$p = 0.355$	$p = 0.466$
	dCA3-pcl volume	12	$p = 0.969$	$p = 0.994$	$p = 0.427$	$p = 0.778$	$p = 0.493$	$p = 0.163$	$p = 0.249$
Neuronal reconstruction	*dDG dendritic length*	12	$p = 0.711$	$p = 0.169$	$p = 0.095$	$p = 0.700$	$p = 0.226$	**$p = 0.024$**	**$p = 0.014$**
	dDG dendritic ends	12	$p = 0.437$	$p = 0.272$	$p = 0.054$	$p = 0.908$	$p = 0.299$	**$p = 0.010$**	**$p = 0.003$**
	vDG dendritic length	13	$p = 0.969$	$p = 0.279$	**$p = 0.003$**	$p = 0.562$	$p = 0.211$	**$p = 0.022$**	**$p = 0.042$**
	vDG dendritic ends	13	$p = 0.087$	$p = 0.150$	$p = 0.084$	$p = 0.888$	$p = 0.109$	**$p = 0.047$**	**$p = 0.018$**
	CA1 apical dendritic length	12	$p = 0.568$	$p = 0.182$	$p = 0.386$	$p = 0.543$	$p = 0.197$	$p = 0.150$	**$p = 0.040$**
	CA1 apical dendritic ends	12	$p = 0.959$	$p = 0.313$	$p = 0.682$	$p = 0.345$	$p = 0.515$	$p = 0.315$	$p = 0.140$
	CA3 apical dendritic length	12	$p = 0.646$	**$p = 0.006$**	$p = 0.070$	$p = 0.193$	**$p = 0.006$**	**$p = 0.027$**	**$p = 0.036$**
	CA3 apical dendritic ends	12	$p = 0.342$	$p = 0.452$	$p = 0.814$	$p = 0.599$	$p = 0.340$	$p = 0.662$	$p = 0.437$
Blood leukocyte profile	*% of eosinophils*	116	$p = 0.137$	$p = 0.513$	**$p = 0.013$**	$p = 0.197$	$p = 0.383$	$p = 0.242$	$p = 0.735$
	Number of neutrophils	75	**$p = 0.036$**	**$p = 0.002$**	**$p < 0.001$**	$p = 0.054$	**$p = 0.002$**	**$p = 0.003$**	**$p = 0.020$**
	% of neutrophils	116	**$p < 0.001$**	**$p < 0.001$**	$p = 0.448$	**$p < 0.001$**	**$p < 0.001$**	$p = 0.250$	**$p = 0.031$**
	% of $Ly6C^{high}$ NK cells	116	**$p < 0.001$**	**$p < 0.001$**	**$p = 0.012$**	**$p < 0.001$**	**$p < 0.001$**	$p = 0.728$	**$p = 0.033$**
	% of $Ly6C^{low}$ NK cells	116	**$p < 0.001$**	$p = 0.258$	**$p < 0.001$**	$p = 0.618$	$p = 0.559$	**$p < 0.001$**	**$p < 0.001$**
	% of B cells	116		**$p < 0.001$**	$p = 0.450$	**$p < 0.001$**	**$p < 0.001$**	**$p = 0.003$**	**$p < 0.001$**
	% of T cells	116	$s = 0.439$		$p = 0.599$	**$p < 0.001$**	**$p < 0.001$**	$p = 0.607$	$p = 0.914$
	% of $CD44^{low:int}$, $CD62L^{int}$ **(1)**, *$CD4^+$ T cells*	116	$s = -0.071$	$r = 0.049$		$p = 0.761$	$p = 0.097$	**$p < 0.001$**	**$p < 0.001$**
	% of $CD44^{int:high}$, $CD62L^{low}$ **(2)**, *$CD4^+$ T cells*	116	$s = -0.438$	$s = -0.605$	$s = 0.029$		**$p < 0.001$**	$p = 0.285$	$p = 0.409$
	% of $CD8^+$ T cells	116	$s = 0.447$	$r = 0.889$	$r = 0.155$	$s = -0.553$		$p = 0.115$	$p = 0.148$
	% of $Ly6C^{high}$, $CD62L^{high}$ **(3)**, *$CD8^+$ T cells*	116	$s = 0.276$	$r = -0.048$	$r = -0.831$	$s = -0.100$	$r = -0.147$		**$p < 0.001$**
	% of $Ly6C^{low}$, $CD62L^{int}$ **(4)**, *$CD8^+$ T cells*	116	$s = -0.363$	$r = -0.010$	$r = 0.553$	$s = 0.077$	$r = 0.135$	$r = -0.789$	
	Number of leukocytes	76	$s = 0.019$	$s = -0.140$	$s = -0.304$	$s = 0.078$	$s = -0.093$	$s = 0.295$	$s = -0.312$
Lymph nodes leukocyte profile	*Number of dcLN B cells*	98	$s = -0.551$	$s = -0.296$	$s = 0.006$	$s = 0.534$	$s = -0.256$	$s = -0.234$	$s = 0.393$
	% of ingLN B cells	98	$s = 0.034$	$r = -0.365$	$r = -0.366$	$s = 0.339$	$r = -0.502$	$r = 0.461$	$r = -0.526$
	Number of dcLN T cells	98	$s = -0.545$	$s = -0.192$	$s = 0.018$	$s = 0.459$	$s = -0.136$	$s = -0.253$	$s = 0.435$
	% of ingLN T cells	98	$s = 0.002$	$s = 0.305$	$s = 0.226$	$s = -0.383$	$s = 0.460$	$s = -0.355$	$s = 0.534$
	Number of dcLN $CD4^+$ T cells	98	$s = -0.562$	$s = -0.202$	$s = 0.012$	$s = 0.465$	$s = -0.152$	$s = -0.253$	$s = 0.436$
	% of ingLN $CD4^+$ T cells	98	$s = -0.059$	$s = 0.263$	$s = 0.125$	$s = -0.303$	$s = 0.309$	$s = -0.267$	$s = 0.473$
	Number of dcLN $CD8^+$ T cells	98	$s = -0.521$	$s = -0.182$	$s = 0.031$	$s = 0.430$	$s = -0.114$	$s = -0.262$	$s = 0.443$
	% of ingLN $Ly6C^{low}$, $CD62L^{high}$ **(5)**, *$CD8^+$ T cells*	98	$s = 0.503$	$r = 0.252$	$r = -0.161$	$s = -0.407$	$r = 0.192$	$r = 0.270$	$r = -0.361$
	% of dcLN $Ly6C^{low}$, $CD62L^{high}$ **(6)**, *$CD8^+$ T cells*	98	$s = 0.475$	$s = 0.293$	$s = -0.122$	$s = -0.471$	$s = 0.249$	$s = 0.238$	$s = -0.237$
	Number of dcLN leukocytes	98	$s = -0.552$	$s = -0.248$	$s = 0.018$	$s = 0.505$	$s = -0.195$	$s = -0.243$	$s = 0.411$

The *r* and *s* coefficients are shown in white and the *p*-values in grey. Statistical significance ($p < 0.05$) is highlighted in bold.

Supplementary table 3. Continuation.

	Feature	Sample size	BLP	Lymph nodes leukocyte profile					
			Number leukocytes	Number dcLN B cells	% ingLN B cells	Number dcLN T cells	% ingLN T cells	Number dcLN $CD4^+$ T cells	% ingLN $CD4^+$ T cells
	Sample size		76	98	98	98	98	98	98
BMT	*Latency to reach the target hole*	70	$p = 0.646$	$p = 0.893$	**$p = 0.019$**	$p = 0.676$	$p = 0.159$	$p = 0.706$	$p = 0.605$
BMT	*Time spent in the target quadrant*	70	$p = 0.472$	$p = 0.813$	$p = 0.267$	$p = 0.729$	$p = 0.281$	$p = 0.802$	$p = 0.309$
BMT	*% of pokes in the target hole*	69	$p = 0.240$	$p = 0.703$	**$p = 0.025$**	$p = 0.424$	$p = 0.485$	$p = 0.531$	$p = 0.670$
	YMT Number of arm alternations	28	**$p = 0.025$**	**$p = 0.009$**	$p = 0.099$	**$p = 0.012$**	**$p = 0.039$**	**$p = 0.016$**	$p = 0.093$
OFT	*Total distance*	117	$p = 0.116$	**$p = 0.028$**	**$p = 0.046$**	**$p = 0.041$**	**$p = 0.014$**	**$p = 0.046$**	**$p = 0.040$**
OFT	*Rearing time*	76	$p = 0.496$	$p = 0.828$	$p = 0.602$	$p = 0.735$	$p = 0.514$	$p = 0.865$	$p = 0.763$
OFT	*Rearing counts*	76	$p = 0.585$	$p = 0.687$	$p = 0.367$	$p = 0.564$	$p = 0.291$	$p = 0.694$	$p = 0.494$
	Nadir corticosterone concentration	118	**$p < 0.001$**	$p = 0.873$	$p = 0.496$	$p = 0.853$	$p = 0.415$	$p = 0.844$	$p = 0.942$
	Final body weight	118	**$p = 0.001$**	**$p < 0.001$**	$p = 0.492$	**$p < 0.001$**	$p = 0.142$	**$p < 0.001$**	$p = 0.283$
qRT-PCR	*Ido gene expression*	115	$p = 0.787$	**$p < 0.001$**	$p = 0.140$	**$p = 0.001$**	$p = 0.106$	**$p = 0.001$**	$p = 0.151$
qRT-PCR	*Ifnγ gene expression*	115	$p = 0.202$	**$p = 0.006$**	$p = 0.513$	**$p = 0.027$**	$p = 0.478$	**$p = 0.026$**	$p = 0.755$
qRT-PCR	*Inos gene expression*	115	$p = 0.796$	**$p = 0.023$**	$p = 0.073$	$p = 0.134$	$p = 0.083$	$p = 0.137$	$p = 0.422$
qRT-PCR	*Tnf gene expression*	115	$p = 0.138$	$p = 0.081$	$p = 0.857$	$p = 0.081$	$p = 0.976$	$p = 0.082$	$p = 0.341$
Hippocampal stereological analysis	*Number of neurons in the dDG-gcl*	12	$p = 0.497$	$p = 0.714$	$p = 0.628$	$p = 0.658$	$p = 0.803$	$p = 0.658$	$p > 0.999$
Hippocampal stereological analysis	*Number of neurons in the dCA1-pcl*	12	$p = 0.714$	$p = 0.658$	$p = 0.910$	$p > 0.999$	$p = 0.919$	$p > 0.999$	$p = 0.919$
Hippocampal stereological analysis	*Number of neurons in the dCA3-pcl*	12	$p = 0.714$	$p = 0.356$	$p = 0.970$	$p = 0.103$	$p = 0.497$	$p = 0.103$	$p = 0.803$
Hippocampal stereological analysis	*Number of neurons in the vCA1-pcl*	12	$p = 0.175$	$p = 0.136$	$p = 0.477$	$p = 0.297$	$p = 0.564$	$p = 0.297$	$p > 0.999$
Hippocampal stereological analysis	*Total dDG volume*	12	$p = 0.803$	$p = 0.233$	$p = 0.420$	$p = 0.072$	$p = 0.333$	$p = 0.072$	$p = 0.372$
Hippocampal stereological analysis	*Total dCA1 volume*	12	$p = 0.658$	$p = 0.497$	$p = 0.151$	$p = 0.356$	$p = 0.175$	$p = 0.356$	$p = 0.103$
Hippocampal stereological analysis	*Total dCA3 volume*	12	$p = 0.803$	$p = 0.242$	$p = 0.617$	$p = 0.242$	$p = 0.658$	$p = 0.242$	$p > 0.999$
Hippocampal stereological analysis	*dDG-ml volume*	12	$p = 0.803$	$p = 0.497$	$p = 0.386$	$p = 0.175$	$p = 0.356$	$p = 0.175$	$p = 0.297$
Hippocampal stereological analysis	*dDG-gcl volume*	12	$p > 0.999$	$p = 0.242$	$p = 0.368$	$p = 0.058$	$p = 0.242$	$p = 0.058$	$p = 0.242$
Hippocampal stereological analysis	*dDG-pl volume*	12	$p = 0.803$	$p = 0.658$	$p = 0.646$	$p = 0.297$	$p = 0.658$	$p = 0.297$	$p = 0.658$
Hippocampal stereological analysis	*dCA1-so volume*	12	$p = 0.658$	$p = 0.658$	$p = 0.265$	$p = 0.419$	$p = 0.242$	$p = 0.419$	$p = 0.175$
Hippocampal stereological analysis	*dCA1-pcl volume*	12	$p = 0.658$	$p = 0.175$	$p = 0.085$	$p = 0.103$	$p = 0.136$	$p = 0.103$	$p = 0.103$
Hippocampal stereological analysis	*dCA1-sr volume*	12	$p = 0.658$	$p = 0.497$	$p = 0.143$	$p = 0.356$	$p = 0.175$	$p = 0.356$	$p = 0.103$
Hippocampal stereological analysis	*vCA1-pcl volume*	12	$p = 0.297$	$p = 0.564$	$p = 0.907$	$p = 0.803$	$p = 0.803$	$p = 0.803$	$p = 0.564$
Hippocampal stereological analysis	*dCA3-so volume*	12	$p = 0.778$	$p = 0.356$	$p = 0.432$	$p = 0.356$	$p = 0.714$	$p = 0.356$	$p > 0.999$
Hippocampal stereological analysis	*dCA3-pcl volume*	12	$p = 0.919$	$p = 0.242$	$p = 0.431$	$p = 0.058$	$p = 0.419$	$p = 0.058$	$p = 0.658$
Neuronal reconstruction	*dDG dendritic length*	12	$p = 0.072$	$p = 0.419$	$p = 0.319$	$p = 0.497$	$p = 0.297$	$p = 0.497$	**$p = 0.033$**
Neuronal reconstruction	*dDG dendritic ends*	12	$p = 0.144$	$p = 0.333$	$p = 0.158$	$p = 0.378$	$p = 0.300$	$p = 0.378$	**$p = 0.044$**
Neuronal reconstruction	*vDG dendritic length*	13	$p = 0.090$	**$p = 0.017$**	$p = 0.186$	**$p = 0.033$**	$p = 0.356$	**$p = 0.033$**	$p = 0.497$
Neuronal reconstruction	*vDG dendritic ends*	13	**$p = 0.003$**	**$p = 0.044$**	$p = 0.218$	**$p = 0.044$**	$p = 0.200$	**$p = 0.044$**	$p = 0.272$
Neuronal reconstruction	*CA1 apical dendritic length*	12	$p = 0.494$	$p = 0.803$	$p = 0.285$	$p = 0.658$	$p = 0.419$	$p = 0.658$	$p = 0.242$
Neuronal reconstruction	*CA1 apical dendritic ends*	12	$p = 0.778$	$p = 0.711$	$p = 0.990$	$p = 0.933$	$p = 0.778$	$p = 0.933$	$p = 0.711$
Neuronal reconstruction	*CA3 apical dendritic length*	12	$p = 0.328$	$p = 0.356$	$p = 0.076$	$p = 0.419$	$p = 0.497$	$p = 0.419$	$p = 0.103$
Neuronal reconstruction	*CA3 apical dendritic ends*	12	$p = 0.467$	$p = 0.564$	$p = 0.592$	$p = 0.919$	$p = 0.714$	$p = 0.919$	$p = 0.658$
Blood leukocyte profile	*% of eosinophils*	116	**$p = 0.012$**	$p = 0.348$	**$p = 0.008$**	$p = 0.448$	**$p = 0.010$**	$p = 0.445$	$p = 0.288$
Blood leukocyte profile	*Number of neutrophils*	75	**$p < 0.001$**	$p = 0.869$	$p = 0.710$	$p = 0.928$	$p = 0.745$	$p = 0.971$	$p = 0.666$
Blood leukocyte profile	*% of neutrophils*	116	$p = 0.147$	**$p < 0.001$**	$p = 0.677$	**$p = 0.004$**	$p = 0.561$	**$p = 0.003$**	$p = 0.382$
Blood leukocyte profile	*% of $Ly6C^{high}$ NK cells*	116	$p = 0.504$	**$p < 0.001$**	**$p = 0.041$**	**$p < 0.001$**	**$p = 0.039$**	**$p < 0.001$**	$p = 0.058$
Blood leukocyte profile	*% of $Ly6C^{low}$ NK cells*	116	**$p = 0.014$**	**$p = 0.016$**	**$p < 0.001$**	**$p = 0.007$**	**$p < 0.001$**	**$p = 0.007$**	**$p = 0.005$**
Blood leukocyte profile	*% of B cells*	116	$p = 0.871$	**$p < 0.001$**	$p = 0.739$	**$p < 0.001$**	$p = 0.982$	**$p < 0.001$**	$p = 0.565$
Blood leukocyte profile	*% of T cells*	116	$p = 0.231$	**$p = 0.003$**	**$p < 0.001$**	$p = 0.060$	**$p = 0.003$**	**$p = 0.048$**	**$p = 0.010$**
Blood leukocyte profile	*% of $CD44^{low:int}$, $CD62L^{int}$* **(1)**, *$CD4^+$ T cells*	116	**$p = 0.008$**	$p = 0.955$	**$p < 0.001$**	$p = 0.860$	**$p = 0.027$**	$p = 0.905$	$p = 0.225$
Blood leukocyte profile	*% of $CD44^{int:high}$, $CD62L^{low}$* **(2)**, *$CD4^+$ T cells*	116	$p = 0.504$	**$p < 0.001$**	**$p = 0.001$**	**$p < 0.001$**	**$p < 0.001$**	**$p < 0.001$**	**$p = 0.003$**
Blood leukocyte profile	*% of $CD8^+$ T cells*	116	$p = 0.427$	**$p = 0.012$**	**$p < 0.001$**	$p = 0.186$	**$p < 0.001$**	$p = 0.139$	**$p = 0.002$**
Blood leukocyte profile	*% of $Ly6C^{high}$, $CD62L^{high}$* **(3)**, *$CD8^+$ T cells*	116	**$p = 0.010$**	**$p = 0.022$**	**$p < 0.001$**	**$p = 0.013$**	**$p < 0.001$**	**$p = 0.013$**	**$p = 0.009$**
Blood leukocyte profile	*% of $Ly6C^{low}$, $CD62L^{int}$* **(4)**, *$CD8^+$ T cells*	116	**$p = 0.006$**	**$p < 0.001$**	**$p < 0.001$**	**$p < 0.001$**	**$p < 0.001$**	**$p < 0.001$**	**$p < 0.001$**
Blood leukocyte profile	*Number of leukocytes*	76		$p = 0.966$	$p = 0.795$	$p = 0.884$	$p = 0.810$	$p = 0.998$	$p = 0.940$
Lymph nodes leukocyte profile	*Number of dcLN B cells*	98	$s = 0.006$		$p = 0.869$	**$p < 0.001$**	$p = 0.692$	**$p < 0.001$**	$p = 0.718$
Lymph nodes leukocyte profile	*% of ingLN B cells*	98	$s = -0.036$	$s = 0.017$		$p = 0.444$	**$p < 0.001$**	$p = 0.412$	**$p < 0.001$**
Lymph nodes leukocyte profile	*Number of dcLN T cells*	98	$s = 0.020$	$s = 0.965$	$s = -0.078$		$p = 0.559$	**$p < 0.001$**	$p = 0.252$
Lymph nodes leukocyte profile	*% of ingLN T cells*	98	$s = 0.033$	$s = -0.041$	$s = -0.994$	$s = 0.060$		$p = 0.523$	**$p < 0.001$**
Lymph nodes leukocyte profile	*Number of dcLN $CD4^+$ T cells*	98	$s = 0.001$	$s = 0.969$	$s = -0.084$	$s = 0.997$	$s = 0.065$		$p = 0.201$
Lymph nodes leukocyte profile	*% of ingLN $CD4^+$ T cells*	98	$s = -0.010$	$s = 0.037$	$s = -0.875$	$s = 0.117$	$s = 0.874$	$s = 0.130$	
Lymph nodes leukocyte profile	*Number of dcLN $CD8^+$ T cells*	98	$s = 0.047$	$s = 0.959$	$s = -0.117$	$s = 0.989$	$s = 0.099$	$s = 0.987$	$s = 0.130$
Lymph nodes leukocyte profile	*% of ingLN $Ly6C^{low}$, $CD62L^{high}$* **(5)**, *$CD8^+$ T cells*	98	$s = -0.225$	$s = -0.419$	$r = 0.133$	$s = -0.418$	$s = -0.106$	$s = -0.427$	$s = -0.100$
Lymph nodes leukocyte profile	*% of dcLN $Ly6C^{low}$, $CD62L^{high}$* **(6)**, *$CD8^+$ T cells*	98	$s = -0.166$	$s = -0.481$	$s = 0.068$	$s = -0.485$	$s = -0.039$	$s = -0.481$	$s = -0.076$
Lymph nodes leukocyte profile	*Number of dcLN leukocytes*	98	$s = 0.014$	$s = 0.981$	$s = -0.017$	$s = 0.992$	$s = -0.003$	$s = 0.988$	$s = 0.063$

The *r* and *s* coefficients are shown in white and the *p*-values in grey. Statistical significance ($p < 0.05$) is highlighted in bold.

Supplementary table 3. Continuation.

	Feature	Sample size	Lymph nodes leukocyte profile			
			Number dcLN $CD8^+$ T cells	% ingLN (5) $CD8^+$ T cells	% dcLN (6) $CD8^+$ T cells	Number dcLN leukocytes
	Sample size		98	98	98	98
BMT	*Latency to reach the target hole*	70	$p = 0.645$	$p = 0.626$	$p = 0.719$	$p = 0.792$
BMT	*Time spent in the target quadrant*	70	$p = 0.654$	$p = 0.494$	$p = 0.634$	$p = 0.785$
BMT	*% of pokes in the target hole*	69	$p = 0.371$	$p = 0.919$	$p = 0.614$	$p = 0.565$
	YMT Number of arm alternations	28	**$p = 0.012$**	**$p = 0.046$**	**$p = 0.001$**	**$p = 0.015$**
OFT	*Total distance*	117	**$p = 0.031$**	$p = 0.218$	$p = 0.578$	**$p = 0.041$**
OFT	*Rearing time*	76	$p = 0.853$	$p = 0.313$	$p = 0.444$	$p = 0.697$
OFT	*Rearing counts*	76	$p = 0.680$	$p = 0.388$	$p = 0.629$	$p = 0.549$
	Nadir corticosterone concentration	118	$p = 0.957$	$p = 0.795$	$p = 0.684$	$p = 0.830$
	Final body weight	118	**$p < 0.001$**	**$p = 0.001$**	**$p < 0.001$**	**$p < 0.001$**
qRT-PCR	*Ido gene expression*	115	**$p = 0.001$**	**$p = 0.001$**	**$p = 0.001$**	**$p < 0.001$**
qRT-PCR	*Ifnγ gene expression*	115	**$p = 0.038$**	$p = 0.135$	$p = 0.073$	**$p = 0.016$**
qRT-PCR	*Inos gene expression*	115	$p = 0.139$	$p = 0.193$	$p = 0.316$	$p = 0.081$
qRT-PCR	*Tnf gene expression*	115	$p = 0.063$	**$p = 0.006$**	**$p = 0.013$**	$p = 0.100$
Hippocampal stereological analysis	*Number of neurons in the dDG-gcl*	12	$p > 0.999$	$p = 0.824$	$p = 0.803$	$p = 0.714$
Hippocampal stereological analysis	*Number of neurons in the dCA1-pcl*	12	$p = 0.919$	$p = 0.307$	$p = 0.497$	$p = 0.658$
Hippocampal stereological analysis	*Number of neurons in the dCA3-pcl*	12	$p = 0.297$	$p = 0.848$	$p = 0.803$	$p = 0.356$
Hippocampal stereological analysis	*Number of neurons in the vCA1-pcl*	12	$p = 0.356$	$p = 0.150$	$p = 0.919$	$p = 0.136$
Hippocampal stereological analysis	*Total dDG volume*	12	$p = 0.122$	$p = 0.409$	$p = 0.600$	$p = 0.233$
Hippocampal stereological analysis	*Total dCA1 volume*	12	$p = 0.242$	$p = 0.389$	$p = 0.564$	$p = 0.497$
Hippocampal stereological analysis	*Total dCA3 volume*	12	$p = 0.356$	$p = 0.423$	$p = 0.919$	$p = 0.242$
Hippocampal stereological analysis	*dDG-ml volume*	12	$p = 0.242$	$p = 0.448$	$p = 0.714$	$p = 0.497$
Hippocampal stereological analysis	*dDG-gcl volume*	12	$p = 0.103$	$p = 0.249$	$p = 0.497$	$p = 0.242$
Hippocampal stereological analysis	*dDG-pl volume*	12	$p = 0.419$	$p = 0.594$	$p > 0.999$	$p = 0.658$
Hippocampal stereological analysis	*dCA1-so volume*	12	$p = 0.356$	$p = 0.736$	$p = 0.919$	$p = 0.658$
Hippocampal stereological analysis	*dCA1-pcl volume*	12	$p = 0.058$	$p = 0.225$	$p = 0.297$	$p = 0.175$
Hippocampal stereological analysis	*dCA1-sr volume*	12	$p = 0.242$	$p = 0.301$	$p = 0.564$	$p = 0.497$
Hippocampal stereological analysis	*vCA1-pcl volume*	12	$p = 0.919$	$p = 0.403$	$p = 0.803$	$p = 0.564$
Hippocampal stereological analysis	*dCA3-so volume*	12	$p = 0.419$	$p = 0.326$	$p > 0.999$	$p = 0.356$
Hippocampal stereological analysis	*dCA3-pcl volume*	12	$p = 0.175$	$p = 0.357$	$p = 0.919$	$p = 0.242$
Neuronal reconstruction	*dDG dendritic length*	12	$p = 0.497$	**$p = 0.002$**	**$p = 0.033$**	$p = 0.497$
Neuronal reconstruction	*dDG dendritic ends*	12	$p = 0.378$	**$p = 0.002$**	**$p = 0.006$**	$p = 0.378$
Neuronal reconstruction	*vDG dendritic length*	13	**$p = 0.033$**	$p = 0.218$	$p = 0.419$	**$p = 0.033$**
Neuronal reconstruction	*vDG dendritic ends*	13	**$p = 0.044$**	$p = 0.483$	$p = 0.300$	**$p = 0.044$**
Neuronal reconstruction	*CA1 apical dendritic length*	12	$p = 0.658$	$p = 0.252$	**$p = 0.033$**	$p = 0.658$
Neuronal reconstruction	*CA1 apical dendritic ends*	12	$p = 0.933$	$p = 0.495$	$p = 0.333$	$p = 0.933$
Neuronal reconstruction	*CA3 apical dendritic length*	12	$p = 0.419$	$p = 0.051$	$p = 0.136$	$p = 0.419$
Neuronal reconstruction	*CA3 apical dendritic ends*	12	$p = 0.919$	$p = 0.174$	$p = 0.564$	$p = 0.919$
Blood leukocyte profile	*% of eosinophils*	116	$p = 0.695$	$p = 0.432$	$p = 0.964$	$p = 0.325$
Blood leukocyte profile	*Number of neutrophils*	75	$p = 0.802$	$p = 0.057$	$p = 0.310$	$p = 0.923$
Blood leukocyte profile	*% of neutrophils*	116	**$p = 0.003$**	**$p < 0.001$**	**$p = 0.003$**	**$p = 0.002$**
Blood leukocyte profile	*% of $Ly6C^{high}$ NK cells*	116	**$p < 0.001$**	**$p < 0.001$**	**$p < 0.001$**	**$p < 0.001$**
Blood leukocyte profile	*% of $Ly6C^{low}$ NK cells*	116	**$p = 0.007$**	**$p < 0.001$**	**$p = 0.001$**	**$p = 0.009$**
Blood leukocyte profile	*% of B cells*	116	**$p < 0.001$**	**$p < 0.001$**	**$p < 0.001$**	**$p < 0.001$**
Blood leukocyte profile	*% of T cells*	116	$p = 0.076$	**$p = 0.013$**	**$p = 0.004$**	**$p = 0.015$**
Blood leukocyte profile	*% of $CD44^{low:int}$, $CD62L^{int}$* **(1)**, *$CD4^+$ T cells*	116	$p = 0.766$	$p = 0.116$	$p = 0.237$	$p = 0.861$
Blood leukocyte profile	*% of $CD44^{int:high}$, $CD62L^{low}$* **(2)**, *$CD4^+$ T cells*	116	**$p < 0.001$**	**$p < 0.001$**	**$p < 0.001$**	**$p < 0.001$**
Blood leukocyte profile	*% of $CD8^+$ T cells*	116	$p = 0.268$	$p = 0.061$	**$p = 0.015$**	$p = 0.057$
Blood leukocyte profile	*% of $Ly6C^{high}$, $CD62L^{high}$* **(3)**, *$CD8^+$ T cells*	116	**$p = 0.010$**	**$p = 0.008$**	**$p = 0.02$**	**$p = 0.017$**
Blood leukocyte profile	*% of $Ly6C^{low}$, $CD62L^{int}$* **(4)**, *$CD8^+$ T cells*	116	**$p < 0.001$**	**$p < 0.001$**	**$p = 0.02$**	**$p < 0.001$**
Blood leukocyte profile	*Number of leukocytes*	76	$p = 0.732$	$p = 0.096$	$p = 0.223$	$p = 0.919$
Lymph nodes leukocyte profile	*Number of dcLN B cells*	98	**$p < 0.001$**	**$p < 0.001$**	**$p < 0.001$**	**$p < 0.001$**
Lymph nodes leukocyte profile	*% of ingLN B cells*	98	$p = 0.252$	$p = 0.191$	$p = 0.508$	$p = 0.867$
Lymph nodes leukocyte profile	*Number of dcLN T cells*	98	**$p < 0.001$**	**$p < 0.001$**	**$p < 0.001$**	**$p < 0.001$**
Lymph nodes leukocyte profile	*% of ingLN T cells*	98	$p = 0.334$	$p = 0.298$	$p = 0.704$	$p = 0.974$
Lymph nodes leukocyte profile	*Number of dcLN $CD4^+$ T cells*	98	**$p < 0.001$**	**$p < 0.001$**	**$p < 0.001$**	**$p < 0.001$**
Lymph nodes leukocyte profile	*% of ingLN $CD4^+$ T cells*	98	$p = 0.201$	$p = 0.326$	$p = 0.456$	$p = 0.536$
Lymph nodes leukocyte profile	*Number of dcLN $CD8^+$ T cells*	98		**$p < 0.001$**	**$p < 0.001$**	**$p < 0.001$**
Lymph nodes leukocyte profile	*% of ingLN $Ly6C^{low}$, $CD62L^{high}$* **(5)**, *$CD8^+$ T cells*	98	$s = -0.401$		**$p < 0.001$**	**$p < 0.001$**
Lymph nodes leukocyte profile	*% of dcLN $Ly6C^{low}$, $CD62L^{high}$* **(6)**, *$CD8^+$ T cells*	98	$s = -0.451$	$s = 0.776$		**$p < 0.001$**
Lymph nodes leukocyte profile	*Number of dcLN leukocytes*	98	$s = 0.976$	$s = -0.421$	$s = -0.495$	

The *r* and *s* coefficients are shown in white and the *p*-values in grey. Statistical significance ($p < 0.05$) is highlighted in bold.